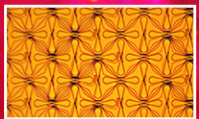
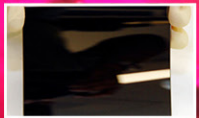
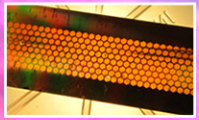
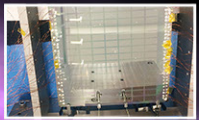
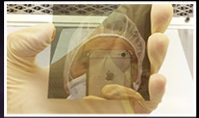
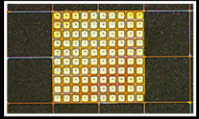


# Physics of the Cosmos Program Annual Technology Report



Physics of the Cosmos  
Program Office  
October 2016



## PCOS Program

### Program Office

**Program Manager:** Mansoor Ahmed ([mansoor.ahmed@nasa.gov](mailto:mansoor.ahmed@nasa.gov))  
**Deputy Program Manager:** Azita Valinia ([azita.valinia-1@nasa.gov](mailto:azita.valinia-1@nasa.gov))  
**Chief Scientist:** Ann Hornschemeier ([ann.hornschemeier@nasa.gov](mailto:ann.hornschemeier@nasa.gov))  
**Deputy Chief Scientist:** Peter Bertone ([peter.bertone@nasa.gov](mailto:peter.bertone@nasa.gov))  
**Chief Technologist:** Harley Thronson ([harley.a.thronson@nasa.gov](mailto:harley.a.thronson@nasa.gov))  
**Technology Development Manager:** Thai Pham ([thai.pham@nasa.gov](mailto:thai.pham@nasa.gov))  
**PATR Production Lead and Editor:** Opher Ganel ([opher.ganel@nasa.gov](mailto:opher.ganel@nasa.gov))  
**PATR Co-Editor:** Russell Werneth ([russell.i.werneth@nasa.gov](mailto:russell.i.werneth@nasa.gov))  
**PATR Graphics:** Herbert Eaton ([herbert.e.eaton@nasa.gov](mailto:herbert.e.eaton@nasa.gov))  
DeLee Smith ([delee.i.smith@nasa.gov](mailto:delee.i.smith@nasa.gov))  
**PATR Admin Support:** Kay Deere ([kay.m.deere@nasa.gov](mailto:kay.m.deere@nasa.gov))

### Headquarters

**Program Executive:** Shahid Habib ([shahid.habib-1@nasa.gov](mailto:shahid.habib-1@nasa.gov))  
**Program Scientist:** Rita Sambruna ([rita.m.sambruna@nasa.gov](mailto:rita.m.sambruna@nasa.gov))  
**Deputy Program Scientists:** Daniel Evans ([daniel.a.evans@nasa.gov](mailto:daniel.a.evans@nasa.gov))  
Wilt Sanders ([wilton.t.sanders@nasa.gov](mailto:wilton.t.sanders@nasa.gov))

<http://pcos.gsfc.nasa.gov>

*The report cover links our age-old observation of the skies, seeking to understand the universe we live in and how it works, with modern astrophysics.*

*The step-pyramid of the Mayan Temple of Kukulcan in Chichen Itza incorporates astronomical observations made in ancient times, including 365 steps, the number of days in the Mayan Haab year; and 18 terraces, corresponding to the number of 20-day months in the Haab year. This demonstrates how important astronomical observations have been since ancient times.*

*Modern astrophysics has expanded beyond the spectrum visible to the human eye, searching for B-mode polarization in the cosmic microwave background, an expected signature of the inflationary period immediately following the Big Bang, depicted as vectors at the right edge of our cover; X rays, generated by some of the most energetic and violent cosmic phenomena such as active galactic nuclei similar to the artist's impression shown at the top of the cover; and even gravitational waves, vibrations in the very fabric of space-time caused by such events as massive black holes spiraling into each other.*

*The “chirp,” shown overlaying an artist’s concept of inspiraling black holes, was observed earlier this year by the Laser Interferometer Gravitational-Wave Observatory (LIGO), the first direct evidence of these long-theorized waves. As black holes spiral in, their orbital distance decreases and their speed increases, causing the gravitational-wave frequency to increase. Translating this frequency to sound waves creates a chirp sound.*

*The Strategic Astrophysics Technology project images at the left edge of the cover demonstrate our ongoing efforts to identify and develop the technologies that will advance humankind’s ability to observe and understand our universe.*

# Table of Contents

Executive Summary . . . . .	4
1. Program Science Overview . . . . .	7
2. Strategic Technology Development Process and Portfolio . . . . .	10
3. Technology Gaps, Priorities, and Recommendations . . . . .	16
4. Benefits and Successes Enabled by the PCOS SAT Program . . . . .	21
5. Closing Remarks . . . . .	26
References . . . . .	27
Appendix A – Technology Gaps Evaluated by the TMB in 2016 . . . . .	28
Appendix B – Program Technology Development Quad Charts . . . . .	63
Appendix C – Program Technology Development Status . . . . .	77
Appendix D – Acronyms. . . . .	179

# PCOS 2016 PATR

## Executive Summary

### What is NASA's Physics of the Cosmos (PCOS) Program?

From ancient times, humans have looked up at the night sky and wondered: Are we alone? How did the universe come to be? **How does the universe work?** PCOS focuses on that last question. Scientists investigating this broad theme use the universe itself as their laboratory, investigating its fundamental laws and properties. They test Einstein's General Theory of Relativity to see if our current understanding of space-time is borne out by observations. They examine the behavior of the most extreme environments – supermassive black holes, active galactic nuclei, and others – and the farthest reaches of the universe, to expand our understanding. With instruments sensitive across the spectrum, from radio, through infrared (IR), visible light, ultraviolet (UV), to X rays and gamma rays, as well as gravitational waves (GWs), they peer across billions of light-years, observing echoes of events that occurred instants after the Big Bang.

The Laser Interferometer Gravitational-Wave Observatory (LIGO) recently recorded the first direct measurement of long-theorized GWs. Another surprising recent discovery is that the universe is expanding at an ever-accelerating rate, the first hint of so-called “dark energy,” estimated to account for 75% of mass-energy in the universe. Dark matter, so called because we can only observe its effects on regular matter, accounts for another 20%, leaving only 5% for regular matter and energy. Scientists now also search for special polarization in the cosmic microwave background to support the notion that in the split-second after the Big Bang, the universe inflated faster than the speed of light! The most exciting aspect of this grand enterprise today is that we can finally develop the tools needed for such discoveries.

### Why is PCOS Technology Development Critical?

A 2008 Space Review paper noted that robust technology development and maturation is crucial to reducing flight project schedule and cost over-runs: “...in the mid-1980s, NASA's budget office found that during the first 30 years of the civil space program, no project enjoyed less than a 40% cost overrun unless it was preceded by an investment in studies and technology of at least 5 to 10% of the actual project budget that eventually occurred” [1]. Such a technology maturation program is most efficiently addressed through focused R&D projects, rather than in flight projects, where “marching armies” make the cost of delays unacceptably high. The National Academies of Sciences 2010 Decadal Survey, [New Worlds, New Horizons in Astronomy and Astrophysics](#) (NWNH) stressed that “*Technology development is the engine powering advances in astronomy and astrophysics... Failure to develop adequately mature technology prior to a program start also leads to cost and schedule overruns*” [2].

NASA requires flight projects to demonstrate technology readiness level (TRL) 6<sup>\*</sup> by Preliminary Design Review (PDR) for all required technologies. However, this can only occur with a process in place to correctly identify and adequately fund development of relevant “blue sky” technologies to TRL 3<sup>†</sup>, and then mature them to TRL 5<sup>‡</sup> or 6, across the so-called “mid-TRL gap,” where sustained funding frequently falls short.

### What's in this Report? What's New?

This sixth Program Annual Technology Report (PATR) summarizes the Program's technology development activities for fiscal year (FY) 2016. It lists technology gaps identified by the PCOS community and two mission-concept studies with priorities assigned by the PCOS Technology Management Board (TMB; p. 20).

\* TRLs are fully described in NPR 7123.1B, Appendix E, with TRL definitions reproduced in Appendix A below; TRL 6 is defined as: “System/sub-system model or prototype demonstration in a relevant environment.”

† TRL 3 is defined as: “Analytical and experimental critical function and/or characteristic proof-of-concept.”

‡ TRL 5 is defined as: “Component and/or breadboard validation in relevant environment.”



Following this year's prioritization, the Program Office recommends NASA Astrophysics Division at HQ solicit and fund the maturation of the following technologies with the highest priority:

- Highly stable low-stray-light telescope;
- High-power, narrow-line-width laser sources;
- Low-mass, long-term-stability optical bench;
- Phase measurement system (PMS);
- Fast, low-noise, megapixel X-ray imaging arrays with moderate spectral resolution; and
- High-resolution, lightweight X-ray optics.

These recommendations represent technologies most critical for substantive near-term progress on strategic priorities and take into account ongoing discussions between NASA and the European Space Agency (ESA) about potential US contributions to the Advanced Telescope for High ENergy Astrophysics (Athena), recently selected for ESA's L2 slot planned to launch in 2028, and a yet-to-be-selected GW mission for ESA's L3, planned to launch in the mid-2030s. The latter were captured by recommendations from the NASA L3 Study Team (L3ST). Technology needs for X-ray missions such as Athena and an X-Ray Surveyor (XRS) are represented by gaps submitted by the XRS Science and Technology Definition Team (STDT). The XRS STDT, along with STDTs for a Large UV/Optical/IR (LUVOIR) Surveyor, a Far-IR Surveyor, and a Habitable Exoplanet (HabEx) imaging mission, were charged by the Astrophysics Division Director to develop the science case, technology assessment, design reference mission with strawman payload, and cost assessment. This is being done in preparation for the upcoming 2020 Decadal Survey. These Surveyors are three of five described in the Astrophysics Roadmap, "[Enduring Quests, Daring Visions](#)," released in December 2013, while HabEx was described in the NWNH.

The Astrophysics Division has awarded 22 PCOS SAT projects to date, funded by PCOS Supporting Research and Technology (SR&T), intended to develop telescopes, optics, detectors, electronics, micro-thruster subsystems, and laser subsystems, applicable to future strategic PCOS missions. Nine projects continue from previous years, each reporting significant progress, with several prepared for TRL advancement review. With four new projects begun in FY 2016, this PATR reports on the progress, current status, and planned activities for 13 projects funded in FY 2016. We thank the PIs of our ongoing projects for their informative progress reports (Appendix B – Quad Charts, p. 63; Appendix C – Development Status, p. 77). As of this writing, no new SATs have been awarded yet for 2017 start.

The following are examples where Program-funded technologies were infused, or are planned to be infused, into projects and missions:

- Advancements made to X-ray detectors and readout technologies are allowing meaningful NASA contributions to Athena;
- REgolith X-ray Imaging Spectrometer (REXIS), an MIT student instrument on the Origins-Spectral Interpretation-Resource Identification-Security-Regolith Explorer (OSIRIS-REx), incorporated Program-funded directly deposited X-ray blocking filter technology on its CCDs (launched September 8, 2016);
- Antenna-coupled transition-edge superconducting (TES) bolometer technology was deployed in the ground-based Background Imaging of Cosmic Extragalactic Polarization 2 (BICEP2) experiment to measure B-mode polarization, and performance-tested in a realistic environment on a long-duration balloon flight of the Suborbital Polarimeter for Inflation Dust and the Epoch of Reionization (Spider) during the 2014/15 Antarctic season; and
- High-efficiency 40-GHz feedhorn-coupled TES-based detector architecture being matured by another SAT project was deployed in the Cosmology Large Angular Scale Surveyor (CLASS) telescope in the Atacama Desert.

Additionally, SAT-funded advances in X-ray mirrors, high-stability lasers, low-scattered-light stable telescopes, micro-propulsion, and phase-measurement systems are allowing potential significant US contributions to ESA's Athena and L3 missions.

While infusion into ground-based and suborbital projects is not the goal of the SAT program, these are successes in that they support actual projects while proving technical performance on the path to infusion into space-based missions.



# 1. Program Science Overview

PCOS lies at the intersection of physics and astronomy. It uses the universe – the cosmic scale, the diversity of conditions, and the extreme objects and environments – as a laboratory to study the basic properties of nature. PCOS science addresses the fundamental physical laws and properties of the universe. The science objectives of the PCOS Program are to probe Einstein's General Theory of Relativity and the nature of space-time, better understand the behavior of matter and energy in the most extreme environments, expand our knowledge of dark energy and the accelerating universe, precisely measure the cosmological parameters governing the evolution of the universe, test the Inflation hypothesis of the Big Bang, and uncover the connection between galaxies and supermassive black holes.

The Program encompasses multiple missions aimed at meeting Program objectives, each with unique capabilities and goals. The Program was established to integrate those missions into a cohesive effort, enabling each project to build on the technological and scientific legacy of its contemporaries and predecessors. Each project operates independently to achieve its unique set of mission objectives, which contribute to overall Program objectives.

## Current Operating Missions

### *The Chandra X-ray Observatory*

The [Chandra X-ray Observatory](#), named the Advanced X-ray Astrophysics Facility (AXAF) until its launch, is a flagship mission and one of NASA's "Great Observatories." Chandra was launched and deployed by Space Shuttle Columbia on July 23, 1999. It is the most sophisticated X-ray observatory built to date and was specially designed to detect X-ray emission from very hot regions of the universe. Chandra's scientific impact has been enormous. Its discoveries include the first observation of an X-ray-emitting ring around the pulsar at the center of the Crab Nebula, the first X-ray emission seen from the super-massive black hole in the center of the Milky Way, and the first image of the compact object (neutron star or black hole) at the center of the Cassiopeia A supernova remnant.

### *The X-ray Multi-Mirror Mission-Newton (XMM-Newton)*

[XMM-Newton](#), named after physicist and astronomer Sir Isaac Newton, was launched on December 10, 1999, the second cornerstone mission of ESA's Horizon 2000 program. The observatory's science objectives include investigating interstellar X-ray sources, performing narrow- and broad-range spectroscopy, and the first simultaneous imaging of objects in both X-ray and optical (visible and UV) wavelengths. NASA funded elements of the instrument package and provided the Guest-Observer Facility (GOF) at Goddard Space Flight Center (GSFC). The GOF provides a clearinghouse for project-generated technical information and analysis software, as well as budget support for US astronomers who apply for observation time. XMM-Newton's scientific legacy includes the determination that the black hole at the center of the Milky Way woke up violently about 400 years ago, turning off about 100 years later; acquisition of the first large-scale map of the dark matter and baryon distributions in the universe; and construction of the largest catalog of cosmic X-ray-emitting objects.

### *The Fermi Gamma-ray Space Telescope*

The [Fermi Gamma-ray Space Telescope](#), formerly Gamma-ray Large-Area Space Telescope (GLAST), launched on June 11, 2008, bringing together the astrophysics and particle physics communities. Fermi is a NASA-led mission in collaboration with the Department of Energy, with contributions from France, Germany, Japan, Italy, and Sweden. Its science objectives are to explore the most extreme environments in the universe, search for signs of new laws of physics, explain how black holes accelerate relativistic jets, help understand the physics of gamma-ray bursts, and answer long-standing questions across a broad range of topics, including solar flares, pulsars, and the origin of cosmic rays. Fermi made numerous discoveries, including the first observation of gamma-ray emission from a pulsar (Vela), evidence that supernova remnants are acceleration sites for lower-energy cosmic rays, and the first detection of the two gamma-ray and X-ray "Fermi Bubbles" extending 25,000 light years above and below the center of the Milky Way.

### ***LISA Pathfinder (LPF)***

[LPF](#), launched on December 3, 2015, is a technology demonstration mission and the first PCOS mission to launch since the Program was created in 2009. The LPF launch, coupled with the momentous direct detection of GWs by the LIGO collaboration, made 2015 a watershed year for GW astrophysics. LPF is intended to validate a number of key technologies for space-based GW observatories, including inertial reference sensors, ultra-low-noise drag-free flight, and micro-Newton thrusters, retiring technical risks for a LISA-like mission. LPF contains two payloads, the European LISA Technology Package (LTP) and NASA's Space Technology 7 (ST-7) experiment, the latter managed by JPL. Science operations at the Earth-Sun L1 Lagrange point began on March 1, 2016. Results from the European phase of the mission were announced on June 7, 2016 and published in Physical Review Letters [3]. LTP's measured acceleration noise performance far exceeds its requirement and approaches that of a full-scale observatory such as LISA. This represents a major step toward realizing a LISA-like observatory. The transition to ST-7 operations began in the first week of July 2016. NASA participation in an extended mission of 7–8 months has been formally approved by NASA HQ Astrophysics Division Director Paul Hertz. The purpose of the extended mission is to gain a deeper understanding of instrument performance by undertaking experiments deemed too risky for prime-mission operation.

### **Mission in Development**

[Euclid](#) is the sole mission currently in development addressing the PCOS science. Euclid is a dark-energy survey mission, led by ESA. The NASA portion of Euclid is a PCOS project managed by JPL. Scheduled for a 2020 launch, Euclid will perform a six-year photometric and spectroscopic survey of about a third of the sky. Euclid's scientific objectives, to improve our understanding of dark energy, gravity, and dark matter, are aligned with PCOS objectives. NASA will provide detectors and associated cryogenic electronics for one of Euclid's two instruments, the Near Infrared Spectrometer and Photometer (NISF).

### **Planning for Future Missions**

The PCOS portfolio currently focuses on technology studies in support of the priorities of the Astrophysics Division as outlined in the [Astrophysics Implementation Plan \(AIP\)](#), [updated in December 2014](#). The highly ranked NWNH priorities addressing PCOS science are:

- [LISA](#) – large mission category (currently incarnated as ESA's L3);
- [International X-ray Observatory \(IXO\)](#) – large mission category (study led to Athena and XRS concepts); and
- [Inflation Probe \(IP\)](#) – medium-size mission category.

The decadal committee ranked as the highest-priority large space mission the [Wide-Field Infrared Survey Telescope \(WFIRST\)](#). Managed by the Exoplanet Exploration Program (ExEP) Program Office at JPL, with the implementation project located at GSFC, WFIRST is envisioned and designed to settle fundamental questions about the nature of dark energy, to perform studies of exoplanets, and to provide a highly capable near-IR observatory for large-field surveys. Following ESA's announcement of themes for its large-class L2 and L3 launch opportunities, scheduled for 2028 and 2034, respectively, NASA is pursuing partnerships on the X-ray mission Athena for L2 and a future space-based GW observatory for L3 (details below). Since the AIP prioritized the IP lowest among the three, PCOS will not perform an IP mission study in the near future. However, PCOS and the Astrophysics Division continue to support related technologies through SAT and Astrophysics Research and Analysis (APRA) funding.

ESA's L2 theme is "The Hot and Energetic Universe." In July 2014, ESA formally announced its selection of the [Athena X-ray mission concept](#) for L2. Activities related to NASA-ESA collaboration on Athena continue. The year 2015 was quite busy with the first Athena Science Team meeting, the Athena Science Requirements Review and Mission Consolidation Review – all with NASA-funded US participation. The NASA contribution to Athena continues to center around the calorimeter array for the X-ray Integral Field Unit (X-IFU). Discussion is ongoing about NASA also providing part of the Wide Field Imager (WFI).



The L3 theme is the “The Gravitational Universe.” In November 2015, NASA [chartered](#) the L3ST to investigate how the US might contribute to the future ESA GW mission. An [interim report](#) was delivered to the NASA HQ Astrophysics Division Director on June 20, 2016 and the final Phase I report is due on September 30, 2016. NASA provided two representatives to ESA’s Gravitational Observatory Advisory Team (GOAT), which completed its work in March 2016. The purpose of the GOAT was to evaluate and recommend possible scientific and technical approaches for a GW observatory envisaged for a planned launch date in 2034. [The final GOAT report](#) was released in May 2016 with a number of findings, including that a LISA-type laser interferometer is the preferred mission architecture.

Looking further into the future, in October 2015, the PCOS Program Analysis Group (PhysPAG), the Cosmic Origins (COR) Program Analysis Group (COPAG), and Exoplanet Program Analysis Group (ExoPAG) submitted a [joint report to the Astrophysics Subcommittee](#); recommending which large-scale mission concept studies should be initiated. If realized, these candidate mission concepts, as identified by a [January 2015 white paper](#), written by the Director of the Astrophysics Division and in the Astrophysics Roadmap, would explore the nature of the universe from its earliest moments, in its most extreme conditions, and at the largest scales, as well as search for habitable planets beyond our solar system. The four candidate concepts are:

- [Far-IR Surveyor](#);
- [Habitable-Exoplanet Imaging Mission](#);
- [LUVOIR Surveyor](#); and
- [X-Ray Surveyor](#).

Note that all three Program Analysis Groups (PAGs) indicated in their report that they assume an L3 Gravitational-Universe mission study will occur concurrently with these flagship mission studies. They also concurred that the above list identifies the optimal set of large-mission concepts to study, make science cases, assess cost and technology needs, and formulate design reference missions to be considered and prioritized by the upcoming 2020 Decadal Survey. Following the joint PAG report, the Astrophysics Division [chartered](#) four STDs that will accomplish these tasks. For more information about each study team’s activities and progress, click on the relevant mission link above.

In the medium-scale category (i.e., Probe-class, total cost between approximately \$400M and \$1B), NASA solicited proposals to conduct concept studies for Astrophysics Probe missions. Following peer review, NASA will select a small number of proposals for detailed study. The results of the selected studies will also be provided as input to the 2020 Decadal Survey. The Program’s future technology development efforts will be guided by the outcome of the study of both the large-scale and Probe-class mission concepts.

## 2. Strategic Technology Development Process and Portfolio

The PCOS, COR, and ExEP Program Offices were set up by NASA HQ Science Mission Directorate (SMD) Astrophysics Division to manage all aspects of these focused astrophysics programs. The Program Offices shepherd critical technologies toward infusion into Program-relevant flight projects. The Offices follow Astrophysics Division guidance, and base their recommendations on science community input, ensuring the most relevant technologies are solicited and developed. The PCOS Program Office, located at GSFC, serves as HQ's implementation arm on PCOS Program-related matters. The Astrophysics Division achieves efficiency by having the same staff and physical facilities serve both the COR and PCOS Program Offices. The Astrophysics Division funds technology development at all TRLs. Early-stage development ( $\text{TRL} \leq 3$ ) and technologies related to non-strategic missions and suborbital projects are typically funded by APRA. Final maturation ( $\text{TRL} \geq 6$ ) is mission-specific and thus handled by flight missions. The SAT program, launched in 2009, funds maturation of technologies across the mid-TRL gap ( $3 \leq \text{TRL} < 6$ ).

### The PCOS Technology Development Process

The PCOS Program Office is charged to develop and administer a technology development and maturation program, moving innovative technologies across the mid-TRL gap to enable strategic PCOS missions. The Program Office facilitates, manages, and implements the technology policies of the Program. Our goal is to facilitate technology infusion into PCOS missions, including the crucial phase of transitioning nascent technologies into targeted projects' technology programs during mission formulation. PCOS SAT projects are funded by the PCOS SR&T budget. Our work is guided by the priorities set forth in the AIP, the Astrophysics Roadmap, and other strategic guidance from the NASA Astrophysics Division. The AIP describes the Astrophysics Division's planned implementation of space-based priority missions and activities identified in NWNH, updated due to more recent budgetary developments. The Roadmap strives to inspire and challenge the community to pursue the missions and technologies needed over the next three decades to address NWNH-identified science goals.

Our technology development process (Fig. 2-1) places the science community's inputs at the center of our efforts through the Decadal Survey process and ongoing identification of technology gaps. The community is encouraged to submit gaps at any time via the PhysPAG or directly through the PCOS Program website. The PhysPAG Executive Committee (EC) reviews gaps submitted before the annual June 1 cutoff date, consolidating, enhancing, and adding to them as needed to create a complete, accurate, and compelling set of gaps for TMB evaluation. The Program Office charges its TMB annually to evaluate and determine which of the submitted technology developments would meet Program objectives, and to prioritize them for further development consideration. The TMB ranks gaps based on Program objectives, strategic ranking of relevant science/missions, benefits and impacts, and urgency. The TMB, a Program-level functional group, thus provides a formal mechanism for input to, and review of, PCOS technology development activities.



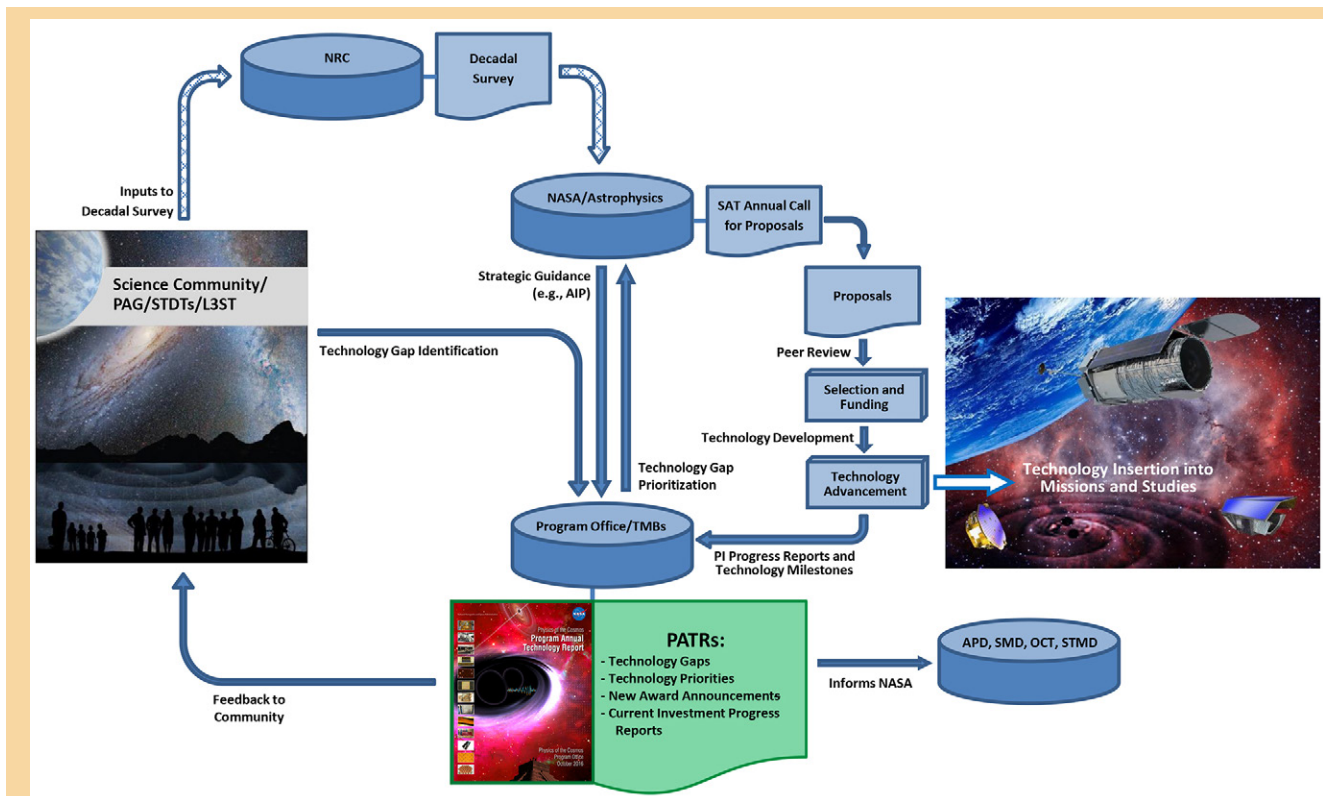


**Fig. 2-1.** The PCOS technology development process receives community input on technology gaps, recommends priorities, manages SAT-funded activities, and informs NASA and the science community about progress (NRC, National Research Council; PAG, Program Analysis Group; APD, Astrophysics Division; OCT, Office of the Chief Technologist; STMD, Space Technology Mission Directorate).

TMB priority recommendations inform Astrophysics Division decisions on what technologies to solicit in the upcoming annual SAT call for proposals, and help guide proposal selections. HQ's investment considerations are made within a broader context, with programmatic factors apparent at the time of selection affecting funding decisions. HQ evaluates submitted technology development proposals, considering overall scientific and technical merit, programmatic relevance, and cost reasonableness given the scope of work. Awardees work to mature their technologies from their initial TRL, normally 3 or 4<sup>§</sup>, through TRL 5. PIs report progress and plans to the Program Office periodically, and submit their technologies for TRL advancement review as appropriate. Progress in these projects allows infusion of newly mature technologies into NASA missions and studies, enabling and enhancing their capabilities with acceptable programmatic costs and risks.

As seen in Fig. 2-1, the PATR plays an important role in our process. Through PI reports and quad charts, it describes the status of all current investments in strategic PCOS technologies. It reports technology gaps articulated by the scientific community, and starting this year also by the large-mission-concept study teams, with a prioritized list of technologies for future solicitation and funding. The PATR is an open source for the public, academia, industry, and the government to learn about the status of enabling technologies required to fulfill PCOS science objectives. The report informs NASA organizations, including but not limited to the Astrophysics Division, and updates the community regarding technology development progress, as input for future technology gap submissions. Technological progress and programmatic decisions change the landscape of requirements for PCOS needs; therefore, the process is repeated annually to ensure continued relevance of priority ranking. Indeed, in any given year, new SAT award decisions are informed by PATRs published over the prior two years, a new SAT solicitation is informed by the prior-year PATR and the current year's TMB priority ranking, and the current PATR provides recommendations for next year's SAT.

§ TRL 4 is defined as: "Component and/or breadboard validation in laboratory environment."

This technology development and maturation process identifies existing and emerging needs in a transparent manner, improves the relevance of PCOS technology investments, provides the community a voice in the process, and promotes targeted external technology investments by defining needs and identifying NASA as a potential customer for innovative technologies. It also identifies providers of technologies and expertise, the Program PIs, to potential customers and collaborators within and beyond NASA. This encourages industry and other players to invest in enabling technologies for future missions, and promotes formation of productive collaborations. Beyond involvement in the Decadal Survey process and technology gap submission, the science and technical community is a key stakeholder in Program technology development activities. The community provides feedback and inputs to the technology development process; and participates in PhysPAG and other committees and workshops, ad-hoc studies, and in technology development by responding to SAT solicitations.

## **TRL Vetting**

SAT funding helps mature technologies expected to enable and/or significantly enhance future strategic astrophysics missions. These technologies typically enter the SAT program at TRLs 3 or 4, and are intended to progress toward higher TRLs. TRL assertions above a technology's approved entry level are not official until a TRL-vetting TMB concurs with the development team's assessment. When PIs believe their team has demonstrated the required progress, they may request a review to present their case for TRL update. The Program Office then convenes a TMB consisting of Program Office and HQ senior staff along with subject matter experts to assess the request and, when warranted, approve the new TRL. The typical forum for such a request is during the PI's end-of-year presentation to the Program Office, but it can be made at any time. Several projects in the PCOS portfolio have already gone through this process (see below), and the PIs of several more are planning to undergo TRL vetting this coming year.

### ***Why review TRLs?***

TRLs are used throughout the agency to help assess the maturity of technologies. The Program Office's charge includes a requirement that it monitor the progress of the Astrophysics Division's investments in technology maturation through SAT projects relative to the TRL plan and milestones submitted by the PI in the SAT proposal. A key indicator of such progress is TRL advancement as vetted by the Program Office, providing a consistent method of assessing progress across our full portfolio of projects.

### ***What does our vetting mean?***

When the Program's TMB approves a higher TRL asserted by the PI, it provides an independent assessment and verification that the project has achieved that TRL. The TMB consists of scientists, technologists, and systems engineers from the Program; and subject matter experts from the community and Aerospace Corporation; who provide an objective and informed assessment. The primary purpose for issuing this assessment is to inform the Program Office of significant progress in preparing the technology for possible infusion into strategic missions. It also informs the community of an improved state of readiness.

### ***What is expected?***

The TRL vetting process is initiated when a PI notifies the Program Office that the milestones necessary for TRL advancement have been met. The PI team prepares a brief but compelling presentation that makes the case for the higher TRL, and the PI presents it to the TRL-vetting TMB which considers the TRL assertion. The TMB is guided by TRL definitions in [NASA Systems Engineering Processes and Requirements](#), also known as NASA Procedural Requirement (NPR) 7123.1B. Recognizing that PI teams are busy and must concentrate their efforts on the work of maturing their technology, the Program Office is satisfied to rely on a cogent exposition of the same reports, graphs, and test results the team captures for its own records.

The Program Office has tools to help PIs assess their progress and is available to provide information on the TRL process. Finally, if the project is still ongoing, we recommend the PI present a plan for further TRL advances, if any, allowing the TMB to offer feedback and make recommendations.



***What are the benefits for the PI and the Program?***

The Program Office's TRL-vetting process serves as an opportunity to capture and collect the needed documentary evidence and present it to a group of independent experts. This can strengthen a potential future TRL case presentation, whether in person or in writing, to flight projects, proposal teams considering adding the technology to their mission, and/or proposal reviewers. Another leveraging opportunity might be in collaboration opportunities. As alluded to above, the TMB can help the PI team fine-tune its plan for future work to achieve the claimed TRL if the current claim was not vetted, or for the next TRL if it was.

Finally, TRLs are NASA's technology-development-assessment language, and TRL advancement is one of the key success criteria for SAT projects. Our TRL vetting is an objective process, rendering an independent verification of achievement, increasing the credibility of the technology's maturity and its potential for continued funding, infusion into flight missions, and consideration by community assessments such as STDT studies and Decadal Surveys.

**The PCOS Technology Development Portfolio as of 2016**

For FY 2016, the driving objective is to maintain progress in key enabling technologies for possible contributions to ESA L-class missions, such as Athena and the L3 GW mission, a future US-led XRS, and a Cosmic Microwave Background (CMB) polarimetry mission.

Twenty-two PCOS SAT grants have been awarded to date. Table 2-1 provides top-level information on the 13 projects that received funding in FY 2016, including where each is described in detail in the appendices. Appendix B provides one-page "quad chart" project summaries, while Appendix C provides in-depth reports detailing development status, progress over the past year, and planned near-term development activities. The appendices provide technology overviews and status, not flight implementation details. For additional information, please contact the PCOS Program Office or the PIs directly. Contact information for each PI appears at the end of his or her report.

When possible, PCOS has leveraged its limited funding by joining with other programs, e.g. the Game-Changing Development Program of NASA's STMD, to co-fund projects that meet both programs' technology goals. Such collaborative investments are "win-win-win" opportunities for the Astrophysics Division, STMD, and the PI. The PCOS Program looks forward to continued relationship with STMD, creating more such opportunities in the future.

Similarly, the PCOS Program Office manages one project that has transitioned from SAT to directed funding. Another SAT project, developing 0.5-arcsec adjustable X-ray optics, follows up on a related project led by the same PI and co-funded by the APRA program and STMD. Since the two are so closely related, the quad chart and PI report in Appendices B and C, respectively, describe progress in both.

**Strategic Astrophysics Technology Selection for FY 2017 Start**

The PCOS Program funds SAT projects to advance the maturation of key technologies to make feasible their implementation in future space-flight missions. The Program focuses on advancing those technologies most critical for substantive near-term progress on strategic priorities. As of this writing, the selection of 2017-start SAT projects has yet to be announced.

Technology Development Title	PI	Institution	Start Year; Duration	Current TRL	Quad Chart & Status Report Page Locations
Demonstration of a TRL-5 Laser System for eLISA	Jordan Camp	GSFC	FY14; 2 yrs	3	64, 78
Phase Measurement System Development for Interferometric Gravitational-Wave Detectors	William Klipstein	JPL	FY14; 3 yrs	4	65, 86
Telescope Dimensional Stability Study for a Space-Based Gravitational-Wave Mission	Jeffrey Livas	GSFC	FY16; 2 yrs	3	66, 92
Directly Deposited Blocking Filters for Imaging X-ray Detectors	Mark Bautz	MIT	FY12; 4 yrs	5	67, 102
Fast Event Recognition for the Athena Wide-Field Imager	David Burrows	PSU	FY15; 2 yrs	3	68, 115
Providing Enabling and Enhancing Technologies for a Demonstration Model of the Athena X-IFU (directed funding)	Caroline Kilbourne	GSFC	FY16; 2 yrs	4	69, 120
Reflection Grating Modules: Alignment and Testing	Randall McEntaffer	PSU	FY15; 2 yrs	4	70, 129
Development of 0.5 Arcsecond Adjustable Grazing-Incidence X-ray Mirrors for the SMART-X Mission Concept	Paul Reid	SAO	FY15; 3 yrs	3	71, 137
Advanced Packaging for Critical-Angle X-ray Transmission Gratings	Mark Schattenburg	MIT	FY15; 2 yrs	4	72, 148
Technology Development for an AC-Multiplexed Calorimeter for Athena	Joel Ullom	NIST	FY15; 2 yrs	3	73, 154
Affordable and Light-Weight High-Resolution Astronomical X-ray Optics	William Zhang	GSFC	FY15; 2 yrs	5	74, 160
Superconducting Antenna-Coupled Detectors and Readouts for Space-Borne CMB Polarimetry	James Bock	Caltech/JPL	FY16; 2 yrs	3-6	75, 166
High-Efficiency, Feedhorn-Coupled, TES-Based Detectors for CMB Polarization Measurement	Edward Wollack	GSFC	FY16, 2 yrs	3	76, 175

**Table 2-1.** PCOS Technology Development Portfolio as of FY 2016 (organized by science topic and PI name). Project durations include approved no-cost extensions.

## Large-Mission-Concept Studies toward the 2020 Decadal Survey

As mentioned in Section 1, this year the Astrophysics Division set up STDs to study four large-mission concepts – Far-IR Surveyor, HabEx Imaging Mission, LUVOIR Surveyor, and XRS. The STDs are each charged to develop the science case and design reference mission, assess technology development needs, and estimate the cost of their mission concept. These studies will guide our efforts to mature technology components and architectures required to offer four equally compelling cases for the 2020 Decadal Survey’s consideration. Similarly, the L3ST was chartered to help us understand how NASA might participate in ESA’s L3 GW mission, inform our engagement through L3’s earliest stages, and prepare for the 2020 Decadal Survey.

Each of these ambitious mission concepts promises breakthrough science results, but implementing them will require us to overcome daunting technology development challenges. The SAT program is certain to play a major role in funding these technology development efforts. We encourage all members of the community to support our efforts to identify the highest-priority technology gaps we need to close to make these missions feasible, and continue to submit proposals in response to SAT solicitations. As of this writing, notices of intent to submit for the next SAT round are due January 20, 2017, with proposals due March 17, 2017.

As described in Section 3, starting this year, the XRS STDT and the L3ST provide their own technology gap lists to the PCOS Program Office. The Program Office combines these lists with the one consolidated by the PhysPAG EC, and submits the resulting list to the TMB for prioritization.

## Historical Record of TPCOS Proposals and Awards

The Technology development for Physics of the Cosmos (TPCOS) section of the SAT program (Table 2-2) received 21 proposals in response to the 2010 solicitation, its first year; 26 for 2011; 10 for 2012; eight for 2013; six for 2014, and nine for 2015. Of the first set, five proposals were selected, with five more the following year, three in the third year, six in year four, and three last year. As stated above, 2017-start SATs have yet to be selected. This makes the historical selection rate for PCOS SAT proposals 31%, excluding 2015, with the three most recent selection rounds hitting 30%, 75%, and 50%, respectively.

Solicitation Year	TPCOS Proposals		Proposal Success Ratio
	Submitted	Awarded	
2010	21	5	24%
2011	26	5	19%
2012	10	3	30%
2013	8	6	75%
2014	6	3	50%
2015	9	TBA	TBD
Total to Date	80	TBD	TBD

**Table 2-2.** Numbers of TPCOS SAT Proposals and Awards. The number of 2015 SAT proposals selected has yet to be announced (TBA), and thus the proposal success ratio for that cycle is to be determined (TBD).



### 3. Technology Gaps, Priorities, and Recommendations

Enabling strategic astrophysics missions that are decades away requires identifying and closing gaps between state-of-the-art (SOTA) performance and that required for those missions. As current technologies develop and mature and as our understanding of the missions' concept designs mature, those gaps evolve.

As shown in Fig. 2-1, we solicit technology gaps from the community on an ongoing basis. Anyone may submit a technology gap directly to the Program Office, [downloading a form](#) from the PCOS website, or through the PhysPAG. Gaps may be submitted throughout the year, however, since gaps are assessed and prioritized annually in late July, the Program Office set a June 1 cutoff date for consideration in the same year. This allows the PhysPAG EC to review the list of gaps for completeness, merge overlapping gaps, and complete and improve entries where the submission did not adequately address the requested information. Then, the EC returns the list to the Program Office for final preparation for the TMB's assessment.

To maximize the likelihood of high priority ranking, the Program Office encourages submitters to include as much of the information requested as possible. Importantly, we ask submitters to describe a capability gap, not a specific implementation process or methodology. The goals and objectives should be clear and quantified. Additionally, a complete description of the needed capability with specific performance goals based on mission needs is very valuable. Such information serves several important purposes:

1. The TMB is best able to understand and thus correctly assess the identified technology gap.
2. NASA HQ is best able to develop accurate technology development proposal calls.
3. The community is clearly informed and best able to match candidate technologies to mission needs.

Aside from submitter information, the technology gap form requests the following information:

- **Technology gap name:** Identifies the gap, and optimally the type of mission filling it would enable;
- **Brief description:** Summarizes the technology gap and associated key performance criteria; in general, well-defined technology gaps receive higher priority than vague ones;
- **Assessment of current SOTA and TRL:** Describes the SOTA, allowing the TMB to appreciate the gap between what's available and what's needed; **SOTA TRL** specifies the current TRL per NPR 7123.1B Appendix E of relevant SOTA technology; and **Full-Solution TRL** specifies the current TRL of candidate technologies that could provide a full solution; the SAT program funds projects to advance technologies from TRL 3 up through TRL 5, so those with full solutions already at TRL 6 rank lower unless the existing technology is significantly deficient in some way (e.g., cost, complexity, yield, etc.); note that full-solution TRL can never exceed the SOTA TRL, else this full-solution technology would be the SOTA;
- **Target goals and objectives:** Details the quantifiable goals and/or objectives for a candidate technology to fill the described gap. For example, "*The goal is to produce a detector with a sensitivity of X over a wavelength of Y to Z nm;*" Technology gaps with clearly quantified objectives may receive higher priority than those without quantified objectives;
- **Scientific, engineering, and/or programmatic benefits:** Describes the benefits of closing the technology gap; for enabling technology, this describes how and why it is such; for an enhancing technology, it describes, and if possible quantifies, the impact; benefits could be better science, lower resource requirements (e.g., mass, power, etc.), and/or programmatic (e.g., reduced risk, cost, or schedule); for example, "*Material X is 50% stronger than the current state of the art and will enable the optical subsystem for a 2-m telescope to be Y kg lighter;*" technology gaps with greater potential mission benefits receive higher scores;

- **Application and potential relevant missions:** Technologies enabling or enhancing missions ranked highly by the AIP, Astrophysics Roadmap, or NWNH, will score higher; technologies applicable to a wide range of PCOS missions, as well as COR and/or ExEP missions will rank better; and
- **Time to Anticipated Need:** Specifies when the strategic mission enabled or enhanced by the technology is planned to launch; in cases where there is a more immediate driving need (e.g., ESA requirements for achieving TRL 5 or 6 by a certain date to be considered for inclusion in a mission considered strategic by NASA Astrophysics Division), this driving requirement is also considered; technology gaps with shorter time windows relative to required development times receive higher priority.

## Technology Gaps Submitted to the 2016 TMB

As in 2015, the PhysPAG EC agreed to review the list of technology gaps compiled by the Program Office. The Program Office forwarded to the EC 22 gaps from the 2015 TMB list plus 17 new community entries, some of which simply suggested edits to 2015 gaps. We thank the community for their engagement in this process and for their thoughtful gap submissions. The EC consolidated gaps with significant overlap, improved some wording to make them more compelling, added entries if and where appropriate, and recommended removing entries that were not technologies, were too incomplete, or were outside the charge of the SAT program. The EC returned to the Program Office a list of 24 gaps. In parallel, the L3ST submitted seven gaps to the Program Office, while the XRS STDT submitted four gaps “vital” for X-ray science, where optics development “*should be the primary focus.*” Five of the seven L3ST gaps were revisions of 2015 gaps, with the remaining two split from a single 2015 gap. Of the four XRS STDT gaps, three were revisions of 2015 gaps, and one was a new entry. To facilitate and streamline the TMB prioritization process, a subset of the full TMB consolidated the 35 entries into 25 distinct gaps. Almost all technologies developed to close these gaps would enable and/or enhance high-priority strategic missions per the AIP, the Astrophysics Roadmap, and/or NWNH. We deeply appreciate the efforts of the EC, L3ST, and XRS STDT, and look forward to continued collaboration in the future. Having the EC and study teams review gap entries and propose new ones where appropriate, prior to TMB prioritization, serves several important purposes:

- Providing a set of expert-vetted, unique, and compelling technology gaps, such that the resulting entries potentially merit higher priority ranking;
- Ensuring the gaps accurately reflect the current situation per the community and study teams; and
- Making the process of generating unique technology gaps more transparent to the community.

## Prioritizing Technology Gaps

In its prioritization meeting, the TMB followed an agreed-upon set of evaluation criteria, resulting in the priorities shown below. TMB membership included senior staff from NASA HQ Astrophysics Division, the Program Office, STMD, and the Aerospace Corporation. For 2016, the TMB used a prioritization approach similar to that used in prior years, with a streamlined set of four criteria. These included strategic alignment, benefits and impacts, scope of applicability, and urgency.

- **Strategic alignment:** How well does the technology align with PCOS science and programmatic priorities of current programmatic guidance (i.e., AIP, Roadmap, and NWNH)?
- **Benefits and impacts:** How much impact does the technology have on PCOS-relevant science in applicable mission(s)? To what degree does the technology enable and/or enhance achievable science objectives, reduce cost, and/or reduce mission risks?
- **Scope of applicability:** How cross-cutting is the technology? How many Astrophysics programs and/or mission concepts could it benefit?
- **Urgency:** When are launches and/or other schedule drivers of missions enhanced or enabled by this technology anticipated?

The TMB assigned weighting factors, reflecting the relative importance of each criterion. Each gap received a score of 0 to 4 for each criterion. The scores were multiplied by their respective weights, and the products were summed. Technologies that could be scored based on several missions or mission classes were scored for each scenario independently, assigning the highest overall score (e.g., if a gap could receive an overall score of 91 for one mission and 75 for another, it would be assigned the higher score). Table 3-1 details the criteria descriptions, weighting factors, and TMB scoring guidelines.

Criterion	Weight	Max Score	Max Weighted Score	General Description/ Question	4	3	2	1	0
<b>Strategic Alignment</b>	10	4	40	How well does the technology align with PCOS science and programmatic priorities of current programmatic guidance (i.e., AIP, Roadmap, and NWNH)?	Technology enables PCOS-relevant science within mission concept receiving highest programmatic consideration or recommended by STDT or L3ST	Technology enables PCOS-relevant science within mission concept receiving mid to high programmatic consideration in AIP or in Roadmap as “Surveyor” but not being studied	Technology enables PCOS-relevant science within mission concept receiving low current programmatic consideration in AIP or Roadmap	Technology enables PCOS-relevant science within mission concept not considered in AIP or Roadmap, but positively addressed in NWNH	Technology does not enable PCOS-relevant science within any mission concept considered by current programmatic guidance
<b>Benefits and Impacts</b>	8	4	32	How much impact does the technology have on PCOS-relevant science in applicable mission(s)? To what degree does the technology enable and/or enhance achievable science objectives, reduce cost, and/or reduce mission risks?	Critical and key enabling technology; required to meet PCOS-science-relevant mission concept objectives; without this technology, mission would not launch or PCOS science return would be significantly impaired	Highly desirable; not mission-critical to PCOS-science-relevant objectives, but significantly enhances PCOS science capability, reduces critical resources needed, and/or reduces mission risks; without it, missions may launch, but PCOS science return would be compromised	Desirable; not required for PCOS-science-relevant mission success, but offers significant PCOS-relevant science or implementation benefits; if technology is available, would almost certainly be implemented in missions for PCOS purposes	Minor PCOS-relevant science impact or implementation improvements; if technology is available would be considered for implementation in missions for PCOS purposes	No PCOS-relevant science impact or implementation improvement; even if available, technology would not be implemented in missions for PCOS purposes
<b>Scope of Applicability</b>	3	4	12	How cross-cutting is the technology? How many Astrophysics programs and/or mission concepts could it benefit?	Applies widely to PCOS mission concepts and both COR and exoplanet mission concepts	Applies widely to PCOS mission concepts and either COR or exoplanet mission concepts	Applies widely to PCOS mission concepts	Applies to a single PCOS mission concept	No known applicable PCOS mission concept
<b>Urgency</b>	4	4	16	When are launches and/or other schedule drivers of missions enhanced or enabled by this technology anticipated?	Launch anticipated in next 5-9 years (2021-2025) or other schedule driver requires progress in 3-4 years (2019-2020)	Launch anticipated in next 10-14 years (2026-2030) or other schedule driver requires progress in 5-9 years (2021-2025)	Launch anticipated in next 15-19 years (2031-2035)	Launch anticipated in next 20-24 years (2036-2040)	Launch anticipated in 25 or more years (2041 or later)

**Table 3-1.** Clear, strategic criteria provide a rigorous, transparent process for prioritizing technology gaps.



This process provides a rigorous and transparent ranking of technology gaps based on the Program's goals, community scientific rankings of relevant missions, Astrophysics Division priorities as outlined in the AIP and Astrophysics Roadmap, and the external programmatic environment. Since the SAT program is intended to promote development and maturation of technologies relevant to missions and concepts identified as strategic, the strategic alignment criterion is driven by strategic documents such as the AIP, the Astrophysics Roadmap, and the NWNH. The AIP details highly ranked science missions and technology development, which for PCOS include dark energy, GWs, X-ray astronomy, and Cosmic Inflation; and prioritizes those based on current budget realities. This year, the TMB considered technologies identified by the XRS STDT and the L3ST as having the highest possible strategic alignment. The CMB Polarization Surveyor mentioned in the Astrophysics Roadmap was also given points for strategic alignment.

## Prioritization Results

As mentioned above, in 2016, the PCOS TMB received and scored 25 technology gap entries. Reviewing the scores, the TMB binned the technology gaps into three groups based on a number of factors, including primarily a natural grouping of overall scores.

**Priority 1:** Technologies the TMB determined to be of the highest interest to the PCOS Program. Advancing these key enabling technologies is judged to be most critical to making substantive near-term PCOS-science-relevant progress on the highest-priority strategic astrophysics missions, including the XRS and GW missions such as participation in ESA's L3 mission. The TMB recommends SAT calls and award decisions address these technology gaps first.

**Priority 2:** Typically, technologies the TMB believes would be highly desirable or desirable for a variety of strategic missions. The TMB recommends that should sufficient funding be available, SAT calls and award decisions address closing these technology gaps as well.

**Priority 3:** Technologies the TMB deemed supportive of PCOS objectives, but scoring lower than Priority 1 and 2 technology gaps.

Table 3-2 lists the gaps prioritized by the TMB, including 2016 assigned priorities, gap names, science topics addressed, gap submission sources, and where in Appendix A you can find detailed gap entries.

From 2011 through 2016, nearly all gaps achieving Priority 1 maintained that rank or changed by one level due to minor shifts in how priority scores break up naturally into groups. Also, funded projects have addressed high-priority gaps, mostly Priority 1, and occasionally Priority 2. For example, four of the six 2016 Priority 1 gaps have already been addressed by SAT projects, as have four of the eight Priority 2 gaps.

2016 Priority	Technology Gap Name	Science Addressed	Submitted By	Gap Detail Page Location
Priority 1	Highly stable low-stray-light telescope	GW	L3ST and General Community	46
	High-power, narrow-line-width laser sources	GW	L3ST and General Community	44
	Low-mass, long-term-stability optical bench	GW	L3ST and General Community	48
	Phase measurement system (PMS)	GW	L3ST and General Community	49
	Fast, low-noise, megapixel X-ray imaging arrays with moderate spectral resolution	X Ray	XRS STDT and General Community	29
	High-resolution, lightweight X-ray optics	X Ray	XRS STDT and General Community	35
Priority 2	Precision Microthrusters	GW	L3ST	53
	Non-contact charge control for Gravitational Reference Sensors (GRS)	GW	L3ST and General Community	51
	Advanced millimeter-wave focal plane arrays for CMB polarimetry	IP	General Community	41
	Millimeter-wave optical elements	IP	General Community	43
	Large-format, high-spectral-resolution, small-pixel X-ray focal plane arrays	X Ray	XRS STDT and General Community	30
	High-efficiency X-ray grating arrays for high-resolution spectroscopy	X Ray	XRS STDT	34
	Rapid readout electronics for X-ray detectors	X Ray	General Community	33
	High-efficiency cooling systems for temperatures covering the range 20 K to below 1 K	X Ray, IP	General Community	62
Priority 3	High-performance gamma-ray telescope	Gamma Ray	General Community	55
	Gravitational reference sensor (GRS)	GW	L3ST and General Community	52
	Lattice optical clock for Solar Time Delay (STD) mission and other applications	STD	General Community	60
	Fast, few-photon UV detectors	UHECR	General Community	56
	Lightweight, large-area reflective optics	UHECR	General Community	57
	Low-power time-sampling readout	UHECR	General Community	58
	Low-power comparators and logic arrays	UHECR	General Community	59
	Low-stress or stress-free coating for X-ray optics	X Ray	General Community	36
	Ultra-high-resolution focusing X-ray observatory telescope	X Ray	General Community	37
	Very-wide-field focusing instrument for time-domain X-ray astronomy	X Ray	General Community	39
	Advancement of X-ray polarimeter sensitivity using negative ion gas	X Ray	General Community	32

**Table 3-2.** Summary of 2016 PCOS technology gaps and their TMB-assigned priorities. Gaps shown by priority tier and science theme. All gaps within a specific tier have equal priority.

The Program Office continues to solicit and compile technology gap submissions from the community, and as was done this year, will maintain its collaboration with the EC and study teams to ensure the gaps ranked by the TMB continue to be complete, distinct, and compelling. As mentioned above, the next cutoff date for community gap submissions is June 1, 2017. Notices of intent to submit SAT proposals are due January 20, 2017, with proposals due March 17, 2017.

## 4. Benefits and Successes Enabled by the PCOS SAT Program

The main benefit of the SAT program is in maturing technologies across the mid-TRL gap, so they can be infused into strategic PCOS missions and/or international collaborative missions relevant to Program goals, as part of a US contribution. Table 4-1 lists technologies vetted by a Program Office TMB as having advanced in TRL. All SAT projects have made significant progress in maturing their technologies, with at least two asserting TRL advances that have yet to be vetted by a TMB.

Technology Development Title	PI	Vetting Date	Initial TRL	Vetted TRL
Advanced Packaging for Critical-Angle X-ray Transmission Gratings	Mark Schattenburg	5/17/2016	3	4
Reflection Grating Modules: Alignment and Testing	Randall McEntaffer	6/14/2016	3	4

**Table 4-1.** SAT projects with vetted TRL advances.

Where appropriate, newly matured technologies may also be implemented in ground-based projects, suborbital experiments, Explorers, and Probe-class missions. These often extend beyond the PCOS Program to COR, ExEP, and even beyond missions managed by Astrophysics Division.

The following are examples of TPCOS SAT project developments contributing to missions and projects:

- TES micro-calorimeter is expected to be a major US contribution to the ESA [Athena](#) mission's X-IFU (PI, Caroline Kilbourne);
- Continued development of time-division Superconducting QUantum Interference Device (SQUID) multiplexing supported by SAT funding is viewed as a backup to [Athena X-IFU's](#) baseline readout, which is currently at a lower TRL (PI, Joel Ullom);
- An SAT project is maturing a Field-Programmable-Gate-Array (FPGA) -based fast X-ray event recognition that NASA Astrophysics selected for work on a US contribution for [Athena's Wide-Field Imager](#) (PI, David Burrows);
- Phasemeter technology funded by the PCOS SAT program, including phase locking and laser stabilization, was infused into the Laser-Ranging Interferometer (LRI) on the [Gravity Recovery and Climate Experiment \(GRACE\) Follow-On mission](#). Advances from this LRI work were then leveraged by the PI back into his SAT project (PI, William Klipstein);
- Antenna-coupled TES bolometer technology developed with SAT support was deployed in the [BICEP2](#) experiment in Antarctica, helping search for B-mode polarization in the CMB signal; this provided an order-of-magnitude increase in measurement speed compared to the BICEP1 experiment; detector-array technology from this SAT project was then incorporated into [BICEP3](#) and Keck Array, and flown on the [Spider](#) long-duration balloon mission during the 2014/15 Antarctic season, measuring CMB polarization at 90 and 150 GHz with excellent low-frequency stability and low cosmic-ray event rates (PI, James Bock);
- Directly deposited optical blocking filters developed by another SAT project were incorporated into flight CCDs of [REXIS](#), an MIT student instrument on the [OSIRIS-REx](#) mission (launched Sep. 8, 2016); this filter technology meets the experiment's stringent performance requirements without straining its technical budgets; as a bonus, this provides the SAT project a nearly free opportunity to space-qualify its development, with environmental testing leading to the discovery and subsequent resolution of unexpected light leaks (PI, Mark Bautz);



- High-efficiency 40-GHz feedhorn-coupled TES-based detector architecture being matured by another SAT project was deployed in the [CLASS](#) telescope in the Atacama Desert (PI, Edward Wollack); and
- SAT team member, R.S. Shiri, has applied for a patent (GSC-17289-1, “Design and fabrication of partially transparent petaled mask or occulter using grayscale lithography,” filed May 23, 2016), which may one day be used for flight missions (PI, Jeffrey Livas).

As mentioned above, SAT-funded advances in X-ray mirrors, high-stability lasers, micro-propulsion, and low-scattered-light stable telescopes also allow potential significant US contributions to ESA’s Athena and L3 missions.

As in prior years, the Program Office surveyed current PIs about additional benefits resulting from their SAT funding. Of the 13 PIs represented in this PATR, 10 provided information about collateral benefits. Of these, five reported they were able to leverage SAT funding to generate matching internal research and development funding (e.g., GSFC IRAD funding); fellowships (e.g., Smithsonian Astrophysical Observatory, SAO, internal funding including two Leon Van Speybroeck, LVS, Fellowships in X-ray Optics; an NRC fellowship; a National Science Foundation, NSF, post-doctoral fellowship; and university funding for undergraduate research); cost sharing with a flight project; and/or funded parallel efforts on related projects (e.g., APRA). Six PIs responding report having hired students and/or post-doctoral fellows to assist their technology development work (slightly more on average than one undergraduate student, one graduate student, and one post-doctoral fellow per project), helping train the next generation of researchers and technologists needed to support future missions (Fig. 4-1). One student converted to a full-time research position at his organization, another was accepted to a graduate program, and several received their PhDs; proving that the SAT Program is helping train and shape the future astrophysics work force. Several PIs went on to successfully propose additional technology development projects through both the SAT and APRA programs.

## Involving Students and Postdocs in SAT Projects

The PCOS SAT projects have involved dozens of students and postdocs, helping train the future astrophysics workforce. As can be seen in the following quotes, the Program is making a deep impact on these future technologists, and through them promotes astrophysics missions over many decades to come.

*"I feel well-prepared to lead efforts in optical design, modeling and simulation, and experiment design and implementation."*

*"Immersed in an environment of frequent discussion, compelling ideas, and passionate problem-solving, I had the opportunity to constantly inquire and learn."*

*"By graduation, I will be prepared to serve as a PI for future missions and a contributor to the fields of space technology and astrophysics."*

*"The SAT project enabled me to gain understanding of the systems-level engineering challenges further up the optical path."*

*"I've gained valuable microfabrication knowledge and skills that I know will serve me well in future efforts to ready new technology for broader use."*

**Fig. 4-1.** SAT projects hire many students and post-doctoral fellows, helping train the future astrophysics workforce.



**Fig. 4-2.** Poster presented at the June 2016 SPIE meeting in Edinburgh, Scotland. The Program promotes exposure of current technology developments and investment priorities at national and international meetings, and informs the community of upcoming SAT funding opportunities.



**Fig. 4-2.** Poster presented at the June 2016 SPIE meeting in Edinburgh, Scotland. The Program promotes exposure of current technology developments and investment priorities at national and international meetings, and informs the community of upcoming SAT funding opportunities.



## The Broad Impacts of the SAT Program

Figure 4-3 depicts the geographic breadth of SAT program (both COR and PCOS) impacts, showing the locations of our PI institutions, their collaborators and partners, and the universities and colleges where the students and post-doctoral fellows involved in SAT projects attend school and work.

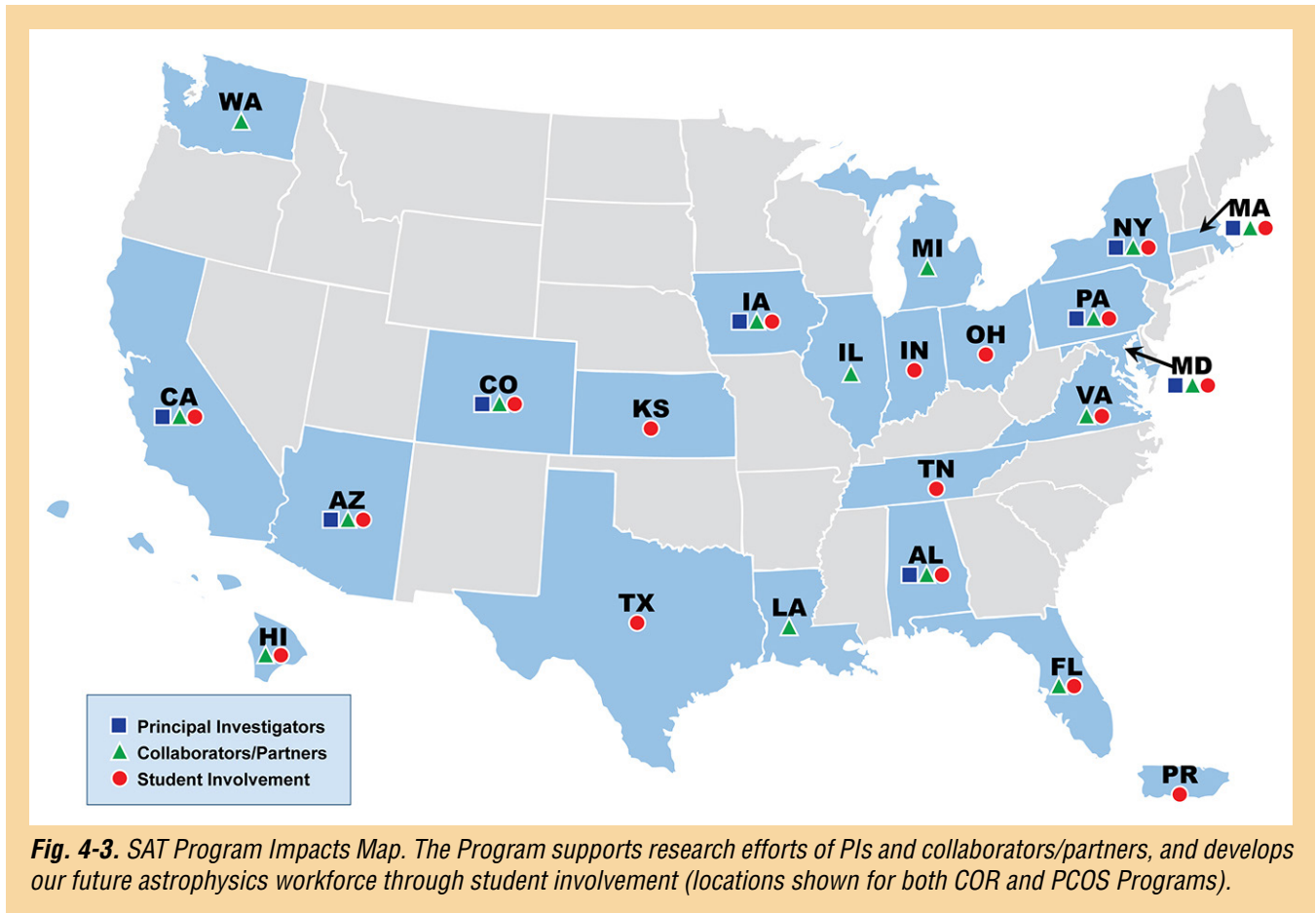


**Fig. 4-3.** SAT Program Impacts Map. The Program supports research efforts of PIs and collaborators/partners, and develops our future astrophysics workforce through student involvement (locations shown for both COR and PCOS Programs).

## 5. Closing Remarks

This 2016 PCOS PATR serves as a snapshot of the dynamic state of technology development managed by the Program Office and provides future directions for technology planning and maturation. As we complete another year of PCOS technology development activities, we see many positive developments.

Our technology development portfolio is growing, and continues to deliver significant advancements. All funded technologies are maturing toward higher TRLs, with several providing direct benefit to ground-based experiments and flight missions. PCOS SAT investments are also generating benefits beyond direct advancement of strategic technologies. This includes leveraging internal and external (including non-NASA) funding; using contributed materials, parts, and facility/equipment; hiring students and post-docs, thereby training our future astrophysics workforce; and generating research collaborations and industry partnerships, in support of PCOS science goals.

Our technology gap prioritization process continues to adhere to strategic guidance based on the AIP; Astrophysics Roadmap “Surveyor” concepts, especially those being studied by STDs and the L3ST; and NWNH; with the TMB assigning the most significant weight in technology gap prioritization to strategic alignment. As a result, the Astrophysics Division is likely to continue to fund SAT proposals addressing technology gaps identified by the TMB as having the highest priority. The latest set of highest-priority TMB recommendations, submitted to the Astrophysics Division and reported here, include technology developments related to GW missions, as well as X-ray focal plane arrays and optics.

To support the ever-evolving technology needs of the PCOS community, we continue to interact with the broad scientific and technical communities through the PhysPAG, through various workshops, via public outreach activities, and at public scientific conferences. These activities identify and incorporate the astrophysics community’s ideas about new science, current technology progress, and new needs for technology in an open and proven process. Each year, we incorporate new lessons learned and make appropriate improvements to our process. In parallel, we incorporate the technology needs identified by the large-mission-concept study teams into our technology gaps identification and prioritization process.

We would like to thank the PCOS scientific and technical communities, the PIs and their teams, the PhysPAG EC, and the large-mission-concept study teams for their efforts and inputs that make this annual report current and meaningful. We welcome continued feedback and inputs from the community in developing next year’s PATR, which should be sent to the [Program Office Technology Development Manager](#). For more information about the PCOS Program and its activities, please visit the [PCOS website](#).

## References

- [1] J. Mankins, “*The critical role of advanced technology investments in preventing spaceflight program cost overrun*”, The Space Review, December 1, 2008. Available at <http://www.thespacereview.com/article/1262/1>. Accessed May 2014.
- [2] National Research Council, “*New Worlds, New Horizons in Astronomy and Astrophysics*,” Washington, DC: The National Academies Press, 2010. Available at <http://www.nap.edu/catalog/12951/>. Accessed May 2014.
- [3] M. Armano et al., “*Sub-Femto-g Free Fall for Space-Based Gravitational Wave Observatories: LISA Pathfinder Results*,” Phys. Rev. Lett. **116**, 231101, DOI: 10.1103/PhysRevLett.116.231101 (2016).

# Appendix A

## Technology Gaps Evaluated by the TMB in 2016

This appendix details the technology gaps prioritized by the Physics of the Cosmos (PCOS) Program Technology Management Board (TMB) in 2016. These are gaps between the current state-of-the-art (SOTA) technology readiness levels (TRLs, defined in Table A-1) and capabilities needed for future missions.

The order of the gaps is similar to that of prior-year Program Annual Technology Reports (PATRs). Specifically, we've grouped the gaps by science topic, and within that, by technology type. Where submitted gaps had significant overlap, they were merged into a single gap by the PCOS Program Analysis Group (PhysPAG) Executive Committee (EC) or by the TMB. Gap priority ranking is shown on p. 20 above. Submitted entries not ranked may have been merged into others; deemed outside the purview of the PCOS program (e.g., better addressed by Strategic Astrophysics Technology, SAT, programs other than PCOS; or associated with launch vehicles, rovers, avionics, spacecraft systems, etc.); deemed as not being technology gaps (i.e., specific implementations or not technologies at all); or deemed too mature for the SAT program.

Each entry lists the source of the gap next to the gap name. Sources include the general community, a large-mission-concept study team, or both. This last case is the case where similar gaps were submitted both by a member of the general community and a study team, and the TMB merged the gaps. We thank the EC, the X-ray Surveyor (XRS) Science and Technology Definition Team (STDT), the L3 Study Team (L3ST), and the general community for their engagement in and support of our technology gap identification process.

The Program Office considers gaps submitted by a study team, or by both the community and a study team, as “owned” by the study team until the team submits its final report. In practical terms, this means that the Program Office will forward to the study team any edits to such a gap that are submitted by the general community by the June 1 deadline. The study team will then consider these edits for possible inclusion into the following-year version of the gap. The study teams’ unmatched expertise in the technology needs of their respective mission concepts gives great credibility to their opinions on such technologies; increasing the likelihood of higher priority ranking for gaps owned by the teams.

TRL	Definition
1	Basic principles observed and reported.
2	Technology concept and/or application formulated.
3	Analytical and experimental critical function and/or characteristic proof-of-concept.
4	Component and/or breadboard validation in laboratory environment.
5	Component and/or breadboard validation in relevant environment.
6	System/subsystem model or prototype demonstration in a relevant environment.
7	System prototype demonstration in an operational environment.
8	Actual system completed and “flight qualified” through test and demonstration.
9	Actual system flight proven through successful mission operations.

**Table A-1.** TRL definitions from [NASA Procedural Requirements \(NPR\) 7123.1B Appendix E](#), which provides a full description of the TRLs.



Gap Name		Fast, low-noise, megapixel X-ray imaging arrays with moderate spectral resolution <i>Submitted by XRS STDT and General Community</i>
Description		<p>XRS requires X-ray imaging arrays covering wide fields of view (FOV) with excellent spatial resolution, i.e., megapixel or higher, and moderate spectral resolution.</p> <p>Much of the science for XRS emphasizes the soft X-ray band, so detector arrays (including optical-blocking filters) should have high efficiency and good spectral resolution down to <math>E \sim 0.2</math> keV.</p> <p>Fast readout time is needed to minimize event pileup and dead time, and radiation hardness must be sufficient to survive likely mission duration and environment.</p>
Current State-of-the-Art (SOTA)		<p>Silicon active pixel sensors (APS) currently satisfy some of the requirements, but further work is needed to meet all requirements simultaneously.</p> <p>APS with 36-<math>\mu\text{m}</math> pixels are at TRL 6, but noise levels are still too high, and sensitivity to soft X rays needs to improve. Sparsified readout, limited to pixels with signals, allows fast frame rates and is at TRL 3.</p>
TRL	SOTA	2–3
	Solution	
Performance Goals and Objectives		<ul style="list-style-type: none"> <li>• XRS requires large format X-ray detectors with sufficient spatial resolution so as not to compromise the imaging performance of the XRS optics (notionally with 0.5" half power diameter, HPD);</li> <li>• Multi-chip abuttablility to build detector surface approximating best focal surface for the mirrors;</li> <li>• Noise &lt; 1e-;</li> <li>• Fano-limited spectral resolution in the 0.2-10 keV energy band;</li> <li>• Frame rates &gt; 100 frames/s;</li> <li>• Optical-blocking filters with minimal X-ray absorption above 0.2 keV;</li> <li>• Radiation hardness supporting &gt; 5 years science operations at Chandra-like or L2 orbit;</li> <li>• Near-room-temperature operation; and</li> <li>• Power/sensor as low as 0.1 W.</li> </ul>
Scientific, Engineering, and/or Programmatic Benefits		Enables X-ray imaging of wide fields with high spatial resolution and sufficient spectral resolution to meet science goals of strategic X-ray missions.
PCOS Applications and Potential Relevant Missions		XRS, Joint Astrophysics Nascent Universe Satellite (JANUS) / X-ray Time Domain Explorer (XTiDE) -like, or any other focused X-ray optics, or coded-aperture wide-field X-ray-monitoring, or X-ray-grating mission.
Time to Anticipated Need		Need to demonstrate credibility before the 2020 Decadal Survey, and would require TRL 6 by mission Preliminary Design Review (PDR) anticipated in the mid-2020s.

Gap Name		Large-format, high-spectral-resolution, small-pixel X-ray focal plane arrays <i>Submitted by XRS STDT and General Community</i>
Description		<p>X-ray microcalorimeters are needed to allow spatially-resolved spectroscopy with the XRS. The arrays need to cover a wide field (<math>&gt; 5</math> arcmin) and with spatial resolution matching future X-ray optics (<math>&lt; \sim 1</math> arcsec).</p> <p>The X-ray focal-plane-array (FPA; e.g., microcalorimeter) pixels need to provide excellent spectral resolution (<math>&lt; \sim 4</math> eV Full-Width at Half-Maximum, FWHM, in the 0.2 – 10 keV band).</p> <p>Current X-ray microcalorimeter FPAs are not yet able to meet these minimum requirements. Fabrication of arrays of sufficiently small pixels, with large-enough pixel counts, with an efficient multiplexed readout capable of simultaneously reading out all X-ray events across the entire array while maintaining high energy resolution, is challenging.</p> <p>Much of the science for XRS emphasizes the soft X-ray band, so detector arrays (and supporting instrumentation including optical blocking filters) should allow a detector with high efficiency down to <math>E \sim 0.2</math> keV.</p>
Current State-of-the-Art (SOTA)		<p>Fabrication of arrays with 1024 transition-edge sensors (TESs), each connected to nine absorbers on a 75-<math>\mu\text{m}</math> pitch has been demonstrated (9216 pixels). Smaller arrays have been fabricated with a 50-<math>\mu\text{m}</math> pitch. Small arrays with nine absorbers attached to a single TES have demonstrated <math>&lt; 3</math> eV FWHM energy resolution. Much larger arrays, with more absorbers per sensor are needed. In the context of the required array size, the array fabrication is currently TRL 3. Small arrays (36 pixels) of much larger microcalorimeter pixels, is at TRL 9 (Hitomi).</p> <p>Multiplexing of TES microcalorimeters with time-division multiplexing has been demonstrated with 32 pixels in a single readout channel with less than 3 eV resolution. This readout option is at TRL 4 / 5.</p> <p>Multiplexing with microwave Superconducting QUantum Interference Devices (SQUIDs) in resonator circuits at GHz frequencies has the potential to read out hundreds or maybe a thousand sensors per readout channel, and thus provides a path to reading out much larger arrays. This has been demonstrated reading out 4 pixels (TRL 3). TESs and magnetically coupled (micro-)calorimeters (MCC) are two of the leading thermal-sensor technologies with potential to meet the XRS requirements, and both can be read out using microwave SQUIDs in GHz resonators.</p>
TRL	SOTA	
	Solution	
Performance Goals and Objectives		<p>The primary objective for XRS is large-format arrays with pixel count <math>&gt; 100\text{k}</math> and spectral resolution <math>&lt; 4</math> eV FWHM at 0.2 – 10 keV. This likely requires a high degree of multiplexing, both thermal and electrical:</p> <p><u>Thermal multiplexing:</u> Sensors attached through varying thermal conductances to multiple absorbers, allowing pixel identification across the entire energy band, up to a multiplexing factor of 25:1, with energy resolution <math>&lt; 4</math> eV and pixel pitch <math>&lt; 50 \mu\text{m}</math>.</p> <p><u>Electrical multiplexing:</u></p> <ul style="list-style-type: none"> <li>• Readout using conventional multiplexing techniques (<math>&lt; 20</math> MHz). Desired multiplexing factor is 64:1.</li> <li>• Readout using microwave resonators, such as with microwave SQUIDs. Desired multiplexing factor is 1000:1.</li> </ul>

<b>Scientific, Engineering, and/or Programmatic Benefits</b>	<p>Science benefits identified for International X-ray Observatory (IXO) in “New Worlds, New Horizons in Astronomy and Astrophysics” (NWNH) and XRS in the 2014 Astrophysics Roadmap update.</p> <p>The more advanced the multiplexed readout becomes, the more engineering benefits there are. These benefits include having less-demanding cryogenic requirements; and also lower instrument mass, power, and cost for the cryogenics and readout.</p>
<b>PCOS Applications and Potential Relevant Missions</b>	<p>XRS.</p> <p>The technology is also synergistic with an enabling technology for the US contribution to Athena.</p>
<b>Time to Anticipated Need</b>	<p>Need to demonstrate credibility before the 2020 Decadal Survey, and would require TRL 6 by mission PDR anticipated in the mid-2020s.</p>

Gap Name		Advancement of X-ray polarimeter sensitivity using negative-ion gas <i>Submitted by General Community</i>
Description		<p>Standard photoelectric X-ray polarimeter designs are both quantum-efficiency (QE) -limited and challenging to calibrate due to diffusion of electron signal as it drifts through the gas.</p> <p>Drifting negative ions decreases diffusion to the thermal limit, thereby decoupling sensitivity from drift distance, and enabling larger detector areas that can be at the focus of larger-diameter mirrors and single-reflection concentrator.</p> <p>Negative-Ion Time-Projection-Chamber (NITPC) polarimeters also allow the selection of constituent gases and pressures to be based on optimization of modulation and QE rather than diffusion properties. This versatility enables a large improvement in sensitivity without driving cost and with only moderate increase to mass and power of the detector and/or instrument. Furthermore, the energy band will be tunable to maximize science return.</p>
Current State-of-the-Art (SOTA)		<p>Several photoelectric polarimeter concepts such as Polarimeter for Relativistic Astrophysical X-ray Sources (PRAXyS, previously Gravity and Extreme Magnetism Small Explorer, GEMS), Imaging X-ray Polarimeter Explorer (IXPE), and Polarimetry of Energetic Transients (POET) etc. were proposed in 2014 to provide the next substantial step exploiting X-ray polarization to answer key scientific questions for some of the brightest sources in the sky.</p> <p>However, proposed measurements remain photon-limited and the need for higher-sensitivity polarimeters for both faint persistent sources such as Active Galactic Nuclei (AGN) and bright transient sources such as Soft-Gamma Repeaters (SGRs) by way of Explorer missions and probe-class missions in the next decade remains critical.</p> <p>The goal of this development is to make practical the technology that will provide an order-of-magnitude improvement in polarization sensitivity over current-generation instruments.</p>
TRL	SOTA	4
	Solution	
Performance Goals and Objectives		<p>Development of gas electron multipliers optimized for negative ion gas.</p> <p>Development of finer-pitch strip readouts to improve the sensitivity at lower energies and higher pressures.</p> <p>Optimization of gas mixtures to maximize sensitivity (QE vs. track length).</p> <p>Demonstrate lifetime of gas and detector materials is commensurate with mission requirements.</p>
Scientific, Engineering, and/or Programmatic Benefits		These developments will allow a factor-of-10 improvement in sensitivity without decreasing the sensitivity per unit mass and without increasing the relative cost of an instrument.
PCOS Applications and Potential Relevant Missions		<p>Flagship and Probe-class X-ray missions.</p> <p>Explorer-class X-ray missions.</p> <p>Sounding rocket experiments.</p>
Time to Anticipated Need		<p><b>Named missions:</b></p> <p><b>Development needed for 2020 Decadal:</b> No</p> <p><b>Other drivers:</b> Explorers, Probes, and Missions of Opportunity (MOs).</p>



Gap Name		Rapid readout electronics for X-ray detectors	
		<i>Submitted by General Community</i>	
Description		Future NASA X-ray missions in both the long term (XRS, which is endorsed by Enduring Quests Daring Visions Report and currently under STDT study) and nearer term (Probe and Explorer-class opportunities), as well as the Athena mission, led by the European Space Agency (ESA), will have focal-plane instruments that have many pixels ( $> 10$ Mpix) and very fast frame rates. A key technology that will need further development to support these focal planes will be electronics boards that can read out and process the events from these detectors at very rapid rates.	
Current State-of-the-Art (SOTA)		<p>The concept for a board that would accomplish the requirements for both JANUS and Athena was initially developed when JANUS was in a phase-A study and Athena had a potential opportunity for US contribution to these electronics.</p> <p>The need still exists for such a board for other future missions such as XRS, Arcus, or other upcoming Explorer and/or Probe-class missions.</p> <p>A design was developed using a Xilinx Field Programmable Gate Array (FPGA) and parallel event processing that enables the required speeds.</p>	
TRL	SOTA	3	
	Solution	3	
Performance Goals and Objectives		Development of an electronics board that can read out and characterize X-ray events at $> 1.6$ Gigapixel/second.	
Scientific, Engineering, and/or Programmatic Benefits		<p>Enable rapid detector readout and event characterization for a variety of possible X-ray missions, large and small: flagship, Probes, Small Explorer (SMEX), Medium-class Explorer (MIDEX), and CubeSats.</p> <p>In particular, this will enable missions such as Arcus, which is being proposed, and/or XRS, which is endorsed by Enduring Quests Daring Visions. These developments could also contribute to efforts by our European colleagues on technology needed for the Athena mission.</p>	
PCOS Applications and Potential Relevant Missions		<p>XRS (currently under study by a NASA STDT as a large strategic mission concept) is one example of a potential mission requiring rapid readout electronics with these characteristics (Kouveliotou et al. 2014, "Enduring Quests, Daring Visions;" &amp; Vikhlinin et al. 2012 gives a possible strawperson example of how this mission might look). The large-FOV instrument on this mission specifically required large-format APS. This instrument would provide a large FOV with excellent spatial and temporal resolution and moderate spectral resolution. The heart of the instrument is a <math>&gt; 16</math> Mpix focal plane with a readout requirement of <math>&gt; 100</math> frames/second and is comprised of an array of X-ray photon-counting APS. This same plan would apply to any other similar mission that couples large effective area with a need for large-format/many-pixel detectors, or missions that require rapid readout of many pixels for other purposes such as timing resolution or background suppression.</p> <p>Examples: XRS, Arcus, Athena, Probe-class X-ray missions with more targeted capabilities, JANUS-like missions, XTIDE-like missions.</p>	
Time to Anticipated Need		<p><b>Named Missions:</b> XRS and Athena (2020)</p> <p><b>Development needed for 2020 Decadal:</b> Yes</p> <p><b>Other drivers:</b> Several Explorer (e.g., Arcus, 2018) and Probe concepts that require pixelated Si sensors operating at high frame rates.</p>	

Gap Name		High-efficiency X-ray grating arrays for high-resolution spectroscopy <i>Submitted by XRS STDT</i>
Description		<p>Light-weight, high-efficiency (<math>&gt; 40\text{-}50\%</math>), large-format X-ray grating arrays enable high spectral resolving power <math>R &gt; 5000</math> in the soft X-ray band (<math>\sim 0.2 - 2 \text{ keV}</math>) for absorption- and emission-line spectroscopy using large X-ray telescopes.</p> <p>These would provide the resolving power needed to address key science goals in the soft X-ray band, such as studying the physical state of baryons in galactic halos and in the Cosmic Web, detailing matter and energy feedback from supermassive black holes (SMBH), and characterizing stellar lifecycles from birth to death.</p> <p>NOTE: The needs of XRS lead to more ambitious requirements than those typically discussed for Explorer-class missions. In particular, resolving powers of <math>R = 5000</math> at the minimum are of interest. The grating arrays should be able to intercept between 50 and 100% of the input beam, and they should be insertable and retractable.</p>
Current State-of-the-Art (SOTA)		<p>Proven technologies (grating spectrometers on Chandra and X-ray Multi-mirror Mission-Newton, XMM-Newton) fall short in efficiency, collecting area, and resolving power, by factors of 5-10. High-efficiency gratings have been demonstrated that place <math>&gt; 40\%</math> of the incident soft X-ray light into the diffracted orders.</p> <p>Separately, high-spectral-resolving-power gratings have achieved resolving powers <math>&gt; 10,000</math> in the soft X-ray band with a single grating element and small collecting area, showing that <math>R &gt; 3000</math> can be achieved with large-collecting-area designs.</p> <p>Current technology readiness is assessed to be at TRL 4.</p>
TRL	SOTA	4
	Solution	4
Performance Goals and Objectives		<p>Large-format grating arrays with high efficiency (<math>\sim 40\%</math> or more) in the <math>0.2 - 2 \text{ keV}</math> energy band. Dispersion must be large enough to allow <math>R &gt; 5000</math>.</p> <p>Gratings must be scalable in size, with the goal of covering at least 50% of the XRS beam. The STDT is particularly interested in exploring approaches to facilitate manufacturing and assembly of gratings arrays of the size required for XRS.</p> <p>Gratings must be insertable and fail-safe retractable.</p>
Scientific, Engineering, and/or Programmatic Benefits		<p>Spectrometers achieving <math>R &gt; 5000</math> throughout the soft X-ray band are mission-enabling, as microcalorimeters cannot achieve that. Priority science goals for soft X-ray spectroscopy are studying the physical state of baryons in galactic halos and in the Cosmic Web, detailing matter and energy feedback from SMBH, and characterizing stellar lifecycles from birth to death.</p>
PCOS Applications and Potential Relevant Missions		<p>A spectrometer using gratings with this performance is envisioned for XRS, has been studied by NASA as a Probe, has been proposed for an Explorer, and will be flown on the Off-plane Grating Rocket Experiment (OGRE).</p>
Time to Anticipated Need		<p>Need to demonstrate credibility before the 2020 Decadal Survey, and would require TRL 6 by mission PDR anticipated in the mid-2020s.</p>

Gap Name		High-resolution, lightweight X-ray optics <i>Submitted by XRS STDT and General Community</i>
Description		<p>The science of XRS requires a large-throughput mirror assembly with sub-arcsec angular resolution. These future X-ray mirrors have a set of requirements which collectively represent very substantial advances over any currently in operation or planned for missions other than XRS. Of particular importance is achieving low mass per unit collecting area, while maintaining Chandra-like angular resolution.</p> <p>Proposed technology improvements may include: piezo cells to adjust figure, magnetic-smart-material (MSM) shaping with magnetic field; ion implantation, zero-stress Si (single-crystal silicon), differential deposition, coating the substrate back with a localized and controlled “stressy” material. Development of X-ray-reflecting coatings with low stress, or controlled stress, is an essential component of the high-resolution, lightweight optics work.</p>
Current State-of-the-Art (SOTA)		<p>Chandra optics:</p> <ul style="list-style-type: none"> <li>• Angular resolution <math>&lt; \sim 0.5</math> arcsec;</li> <li>• Effective area <math>750 \text{ cm}^2</math> at 1 keV; and</li> <li>• Mirror mass 951 kg.</li> </ul> <p>TRL 2-3 for various technologies for high-resolution, light-weight mirrors mentioned above.</p>
TRL	SOTA	2-3
	Solution	
Performance Goals and Objectives		<ul style="list-style-type: none"> <li>• Mirror technologies must be scalable to a few-square-meter-class assemblies; and</li> <li>• Angular resolution of order 0.5 arcsec.</li> </ul>
Scientific, Engineering, and/or Programmatic Benefits		This type of X-ray optics will enable study of the early universe to complement the James Webb Space Telescope (JWST), maintain US leadership in lightweight X-ray optics for space, and facilitate future missions and minimize their schedule and costs.
PCOS Applications and Potential Relevant Missions		Enabling technology for XRS. May be used in future Explorer-class missions.
Time to Anticipated Need		Need to demonstrate credibility before the 2020 Decadal Survey, and would require TRL 6 by mission PDR anticipated in the mid-2020s.

Gap Name		Low-stress or stress-free coating for X-ray optics <i>Submitted by General Community</i>
Description		All X-ray optics need reflecting-surface coating with a heavy metal, such as iridium, platinum, or gold. Such a coating layer usually has strong residual stress from the deposition process. This residual stress will deform a mirror substrate, particularly a segmented thin substrate, and degrade its angular resolution dramatically. This is an especially serious issue for multilayer coatings required for hard X-ray ( $E > 10$ keV) applications, as they can be very thick and their stress can be extremely high.
Current State-of-the-Art (SOTA)		For soft X-ray mirror coating, the residual stress can be minimized by thinning the surface coating, but it could slightly lower X-ray reflectivity. However, there is no real solution to this issue at this point for multilayer coating.  The (multilayer) Nuclear Spectroscopic Telescope ARray (NuSTAR) mirror suffers from stress and ends up with a 58-arcsec resolution, while the substrate was about 20 arcsec. Stress-free coating is crucial for future high resolution soft/hard-X-ray mirrors.
TRL	SOTA	
	Solution	
Performance Goals and Objectives		To be able to coat a thick enough layer or a multilayer on a segmented thin mirror substrate, with substrate thickness of 0.2 - 0.4 mm, and with minimal distortion.
Scientific, Engineering, and/or Programmatic Benefits		Would enable some implementations of lightweight, high-resolution, affordable X-ray optics; and dramatically improve the angular resolution of large-area, hard X-ray optics.
PCOS Applications and Potential Relevant Missions		All future X-ray missions utilizing segmented thin X-ray optics, especially in the hard-X-ray band, including Explorers, Probes, and MOs.
Time to Anticipated Need		<b>Named missions:</b>  <b>Development needed for 2020 Decadal:</b> No  <b>Other drivers:</b> Explorer, Probe, and MO opportunities.



Gap Name		Ultra-high-resolution focusing X-ray observatory telescope <i>Submitted by General Community</i>
Description		<p>Very high angular resolution in the X-ray band is needed to study the structure surrounding and jets emanating from SMBHs at the cores of galaxies. However, the Chandra X-ray observatory's 0.5-arcsec resolution is already near the best that can be expected from grazing-incidence reflection.</p> <p>Simulations suggest that above 4 keV, a transmitting diffractive-refractive pair in direct contact in which the focal length of the refractive component is minus twice that of the diffractive element can achieve milliarcsec resolution by nullifying chromatic aberration over a 15% bandwidth. However, a 1-m-diameter system would have a focal length of the order of 1000 km. Optics and detector would be aboard separate spacecraft that engage in "formation flying." Only one spacecraft can be in a true orbit; the other has to be powered by an engine to overcome the gravity gradient to maintain alignment and to reposition for target changes. The center of the detector spacecraft has to be &lt; 10 cm from the optical axis or a designated position in a raster scan. The position of the optical axis has to be known to &lt; 5 mm for milliarcsec resolution. Pointing direction of the optics and the distance between the two spacecraft are not critical.</p>
Current State-of-the-Art (SOTA)		<p>This system requires new technology in two areas, X-ray optics and mission operations. Construction of the optics is not expected to be difficult, in fact, it should be much less demanding and much lower mass than a grazing-incidence optic. However, the very long focal length precludes laboratory tests of large-diameter optics.</p> <p>The principle but not the level of performance can be verified by testing miniature components at synchrotron radiation facilities with a very long vacuum pipe to accommodate the large distance between the optics and detector. Mission operations have to be studied analytically. No other high-energy mission or mission concept that this author knows of has had operational requirements comparable in difficulty to this, but there is no apparent reason why they cannot be satisfied.</p>
TRL	SOTA	1
	Solution	
Performance Goals and Objectives		<p>The mission should be considered only after the development of a successor to Chandra (XRS) has begun. It would begin with a study of formation flying of two spacecraft separated by 1000 km to determine the feasibility and costs of maintaining the position of the detector within 10 cm of the optical axis, or a designated point on the focal surface of a raster scan, with a positional uncertainty &lt; 5 mm for a period of several years, during which time there will be target changes.</p> <p>Propulsion, most likely by ion engines, is needed for both maintaining pointing and changing targets. The quantity of propellant that can be accommodated determines the lifetime of the mission. The presence of either two optics or detector spacecraft will result in more efficient utilization of propellant. One spacecraft navigates to the next target position while the other is observing.</p>
Scientific, Engineering, and/or Programmatic Benefits		<p>This X-ray telescope system offers in theory three orders-of-magnitude higher angular resolution than any current or future grazing-incidence X-ray telescope and any single-lens telescope in any wavelength band. The formation-flying capability that would be developed for this mission is applicable to an even more ambitious project, X-ray interferometry with multiple lenses. Development of formation-flying capability between two or more spacecraft should be useful in other space projects.</p>

<p><b>PCOS Applications and Potential Relevant Missions</b></p>	<p>A very-high-angular-resolution X-ray telescope would be enabled by the development of technology for long distance formation flying between two spacecraft with 5-cm pointing accuracy of the detector with respect to the optical axis or another direction of a raster scan, and changing targets.</p> <p>The principal objectives are observing the structure of the environment surrounding SMBH and the small clumps of material in their jets. The same would apply to the nebula surrounding neutron stars and the jets emanating from them.</p>
<p><b>Time to Anticipated Need</b></p>	<p><b>Named missions:</b></p> <p><b>Development needed for 2020 Decadal:</b> No</p> <p><b>Other drivers:</b> Applicability would be a decade after the next high-angular-resolution telescope, i.e. the XRS, has operated for several years and has revealed specific targets that require higher-angular-resolution observations to probe more deeply.</p>

Gap Name		Very-wide-field focusing instrument for time-domain X-ray astronomy <i>Submitted by General Community</i>
Description		<p>There exists considerable support in the astronomical community for a Probe-type mission dedicated to Time-Domain X-ray Astronomy. Given the large number of X-ray sources across the sky that are variable, or transient, the key instrument would be a focusing telescope with an extremely large field of view, i.e. several steradians. The type of optics with the large field of view is known as a “lobster-eye”. There are two types. One is based on an array of square pores slumped onto a spherical surface. Small units have been constructed and, in fact, such an optic is scheduled to be aboard the ESA mission to Mercury. The other type of lobster-eye is a hybrid consisting of an equally spaced array of flat mirrors that lie along the radii of a cylinder. Both faces of the mirrors are coated with a heavy metal with good X-ray reflectivity. It provides position information in one dimension. A circumferential cylindrical coded mask provides positions in the other dimension. Both types require similar detector systems, which would consist of an array of CCD, CMOS or other type of pixelated detectors. While the detector chips currently exist, there has not been an array of X-ray devices that covers efficiently a very large area (up to a square meter). Compared to the 2D channel-plate optic, the hybrid has an order of magnitude more effective area and much broader bandwidth but more background. For very short-lived transients, such as gravitational waves (GWs) and short gamma-ray bursts (GRBs), where little background accumulates, the larger area and broader bandwidth is desirable.</p>
Current State-of-the-Art (SOTA)		<p>Small prototype telescopes of both types have been constructed but are not close to the optics size required for the Transient X-ray Astrophysics Probe. Leicester University in the UK has been leading the thermally slumped channel-plate effort. So far, the angular resolution of small units has been ~5 arcmin, far short of the 20-arcsec theoretical value. Also, the coatings on the walls of the channel plate have not been optimal. Small versions of the cylindrical-geometry 1D focusing lobster-eye telescopes have been constructed at SAO and in the Czech Republic. However, the problem of a low-mass structure for the mirrors has not been addressed and no effort has been made to develop a circumferential cylindrical coded mask to go with the cylindrical 1D lobster-eye. While optical astronomers have successfully made large arrays of optical/infrared CCDs, there has not been the need so far for a comparable X-ray detector.</p> <p>Technologies for the channel plate version are ~TRL 4. Technologies for the hybrid exist in concept but insufficient support delays design of a prototype optic integrated with a coded mask. Optics are at ~TRL 2 and the 1D cylindrical coded mask at TRL 3 thanks to the success of Swift and XMM coded masks. The UK is supporting most channel-plate telescope development efforts. Support for the hybrid would have to be provided by NASA. The detector array for both 2D and 1D focusing systems is at TRL 3. Comparable-size arrays have been constructed for optical telescopes but with less need for continuous focal surface coverage. Kepler is an example of a large focal plane detector array in space.</p>
TRL	SOTA	Channel-plate telescope 3 – 4; cylindrical hybrid 2 – 3
	Solution	4



<b>Performance Goals and Objectives</b>	<p>With a 1-m focal length and 120° azimuth coverage, the lobster-eye focal plane would be a closely packed cylindrical array of pixelated X-ray detectors over a focal surface with <math>\sim 1\text{-m}^2</math> total area. Ideally, the detector active region would occupy a very large fraction of that area, efficient to at least 10 keV, with 50-<math>\mu\text{m}</math> pixels sufficient.</p> <p>Telescope technical goals are: several arcmin or better angular resolution and sub-arcmin position determination (by finding image centroid) with a <math>\text{FOV} \geq 2</math> ster.</p> <p>Sensitivity for GRB detection at least <math>\times 10</math> better than Swift, capable of detecting and positioning all kinds of variable (and static) sources at least <math>\times 10</math> better than the scanning Rossi X-ray Timing Explorer (RXTE) All-Sky Monitor and Japan's Monitor of All-sky X-ray Image (MAXI) on the International Space Station (ISS).</p> <p>Many sources are nearly constantly in the FOV (except during Earth occultation in Low Earth Orbit, LEO) for both types of lobster-eye telescopes. The hybrid's larger exposure time and area ensure superior sensitivity to the scanning collimated monitors, with background reduction of focusing adding another level of superiority.</p>
<b>Scientific, Engineering, and/or Programmatic Benefits</b>	<p>Both types of lobster-eye telescopes are new types of X-ray optics that have not been in orbit. The channel-plate type will be very low mass. The FOV of both types is several ster whereas current and previous focusing telescopes, e.g. Chandra and XMM, have fields that are a fraction of a square degree. The difference in sky coverage is a factor of <math>10^4</math>. Large non-focusing detectors with similar large FOVs, e.g. Swift, do not cover the same bandwidth, and have much less sensitivity and angular resolution. The lobster-eye telescopes enable an entire new class of measurements, detecting and positioning short-lived transient sources such as distant GRBs and likely transients with sub-second duration transients associated with GWs. They have much more sensitivity than the non-focusing scanning all-sky monitors for all types of temporal variations.</p>
<b>PCOS Applications and Potential Relevant Missions</b>	<p>The very-wide-field lobster-eye X-ray telescope enables the development of the Transient Astrophysics Probe, a candidate PCOS mission that carries out studies of multiple sources varying over a large range of time scales simultaneously from the same pointing position. By detecting and positioning very distant GRBs, Cosmic Origins (COR) objectives will be fulfilled because the distant GRBs' host galaxies will be the youngest galaxies in the universe. Lobster-eye telescopes can map X-ray emission from planets and asteroids in our solar system. Depending on the viewing distance and the size of the object, X rays from a large part or the entire front-facing surface of the planet can be mapped much more quickly with the lobster-eye telescope's large FOV.</p>
<b>Time to Anticipated Need</b>	<p><b>Named missions:</b></p> <p><b>Development needed for 2020 Decadal:</b> No</p> <p><b>Other drivers:</b> NASA is not likely to launch a Probe-type mission in less than five years. Meanwhile technology development of the optics and X-ray detector arrays can proceed via Astrophysics Research and Analysis (APRA) and SAT programs.</p>

Gap Name		Advanced millimeter-wave focal-plane arrays for CMB polarimetry <i>Submitted by General Community</i>	
Description		<p>The Inflation Probe (IP) requires arrays of detectors with background-limited sensitivity, dual-polarization detection capability, and control of systematic errors at multiple frequencies between ~30 and ~600 GHz for foreground removal.</p> <p>Architectures must be scalable to large arrays for the requisite sensitivity. Simultaneous multiband operation, high multiplexing factors, and efficient detector and readout focal-plane packaging represent desirable design qualities. Detector systems must be compatible with the space environment. This includes low dielectric exposure to low-energy electrons and robust performance in the presence of cosmic rays.</p> <p>Continued deployment in ground-based and balloon-borne platforms will benefit development efforts.</p>	
Current State-of-the-Art (SOTA)		<p>A great deal of progress has been made with a variety of approaches, including feedhorn and antenna-coupling waveguide probes, and filled absorber structures.</p> <p>TESs are currently the leading candidate technology for the detecting element in these integrated sensors. Arrays of several thousand detectors are operating in ground-based Cosmic-Microwave-Background (CMB) -polarization experiments. Balloon experiments E and B Experiment (EBEX) and Suborbital Polarimeter for Inflation Dust and the Epoch of Reionization (Spider) have demonstrated two TES architectures in the environment closest to space. Primordial Inflation Polarization Explorer (PIPER) will soon demonstrate a third.</p> <p>Fabrication of TES arrays on 150-mm diameter substrates, which addresses pixel-count scalability, is now maturing at multiple fabrication foundries. However, no fielded 150-mm arrays exist at this time.</p>	
TRL	SOTA	4	
	Solution	3	
Performance Goals and Objectives		<p>The detectors must demonstrate high efficiency, background-limited sensitivity, and linearity over a wide spectral range (~30 to ~600 GHz), while at the same time controlling systematic errors to a level sub-dominant to the instrument statistical-noise floor. The technology must demonstrate extremely low levels of polarized-beam systematic errors to achieve this goal.</p> <p>The technology must be compatible with space-borne operation, and provide appropriate magnetic shielding, cosmic-ray immunity, vibration tolerance, and excellent noise stability. Process uniformity, high detector efficiency, and high yield are also important.</p> <p>One technical development that would have a large impact on instrument design is a reduction of the TES detector-to-readout interconnects at the milliKelvin stage. Current TES readout schemes demand a large number of additional hardware elements, which require interconnects and an associated mechanical support structure. Technical approaches that do away with additional readout hardware elements will reduce the mass, volume, and complexity of the entire instrument. Integrated fabrication of TES detectors and SQUID readouts represents one avenue to achieve this goal.</p>	

<b>Scientific, Engineering, and/or Programmatic Benefits</b>	<p>Measurement of CMB polarization to search for evidence of, and characterize, Inflation is a top NASA priority.</p> <p>Such detectors are a key enabling technology. A space-borne measurement can probe for a polarization pattern imprinted by a background of GWs generated at the time of Inflation in the early universe.</p> <p>Polarization measurements on finer angular scales probe large-scale structure sensitive to neutrino mass and dark energy.</p>
<b>PCOS Applications and Potential Relevant Missions</b>	<p>These are needed for measuring CMB polarization to search for and characterize the faint polarized signature of Inflation.</p> <p>The targeted mission is IP as recommended in the NWNH report. Other possibilities include Explorer and international CMB-polarization and absolute-spectrum experiments.</p> <p>Development also has technological overlaps with superconducting far-IR and X-ray detectors.</p>
<b>Time to Anticipated Need</b>	<p><b>Named missions:</b> IP (2020s)</p> <p><b>Development needed for 2020 Decadal:</b> Yes, IP</p> <p><b>Other drivers:</b> IP technology development is a NWNH priority that was recently revisited by the mid-Decadal review.</p> <p>US contribution to the Japanese Aerospace eXploration Agency (JAXA) mission Lite (light) satellite for the study of B-mode polarization and Inflation from cosmic background Radiation Detection (LiteBIRD) is already in a phase A study through the Explorer's program. An additional Explorer proposal to contribute to a European Space Agency (ESA) mission is likely this year.</p>

Gap Name		Millimeter-wave optical elements	Submitted by General Community
<b>Description</b>		High-throughput telescopes and optical elements with controlled polarization properties are required for the IP. These require development of cryogenic mm-wave filters and coatings.  Measurement of CMB polarization on large scales may require rapid polarization modulation to separate sky-signal polarized intensity from instrumental effects. Employing modulators large enough to span the telescope primary aperture is an advantage in that sky polarization can be separated from instrumental effects.	
<b>Current State-of-the-Art (SOTA)</b>		Single-layer anti-reflection (AR) coatings are in widespread use. Meta-material AR structures are in development and early use.  Several experiments in the field are currently using rapidly spinning half-wave plates as the primary means of modulating the signal and separating it from longer time variations.  More experiments are coming online using both half-wave plates and variable-delay polarization modulators that endeavor to measure larger areas of the sky.	
<b>TRL</b>	<b>SOTA</b>	2 – 5	
	<b>Solution</b>		
<b>Performance Goals and Objectives</b>		Develop robust multi-layer coatings for broadband applications for commonly used dielectrics (e.g., silicon, alumina, and sapphire).  Develop thermal filtering technologies suitable for large Focal-Plane Arrays (FPAs) operating at sub-Kelvin temperatures.  Develop space-compatible modulators, including work on frequency-selective surfaces and mechanisms compatible with the space radiation environment. Minimizing dielectric cross-section to low-energy electrons is a priority.  Develop and compare strategies for instrument architectures with and without rapid modulators.  A secondary goal is to ensure that the technology can be implemented in a cost-effective way for large optical elements. Large in this context is up to 100 cm in diameter.	
<b>Scientific, Engineering, and/or Programmatic Benefits</b>		Broadband optics can reduce the necessary focal-plane mass and volume for CMB polarization measurements. This may open options for compact optical systems appropriate for lower-cost Explorer opportunities; an international mission concept using broadband refracting optics is in the planning stages. Modulators are potentially a key enabling technology.	
<b>PCOS Applications and Potential Relevant Missions</b>		IP, Far-IR, Explorer, and international experiments to study CMB polarization and absolute spectrum.	
<b>Time to Anticipated Need</b>		<b>Named missions:</b> IP (2020s)  <b>Development needed for 2020 Decadal:</b> Yes, IP  <b>Other drivers:</b> IP technology development is a NWNH priority that was recently revisited by the mid-Decadal review.  International and Explorer implementations of the IP have proposed launch dates during the second half of the next decade.	



Gap Name		High-power, narrow-line-width laser sources <i>Submitted by L3ST and General Community</i>
Description		GW missions need lasers that are either intrinsically stable or can be stabilized to external references. The laser phase must also be modulated to allow exchange of clock-noise information, ranging tones, and potentially data.
Current State-of-the-Art (SOTA)		<p>The laser system is usually envisioned as a master oscillator power amplifier (MOPA) system. The Tesat laser flying on LISA Pathfinder (LPF) meets most of the master laser requirements for Laser Interferometer Space Antenna (LISA). Lasers of a similar type Non-Planar Ring Oscillator (NPRO) exist commercially in the US.</p> <p>GSFC has partnered with LGS to develop an alternative master laser based on an External Cavity Laser (ECL), which is currently at TRL 3.</p> <p>Commercial amplifier products exist in the US and Europe but are typically intended for other applications and require integration into a laser system and subsequent testing. A 2-W laser amplifier was constructed by LGS, tested at GSFC, and is at TRL 4.</p> <p>An alternative to the MOPA approach is a single-stage laser. Commercial (not space-qualified) single-stage laser systems with 2-W output power exist that can be controlled to meet power and frequency noise requirements but lack capability to sufficiently modulate the laser field. This could be remedied with the inclusion of a high-power phase modulator which would require some development.</p>
TRL	SOTA	3
	Solution	3
Performance Goals and Objectives		<p>The goal is to assemble and test a full space-qualified laser system meeting all requirements listed below. This includes laser power, frequency noise, intensity noise, and a possibility to modulate the laser with GHz sidebands, Pseudo-Random Noise (PRN) codes, and maintain phase fidelity throughout the laser system.</p> <p>The key performance parameters are:</p> <ul style="list-style-type: none"> <li>• Laser power &gt; 1W;</li> <li>• Frequency noise: <math>\sim 100 \text{ Hz}/\sqrt{\text{Hz}}</math>;</li> <li>• Relative intensity noise:                         <ul style="list-style-type: none"> <li>- <math>10^{-4}/\sqrt{\text{Hz}}</math> in LISA band,</li> <li>- <math>10^{-8}/\sqrt{\text{Hz}}</math> above <math>\sim 2 \text{ MHz}</math>;</li> </ul> </li> <li>• Phase fidelity of GHz phase modulation <math>&lt; 6 \times 10^{-4}/\sqrt{\text{Hz}}</math> in LISA band; and</li> <li>• Lifetime: &gt; 3 years hot; 5 years with 3 yrs in cold redundancy.</li> </ul> <p>All parameters measured at output of single-mode polarization-maintaining fiber.</p>
Scientific, Engineering, and/or Programmatic Benefits		<p>The laser is a potential US contribution to an ESA-led L3 mission addressing the “Gravitational Universe” science theme. It is also required for a potential future US-led laser-interferometric GW mission. Laser technology is in general a critical technology for a vast range of future applications.</p> <p>All formation-flying plans in the 30-year Astrophysics Roadmap require laser systems that meet at least some of these requirements. Having a space-qualified commercial-off-the-shelf (COTS) laser system meeting the GW mission requirements should be a general goal of NASA.</p>

<p><b>PCOS Applications and Potential Relevant Missions</b></p>	<p>Space-based laser-interferometric GW detectors such as LISA or Space-based Gravitational-wave Observatory at a Middle price point (SGO-Mid) or the European evolved LISA (eLISA) concept.</p> <p>Space-based geodesy missions, such as Gravity Recovery and Climate Experiment (GRACE) II, require low-power versions of these types of lasers.</p> <p>Future missions: Interferometry was named as one of the crosscutting, game-changing technologies in the Astrophysics Roadmap, and ultra-stable lasers are essential for this.</p>
<p><b>Time to Anticipated Need</b></p>	<p><b>Named missions:</b> L3 (late 2020s / early 2030s)</p> <p><b>Development needed for 2020 Decadal:</b> Yes, L3</p> <p><b>Other drivers:</b> ESA is considering accelerating the L3 schedule in response to the recent GW detections and the LPF results. The earliest expected date for mission adoption would be 2020. Targeting TRL 6 by 2020 would enable NASA to offer the laser as a contribution to L3. The schedule for a US-led mission would likely lag by 2-3 years.</p>

Gap Name		Highly stable low-stray-light telescope <i>Submitted by L3ST and General Community</i>
Description		<p>LISA-like missions need optical telescopes to expand and compress laser beams.</p> <p>A robust design is needed for small-scale manufacturability of functionally interchangeable units. A total of order 10 telescopes is required, including 6 flight units, 1-2 spares, and additional units for ground testing and test beds.</p> <p>The need for in-field guiding will depend on the orbits and progress in other areas, such as designs that allow correlating the two local lasers at the <math>\text{pm}/\sqrt{\text{Hz}}</math> level (back-link fiber or free-space link).</p>
Current State-of-the-Art (SOTA)		<p>The most unusual performance parameters are <math>\text{pm}/\sqrt{\text{Hz}}</math> stability and stray-light requirements. Telescopes that meet the phase-front quality, FOV, and diameter requirements are fairly standard.</p> <p>The long-term imaging requirement with a set-and-forget focus adjustment is probably also standard. However, this adjustment mechanism might introduce unacceptable dimensional noise beyond the <math>\text{pm}/\sqrt{\text{Hz}}</math> level and some realizations have shown increased scattered-light levels. Relying on the passive absolute stability of the secondary/primary distance (<math>\sim\mu\text{m}</math>) would eliminate the need for a focus adjustment.</p> <p>The <math>\text{pm}/\sqrt{\text{Hz}}</math> stability has been tested for several spacer materials but never for a realistic telescope that includes mirrors and mounts. Additional work on stable materials may be needed.</p> <p>The backscatter has been studied in small tabletop experiments for the secondary mirror for on-axis telescopes but not for a full telescope. On- and off-axis telescopes have been studied with ray-tracing programs, which are not ideal for laser interferometric applications. In-field guiding has not been integrated into any telescope test, and would require development of a mechanism.</p> <p>These tests and simulations put the telescope at TRL 4 without in-field guiding and below TRL 4 with it.</p>
TRL	SOTA	4
	Solution	4
Performance Goals and Objectives		<p>The key performance parameters are: <math>\text{pm}/\sqrt{\text{Hz}}</math> stability at <math>f &gt; 1 \text{ mHz}</math> <math>\sqrt{[1 + (3 \text{ mHz}/f)^4]}</math>; <math>&lt; 100 \text{ pW}</math> of stray light from the telescope back into the fundamental spatial mode on the optical bench (for up to 2-W input power); long-term imaging stability (set-and-forget focus adjustment or passive absolute stability) to generate small (5-mm) collimated beam on optical bench; aperture stop for transmitted beam; phase-front quality: <math>\lambda/30</math>; FOV: <math>\pm 200 \text{ mrad}</math>; diameter: 20 - 40 cm.</p> <p>The goal is to build a prototype telescope (ideally two: one on-axis, one off-axis) and test for <math>\text{pm}/\sqrt{\text{Hz}}</math> stability and minimal backscatter while also evaluating the received and transmitted laser fields. Tests with a full telescope would lead to TRL 5 and allow a decision between a simple on-axis design and a more complex off-axis design.</p> <p>In-field guiding should be studied through design and simulation first, and the need should be evaluated against progress in other areas including mission design (orbits, lifetime). In-field guiding would require development of a mechanism that could change the direction of propagation of a beam without inducing any change in the optical path length.</p>
Scientific, Engineering, and/or Programmatic Benefits		<p>The telescope is one of the potential US contributions to an ESA-led L3 mission that addresses the “Gravitational Universe” science theme. It is also required for a potential future US-led laser-interferometric GW mission.</p>

<b>PCOS Applications and Potential Relevant Missions</b>	<p>Space-based laser-interferometric GW detectors such as LISA, SGO-Mid, or the European eLISA concept.</p> <p>Potentially other precision interferometric measurement applications.</p>
<b>Time to Anticipated Need</b>	<p><b>Named missions:</b> L3 (late 2020s / early 2030s)</p> <p><b>Development needed for 2020 Decadal:</b> Yes, L3</p> <p><b>Other drivers:</b> ESA is considering accelerating the L3 schedule in response to the recent GW detections and the LPF results. The earliest expected date for mission adoption would be 2020. Targeting TRL 6 by 2020 would enable NASA to offer the telescope as a contribution to L3. The schedule for a US-led mission would likely lag by 2-3 years.</p>



Gap Name		Low-mass, long-term-stability optical bench <i>Submitted by L3ST and General Community</i>
Description		Space-based laser-interferometric GW missions need optical benches to prepare, split, direct, and combine the different laser fields to form all required beat signals.
Current State-of-the-Art (SOTA)		<p>Europe developed the optical bench for LPF using an all Zerodur®, hydroxide-bonded bench (TRL 8 now). Recent LPF results show that the optical bench greatly exceeds the stability requirement. However, the assembly of the bench took very long and was always on or near the critical path. This technology does not scale well for the 4× larger LISA bench, which also carries 4× more components, and LISA requires six flight units instead of one.</p> <p>The European team is exploring a robotic assembly technique to reduce assembly time. This technology is probably at TRL 2 or 3. Alternatively, or more likely in addition, the optical bench could be re-designed to trade some of the performance margin in stability for ease in manufacturing. This technology is probably at TRL 2 or 3.</p>
TRL	SOTA	8
	Solution	2
Performance Goals and Objectives		<p>At least two approaches should be considered. The first is to develop a manufacturing technique to robustly produce optical benches using the LPF-proven approach but with reduced assembly time and labor. This is the approach being taken in Europe.</p> <p>The second approach is to re-visit the optical bench design and look for trades to reduce the difficulty of assembly at the expense of the significant performance margin in dimensional stability demonstrated by the LPF bench. This might include replacing some (or most) of the bench with a classical mechanical structure and only applying the labor-intensive hydroxy catalysis techniques for the most critical components. Composite structure using other materials such as single-crystal silicon and non-carbon-fiber-based composites should be investigated, as should metals.</p> <p>Key performance parameters are: dimensional stability of <math>\sqrt{(1+(1\text{mHz/f})^4)}</math> pm/<math>\sqrt{\text{Hz}}</math>; long-term-alignment stability; low mass; and assembly procedures that allow for small-scale manufacturability, perhaps through automation, modular design, simplified bonding techniques, and/or optical fiber techniques (LISA-like missions will require of order 10 optical benches, including 6 flight units, 1-2 spares, and additional units for ground testing).</p>
Scientific, Engineering, and/or Programmatic Benefits		<p>A lighter and easier-to-assemble optical bench would significantly reduce cost and programmatic risks associated with any complex assembly process.</p> <p>In addition, the bench could be a deliverable for NASA in the ESA-led mission which addresses the L3 “Gravitational Universe” science theme.</p>
PCOS Applications and Potential Relevant Missions		<p>NASA contribution to ESA’s L3 mission.</p> <p>Rapid (perhaps automated) construction of dimensionally stable optical structures could in principle be generalized to other applications including telescopes.</p>
Time to Anticipated Need		<p><b>Named missions:</b> L3 (late 2020s / early 2030s)</p> <p><b>Development needed for 2020 Decadal:</b> Yes, L3</p> <p><b>Other drivers:</b> ESA is considering accelerating the L3 schedule in response to the recent GW detections and the LPF results. The earliest expected date for mission adoption would be 2020. Targeting TRL 6 by 2020 would enable NASA to offer the optical bench as a contribution to L3. The schedule for a US-led mission would likely lag by 2-3 years.</p>

Gap Name		Phase measurement system (PMS) <i>Submitted by L3ST and General Community</i>
<b>Description</b>		<p>Space-based laser-interferometric GW missions measure the phase evolution of laser beat signals to monitor the minute length changes caused by GWs (<math>\sim \text{pm}/\sqrt{\text{Hz}}</math> level), extract the phase of the clock noise tones (<math>\sim 0.1</math> millicycle/<math>\sqrt{\text{Hz}}</math>), measure absolute spacecraft distances at the sub-meter level, and provide signals for phase-locking and arm-locking the lasers and for aligning the constellation.</p> <p>The PMS includes the analog front end, quadrant photo-receivers, anti-aliasing filters, and Analog to Digital Converters (ADCs). An ultra-stable oscillator (USO) and a frequency distribution system that includes frequency multipliers are also considered part of the PMS.</p>
<b>Current State-of-the-Art (SOTA)</b>		<p>A fully functional LISA Phasemeter has been developed to TRL 4. The system consists of many subcomponents which are at different TRLs. The most critical parts are the analog front end of the measurement system, which is at TRL 4.</p> <p>Quadrant photo-receivers based on COTS detectors have been developed at ANU, and a custom-designed detector with much lower capacitance (and therefore lower noise) has been developed through the Small Business Innovation Research (SBIR) program. Both alternatives need further development or at least flight qualification.</p> <p>The frequency multipliers in the frequency distribution system are at TRL 5. The phasemeter core is at TRL 6, although general advances in digital signal processing should be used to simplify and advance the capabilities of the PMS over time.</p> <p>A phasemeter has been developed to flight maturity for NASA's GRACE Follow-On mission, for the Laser Ranging Interferometer (LRI) instrument. The LRI phasemeter represents relevant flight heritage for a LISA-like missions. While several phasemeter performance requirements on the LRI are relaxed compare to LISA requirements, the LRI phasemeter is expected to meet LISA requirement levels.</p>
<b>TRL</b>	<b>SOTA</b>	4
	<b>Solution</b>	4
<b>Performance Goals and Objectives</b>		<p>Advance the maturity of the LISA Phasemeter based on the flight Phasemeter developed for LRI. There are several clear ways to achieve this:</p> <ol style="list-style-type: none"> <li>1. Test the LRI phasemeter to LISA performance requirements, thereby validating the technology for use in LISA.</li> <li>2. Incorporate flight LRI phasemeter developments, such as automatic laser lock acquisition sequences, into the TRL 4 LISA PMS.</li> <li>3. Study the best options for increasing channel count from the LRI to LISA phasemeters.</li> </ol> <p>Quadrant photo-receivers and ADCs should be developed to meet the original LISA requirements (which serve as benchmarks for all currently discussed mission designs) and reach TRL 5. These analog parts present the largest remaining risk for the PMS. Further development of the frequency multipliers requires a final mission design that includes a frequency distribution plan.</p>
<b>Scientific, Engineering, and/or Programmatic Benefits</b>		<p>The PMS, in the form discussed here, meeting the requirements presented here, is critical for all LISA-like missions. A working PMS with an adequate analog front end is also important for many tests for other subsystems in LISA-like missions such as the optical bench or the telescope.</p> <p>The PMS is a strategic technology with multiple uses in many areas; the initial phasemeter evolved out of the Blackjack receivers used in GPS. The analog front end would allow application to optical signals, which vastly improves the sensitivity compared to GPS.</p>

<b>PCOS Applications and Potential Relevant Missions</b>	<p>Space-based laser-interferometric GW detectors such as LISA, SGO-Mid, or the European L3 concept.</p> <p>GRACE follow-on missions.</p> <p>Other future interferometric missions; interferometry has been named as one of the crosscutting, game-changing technologies in the Astrophysics Roadmap.</p>
<b>Time to Anticipated Need</b>	<p><b>Named missions:</b> L3 (late 2020s / early 2030s)</p> <p><b>Development needed for 2020 Decadal:</b> Yes, L3</p> <p><b>Other drivers:</b> ESA is considering accelerating the L3 schedule in response to the recent GW detections and the LPF results. The earliest expected date for mission adoption would be 2020. Targeting TRL 6 by 2020 would enable NASA to offer the PMS as a contribution to L3. The schedule for a US-led mission would likely lag by 2-3 years.</p>

Gap Name		Non-contact charge control for Gravitational Reference Sensors (GRS) <i>Submitted by L3ST and General Community</i>
Description		<p>Space-based GW observatories like LISA use free-floating test masses (TMs) as references for measuring GWs. The free-floating TMs can become electrically charged due to cosmic-ray impacts and during release from the TM caging system. This charge introduces a force on the TM due to stray electric fields associated with the spacecraft, limiting the sensitivity of the entire system to GWs.</p> <p>A charge control system is needed to control the TM with respect to its housing. A standard approach used on flight accelerometers is to use a thin metallic wire for charge control. However, the mechanical coupling produced by these wires would introduce disturbances that exceed the requirements for a GW mission. Non-contact charge control units use ultraviolet (UV) light to control charge via the photoelectric effect.</p> <p>The LPF charge control system, which uses ultraviolet (UV) light generated by Hg lamps, operates in a maintenance mode. This means that it requires a pause in science operations in order to provide charge control. A charge control system that could operate without disturbing the science measurement would be advantageous.</p>
Current State-of-the-Art (SOTA)		<p>In the current LPF charge management design, UV light generated by Hg lamps is directed via a UV fiber feedthrough toward the TM surface if the goal is to increase the TM potential, or toward the electrode housing surface if the goal is to decrease the potential. The Hg-lamp-based charge management system on LPF was successfully demonstrated in 2016. The TRL in Europe is high (8).</p> <p>Non-contact charge control using deep-UV LEDs operating at 240 - 255 nm are a promising new UV source for controlling TM charge. Compared to the Hg lamps, UV LEDs are smaller, lighter, consume less power, have a wider spectrum selection, and have a higher dynamic range, with at least an order-of-magnitude improvement in each performance area.</p>
TRL	SOTA	8
	Solution	
Performance Goals and Objectives		<p>Develop a non-contact charge management system that can be integrated seamlessly into the LPF GRS, with bi-directional charge control at an average rate of 50 e/s.</p> <p>For maintenance activity, the charge control rate of the device needs to be increased by the maintenance duty cycle (~2 hrs/week) or ~9 ke/s.</p> <p>Demonstrate AC charge control in a low-disturbance environment and assess whether the science measurement is disturbed (TM force &lt; 1 fN/√Hz at modulation frequency).</p>
Scientific, Engineering, and/or Programmatic Benefits		Non-contact charge control is an essential element of a space-based GW instrument and will enable the science that has been endorsed by the past two decadal surveys. A charge management system is a candidate NASA contribution to the ESA-led L3 GW mission.
PCOS Applications and Potential Relevant Missions		GW observatories.
Time to Anticipated Need		<p><b>Named missions:</b> L3 (late 2020s / early 2030s)</p> <p><b>Development needed for 2020 Decadal:</b> Yes, L3</p> <p><b>Other drivers:</b> ESA is considering accelerating the L3 schedule in response to the recent GW detections and the LPF results. The earliest expected date for mission adoption would be 2020. Targeting TRL 6 by 2020 would enable NASA to offer the charge control as a contribution to L3. The schedule for a US-led mission would likely lag by 2-3 years.</p>



Gap Name		Gravitational Reference Sensor (GRS) <i>Submitted by L3ST and General Community</i>
Description		The ideal GRS is a free-falling TM subject only to the tidal forces caused by GWs. The GRS envisioned for LISA-like missions is a 2 kg gold/platinum cube surrounded by electrodes used to sense the position of the TM with respect to the spacecraft, and also apply forces to the TM in all non-sensitive directions. This GRS, as a technical unit, also includes the electrode housing, caging mechanisms, vacuum systems, and front-end electronics.
Current State-of-the-Art (SOTA)		The European GRS was successfully demonstrated on LPF, exceeding the LPF requirements and nearly meeting the LISA requirements. NASA has nothing comparable and it is difficult to assign a reasonable TRL for this specific case.
TRL	SOTA	8
	Solution	
Performance Goals and Objectives		The long-term target is to develop competency in the US in GRS technology. The immediate goals are to design and fabricate a TRL-3 electrode housing, to construct a torsion pendulum test facility to evaluate the performance of the GRS housing, and to develop capacitive readout and electrostatic actuation electronics, as well as an interferometric readout for calibration and high resolution measurements.
Scientific, Engineering, and/or Programmatic Benefits		GRS technology is absolutely critical for any GW detector mission. Having zero competency in the US puts us in a difficult position for a NASA-led mission which would address one of the leading science goals of the last two decadal surveys.
PCOS Applications and Potential Relevant Missions		LISA-like space-based GW missions and, with relaxed requirements, geodesy missions.
Time to Anticipated Need		NASA-led: TRL 3 by 2018 latest. TRL 5 by 2022.  ESA-led: TRL 3 by 2018 to develop competency and the possibility of alternative vendors should the single vendor in Italy become unavailable.

Gap Name		Precision Microthrusters
		<i>Submitted by L3ST</i>
<b>Description</b>		<p>GW observatories, large exoplanet observatories including the star shade concept, and potentially any astronomy or astrophysics observatory currently planning to use reaction wheels, demand extraordinary fine pointing and precision attitude control. Especially for the drag-free platforms necessary to measure GWs, high-precision microthrusters are necessary to meet <math>\sim 10 \text{ nm}/\sqrt{\text{Hz}}</math> position stability requirements.</p> <p>Microthrusters must have precise thrust steps (<math>\leq 0.1 \text{ } \mu\text{N}</math>) with low noise (<math>0.1 \text{ } \mu\text{N}/\sqrt{\text{Hz}}</math>) over a range of 5-50 <math>\mu\text{N}</math> for a primary application of a GW observatory. In all applications, higher specific impulse (<math>&gt;100 \text{ s}</math>) is also beneficial for low-mass systems.</p> <p>For example, studies have shown that using microthrusters instead of reaction wheels can actually be a net savings in terms of mass due to the elimination of heavy vibration isolation systems.</p> <p>Finally, a lifetime of <math>\geq 5</math> years is key for all major observatories. Currently, colloid microthrusters provide the most advanced microthruster technology, now being demonstrated on LPF, but still require a longer lifetime demonstration along with fully redundant architectures.</p>
<b>Current State-of-the-Art (SOTA)</b>		<p>Both cold-gas and colloid microthrusters are being demonstrated on LPF and other missions to reach TRL 7.</p> <p>Meeting once very challenging thrust-precision performance requirements is now absolutely feasible. However, many of these systems are single-string and only have space-based demonstrations on the order of 90 days of operation.</p> <p>To reach TRL 6 for flagship-class missions, additional developments and demonstrations of lifetime and reliability need to be addressed.</p> <p>PCOS SAT funding has already pushed a fully redundant colloid-thruster feed system to TRL 5 with enough capacity for a 5-year GW observatory mission. However, the fully redundant thruster system, including the thruster head itself, has not been tested, nor has lifetime been demonstrated greater than 1/3 of a year.</p>
<b>TRL</b>	<b>SOTA</b>	7
	<b>Solution</b>	5
<b>Performance Goals and Objectives</b>		<p>Performance targets have already been met by existing systems, such as the colloid microthruster. However, lifetimes of only <math>\sim 3000</math> hours have been demonstrated on the ground.</p> <p>For flagship-class missions, additional development regarding reliability, maintaining performance while improving redundancy, and lifetime (<math>\geq 5</math> year) demonstrations will be required prior to adoption and infusion.</p>
<b>Scientific, Engineering, and/or Programmatic Benefits</b>		<p>While the main application of precision microthrusters relates to drag-free GW observatories, further development of these systems would allow reaction wheel replacement on many future missions.</p> <p>Precision thrusters do not require the heavy vibration-isolation systems that current reaction wheel based systems (e.g., Hubble, Kepler, etc.) employ.</p> <p>Furthermore, if reliability and lifetime greater than current reaction-wheel technology can be proven, a leading cause to observatory failure (reaction-wheel failure) can be mitigated.</p>

<p><b>PCOS Applications and Potential Relevant Missions</b></p>	<p>The main application relates to GW observatory concepts that demand drag-free operation of the observing spacecraft. Other missions, such as exoplanet observatories or X-ray observatories that also require fine positioning and pointing, could also benefit.</p> <p>Eventually, precision microthrusters could be used to replace heavier and less-reliable reaction-wheel-based pointing systems on all future astronomy and astrophysics observatories.</p>
<p><b>Time to Anticipated Need</b></p>	<p><b>Named missions:</b> L3 (late 2020s / early 2030s)</p> <p><b>Development needed for 2020 Decadal:</b> Yes, L3</p> <p><b>Other drivers:</b> ESA is considering accelerating the L3 schedule in response to the recent GW detections and the LPF results. The earliest expected date for mission adoption would be 2020. Targeting TRL 6 by 2020 would enable NASA to offer the microthrusters as a contribution to L3. The schedule for a US-led mission would likely lag by 2-3 years.</p> <p>The main lifetime demonstration necessary for infusion of this technology requires 6-8 years for a 1-to-1 operational hour test. Such was the case for the now successfully infused ion engines, first demonstrated on Deep Space 1 and now used on Dawn, which had a 30,000-hour ground-based lifetime test that lasted approximately 5 years. Significant investment in microthruster technology now would be required to meet normal NASA standards of a <math>\geq 1.5\times</math> lifetime demonstration by mission PDR or Critical Design Review (CDR).</p>

Gap Name		High-performance gamma-ray telescope
		<i>Submitted by General Community</i>
Description		<p>Two technologies are needed to enable gaseous detectors, e.g., Time Projection Chambers (TPC), with large volumes, tens to hundreds of m<sup>3</sup>, to be inflated on orbit:</p> <ol style="list-style-type: none"> <li>1. The inflatable pressure shell must contain the detector gas at pressures up to ~3 Atm, be capable of self-sealing against micro-meteors, and have a surface density of &lt; 1 g/cm<sup>2</sup>.</li> </ol> <p>The TPC field-shaping electrodes are mounted on the inner surface of the inflatable shell and deploy as the shell inflates to positions accurate to ~1 mm.</p> <ol style="list-style-type: none"> <li>2. The TPC readout structure at the bottom of the TPC must unfold within the gas volume, be rigid, and have position accuracy of ~1 mm.</li> </ol>
Current State-of-the-Art (SOTA)		<p>Thin Red Line Aerospace developed and supplied 20 full-fidelity inflatable pressure shells of up to 320 m<sup>3</sup> volume for Bigelow Aerospace inflatable habitat Genesis spacecraft flight hardware. Thin Red Line designed, engineered, and manufactured the pressure-restraining hulls of Genesis 1 and 2 (launched 07/06 and 06/07, respectively), the first spacecraft on orbit successfully incorporating large-volume, high-stress inflatable architecture (other projects at <a href="http://www.thin-red-line.com/projects.html">http://www.thin-red-line.com/projects.html</a>).</p> <p>Large deployable mirrors have been developed for JWST. This technology could be adapted for the deployable TPC readout.</p>
TRL	SOTA	6
	Solution	
Performance Goals and Objectives		<p>The goal is to enable construction of a ~100 m<sup>3</sup> gamma-ray pair telescope with arcmin angular resolution and continuum sensitivity of better than <math>5 \times 10^{-7}</math> between ~100 MeV and ~10 GeV.</p> <p>The objectives can be met by demonstrating an inflatable TPC gas shell with volume ~10 m<sup>3</sup> at ~1 Atm and deployable readout electrodes with area of ~2 m<sup>2</sup>.</p>
Scientific, Engineering, and/or Programmatic Benefits		Inflatable gaseous detectors would enable gamma-ray telescopes to achieve arcmin angular resolution. Deployable 2-D readout structures within a large gas volume would increase telescope sensitivity.
PCOS Applications and Potential Relevant Missions		Arcmin gamma-ray telescope.
Time to Anticipated Need		<p><b>Named missions:</b></p> <p><b>Development needed for 2020 Decadal:</b> No</p> <p><b>Other drivers:</b> Applicability to Explorer opportunities.</p>



Gap Name		Fast, few-photon UV detectors
		<i>Submitted by General Community</i>
Description		Near-UV (300 – 400 nm) single-photon detectors for measuring from space atmospheric fluorescence light produced by particle cascades induced by ultra-high-energy cosmic rays (UHECR).
Current State-of-the-Art (SOTA)		<p>Current SOTA are multi-anode vacuum photomultipliers (PMTs). These are high TRL (quoted TRL applies only to these devices) and high performance, but are relatively costly per channel, heavy, sensitive to over-exposure, and delicate.</p> <p>Silicon photomultipliers (SiPM, also called multi-pixel photon counters or MPPC), based on arrays of avalanche-diode micro-pixels operating in quenched Geiger mode, are promising but current SOTA SiPM have unacceptable noise without cooling to <math>&lt; 20^{\circ}\text{C}</math>. In the large imaging arrays needed with <math>2 \times 10^5 - 1 \times 10^6</math> pixels, uncooled noise produces high false-detection rate and cooling consumes unacceptable power. Also, most SiPM are not optimized for near-UV detection (although thinned, back-side-illuminated SiPM are possible).</p>
TRL	SOTA	8
	Solution	
Performance Goals and Objectives		<ul style="list-style-type: none"> <li>Active area <math>8 \text{ mm}^2</math> to <math>300 \text{ mm}^2</math>;</li> <li>Active-area fraction <math>&gt; 85\%</math>;</li> <li>Read out at <math>&gt; 10 \text{ MHz}</math>;</li> <li>Suitable for use in <math>\geq 4 \text{ m}^2</math> arrays with <math>\geq 2 \times 10^5</math> detectors (pixels);</li> <li>QE at <math>330 \text{ nm} \geq 30\%</math> (goal <math>60\%</math>);</li> <li>Gain <math>\geq 10^4</math> to allow few-photon (single-photoelectron) detection;</li> <li>Noise <math>&lt; 10^6</math> counts/(<math>\text{mm}^2 \text{ sec}</math>) at half of single-photoelectron signal;</li> <li>Signal duration <math>&lt; 10 \text{ ns}</math>;</li> <li>Recovery from single-photoelectron pulse to <math>99.9\%</math> resolution of <math>10^3</math> photon pulse <math>&lt; 10 \text{ ns}</math>;</li> <li>Inactive area <math>&lt; 20\%</math> when in array (<math>&lt; 5\%</math> goal), and scalable detector (pixel) dimensions to match the imaging optics;</li> <li>Minimum mass (goal <math>&lt; 2 \text{ g/cm}^2</math>);</li> <li>Individual pixel readout is required; and</li> <li>Active lifetime <math>\geq 5</math> years (goal 10 years) with integrated background exposure <math>\geq 3 \times 10^{14}</math> photons/<math>\text{mm}^2</math>.</li> </ul>
Scientific, Engineering, and/or Programmatic Benefits		<p>This technology would enable focal planes for UHECR (see below) instruments to be built at a small fraction of the cost, mass, and power that would be required for the current SOTA. This would in turn vastly increase the probability that a useful space-based UHECR instrument could be built.</p> <p>Coupled with light-weight, low-cost optics, this could enable a pathfinder instrument to be built as a MDEX (possibly as a class-D SMEX, although this is ambitious).</p>
PCOS Applications and Potential Relevant Missions		<p>Focal planes for missions to measure UHECR by imaging, from LEO, the giant particle showers caused by UHECR (<math>E \geq 10^{18} \text{ eV}</math>) interacting in the Earth's atmosphere. This requires determining the time and spatial development of the UV light emitted by air fluorescence after excitation of atmospheric constituents, primarily <math>\text{N}_2</math>, by the particle cascade.</p> <p>A possible pathfinder mission, JEM-EUSO (Japanese Experiment Module Extreme Universe Space Observatory), is in the Astrophysics Roadmap but development would also be applicable to the more advanced OWL (Orbiting Wide-angle Light collectors) mission or other formulations. Detectors would also be important for ground Cherenkov arrays such as Cherenkov Telescope Array (CTA) and would have a variety of other astrophysics, accelerator, and medical imaging applications.</p>
Time to Anticipated Need		<p><b>Named missions:</b></p> <p><b>Development needed for 2020 Decadal:</b> No</p> <p><b>Other drivers:</b> Flight mission estimated no earlier than 2022 for JEM-EUSO or an OWL Pathfinder. Full balloon-flight prototype 2019.</p>

Gap Name		Lightweight, large-area reflective optics
		<i>Submitted by General Community</i>
Description		Lightweight, easily deployable mirror as the primary of a Schmidt telescope (or similar) for measurements from space of atmospheric fluorescence light in the near UV (~330 - 390 nm) produced by particle cascades induced by UHECRs.
Current State-of-the-Art (SOTA)		<p>SOTA is the optical system developed in NASA studies for the OWL mission concept, based on smaller mirrors that have flown. This was an f/1 Schmidt with 45° full FOV. The deployable primary mirror diameter was 7.1 m (Schmidt corrector diameter was 3.0 m, and focal plane was 2.3 m). This had eight petals, launching with the petals folded upward with four inner and four outer petals interleaved. After deployment, the outer ring of four petals unfolded and the inner ring unfolded and moved outward to form a uniform surface. The mass of the mirror and mechanisms was 581 kg.</p> <p>Publically accessible SOTA in inflatable mirror technology is a 7-m diameter microwave antenna in a convex-convex configuration with the reflective material on the inner surface of one of the sides. This requires highly UV-transparent material for the entrance surface.</p>
TRL	SOTA	5
	Solution	
Performance Goals and Objectives		<p>Spherical or piecewise-spherical surface when deployed with <math>\geq 50\%</math> (goal <math>\geq 90\%</math>) reflective area when compared to a complete spherical segment with the same solid angle. Reflector area <math>\geq 38 \text{ m}^2</math> and full FOV <math>\geq 45^\circ</math>. Needed resolution is <math>\sim 1</math> milliradian, <math>\geq 10^4</math> larger than the diffraction limit, so inflatable optics are one possible solution.</p> <p>Goal is for a <math>\sim 7</math>-m-diameter reflector to be compact enough when stowed for launch and light enough to facilitate a mission on a standard MIDEX-class launch vehicle or a vehicle similar to the SpaceX Falcon 9 using a <math>\leq 4.6</math>-m-diameter fairing. Goal for mass of solid 7-m mirror and mechanism (if any) is <math>&lt; 300 \text{ kg}</math>. Goal for mass of inflatable 7-m mirror is <math>\leq 5 \text{ kg}</math>. Long-term goal is <math>1,400 \text{ m}^2</math> reflector area with mass <math>\leq 100 \text{ kg}</math>.</p>
Scientific, Engineering, and/or Programmatic Benefits		<p>This technology would enable reflective optics for a UHECR (see below) mission to be built at a small fraction of the cost and mass of the OWL optics that represent the current SOTA. In turn, vastly increasing the probability that a useful space-based UHECR instrument could be built.</p> <p>Coupled with a lightweight, low-cost, high-performance focal plane and electronics, this could enable building a pathfinder instrument as a MIDEX (or class-D SMEX, though this is ambitious).</p>
PCOS Applications and Potential Relevant Missions		<p>Optics for missions to measure UHECR by imaging, from LEO, the giant particle showers caused by UHECR (<math>E &gt; 10^{18} \text{ eV}</math>) interacting in the Earth's atmosphere. This requires determining the time and spatial development of the UV light emitted by air fluorescence after excitation of atmospheric constituents, primarily <math>\text{N}_2</math>, by the particle cascade. A possible pathfinder mission, JEM-EUSO, using refractive (Fresnel) optics is in the Astrophysics Roadmap. However, this has not been selected for flight by any space agency. It is generally agreed that a full UHECR mission would use reflective optics similar to the Schmidt telescope designed for the NASA OWL mission. It is possible that an OWL-like pathfinder could fly in the same timeframe as JEM-EUSO.</p> <p>Extending the full measurement aperture down to <math>10^{18} \text{ eV}</math> to enable measurements of neutrinos from UHECR interactions with the CMB would require a 42-m-diameter reflector. This could only be achieved using a very light mirror such as an inflatable. If the lightweight technology could be applied to mirrors with better resolution, then a wide variety of missions would be enabled.</p>
Time to Anticipated Need		<p><b>Named missions:</b></p> <p><b>Development needed for 2020 Decadal:</b> No</p> <p><b>Other drivers:</b> Flight mission estimated no earlier than 2022 for JEM-EUSO or an OWL Pathfinder. Full balloon flight prototype 2019.</p>

Gap Name		Low-power time-sampling readout
		<i>Submitted by General Community</i>
Description		Time-sampling low-power readout electronics to measure pulse amplitude and photon-arrival time for detection from space of atmospheric fluorescence light in the near UV (~330 - 390 nm) produced by particle cascades induced by UHECRs using fast photodetectors (e.g., multi-anode vacuum photomultiplier or silicon photomultiplier).
Current State-of-the-Art (SOTA)		<p>SOTA are switched capacitor arrays with ~1024 sampling cells per channel and switching using a “domino” strobe that causes the input to be sampled continuously until stopped by an external signal. Some devices include onboard digitizer and others clock out charge to an external digitizer.</p> <p>Channels can be cascaded to increase depth.</p> <p>Effective resolution 9 to 11.5 bits. Reported power consumption at 200 MS/s (mega-samples per second) sampling (10× faster than needed) ~4 mW/channel.</p> <p>Development push is toward faster sampling rather than lower power consumption. Sample-to-sample timing is not constant, but can be calibrated.</p> <p>Most implementations require an external amplifier. A competing technology uses a series of delay lines acting as a circular analog memory. Sampling depth depends on the total delay that can be achieved. Depth of 1024 samples has been reported at 500 MS/s but same delay would have a depth of only 40 samples at 20 MS/s.</p>
TRL	SOTA	6
	Solution	
Performance Goals and Objectives		<ul style="list-style-type: none"> <li>• Sampling rate <math>\geq 20</math> MS/s for ~100 ns photon-arrival-time resolution (allowing photodetector pulse to overlap two samples);</li> <li>• Full time sampled <math>3 \times 10^{-4}</math> s so depth 6000 samples at 20 MS/s;</li> <li>• Usable dynamic range <math>\geq 11</math> bits per sample;</li> <li>• Charge resolution ~0.25 pC;</li> <li>• Readout clock speed ~10 – 33 MHz;</li> <li>• Operating power at 20 MS/s <math>\leq 0.5</math> mW/channel (goal 0.25 mW/channel) including any required amplification;</li> <li>• Area required including ancillary components <math>\leq 8</math> mm<sup>2</sup>/channel; and</li> <li>• Channels/ASIC <math>\geq 9</math>.</li> </ul>
Scientific, Engineering, and/or Programmatic Benefits		<p>This technology would enable readout electronics for UHECR (see below) instrument focal planes to be built with a small fraction of the cost and power that would be required for the current SOTA. In turn, this would vastly increase the probability that a useful space-based UHECR instrument could be built.</p> <p>Coupled with lightweight, low-cost, optics and high-performance photodetectors, this could enable building a pathfinder instrument as a MIDEEX (or class-D SMEX, though this is ambitious).</p>
PCOS Applications and Potential Relevant Missions		<p>Readout electronics for the focal planes of missions to measure UHECR by imaging, from LEO, the giant particle showers caused by UHECR (<math>E \geq 10^{18}</math> eV) interacting in the Earth’s atmosphere. This requires determining the time and spatial development of the UV light emitted by air fluorescence after excitation of atmospheric constituents, primarily N<sub>2</sub>, by the particle cascade.</p> <p>A possible pathfinder mission, JEM-EUSO, is in the Astrophysics Roadmap but development would also be applicable to the more advanced OWL mission or other formulations.</p>
Time to Anticipated Need		<p><b>Named missions:</b></p> <p><b>Development needed for 2020 Decadal:</b> No</p> <p><b>Other drivers:</b> Flight mission estimated no earlier than 2022 for JEM-EUSO or an OWL Pathfinder. Full balloon flight prototype 2019.</p>

Gap Name		Low-power comparators and logic arrays
		<i>Submitted by General Community</i>
Description		Low-power space-qualified pulse comparators and logic arrays to implement the event trigger logic for detection from space of atmospheric fluorescence light in the near UV (~330 - 390 nm) produced by particle cascades induced by UHECRs using fast photodetectors (e.g., multi-anode vacuum PMT or SiPM).
Current State-of-the-Art (SOTA)		<p><u>Comparators:</u> SOTA for low-power space-qualified comparators are CMOS devices with 1.2 V output voltage. Many devices are available, but lowest power consumption is ~10 mW/channel. No low-voltage output (0.5 V) comparator development for mobile devices seems to be underway.</p> <p><u>Logic:</u> General SOTA for low-power, space-qualified logic implementations are flash-based FPGAs using 1.2 V logic. It is difficult to define a specific SOTA because of the wide variation in numbers of logic cells and I/O lines. However, devices with <math>6 \times 10^5</math> logic cells suitable for UHECR applications, and <math>\geq 100</math> MHz maximum clock speed (<math>2.5\times</math> faster than needed), are available with power consumptions <math>\leq 100</math> mW. There is tremendous effort toward low-voltage (0.5-V) logic for mobile device applications, but to date this has not been fully realized in space-qualified versions.</p>
TRL	SOTA	9
	Solution	
Performance Goals and Objectives		<p><u>Comparator:</u></p> <ul style="list-style-type: none"> <li>• Voltage threshold range 2 mV to 0.5 V;</li> <li>• Nominal input voltage to 1 V, but overdrive tolerant to 5 V;</li> <li>• Response time <math>\leq 50</math> ns;</li> <li>• Output pulse 0.5 V;</li> <li>• Drive capability <math>\leq 600</math> Ohms;</li> <li>• Supply voltage <math>\leq \pm 5</math> V; and</li> <li>• Quiescent power consumption <math>\leq 0.7</math> mW/channel (goal 0.2 mW/channel).</li> </ul> <p><u>Logic:</u></p> <ul style="list-style-type: none"> <li>• FPGA or similar programmable logic with <math>\geq 6 \times 10^5</math> cells per device;</li> <li>• Clock speed 40 MHz;</li> <li>• I/O lines <math>\geq 210</math>;</li> <li>• Internal logic and I/O logic 0.5 V; and</li> <li>• Power consumption <math>\leq 25</math> mW per unit at 40 Mhz (goal 10 mW per unit).</li> </ul>
Scientific, Engineering, and/or Programmatic Benefits		<p>This technology would enable trigger electronics for UHECR (see below) instrument focal planes to be built with a small fraction of the power required for current SOTA. In turn, this would vastly increase the probability that a useful space-based UHECR instrument could be built.</p> <p>Coupled with lightweight, low-cost, optics and high-performance photodetectors and readout electronics, this could enable building a pathfinder instrument as a MDEX (or class-D SMEX, though this is ambitious).</p>
PCOS Applications and Potential Relevant Missions		<p>Event trigger components for missions to measure UHECR by imaging, from LEO, the giant particle showers caused by UHECR (<math>E \geq 10^{18}</math> eV) interacting in the Earth's atmosphere. This requires determining the time and spatial development of the UV light emitted by air fluorescence after excitation of atmospheric constituents, primarily <math>N_2</math>, by the particle cascade.</p> <p>A possible pathfinder mission, JEM-EUSO, is in the Astrophysics Roadmap but development would also apply to the more advanced OWL mission or other formulations. The proposed technology developments would enable a wide variety of other missions from flagships down to nano-sats.</p>
Time to Anticipated Need		<p><b>Named missions:</b></p> <p><b>Development needed for 2020 Decadal:</b> No</p> <p><b>Other drivers:</b> Flight mission estimated no earlier than 2022 for JEM-EUSO or an OWL Pathfinder. Ground tests (in conjunction with Telescope Array) or limited balloon flight tests ~2017. Full balloon flight prototype 2019.</p>



Gap Name		Lattice optical clock for Solar Time Delay mission and other applications <i>Submitted by General Community</i>
Description		<p>There are a number of probable applications of optical clocks in future PCOS missions. However, a particularly attractive one is looking for a suspected breakdown in General Relativity [e.g., T. Damour and G. Esposito-Farese, Phys. Rev. D <b>53</b>, 5541-5578 (1996)].</p> <p>Probably the most promising place to look for such a breakdown is in a possible small deviation of the space-curvature parameter gamma from unity, suggested by string theory or theories with additional dimensions.</p> <p>The present accuracy for gamma as determined by Doppler measurements of the solar time delay during the Cassini mission is <math>2.3 \times 10^{-5}</math>. A new determination with <math>3 \times 10^{-8}</math> or better accuracy could be made with a high-performance optical clock on a spacecraft near the L-1 point of the Earth-Sun system.</p>
Current State-of-the-Art (SOTA)		<p>Both Sr-87 and Yb-131 optical clocks have reached accuracies in the lab of better than <math>5 \times 10^{-18}</math> over periods of <math>10^4</math> s. This is better than precision of <math>1 \times 10^{-14}/(\sqrt{\text{Hz}})</math> down to <math>1 \times 10^{-6}</math> Hz needed for a high-accuracy Solar Time Delay mission, but has not yet been demonstrated at frequencies below <math>1 \times 10^{-4}</math> Hz.</p> <p>Also, the Physikalisch-Technische Bundesanstalt (PTB, National Metrology Institute) in Germany and the Istituto Nazionale di Fisica Nucleare (INFN, National Institute for Nuclear Physics) in Italy have jointly developed a transportable Sr-88 optical clock with a short term noise level of <math>4 \times 10^{-15}</math> at 1 second that is nearly ready for field use.</p> <p>Other groups in Europe are investigating other types of transportable optical clocks. Some components for cold-atom systems are being tested at a drop tower in Bremen, Germany, for future use in space.</p>
TRL	SOTA	
	Solution	
Performance Goals and Objectives		<p>A proposed Solar Time Delay mission was described by N. Ashby, P.L. Bender, J.L. Hall, et al. in "Measurement of gravitational time delay using drag-free spacecraft and an optical clock" [Relativity in Fundamental Astronomy, Proc. IAU Symp. No. <b>261</b>, 2009, P.K. Seidelman, S. Klioner, and M. Soffel, Eds., Int. Astron. Union].</p> <p>Optical time delay measurements would be made from a drag-free spacecraft near the L-1 point to a small transponder satellite during a period of about 20 days when the optical path between the satellites passed by the Sun. The transponder satellite would be in a two-year period orbit with an eccentricity of 0.37. The clock performance required is a precision of <math>1 \times 10^{-14}/(\sqrt{\text{Hz}})</math> down to <math>1 \times 10^{-6}</math> Hz and an accuracy of <math>1 \times 10^{-17}</math>.</p> <p>Other versions of Solar Time Delay missions are expected to be proposed in response to future PCOS requests for proposals.</p>
Scientific, Engineering, and/or Programmatic Benefits		<p>The primary scientific benefit of a Solar Time Delay mission would be a very strong test of General Relativity (GR). Looking for a small offset of <math>1 \times 10^{-7}</math> or less in the parameter gamma from solar time delay measurements is fairly widely believed to be the best candidate for detecting an effect on GR of its merger with quantum physics.</p> <p>Optical clocks are also expected to have high value in connection with spacecraft communications and navigation applications, and are listed under TA 5.4.1.3 in the May 2015 Draft NASA Technology Roadmaps. A Technology Candidate Snapshot for Cold Atom Lattice Optical Clocks is listed on page TA5-94. However, in view of the scientific benefits of a future PCOS Solar Time Delay Mission, technology development of optical clocks to the necessary TRL should also be listed under TA 8.1.</p>

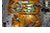


<p><b>PCOS Applications and Potential Relevant Missions</b></p>	<p>Before the proposed Solar Time Delay mission can be fully evaluated, demonstration of the necessary optical clock performance on the ISS may be needed. This will require vibration isolation and some additional precautions because of the on-board noise level. In view of the problem of frequency comparison between the ISS and ground, two clocks on the ISS operating under somewhat different conditions will need to be compared.</p> <p>This demonstration will facilitate applications to other NASA missions, as well as to the expected future PCOS Solar Time Delay mission. The operation on the ISS of the Projet d'Horloge Atomique par Refroidissement d'Atomes en Orbit (PHARAO) clock based on cooled Cs atoms with an accuracy of about <math>1e-16</math> and of a mercury trapped-ion clock will help provide experience on the requirements for optical clock operation.</p>
<p><b>Time to Anticipated Need</b></p>	<p><b>Named missions:</b></p> <p><b>Development needed for 2020 Decadal:</b> No</p> <p><b>Other drivers:</b> Discovery opportunities would benefit from TRL 6 by 2019.</p>

Gap Name		High-efficiency cooling systems for temperatures covering the range 20 K to below 1 K <i>Submitted by General Community</i>
Description		<p>Stable and continuous cooling systems with high thermal-lift capacity and efficiency are needed for the IP and planned X-ray and Far-IR missions.</p> <p>Refrigerators to reach 100 mK are needed, especially refrigerators that are stable, continuous, low mass, have long lifetimes, and are low cost. The cost of reaching 100 mK is an impediment to small or mid-size missions that incorporate sensors requiring such low operating temperatures.</p>
Current State-of-the-Art (SOTA)		<p>The Planck satellite demonstrated continuous cooling to 20 K and 4 K for four years, and continuous cooling to 0.1 K for 2.5 years.</p> <p>The demonstrated open-cycle dilution refrigerator on Planck does not scale to higher power loading. Approaches based on adiabatic demagnetization refrigeration (ADR), <math>^3\text{He}</math> sorption cooling, or closed-cycle dilution offer avenues to provide improved performance.</p>
TRL	SOTA	6
	Solution	
Performance Goals and Objectives		<p>Continuous and stable cooling to 100 mK without cryogens. Cost reductions of 3-5× compared to 100 mK refrigerators demonstrated to date. Mass reductions of 2-3× compared to 100 mK refrigerators demonstrated to date.</p> <p>The cooling power must be increased beyond that provided by the Planck system for large focal planes, and the implementation simplified for lower-cost mission opportunities.</p>
Scientific, Engineering, and/or Programmatic Benefits		<p>Enables next-generation measurements of CMB polarization, Athena, and high-resolution photon counting.</p> <p>Enables improved sensor performance.</p> <p>Enables 100 mK sensors on small or mid-size missions.</p> <p>Extends mission lifetimes.</p>
PCOS Applications and Potential Relevant Missions		IP, Explorer, and international CMB polarization and absolute spectrum experiments; X-ray applications with cryogenic detectors; and Far-IR instrumentation.
Time to Anticipated Need		<p><b>Named missions:</b> IP (2020s), Athena</p> <p><b>Development needed for 2020 Decadal:</b> Yes, IP and XRS</p> <p><b>Other drivers:</b> IP technology development is a NWNH priority that was recently revisited by the mid-Decadal review.</p> <p>International and Explorer implementations of the IP have proposed launch dates during the second half of the next decade.</p>



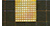




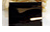
# Appendix B

## Program Technology Development Quad Charts



### Gravitational Waves

	<b>Jordan Camp</b> – “Demonstration of a TRL-5 Laser System for LISA” . . . . .	64
	<b>William Klipstein</b> – “Gravitational-Wave-Mission Phasemeter Technology Development” . . . . .	65
	<b>Jeffrey Livas</b> – “Telescopes for Space-Based Gravitational-Wave Observatories”. . . . .	66

### X Rays

	<b>Mark Bautz</b> – “Directly Deposited Optical-Blocking Filters for Imaging X-ray Detectors” . . . . .	67
	<b>David N. Burrows</b> – “Fast Event Recognition for the Athena Wide-Field Imager”. . . . .	68
	<b>Caroline Kilbourne</b> – “Providing Enabling and Enhancing Technologies for a Demonstration Model of the Athena X-IFU” . . . . .	69
	<b>Randall L. McEntaffer</b> – “Reflection Grating Modules: Alignment and Testing” . . . . .	70
	<b>Paul B. Reid</b> – “Development of 0.5-Arcsecond Adjustable Grazing-Incidence X-ray Mirrors for the SMART-X Mission Concept” . . . . .	71
	<b>Mark L. Schattenburg</b> – “Advanced Packaging for Critical-Angle X-ray Transmission Gratings” . . . . .	72
	<b>Joel Ullom</b> – “Technology Development for an AC-Multiplexed Calorimeter for Athena” . . . . .	73
	<b>William W. Zhang</b> – “Next-Generation X-ray Optics: High Angular Resolution, High Throughput, and Low Cost” . . . . .	74

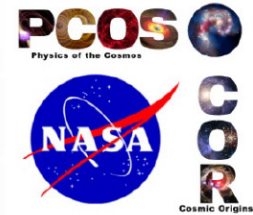
### Cosmic Microwave Background

	<b>James J. Bock</b> – “Planar Antenna-Coupled Superconducting Detectors for CMB Polarimetry” . . . . .	75
	<b>Edward J. Wollack</b> – “High-Efficiency Feedhorn-Coupled TES-based Detectors for Cosmic Microwave Background Polarization Measurements”. . . . .	76



# Demonstration of a TRL-5 Laser System for LISA

PI: Jordan Camp / GSFC



## Objectives and Key Challenges:

- Develop 2.5-W light source for the LISA gravitational-wave (GW) mission using a Master Oscillator Power Amplifier design with a novel diode laser oscillator (External Cavity Laser, ECL) followed by a 2.5-W Yb fiber amplifier, providing a highly stable, compact, and reliable system
- Test the laser system for reliability, and for amplitude and frequency stability, achieving the required noise performance
- Demonstrate system TRL 5
- Develop with industrial partner (Redfern Integrated Optics, RIO) space-qualified, ultra-low-noise oscillator
- Demonstrate low-noise power amplifier with servo controls
- Noise and reliability tests of full laser system

## Significance of Work:

- Required for LISA or any similar GW mission

## Approach:

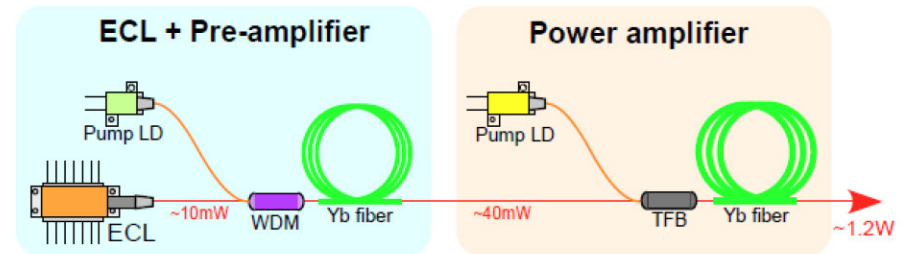
- Noise optimization of 1064-nm ECL (RIO)
- Reliability study of ECL
- Implementation of amplitude and frequency servo controls on full laser system, achieving:
  - $RIN = 10^{-4}$  at  $10^{-3}$  Hz;
  - Frequency noise =  $300 \text{ Hz} / \text{Hz}^{1/2}$  at  $10^{-2}$  Hz; and
  - Differential phase noise =  $6 \times 10^{-4} \text{ rad/Hz}^{1/2}$  at  $10^{-2}$  Hz

## Key Collaborators:

- Kenj Numata, Mike Krainak (NASA/GSFC)
- Lew Stolpner (RIO)

## Development Period:

- Apr 2014 – Dec 2016



**Master Oscillator / Power Amplifier (MOPA)** configuration of LISA laser, including ECL, preamp, and diode-pumped Ytterbium (Yb) fiber amplifier. All components have been tested for noise and reliability except for amplifier reliability, to be tested by fall 2016

## Accomplishments:

- ✓ Fabricated world's first butterfly package layout 1064 nm ECL
- ✓ Procured long lead items: fiber splicers and coaters
- ✓ Developed and constructed 2.5-W laser amplifier
- ✓ Noise tested laser system with ECL
- ✓ Tested reliability of ECL and preamp

## Next Milestones:

- Amplifier reliability tests (Sep 2016)
- ECL optical cavity noise level optimization (Nov 2016)
- Full laser system monitoring (Dec 2016)

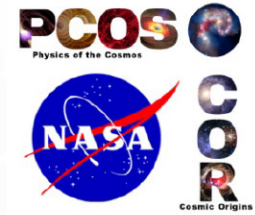
## Applications:

- Laser source for LISA GW mission
- Oscillator for ground-based GW LIGO project
- Oscillator for GRACE-II mission

$TRL_{In} = 3$   $TRL_{Current} = 3$   $TRL_{Target} = 5$

# Gravitational-Wave-Mission Phasemeter Technology Development

PI: William Klipstein / JPL



## Objectives and Key Challenges:

- Advance our phase-measurement system from TRL 4 to 5 through significant system-level hardware-fidelity increase and greater fidelity of signal-test environment by adding low light levels
- Mature the TRL of phase readout with high strain sensitivity through micro-cycle/ $\sqrt{\text{Hz}}$  precision on a 4-16 MHz beat-note in the presence of laser frequency noise and local clock noise, already demonstrated in a lab testbed

## Significance of Work:

- High-performance phase readout is an enabling technology for multi-spacecraft laser-interferometer-based missions such as LISA-like gravitational-wave missions

## Approach:

- Advance component technologies
  - Infuse compatible EM hardware from GRACE Follow-On Laser-Ranging Interferometer (LRI)
  - Demonstrate wavefront sensing with quadrant photoreceivers
- System-level testing
  - Modify interferometer test-bed to include low-light signals
  - Replace COTS components in interferometer test-bed with LRI EM hardware and demonstrate performance

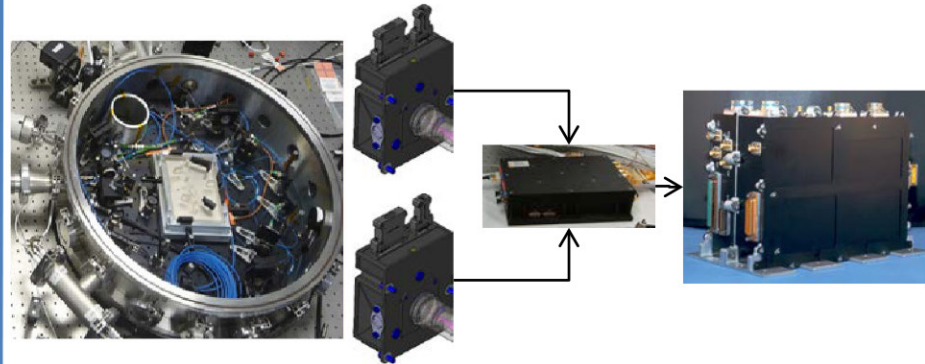
## Key Collaborators:

- Jeff Dickson, Brent Ware, Bob Spero, Kirk McKenzie, Andrew Sutton, and Chris Woodruff (JPL)

## Current Funded Period of Performance:

Apr 2014 – Dec 2016

EM Hardware (quadrant photoreceivers, preamp, and phasemeter) infused into the LISA test-bed



## Recent Accomplishment:

- ✓ Demonstrated phase readout with micro-cycle/ $\sqrt{\text{Hz}}$  precision in the presence of laser frequency noise and local clock noise in an interferometer test-bed

## Next Milestones:

- Incorporate quadrant photoreceivers into test-bed (Sep 2016)
- Demonstrate wavefront sensing (Sep 2016)
- Migrate additional photoreceiver algorithms from LabView phasemeter to EM (Oct 2016)
- Incorporate EM photoreceivers and signal chain (Nov 2016)
- Demonstrate tracking of low-visibility signals with EM Phasemeter (Dec 2016)
- Demonstrate test-bed performance at TRL 5 or higher (Dec 2016)

## Applications:

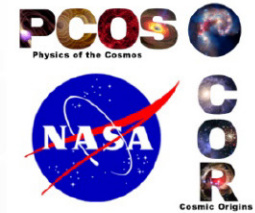
- Inter-spacecraft laser interferometry and pm-precision interferometer readout electronics for future missions, e.g., LISA
- Other interferometry concepts (e.g., planet searches)

$TRL_{In} = 4$     $TRL_{Current} = 4$     $TRL_{Target} = 5$



# Telescopes for Space-Based Gravitational-Wave Observatories

PI: Jeffrey Livas / GSFC



## Objectives and Key Challenges:

- Design, fabricate, and test a lightweight eLISA telescope design in a flight-like environment and demonstrate the ability to satisfy mission requirements for low scattered light and high dimensional stability in time for selection for the eLISA L3 Mission Opportunity
- Key Challenge 1: dimensional stability
- Key Challenge 2: stray-light performance

## Significance of Work:

- First demonstration of a validated scattered-light model combined with a previous demonstration of dimensional stability will provide a firm basis for a realistic engineering model design for a flight-qualifiable telescope
- Potential technology contribution to ESA L3 Cosmic Visions

## Approach:

- Use requirements developed for existing telescope
- Modify based on experience
- Merge a high-thermal-conductivity material in a simple symmetric mechanical configuration with a low-scatter optical design
- Fabricate and test for compliance with specifications

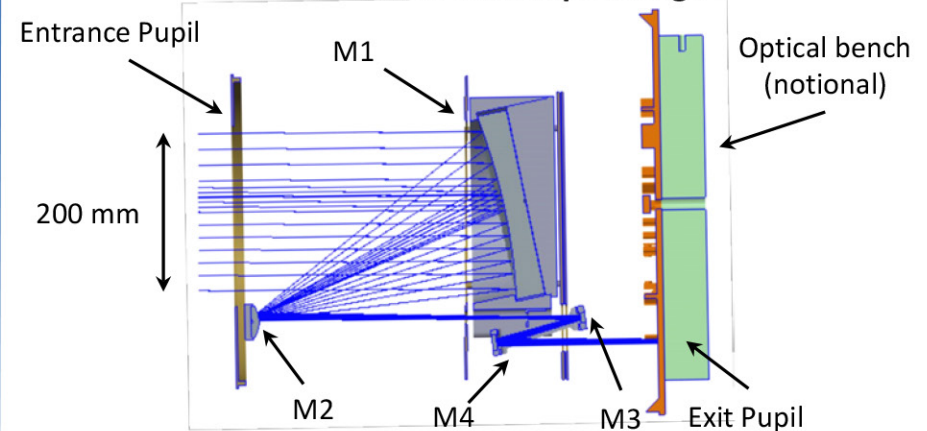
## Key Collaborators:

- J. Howard, G. West, P. Blake, L. Seals, R. Shiri, J. Ward (NASA/GSFC)
- Prof. Guido Mueller (University of Florida)

## Currently Funded Period of Performance:

Oct 2015 – Sep 2017

## Section View of Telescope Design



## Recent Accomplishments:

- ✓ Optical design optimized and toleranced
- ✓ High level mechanical model developed
- ✓ Procurement paperwork submitted

## Key Milestones:

- Design preparation/initiate purchase (May 2016)
- Award contract (Sep 2016)
- Telescope delivery (Dec 2017)
- Demonstrate low scatter performance (Jul 2017)
- Demonstrate optical path-length stability (Sep 2018)

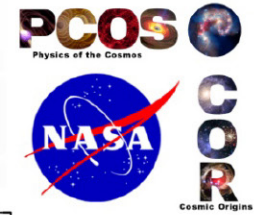
## Applications:

- Flagship gravitational wave missions (eLISA)
- Laser ranging and/or communications
- precision metrology applications

$TRL_{In} = 3$   $TRL_{Current} = 3$   $TRL_{Target} = 4$

# Directly Deposited Optical-Blocking Filters for Imaging X-ray Detectors

PI: Mark Bautz / MIT



## Objectives and Key Challenges:

- Silicon imaging X-ray detectors require thin filters (<300 nm) to block noise/background from UV and optical light
- State-of-the-art, free-standing filters use fragile, thin substrates
- Objective: deposit blocking filter directly on CCD X-ray detector, eliminating substrate
- Challenges:
  - Deposit filter directly without compromising CCD performance
  - Deposit sufficiently thin, uniform filters

## Significance of Work:

- Filter deposited on detector requires no fragile substrate
- Allows cheaper, more robust sensors (no vacuum housing!)
- Improves QE and makes larger focal planes practical

## Approach:

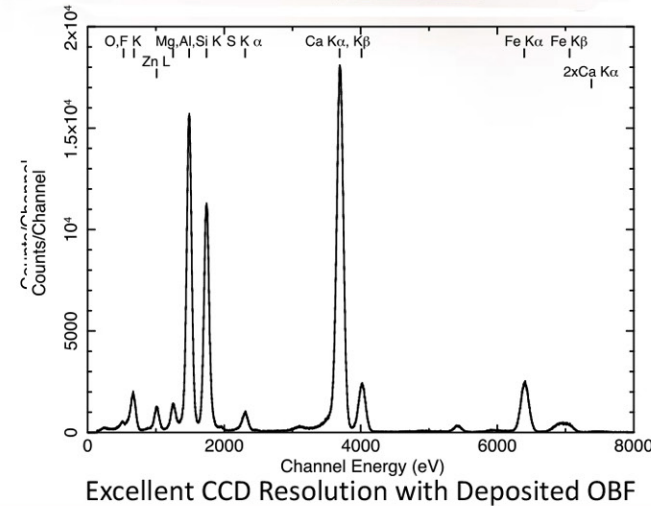
- Exploit existing stocks of (engineering grade/flight spare) X-ray CCD detectors at MIT Lincoln Laboratory
- Screen, thin, passivate, package, and apply filters to detectors
- Filter is Al with AlO<sub>2</sub> cap
- Start thick (220 nm Al), get progressively thinner
- Use existing MIT facilities for X-ray characterization
- Use existing and upgraded facilities for optical characterization

## Key Collaborators:

- Bautz and Kissel (MIT Kavli Institute)
- Suntharalingam, Ryu, Burke, and O'Brien (MIT Lincoln Laboratory)

## Current Funded Period of Performance:

Jul 2012 – Jun 2017



## Recent Accomplishments:

- ✓ Reduced pinhole fraction to < 1% (OD<7) for 220-nm OBF
- ✓ Tested devices with 70 nm and 100 nm thick Al OBF; optical blocking as expected
- ✓ With REXIS, developed and qualified underside coating as effective countermeasure for near-IR leakage through package
- ✓ Supported environmental tests of REXIS flight CCDs/OBFs

## Next Milestones:

- Continue long-term stability test; no degradation in 8 months (Mar 2017)
- Complete post-environmental REXIS OBF performance test and **demonstrate TRL 6, surpassing project goals** (May 2017)

## Applications:

Every X-ray imaging or grating spectroscopy mission

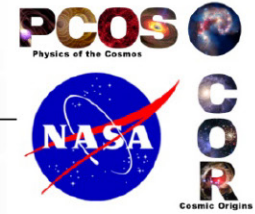
- Explorers (ETA, STAR-X, Arcus, etc.)
- "Probes" (AEGIS, N\_XGS, AXSIO, WFX, etc.)
- Flagship (Athena, X-ray surveyor)

TRL<sub>in</sub> = 5    TRL<sub>Current</sub> = 5    TRL<sub>Target</sub> = 6



# Fast Event Recognition for the Athena Wide-Field Imager

PI: David Burrows / PSU

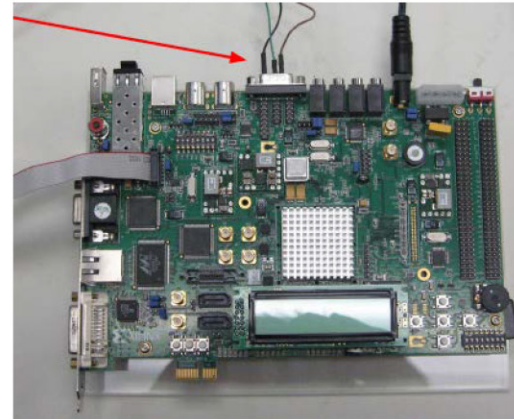


## Objectives and Key Challenges:

- High-speed event recognition and data compression

## Significance of Work:

- Required for several proposed X-ray imagers, including Athena WFI (ESA L2), JANUS XCAT (EX), XTIDE XCAT (SMEX), Arcus (MIDEX), X-ray Surveyor (Astrophysics Roadmap)



Virtex-5 OpenSPARC Evaluation Platform, designed to be a flexible development board for testing high-speed Virtex-5-class FPGAs

## Approach:

- FPGA coding/simulation/testing
- Testing with fixed patterns up to 1GBps
- Testing with real X-ray data up to 1GBps

## Key Collaborators:

- Dr. Karl Reichard and Eli Hughes (PSU/ARL)
- Dr. Abe Falcone and Dr. Tyler Anderson (PSU/ECOS)
- Dr. Mark Bautz (MIT)
- Dr. Ralph Kraft (SAO)

## Current Funded Period of Performance:

Jan 2015 – Dec 2016

## Recent Accomplishments:

- ✓ Completion of Line Processor testing
- ✓ Design of full single-channel ERP
- ✓ Schematic design and PC layout of single-channel ERP board

## Next Milestones:

- Fabrication and test single-channel ERP board (Aug 2016)
- TRL review (Nov 2016)

## Applications:

- Athena WFI (ESA L2)
- JANUS XCAT (EX)
- XTIDE XCAT (SMEX)
- Arcus (MIDEX)
- X-ray Surveyor (Astrophysics Roadmap)

$TRL_{In} = 3$   $TRL_{Current} = 3$   $TRL_{Target} = 4$

# Providing Enabling and Enhancing Technologies for a Demonstration Model of the Athena X-IFU

PI: Caroline Kilbourne / GSFC



## Objectives and Key Challenges:

- Develop large-format arrays of X-ray microcalorimeters and their readout for ESA's Athena X-IFU
- Support European-led primary technology demonstrations using GSFC arrays read out with frequency domain multiplexing (FDM)
- Advance TRL of time/code-division multiplexer (TDM/CDM) to maintain a viable back-up readout scheme

## Significance of Work:

- This solid demonstration of core technologies coupled with demonstrations of targeted enhancements will enable the best possible instrument for Athena
- This development enabled NASA participation in the Athena mission

## Approach:

- Develop large-scale testing infrastructure for Athena technology demonstrations and kilo-pixel array characterization
- Optimize SQUID TDM/CDM components and electronics
- Integrate full Athena-scale TES arrays (Mo/Au TES with Au/Bi absorbers) with optimized multiplexed readout
- Provide arrays for European-led technology demonstrations using FDM
- Develop fabrication techniques for mission-enhancing 'hybrid' arrays

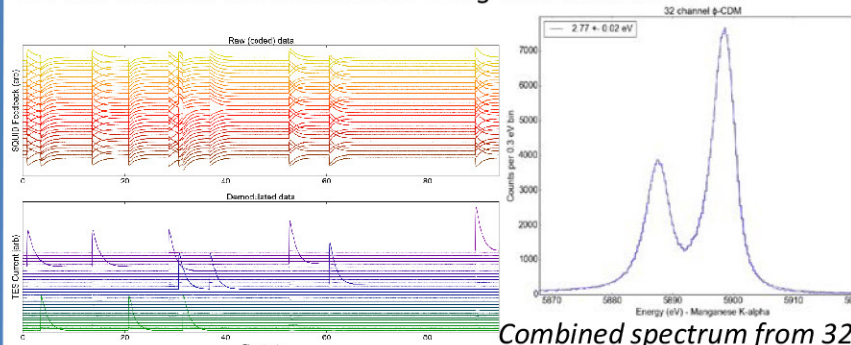
## Key Collaborators:

- J. Adams, S. Bandler, R. Kelley, R.S. Porter, S. Smith, and J. Chervenak (GSFC)
- J. Ullom, W. B. Doriese, and C. Reintsema (NIST)
- K. Irwin (Stanford University)

## Current Funded Period of Performance:

Oct 2015 – Sep 2017

Reaching multiplexer speed and noise goals enabled breakthrough 32-row readout demonstrations using both TDM and CDM



Example raw and demultiplexed TES pulses from CDM demonstration shows  $2.77 \pm 0.02$  eV resolution (FWHM)

## Recent Accomplishment:

- ✓ Multiplexed 32 rows in single column with an average resolution at 6 keV of  $2.55 \pm 0.01$  eV using TDM and  $2.77 \pm 0.02$  eV using CDM

## Next Milestones:

- Complete 3-column  $\times$  32-row TDM demonstration of  $32 \times 32$  array with better than 3 eV resolution at 6 keV (Sep 2016)
- Provide uniform  $32 \times 32$  array for Athena demonstration model and assist with 2-column  $\times$  40-row FDM technology demonstration (also requires  $< 3$  eV resolution at 6 keV) (early 2017)

## Applications:

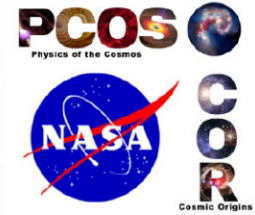
- Contribution to the Athena mission's X-IFU instrument
- Other potential missions needing high-resolution imaging X-ray spectroscopy

TRL<sub>In</sub> = 4    TRL<sub>Current</sub> = 4    TRL<sub>Target</sub> = 5



# Reflection Grating Modules: Alignment and Testing

PI: Randall L. McEntaffer / PSU



## Objectives and Key Challenges:

- Implement an alignment methodology specific to off-plane reflection gratings
- Populate a module with aligned gratings achieving spectral resolution  $> 3000 (\lambda/\delta\lambda)$  with high throughput over the 0.2-2.0-keV band
- Advance the OP-XGS technology to TRL 5

## Significance of Work:

- Enables high throughput and high spectral resolving power below 2 keV, where the majority of X-ray spectral features reside
- This will be the first time that multiple off-plane gratings have been aligned at this tolerance level with associated performance testing

## Approach:

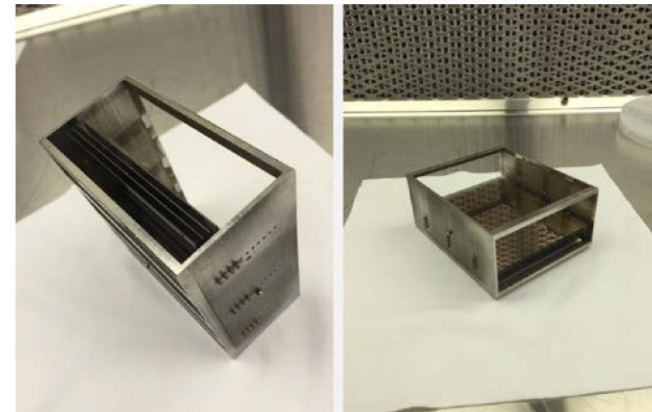
- Quantify alignment tolerances
- Formulate alignment methodology
- Implement alignment methodology
- Performance- and environmental-test an aligned module

## Key Collaborators:

- Will Zhang (NASA/GSFC)
- Jessica Gaskin (NASA/MSFC)

## Current Funded Period of Performance:

Jan 2015 – Dec 2016



An aligned grating module assembly incorporating four full-format (75 mm × 96 mm × 0.5mm) off-plane diffraction gratings

## Recent Accomplishments:

- ✓ TRL 4 vetted
- ✓ Alignment setup used to align four flight-like gratings into a high-fidelity module
- ✓ The module has been performance- and environmental-tested at the Stray Light Facility at MSFC

## Next Milestone:

- Analyze and publish performance/environmental test results from MSFC (Q3-Q4 2016)

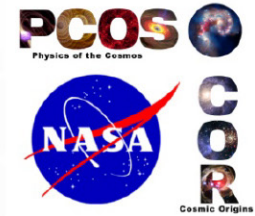
## Applications:

- Large X-ray observatories
- Explorer-class missions
- Suborbital-rocket investigations

$TRL_{In} = 4$   $TRL_{Current} = 4$   $TRL_{Target} = 5$

# Development of 0.5-Arcsecond Adjustable Grazing-Incidence X-ray Mirrors for the SMART-X Mission Concept

PI: Paul Reid / SAO



## Objectives and Key Challenges:

- Develop an alignment and mounting scheme consistent with a large-area, high-resolution X-ray telescope ( $> 2\text{m}^2$  and  $0.5''$ ) that accommodates many ( $\sim 100$ ) closely packed mirror segments, aligned to  $0.25'' = \text{Chandra alignment}$  (mounting distortions  $< 1\text{ }\mu\text{m}$  P/V (correctable with adjusters)
- Approach must allow calibration of mirror surface figure as each segment is mounted so that figure can be corrected before next segment is aligned
- Incorporate developments in high-connection-density flexible cabling and row-column addressing to minimize and simplify electrical connections for mirror-adjuster command and control

## Significance of Work:

- Enables adjustable optics to correct mounting-induced distortion and on-orbit thermal changes with LCD-display electrical simplicity

## Approach:

- Investigate Anisotropic Conductive Films (ACFs) for high connection density (up to 100 contacts/mm)
- Develop ZnO thin film transistor over-layer with insulating top layer for row-column addressing and ease of electrical-contact routing
- Through structural and thermal analysis and design, incorporate and extend alignment and mounting approach being developed for APRA TRL4 X-ray test

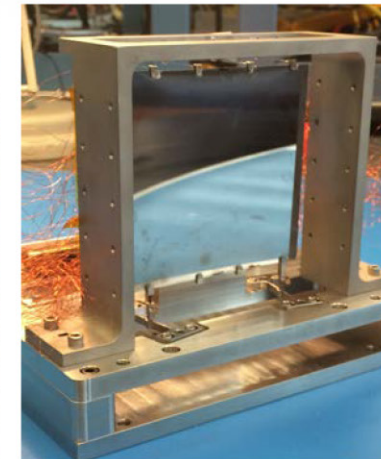
## Key Collaborators:

- Susan Trolier-McKinstry, Tom Jackson, and Tianning Liu (PSU)
- Brian Ramsey and Steve O'Dell (MSFC)

## Current Funded Period of Performance:

Proposed Jan 2015 – Dec 2016

Funding available Apr 2015, so plan Apr 2015 – Mar 2017



Single shell mounting concept with a mounted adjustable mirror

## Recent Accomplishments:

- ✓ Generated preliminary thermal control system requirements
- ✓ Demonstrated ZnO TFT row-column addressing on flat test mirror
- ✓ Demonstrated ACF connections on flat test mirror

## Next Milestones:

- High-fidelity deterministic figure control test (Nov 2016)
- Development of ACF connectivity on conical optics (Nov 2016)
- X-ray-test mounted, corrected, and aligned mirror pair (May 2017)

## Application:

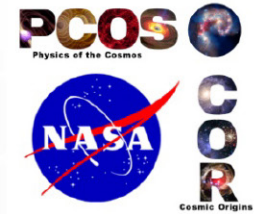
- X-ray Surveyor (formerly SMART-X) mission concept

$TRL_{In} = 3$     $TRL_{Current} = 3$     $TRL_{Target} = 4$



# Advanced Packaging for Critical-Angle X-ray Transmission Gratings

PI: Mark Schattenburg / MIT



## Objectives and Key Challenges:

- Develop key technology to enable a Critical-Angle Transmission X-ray Grating Spectrometer (CATXGS), advancing to TRL 6 in preparation for proposed mid- and large-size missions over the next decade
- Develop improved grating fabrication processes
- Develop frame mounting, alignment, and assembly techniques for CAT grating arrays

## Significance of Work:

- Improved diffraction efficiency and resolving power for CATXGS
- Ability to manufacture large-area, light-weight grating arrays

## Approach:

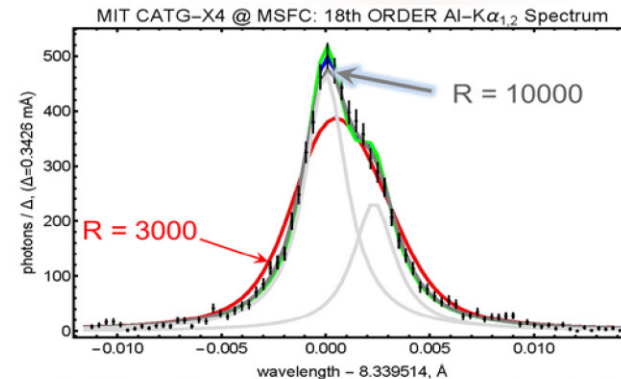
- Integrated wafer front/back-side fabrication process using silicon-on-insulator (SOI) wafers
- Wafer front side: CAT grating and Level 1 support structure
- Wafer back side: Level 2 support mesh structure
- CAT grating fabricated by deep reactive-ion etching (DRIE) followed by KOH polishing
- Bonded to expansion-matched metal support frame (Level 3)
- X-ray tests of prototypes at synchrotron and MSFC facility
- Environmental tests to advance TRL

## Key Collaborators:

- William Zhang (GSFC)
- Steve O'Dell (MSFC)

## Current Funded Period of Performance:

Jan 2015 – Dec 2016



Spectrum of Al K $\alpha_{1,2}$  lines: measured (black), natural width (individual, light gray; combined, green); natural width with R = 3000 broadening (red); natural width with R = 10,000 broadening (dark gray).

## Recent Accomplishments:

- ✓ Demonstrated extension of bandpass toward higher energies and/or increase in critical angle through atomic layer deposition of platinum on silicon CAT gratings
- ✓ Demonstrated resolving power  $R > 10,000$  at the MSFC Stray Light Facility, using GSFC mirror and 30-mm-wide CAT gratings

## Next Milestones:

- Bond gratings to frames (2017)
- Demonstrate X-ray performance of aligned gratings with prototype frame assembly after environmental tests to achieve TRL 5 (fall 2018)

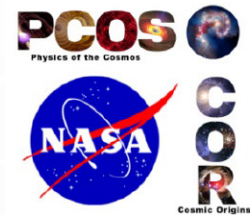
## Application:

- Flagship X-ray missions
- Explorer X-ray missions
- Laboratory X-ray analysis (materials science, energy research)

TRL<sub>In</sub> = 3    TRL<sub>Current</sub> = 4    TRL<sub>Target</sub> = 6

# Technology Development for an AC-Multiplexed Calorimeter for Athena

PI: Joel Ullom / NIST



## Objectives and Key Challenges:

- Increase TRL of AC-biased Transition-Edge Sensor (TES) X-ray microcalorimeters from 3 to 4
- To achieve this, demonstrate that AC-biased TESs can meet the anticipated performance requirements of ESA's Athena mission, in particular, that AC-biased TESs can routinely achieve energy resolutions of 2.5 eV or better at 6 keV
- The key challenge is that, so far, TESs under AC bias do not have as good energy resolution as under DC bias

## Significance of Work:

- AC-biased TESs and Frequency Division Multiplexing (FDM) are the baseline readout architecture for Athena; the performance of this approach strongly impacts mission design and success

## Approach:

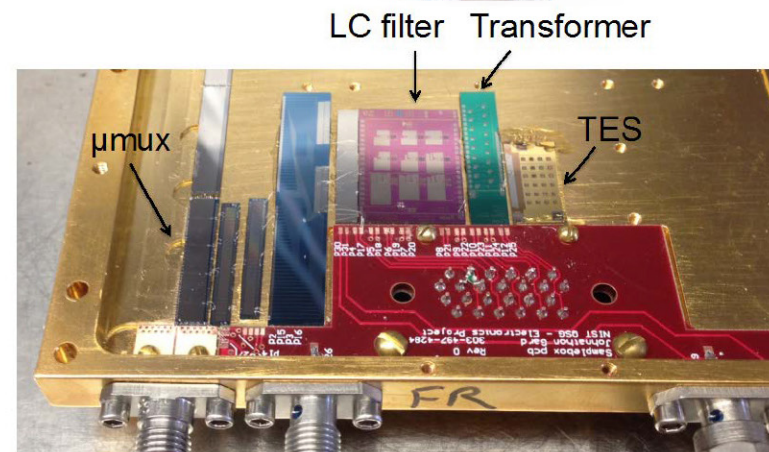
- Study the behavior of single GSFC TESs under AC bias
- In one experiment, maximize the use of readout components from the European Athena team
- In a second experiment, separate the effects of the readout system from the TES by using a novel, open-loop readout architecture based on microwave SQUID amplifiers
- Study interactions among small numbers of AC-biased TES devices

## Key Collaborators:

- Caroline Kilbourne, Simon Bandler, and Richard Kelley (GSFC)
- Kent Irwin (Stanford University)

## Current Funded Period of Performance:

FY 2015 – FY 2016



Sample box for readout of AC-biased TESs using open-loop microwave SQUIDs

## Recent Accomplishments:

- ✓ Completed two new complementary measurement platforms for characterizing AC-biased TESs
- ✓ Successfully demonstrated microwave-SQUID-based readout capable of measuring TESs at a sample rate of 8 MHz
- ✓ Demonstrated 2.9 eV energy resolution for AC-biased TESs @ 6keV

## Next Milestones:

- Characterize AC-biased TESs with both FDM and microwave SQUID amplifiers (Q4 FY16)
- Study interactions among AC-biased TESs (Q4 FY16)

## Applications:

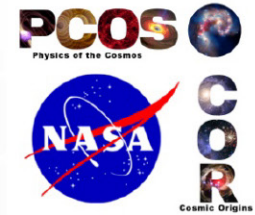
- Athena and future X-ray missions based on TES microcalorimeters

$TRL_{In} = 3$   $TRL_{Current} = 3$   $TRL_{Target} = 4$

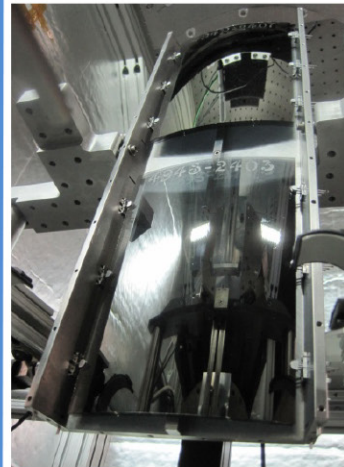


# Next-Generation X-ray Optics: High Angular Resolution, High Throughput, and Low Cost

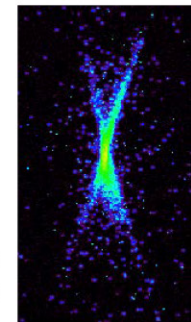
PI: William W. Zhang / GSFC



Technology Development Module containing three pairs of parabolic-hyperbolic mirror segments



X-ray image with 8-arcsec HPD



## Objectives and Key Challenges:

- Develop lightweight X-ray-mirror technology achieving better than 10-arcsec HPD angular resolution while minimizing cost and schedule; advance to TRL 5 to enable missions planned for 2010s and 2020s
- Prepare ways to achieve significantly better than 10-arcsec resolution while keeping the mass and cost at similar levels
- Fabrication and metrology of mirror segments
- Coating mirror segments with 20 nm of iridium w/o distortion
- Alignment and bonding of mirror segments

## Significance of Work:

- Enables major X-ray observatories such as ESA's Athena and NASA's Astrophysics Roadmap X-ray Surveyor

## Approach:

- Precision glass slumping to make mirror substrates
- Use magnetron sputter or atomic layer deposition to maximize X-ray reflectance
- Use interferometer, null lens, and interferometric microscope to conduct measurements
- Use Hartmann tests to align mirror segments
- Develop precision epoxy-bonding techniques

## Key Collaborators:

- Michael Biskach, Kai-Wing Chan, Ryan McClelland, and Timo Saha (GSFC)
- Stephen O'Dell (MSFC)

## Current Funded Period of Performance:

Oct 2014 – Sep 2016

## Recent Accomplishments:

- ✓ Slumped mirror substrates achieving better than 10-arcsec HPD
- ✓ Coated mirror substrates with 15 nm of iridium without distortion
- ✓ Repeatedly co-aligned and bonded multiple mirror pairs, achieving 8-arcsec HPD X-ray images

## Next Milestone:

- Refine mirror bonding process to fully realize mirror segment potential of 6.5-arcsec HPD (Dec 2016)

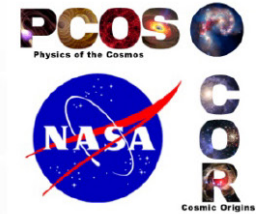
## Applications:

- Flagship and probe-class X-ray missions
- Explorer-type X-ray missions
- Medical research and diagnosis

TRL<sub>In</sub> = 3    TRL<sub>PI-Asserted</sub> = 5    TRL<sub>Target</sub> = 6

# Planar Antenna-Coupled Superconducting Detectors for CMB Polarimetry

PI: James Bock / JPL, Caltech



## Objectives and Key Challenges:

Advance antenna-coupled superconducting detector technologies for space requirements:

- RF propagation properties
- Beam control and polarized matching
- Extended-frequency antennas
- Detector stability and cosmic-ray response
- Readout-noise stability
- Large-format, modular, focal-plane units

## Significance of Work:

- Antenna designs for all bands required by the Inflation Probe
- Detector sensitivity, stability, and minimized particle susceptibility appropriate for space-borne observations

## Approach:

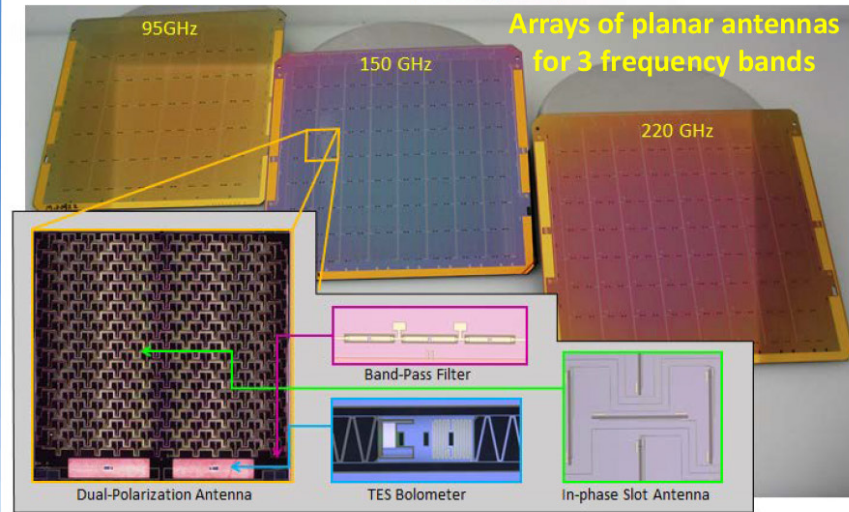
- Planar antennas for entirely lithographed fabrication with no coupling optics
- Detectors provide photon-limited sensitivities in space
- Antennas provide excellent polarization and beam-matching properties
- Modular focal-plane unit for large focal-plane arrays

## Key Collaborators:

- Koko Megerian, Hien Nguyen, Roger O'Brient, Anthony Turner, and Alexis Weber (JPL)
- Jon Hunacek, Howard Hui, Sinan Kefeli, and Bryan Steinbach (Caltech)
- Jeff Filippini (UIUC)

## Current Funded Period of Performance:

Jan 2016 – Dec 2017



## Recent Accomplishments:

- ✓ BICEP3 deploys 20 focal-plane modules at 95 GHz
- ✓ 40 GHz antennas demonstrated
- ✓ 270 GHz and broadband antennas fabricated, in test
- ✓ Ti resistivity and dielectric uniformity characterized on 6" wafers

## Next Milestones:

- Results from 270-GHz antenna test (Jul 2016)
- Results from broad-band antenna test (Jul 2016)
- First cryo run of RF testbed (Aug 2016)
- Develop 6" module design (Sep 2016)

## Applications:

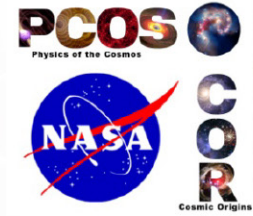
- NASA Inflation Probe mission
- Explorer and international CMB missions
- Technology commonalities with Far-IR and X-Ray missions

$TRL_{In} = 3-4$   $TRL_{PI-Asserted} = 3-6$   $TRL_{Target} = 4-6$



# High-Efficiency Feedhorn-Coupled TES-based Detectors for CMB Polarization Measurements

PI: Edward J. Wollack / NASA GSFC



## Objectives and Key Challenges:

- Development of focal planes for characterization of CMB polarization with the following detector properties:
  - Background-limited millimeter-wave polarimetric sensor with high coupling efficiency and systematic error control
  - Inherently broadband design, scalable to large-format arrays over multiple frequencies of astrophysical interest

## Significance of Work:

- Sub-orbital and space-borne operation of detectors, including:
  - Improved rejection of stray light by detector architecture
  - Improved broadband performance and coupling efficiency
  - Mitigation of space environmental concerns (surface/deep dielectric charging and cosmic rays)

## Approach:

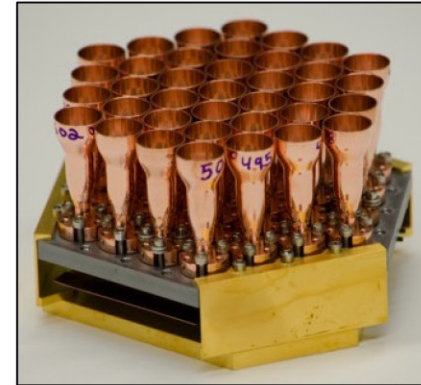
- The effort is focused around 3 fabrication runs to integrate the new technologies into the detector architectures. Specifically, improved:
  - Stray light mitigation and package thermalization
  - Implementation of air-bridge crossovers and ground-plane contacts for large-bandwidth/low-loss signal routing at higher frequencies

## Key Collaborators:

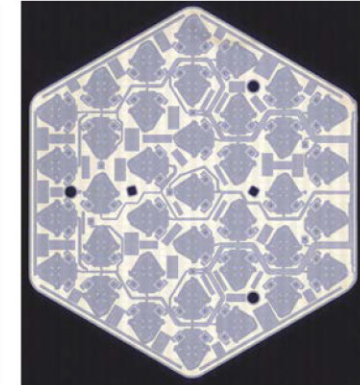
- K. Denis, K. U-Yen, and S.H. Moseley (GSFC)
- K. Rostem (GSFC/JHU)
- D. Chuss (Villanova)
- T. Marriage and C. Bennett (JHU)

## Current Funded Period of Performance:

Jan 2016 – Dec 2017



90 GHz Sensor Module



Detector Wafer

## Recent Accomplishments:

- ✓ Funding received; test and efforts initiated
- ✓ Air bridge prototype devices fabricated
- ✓ Backshort assembly vias and groundplane contacts demonstrated and incorporated in W-band Wafers

## Next Milestones:

- W-band package design validation (Jul 2016)
- Test equipment procurement (Aug 2016)
- Device run #1 (Aug 2016)
- W-band Wafer validation (Sep 2016)

## Application:



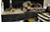
- CMB Polarimetry, suborbital

$TRL_{In} = 3$     $TRL_{Current} = 3$     $TRL_{Target} = 6$



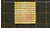





# Appendix C

## Program Technology Development Status



### Gravitational Waves

	<b>Jordan Camp</b> – “Demonstration of a TRL-5 Laser System for LISA” . . . . .	78
	<b>William Klipstein</b> – “Gravitational-Wave-Mission Phasemeter Technology Development” . . . . .	86
	<b>Jeffrey Livas</b> – “Telescopes for Space-Based Gravitational-Wave Observatories”. . . . .	92

### X Rays

	<b>Mark Bautz</b> – “Directly Deposited Optical-Blocking Filters for Imaging X-ray Detectors” . . . . .	102
	<b>David N. Burrows</b> – “Fast Event Recognition for the Athena Wide-Field Imager”. . . . .	115
	<b>Caroline Kilbourne</b> – “Providing Enabling and Enhancing Technologies for a Demonstration Model of the Athena X-IFU” . . . . .	120
	<b>Randall L. McEntaffer</b> – “Reflection Grating Modules: Alignment and Testing” . . . . .	129
	<b>Paul B. Reid</b> – “Development of 0.5-Arcsecond Adjustable Grazing-Incidence X-ray Mirrors for the SMART-X Mission Concept” . . . . .	137
	<b>Mark L. Schattenburg</b> – “Advanced Packaging for Critical-Angle X-ray Transmission Gratings” . . . . .	148
	<b>Joel Ullom</b> – “Technology Development for an AC-Multiplexed Calorimeter for Athena” . . . . .	154
	<b>William W. Zhang</b> – “Next-Generation X-ray Optics: High Angular Resolution, High Throughput, and Low Cost”. . . . .	160

### Cosmic Microwave Background

	<b>James J. Bock</b> – “Planar Antenna-Coupled Superconducting Detectors for CMB Polarimetry” . . . . .	166
	<b>Edward J. Wollack</b> – “High-Efficiency Feedhorn-Coupled TES-based Detectors for Cosmic Microwave Background Polarization Measurements”. . . . .	175

# Demonstration of a TRL-5 Laser System for LISA

Prepared by: Jordan Camp (NASA/GSFC)

## Summary

The gravitational-wave (GW) space mission Laser Interferometer Space Antenna (LISA) [1] is likely to be chosen for the European Space Agency (ESA) L3 GW astronomy opportunity, and NASA intends to contribute instruments to the mission. LISA's eventual flight will open a spectacular new window on the universe, using gravitational waves to reveal the physics and astronomy associated with the merger of massive black hole systems. The backbone of LISA is a highly stable  $\sim 1.5$ -W laser, which enables the picometer interferometry necessary to record the passage of a GW; such a laser is listed as a top priority of the Physics of the Cosmos (PCOS) Program Analysis Group (PhysPAG) technology roadmap. LISA is now under technology development in Europe, and the Europeans have expressed interest in the laser system as a possible contribution from the US. To enable this contribution, we expect to provide a Technology Readiness Level (TRL) 5 demonstration of the full LISA laser system by December 2016, allowing maximum flexibility for mission implementation. The laser system includes a state-of-the-art master-oscillator power-amplifier approach. The oscillator is a compact, low-mass, low-noise, semiconductor External Cavity Laser (ECL) that is robust for operation in space. In addition, our custom-designed fiber amplifier will demonstrate the full range of LISA noise and power requirements.

The activity described here, funded through our Strategic Astrophysics Technology (SAT) grant, involved two steps. First, the understanding gained from our lab prototypes' noise and reliability testing was incorporated into a rebuilt oscillator and amplifier. Second, with the oscillator and amplifier development complete, we performed a full-system test of the laser, using control systems to achieve the laser power, frequency, intensity, and differential phase noise. Environmental testing was also performed on the ECL and preamp. With final amplifier environmental testing and a final factor-of-four improvement in the laser frequency noise at 100 kHz, we expect to complete the laser development and demonstrate a TRL-5 LISA laser system in December 2016.

## Background

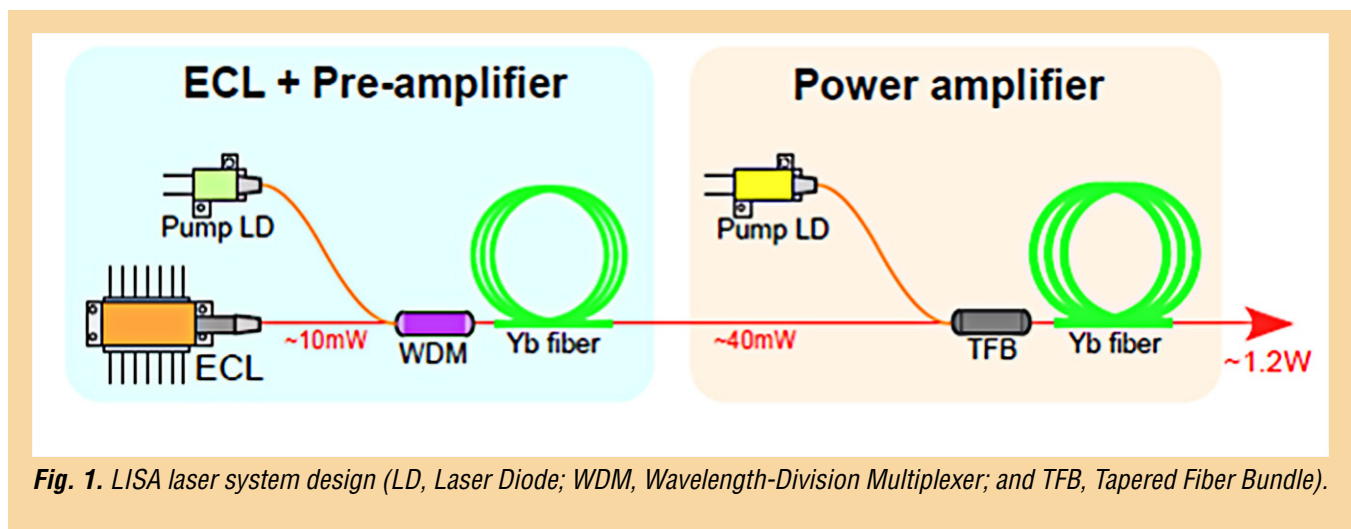
LISA will use laser interferometry to observe the disturbance of freely floating test masses, caused by the passage of GWs. The detection of these GWs will allow LISA to observe the mergers of supermassive black holes, giving unprecedented tests of General Relativity at high precision, as well as views of the astrophysics of merging galaxies back to very high redshift. Because gravity is a very weak force, the GW test-mass disturbance is expected to be very small, on the order of  $10^{-21}$  in strain, or  $10^{-12}$ -m displacement over a  $10^9$ -m arm length, with a timescale of  $\sim 10^3$  seconds. This displacement sensitivity and timescale flows through the LISA laser requirements [2], shown in Table 1.

Power (W)	$\lambda$ (nm)	Intensity Noise ( $1/\sqrt{\text{Hz}}$ )	Frequency Noise ( $\text{Hz}/\sqrt{\text{Hz}}$ )	Differential Phase Noise ( $\text{rad}/\sqrt{\text{Hz}}$ )	Lifetime (Years)
1.5	1064	$10^{-4}$ (at $10^{-3}$ Hz) $10^{-8}$ (at $10^7$ Hz)	300 (at $10^{-2}$ Hz)	$6 \times 10^{-4}$ (at $10^{-2}$ Hz)	2.5

**Table 1.** Laser requirements for LISA

The design of the LISA laser system consists of a low-noise ECL oscillator and preamp, followed by a fiber power amplifier (Fig. 1).





The ECL is a low-mass, low-cost, compact, simple, and highly reliable semiconductor laser, provided by a US vendor [3, 4]. These characteristics make it a compelling choice for the oscillator. The preamp is a simple and highly reliable subsystem that amplifies the ECL output by a factor of 4 to 20.

For the amplifier, a laser design utilizing optical fibers presents many advantages over solid-state bulk crystals, including:

- Insensitivity to contamination problems and ease of alignment, since the light is maintained within the fiber core and waveguide;
- Conveniently redundant design, since higher-risk components such as pump diodes are easily made redundant by splicing them into the gain fiber; and
- Ability to leverage the large resources of the telecommunications fiber industry.

The stringent noise requirements shown in Table 1 are achieved in the laser system design through the use of well-known amplitude- and frequency-stabilization techniques described below, with which our group has had extensive experience. The power and wavelength requirements are compatible with the overall oscillator and power amplifier configuration.

## Objectives and Milestones

The objectives involved three main aspects:

- Optimization of the oscillator (ECL);
- Construction of a preamp and a laser amplifier; and
- Systems and environmental testing of the full laser system (oscillator, preamp, and amplifier).

Optimization of the ECL took place at the laser vendor (Redfern Integrated Optics, RIO). The first version of a 1064-nm-wavelength ECL in the preferred Butterfly package was produced in 2014, and allowed us to incorporate this low-mass, compact oscillator [5] into our laser design. The next step in the ECL development was optimizing its design to provide lower phase noise and high reliability. This was done by iterating the design of the planar Bragg grating which forms the reflector for the ECL optical cavity, and by performing accelerated aging tests on the laser-gain chip.



The laser amplifier was constructed using a mechanically robust design to survive shake-testing and thermal cycling. It also included temperature stabilization, which is needed to limit amplitude noise. This construction involved use of a fiber splicer to combine fibers from the pump diode to the gain elements, and a fiber coater to provide a coating layer with varying index of refraction to keep the light propagating through the fiber with low loss. The laser amplifier was tested for required output power, frequency noise, differential phase noise, and amplitude noise. By fall 2016, it will be environmentally tested for mechanical and thermal robustness.

Finally, the full laser system (oscillator and amplifier) will be monitored for noise and environmental robustness, as shown in Fig. 2. When TRL 5 is achieved individually for the oscillator and amplifier, we will demonstrate TRL 5 through a full-system-level test of the entire laser system, including power, frequency, intensity, and differential phase noise measurements. These studies will take place in the final months of this SAT grant (fall 2016).

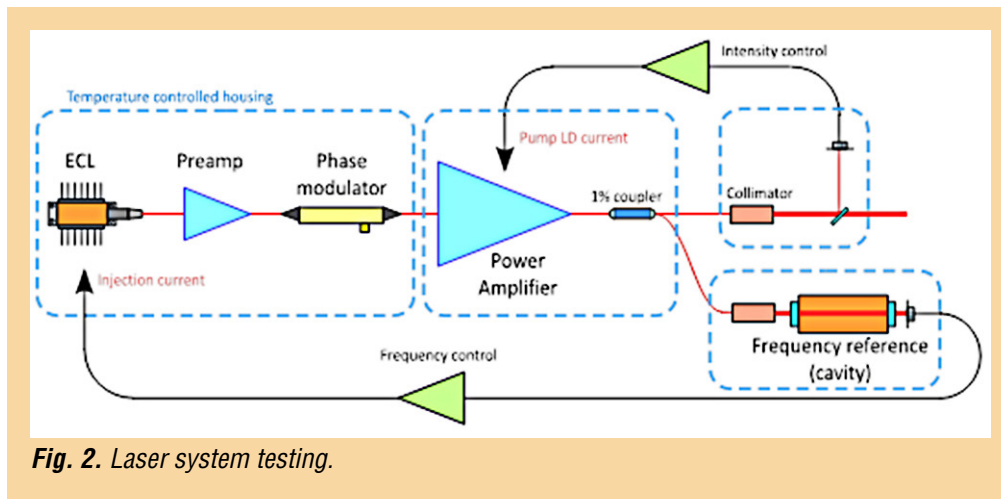


Fig. 2. Laser system testing.

The system test uses the fully fiber-coupled setup shown in Fig. 2 and incorporates the understanding gained in the measurements of the separate components. To simulate the stable space thermal environment, the oscillator and amplifier are located in a temperature-controlled housing, stabilized to 0.1°C over a one-hour timescale. The experimental arrangement of Fig. 2 presents the amplifier, preamp, phase modulator, and amplifier as a single integrated system.

The milestones for these activities are:

- Procurement of long-lead items (**completed**) . . . . . Mar 2015
- Preliminary 1.5-W laser amplifier (**completed**) . . . . . Apr 2015
- Preliminary laser amp test with non-optimized ECL (**completed**) . . . . . May 2015
- ECL optimization contract start (**completed**) . . . . . Jul 2015
- Optimized 2.5-W laser amplifier (**completed**) . . . . . Sep 2015
- Noise tests of stabilized 2.5-W laser amplifier (**completed**) . . . . . Nov 2015
- Reliability testing of ECL and preamp (**completed**) . . . . . Feb 2016
- Laser system test with optimized ECL (**completed**) . . . . . Feb 2016
- Full-laser-system noise testing (**completed**) . . . . . Mar 2016
- Amplifier environmental testing . . . . . Sep 2016
- Noise optimization of ECL . . . . . Nov 2016
- Month-long full laser-system monitoring. . . . . Dec 2016

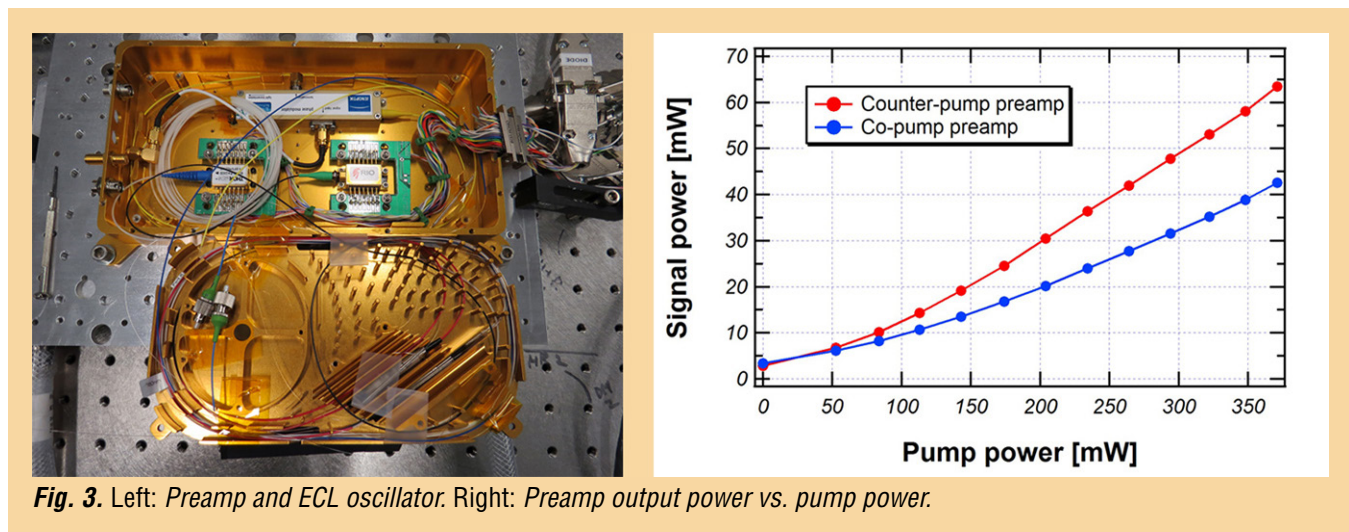
By September 2016, we will have characterized the full-laser-system noise and demonstrated compliance with environmental testing, establishing TRL 5 for this laser.

## Progress and Accomplishments

We received notice of our SAT award in March 2014, and the funding arrived at GSFC in May 2014. Thus, all progress is measured against a start date of May 2014. We describe progress on the major activities of procurements, ECL optimization, preamp build, laser amplifier build, laser systems noise testing, and laser system environmental testing.

**Procurement of Long-Lead Items:** We have prepared a temperature-stabilized enclosure for the laser systems testing. We have also procured all long-lead instruments necessary for the systems testing, including a frequency reference cavity, a fiber-fusion splicer, two fiber coaters, and a mechanical shaker.

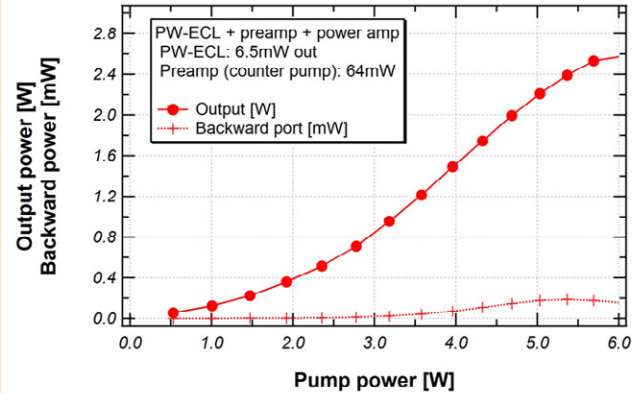
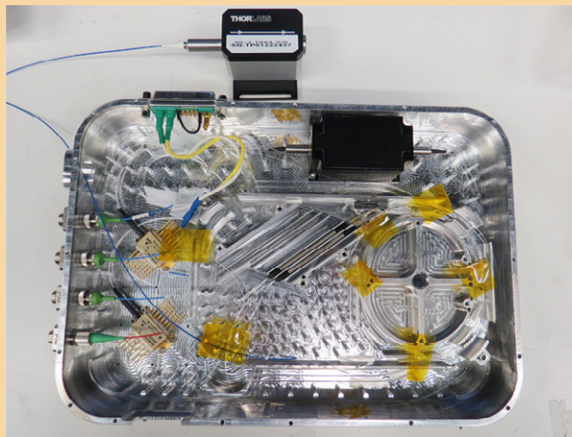
**Preamp Build and Test:** A counter-pumped preamp with a gain of 5 was constructed, using a gain fiber of 1-m length. A clean output spectrum was observed, with low Amplitude-Stimulated Emission (ASE) floor, no output leakage, and an efficiency of  $\sim 20\%$ . The preamp is shown in the left panel of Fig. 3, along with the ECL oscillator mounted with its low-noise current driver. The right panel of Fig. 3 shows the preamp output power plotted against its pump diode power. The preamp enclosure houses two seed ECLs and two pump diodes for redundancy. Its fiber tray design was taken from the Lunar Atmosphere and Dust Environment Explorer (LADEE) flight mission.



**Fig. 3.** Left: Preamp and ECL oscillator. Right: Preamp output power vs. pump power.

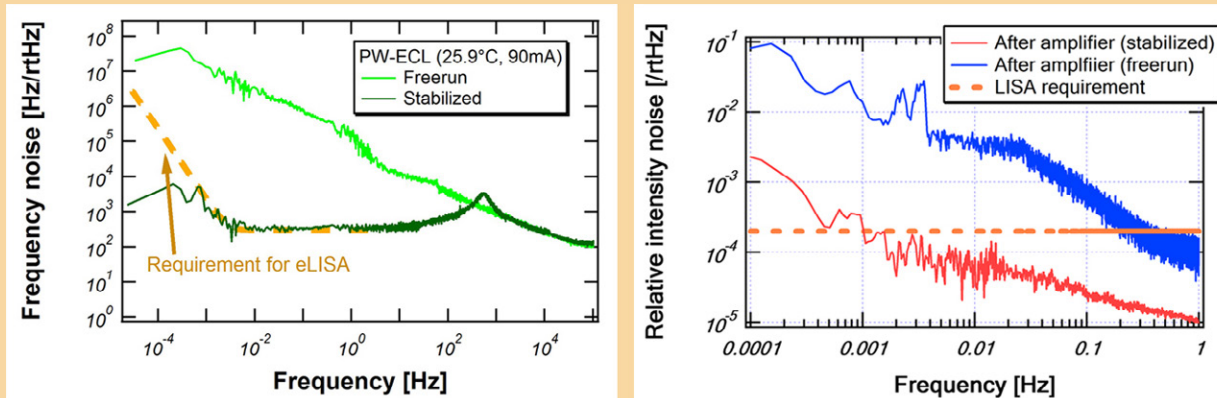
**Amplifier Build and Test:** the newly built 2.5-W fiber amplifier is shown in the left panel of Fig. 4. As shown schematically in Fig. 2, it includes a pump diode to provide power; a TFB to allow redundant power input; and a 2.3-m-length, 10- $\mu\text{m}$  core, double-clad, large-mode-area gain fiber that converts the pump power to amplification gain. The forward-pumped design and optical isolator minimize potential sources of feedback. The amplifier uses a robust mechanical design and temperature stabilization to suppress fiber-length variations.

Testing of the amplifier has shown an unstabilized amplitude variation of about 1% root mean square (rms), and an output power of 2.5 W, significantly above the 1.5-W requirement, as shown in the right panel of Fig. 4. The constant backward-port power as a function of output power indicates that Stimulated Brillouin Scattering (SBS) is likely not a noise concern. Approximately 20 dB polarization extinction ratio (PER) was achieved at the output. A 1064-nm ECL with 6-mW output, followed by a preamplifier of gain  $\sim 10$ , was used as input to the amplifier.



**Fig. 4.** Left: Fiber-based laser amplifier. Right: Laser amplifier output power vs. backward port power.

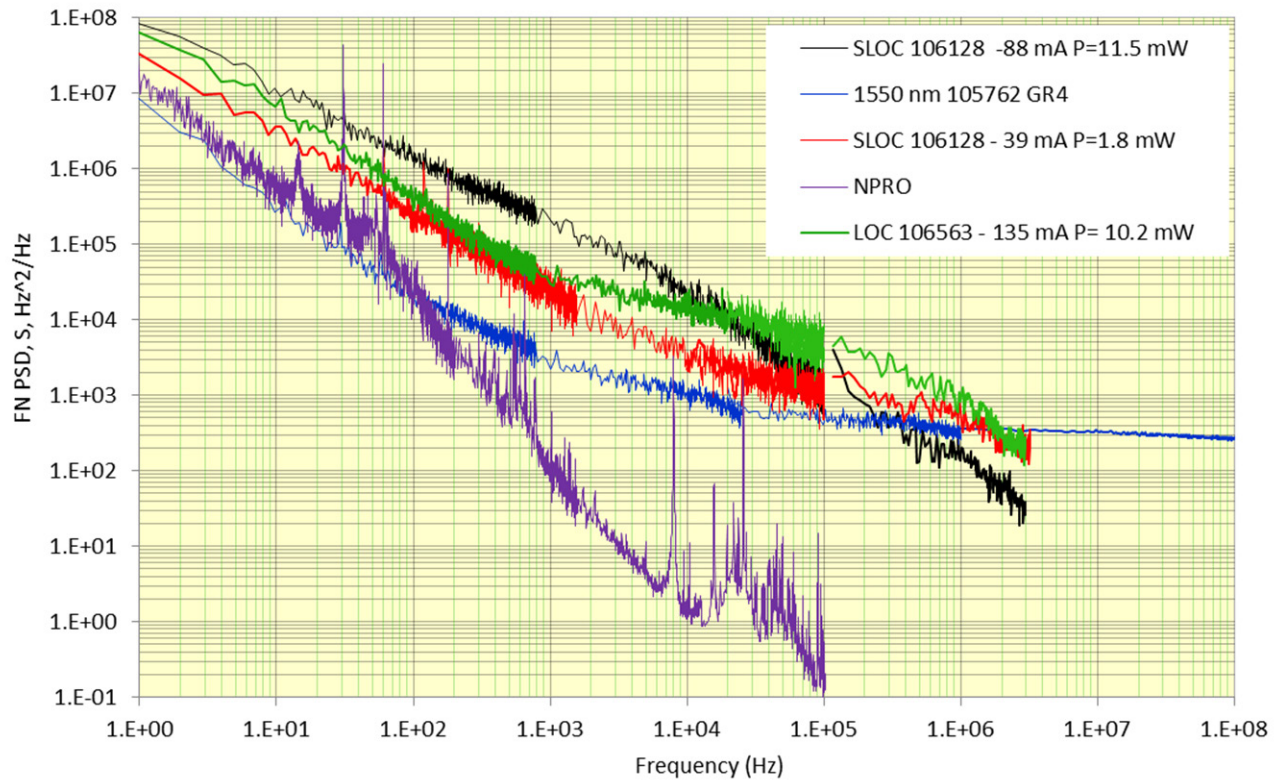
**Laser System Noise Testing:** We have performed laser-system noise tests by amplitude- and frequency-stabilizing the ECL and amplifier (Fig. 5). By stabilizing the amplifier pump-diode current, an amplitude noise attenuation of  $\sim 30$  was achieved at a frequency of 0.1 mHz (a factor of  $\sim 10$  above the LISA requirement, see red curve in right panel of Fig. 5). This noise will decrease significantly once temperature stabilization of the amplifier is applied. The laser system was also frequency-stabilized by locking a small fraction of the amplifier's output to the frequency reference cavity, using either the laser current or an Acousto-Optical Modulator (AOM) as frequency actuator. A control bandwidth of  $\sim 10$  kHz was achieved; future work will increase this to order 1 MHz by optimizing the AOM driver. Finally, the phase-meter necessary to measure LISA phase variations between the lasers on separate spacecraft has been implemented in our lab. It will be used to demonstrate phase locking of a free-running ECL oscillator to an ECL stabilized to the reference cavity.



**Fig. 5.** Frequency (left) and intensity (right) noise of laser system: ECL, preamp, and amplifier.

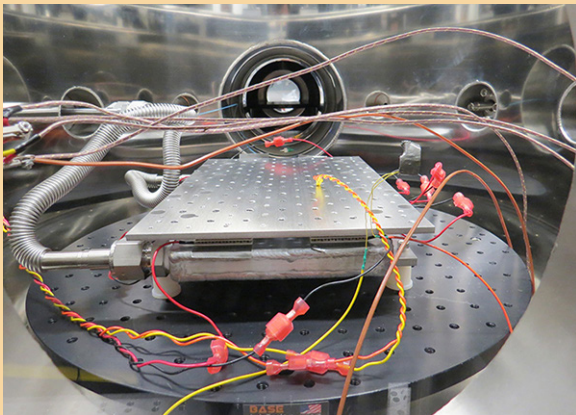
**Design Optimization of ECL:** This work was done at RIO, and involved modeling and analysis of the current-gain chip and Planar Linear Cavity (PLC) that comprise the ECL, and then modeling of the full oscillator. This fed a redesign of the PLC, which was followed by the manufacturing and integration of the new components, and then characterization to verify the improved phase-noise performance. The work also included final reliability testing of the laser gain chip. Three implementations of the ECL optical cavity are shown in Fig. 6 (black, red, and green curves), with the phase noise of each configuration plotted as a function of frequency. The purple and blue curves show for comparison the phase noise of the non-planar ring oscillator (NPRO) and the low-noise 1550-nm ECL, respectively. We chose the implementation providing the red curve, with the lowest noise at 100 kHz (which has a strong effect on laser phase locking). An additional factor-of-four noise reduction is required, which we expect to achieve with a new oscillator scheduled for delivery to GSFC in November 2016.



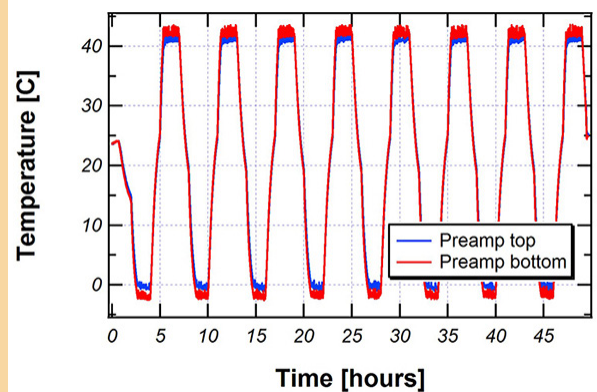


**Fig. 6.** Power spectral density of phase noise of 1064-nm ECL with various optical cavity parameters. The Y-axis units are  $\text{Hz}^2/\text{Hz}$ ; the X-axis units are Hz. The noise at 100 kHz is most significant for phase-locking separate lasers, so we chose the implementation providing the red curve. For comparison, the purple curve shows the phase noise of the NPRO.

**Laser System Environmental Testing:** A critical aspect of this work is environmental testing, which involves thermal-vacuum (TVAC) cycling, vibration testing, and exposure to radiation levels that will be seen in the LISA space environment. These tests have been applied to the ECL oscillator and the preamp, as shown below. Figure 7 shows the TVAC cycling apparatus deployed in our laser lab, and Fig. 8 shows the thermal levels and duration used in the thermal cycling of the preamp.



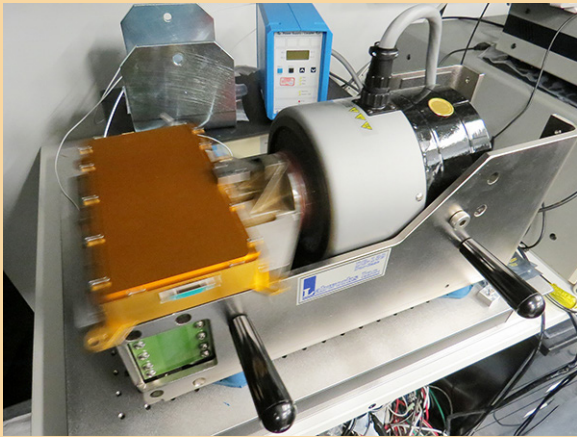
**Fig. 7.** Thermal cycling apparatus in our lab.



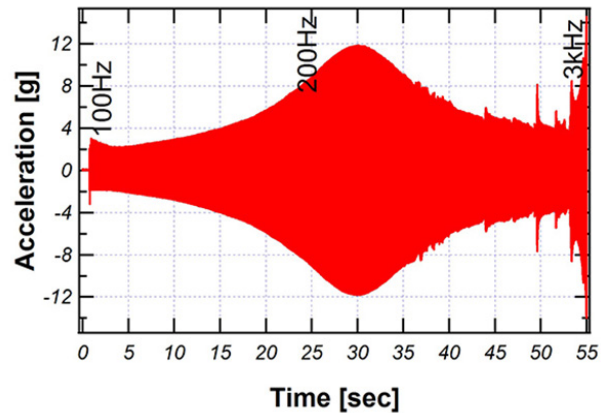
**Fig. 8.** Thermal levels in preamp tests.



Figure 9 shows the vibration (“shaker”) apparatus used to vibrate the preamplifier and other components under test, while Fig. 10 shows the acceleration spectrum that the shaker provides.



**Fig. 9.** Vibration instrument shaking preamp/ECL.



**Fig. 10.** Acceleration from vibration apparatus.

The results of the preamp environmental testing (Fig. 11) show no effect on output power from thermal cycling or vibration, and ~30% drop in output power after gamma-ray radiation exposure, with exposure at the full LISA level of 45 krad in 8 hours, which represents a rate  $10^4$  times the LISA rate experienced during a 5-year orbit. Since radiation damage is related to the exposure rate, this shows the preamp is insensitive to radiation damage at the actual LISA dose rate.

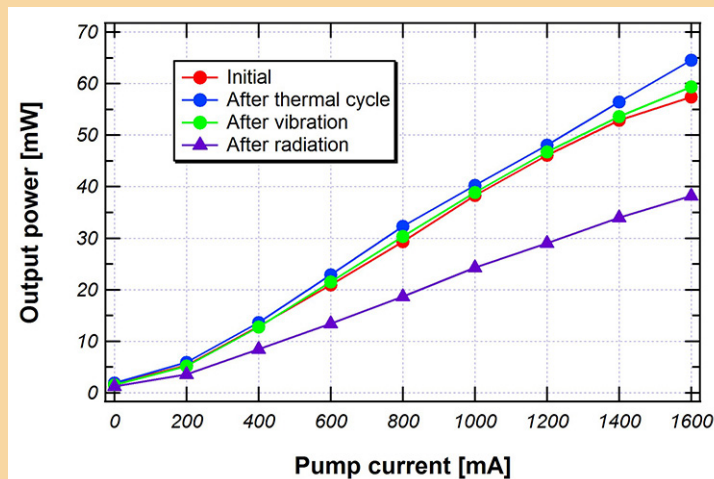


**Fig. 11.** Results of environmental testing on ECL + preamp.

## Path Forward

### Amplifier Environmental Testing, Frequency Noise Reduction, and Long-Term System Monitoring:

The remaining work under this SAT grant involves environmental testing of the amplifier, including thermal cycling, vibration, and radiation exposure; additionally, we plan to work on a factor-of-four reduction in ECL frequency noise at 100 kHz. Finally, the full laser system will be operated and monitored for one month to observe system stability. TRL 5 is expected to be demonstrated with the conclusion of these tests (December 2016).

## References

- [1] T. Prince et al., “*LISA: Probing the Universe with Gravitational Waves*,” LISA-LIST-RP-436 Version 1.2 (2009)
- [2] O. Jennrich and G. Heinzel, “*Laser requirements for a gravitational wave mission*” (2013)
- [3] Redfern Integrated Optics Products Page
- [4] K. Numata et al., “*Performance of planar-waveguide external cavity laser for precision measurements*,” Optics Express **18** 22781 (2010)
- [5] K. Numata et al., “*Characteristics of the single-longitudinal mode planar-waveguide external cavity diode laser at 1064 nm*,” Optics Letters **39** No. 7, 2101 (2014)

For additional information, contact Jordan Camp: [jordan.b.camp@nasa.gov](mailto:jordan.b.camp@nasa.gov)



# Gravitational-Wave-Mission Phasemeter Technology Development

Prepared by: William Klipstein (PI; JPL); Jeff Dickson, Kirk McKenzie, Robert Spero, Brent Ware, and Chris Woodruff (JPL)

## Summary

The proposed work in the framework of this Strategic Astrophysics Technology (SAT) project will advance the Technology Readiness Level (TRL) of our phase measurement electronics, and demonstrate their performance in an upgraded interferometer system-level test bed. The test bed will provide signals representative of gravitational-wave (GW) missions, such as the Laser Interferometer Space Antenna (LISA). Our technology-development effort starts with demonstrating the “photons-to-bits” phase-measurement system (interferometer readout electronics) as a system to TRL 4 in an interferometer test bed providing signals representative of a LISA-like mission. Some components, most notably the digital phasemeter board, have been developed beyond TRL 4, as assessed by NASA’s Earth Science Program.

## Background

LISA-like GW mission concepts rely on heterodyne laser interferometry to measure picometer-level fluctuations in the separation between three widely separated spacecraft. The transmit and receive beams from a spacecraft pair are mixed optically (interfered) on a beam combiner, resulting in a detected signal varying sinusoidally at the frequency difference between the local transmit laser and the laser received from the distant spacecraft. Picometer-level displacement sensitivity requires microcycle-level precision in measuring the phase difference compared to the micron-scale wavelength of the laser light.

Since 2005, we have been developing phase measurement systems to validate and support photons-to-bits interferometer-signal readout based on mission parameters described in the LISA Technology Development Plan. Future variants of GW missions all (except the less-mature atom interferometer concepts) involve laser interferometry between widely separated spacecraft. Thus, they will all rely on a LISA-like phasemeter and time-delay interferometry to mitigate the impact of laser frequency noise on mission performance.

Elements of our phase measurement system include quadrant photoreceivers, an analog signal chain, analog-to-digital converters (ADCs), and digital signal processing for the phase measurement. In addition to measuring the phase (distance) change in the interferometer, the phasemeter also controls laser frequency and provides an optical communication link between spacecraft. We recently used the phasemeter from the Gravity Recovery and Climate Experiment (GRACE) Follow-On to implement differential wavefront sensing using our LISA four-quadrant photoreceivers, and used that signal to maintain relative pointing of incoming and outgoing lasers by feeding back to a steering mirror in the transmitted light path.

## Objectives and Milestones

The objective of this project is to advance our phase measurement system from TRL 4 to 5, through significant system-level hardware-fidelity increase and greater fidelity of the signal-test environment by adding low light levels.

### *Key project milestones:*

1. Incorporate quadrant photoreceivers into test bed.
2. Demonstrate wavefront sensing.
3. Migrate additional photoreceiver algorithms from LabView phasemeter to an Engineering Model (EM).
4. Demonstrate tracking of low-visibility signals with EM phasemeter.
5. Incorporate EM photoreceivers and signal chain.
6. Demonstrate test-bed performance at TRL 5 or better.

## Progress and Accomplishments

Work on this task was postponed in order to take advantage of synergistic developments on the Earth Science mission, GRACE Follow-On, which will carry a Laser Ranging Interferometer (LRI) based on technology development of the phasemeter for a GW mission. LRI will demonstrate inter-spacecraft interferometry with requirements quite similar to the former LISA mission by design. LRI is a partnership between the US and Germany, relying on partners from LISA formulation. The phasemeter team's share in LRI includes the phasemeter, laser, and laser stabilization cavity. LRI will fly LISA phasemeter algorithms implemented and advanced to flight maturity. The hardware complement is shown in Fig. 1.

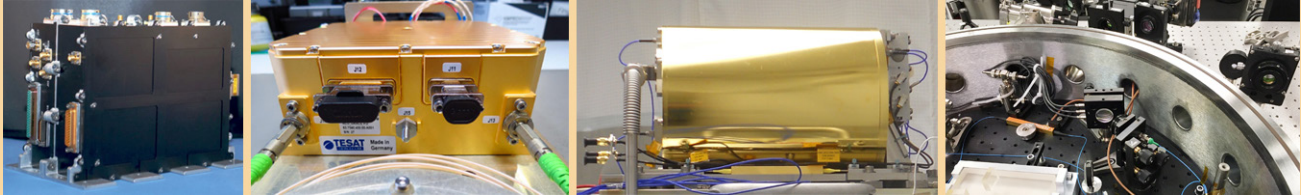


**Fig. 1.** The LRI design requirements and designs came from US and German investments in GW technology as well as geodesy. LRI hardware shown (left to right): Laser Ranging Processor (LRP), Laser, Optical Cavity, and Optical Bench Assembly (OBA).

An EM of the quadrant photoreceivers and signal chain has been delivered to the US to support testing and will be made available to support this task as a complement to the US-developed photoreceivers. A comparison of LRI requirements to LISA requirements is shown in Table 1.

Parameter	LRI	LISA
Measurement noise	0.08 $\mu\text{m}/\sqrt{\text{Hz}}$	$2 \times 10^{-5}$ $\mu\text{m}/\sqrt{\text{Hz}}$
Shot noise	10 $\text{pm}/\sqrt{\text{Hz}}$	7 $\text{pm}/\sqrt{\text{Hz}}$
Photoreceiver noise	1 $\text{nm}/\sqrt{\text{Hz}}$	
Phasemeter noise	1 $\text{nm}/\sqrt{\text{Hz}}$	
Optical pathlength noise	30 $\text{nm}/\sqrt{\text{Hz}}$	
Laser frequency noise	35 $\text{nm}/\sqrt{\text{Hz}}$	
Ultra-stable oscillator (USO) noise	1 $\text{nm}/\sqrt{\text{Hz}}$	
Satellite separation	170 – 270 km	5 million km
Satellite relative velocity	$< \pm 3$ m/s	$< \pm 15$ m/s
Wavelength	1064 nm	1064 nm
Phase precision	40 microcycle/ $\sqrt{\text{Hz}}$	1 microcycle/ $\sqrt{\text{Hz}}$
Nominal carrier-to-noise density (CNR)	$>75$ dB-Hz (single phasemeter channel)	$>75$ dB-Hz (single phasemeter channel)
Intermediate Frequency (IF) signal frequency	4-16 MHz	2-18 MHz
IF signal dynamics (@1Hz)		
Before frequency stabilization	50 kHz/ $\sqrt{\text{Hz}}$	5 kHz/ $\sqrt{\text{Hz}}$
After frequency stabilization	30 Hz/ $\sqrt{\text{Hz}}$	300 Hz/ $\sqrt{\text{Hz}}$
Science bandwidth	2 mHz to 0.1 Hz	0.1 mHz to 1 Hz
Rx optical power	80 pW	80 pW
Number of phasemeter channels	4	64
ADC clocking rate	38.656 MHz	50 MHz
Time coordination	GPS (laser ranging could be used)	Laser ranging code
Laser phase locking	Required	Required
Pointing information	Wavefront sensing	Wavefront sensing

**Table 1.** LRI requirements are closely matched to LISA requirements. The primary differences are that LRI has tighter laser-frequency-noise requirements (demonstrated) and LISA requires more tracking channels, including multiple channels per signal stream. LRI will fly LISA phasemeter algorithms.



The LRI phasemeter has demonstrated the following LISA-relevant requirements:

- Microcycle phase measurement of heterodyne signals with CNR of 66.5 dB-Hz from 4-16 MHz from quadrant photoreceivers (Fig. 2);
- Differential wavefront sensing and steering mirror control at ~60 dB-Hz;
- Phase locking of a flight non-planar ring oscillator (NPRO) laser at 66.5 dB-Hz;
- Laser stabilization of a flight NPRO laser to a flight cavity; and
- Automated inter-spacecraft optical link acquisition.

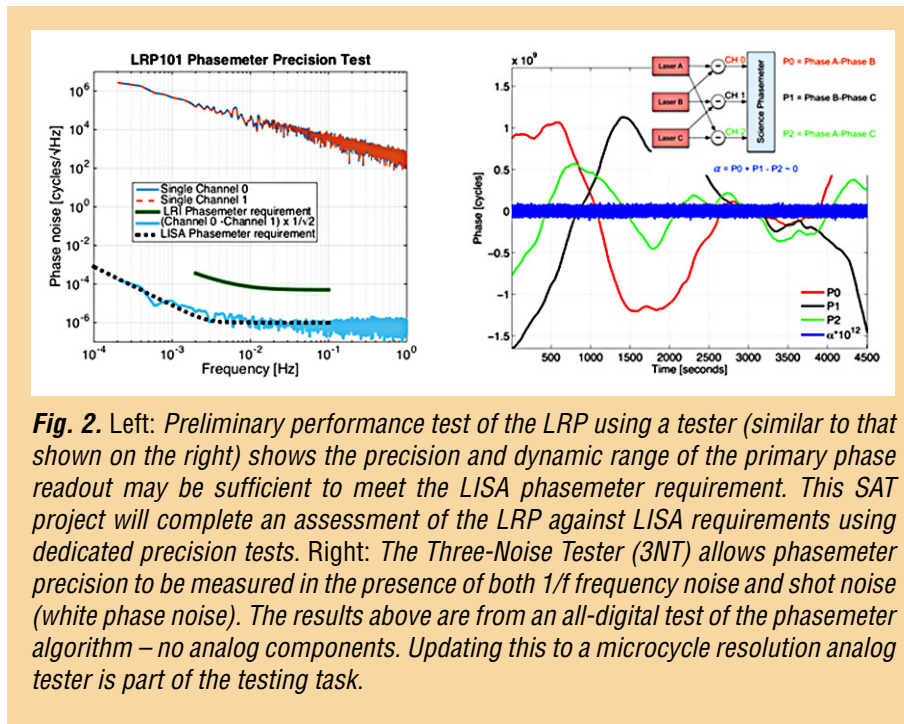


**Fig. 2.** Left: Preliminary performance test of the LRP using a tester (similar to that shown on the right) shows the precision and dynamic range of the primary phase readout may be sufficient to meet the LISA phasemeter requirement. This SAT project will complete an assessment of the LRP against LISA requirements using dedicated precision tests. Right: The Three-Noise Tester (3NT) allows phasemeter precision to be measured in the presence of both  $1/f$  frequency noise and shot noise (white phase noise). The results above are from an all-digital test of the phasemeter algorithm – no analog components. Updating this to a microcycle resolution analog tester is part of the testing task.

The primary functions being added to the LRI phasemeter are the ability to track multiple tones, tracking of a clock-correction signal, and the time/range code used to align time from multiple data streams. These algorithms will be migrated using the same process that was used to migrate the LabView phasemeter algorithms for phase tracking, phase locking, and Pound-Drever-Hall laser-frequency stabilization.

Our Field-Programmable-Gate-Array (FPGA) team from GRACE Follow-On mapped out the tracking-FPGA implementation details of summing the four quadrant signals and performing carrier-assisted tracking of this weaker tone without software changes, which would be relatively straightforward but not within our team's skill base. Timing/ranging-code implementation requires a bit more departure from the current tracking, but is quite similar in practice to what our group does in the BlackJack GPS receivers, with the detailed codes to be used already demonstrated in our Labview Phasemeter.

In addition to adding functionality to the LRI Phasemeter, test infrastructure was developed to test Phasemeter performance. Figure 2 (left) shows a preliminary result of the LRI-phasemeter flight unit showing near-LISA-requirement-level phasemeter error in the presence of representative noise. Using a custom phasemeter noise tester (Fig. 2, right), the residual phasemeter errors can be measured in the presence of both  $1/f$  frequency noise and shot noise (white phase noise), by putting the same signal on both channels and differencing them in post processing. Figure 2 (left) shows the residual noise easily meets the LRI Phasemeter requirement (green trace), but not quite the LISA requirement (dashed black trace). The residual errors may be from the ADC samplers or the test setup itself.

We are completing a move to a new laboratory, which will combine our SAT-funded research with our LRI test equipment. This will help as we transition from our GRACE Follow-On work back to completing our SAT work. We have done preliminary design work to allow testing of a differential-wavefront-sensing (DWS) and control functionality in our Labview phasemeter using the bench shown in Fig. 3. We also made a more compact version with design features to allow use of the EM photoreceivers made by DLR for GRACE Follow-On (Fig. 4). We fabricated a 3D-printed version of this bench, and find it functional, though obviously less stable than a metal structure. Currently, we do not see a need to fabricate a metal structure, as we intend to implement DWS in our test bed, and the bench is primarily used for confirming closed-loop-DWS control, including rotation matrices and signal integrity in the DWS controller.

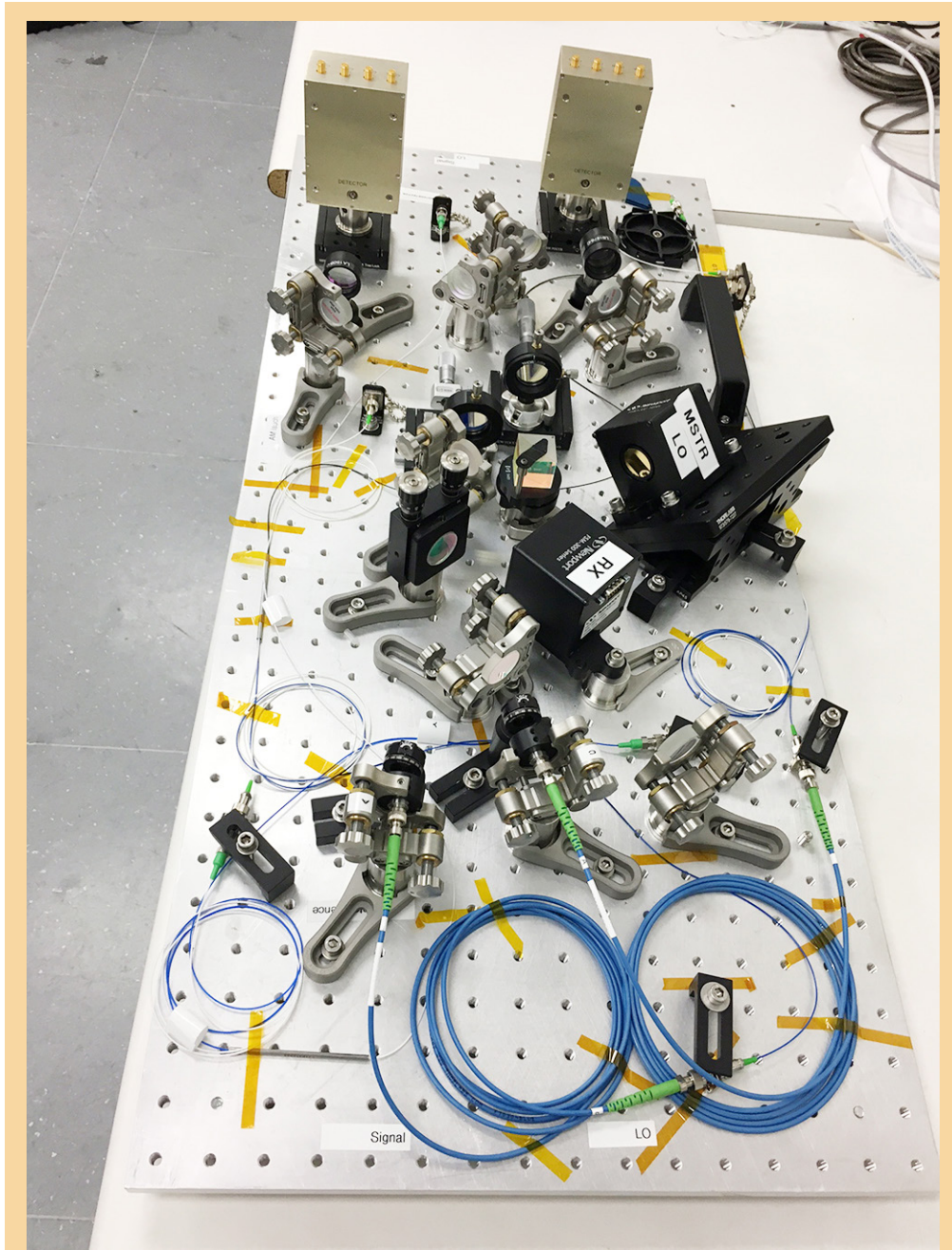


**Fig. 3.** This DWS and control breadboard using quadrant photoreceivers developed for LISA will allow testing of the DWS capability in the Labview phasemeter as a stepping stone to implementation in the test bed, should we want to read out more signals than possible with the LRP EM.



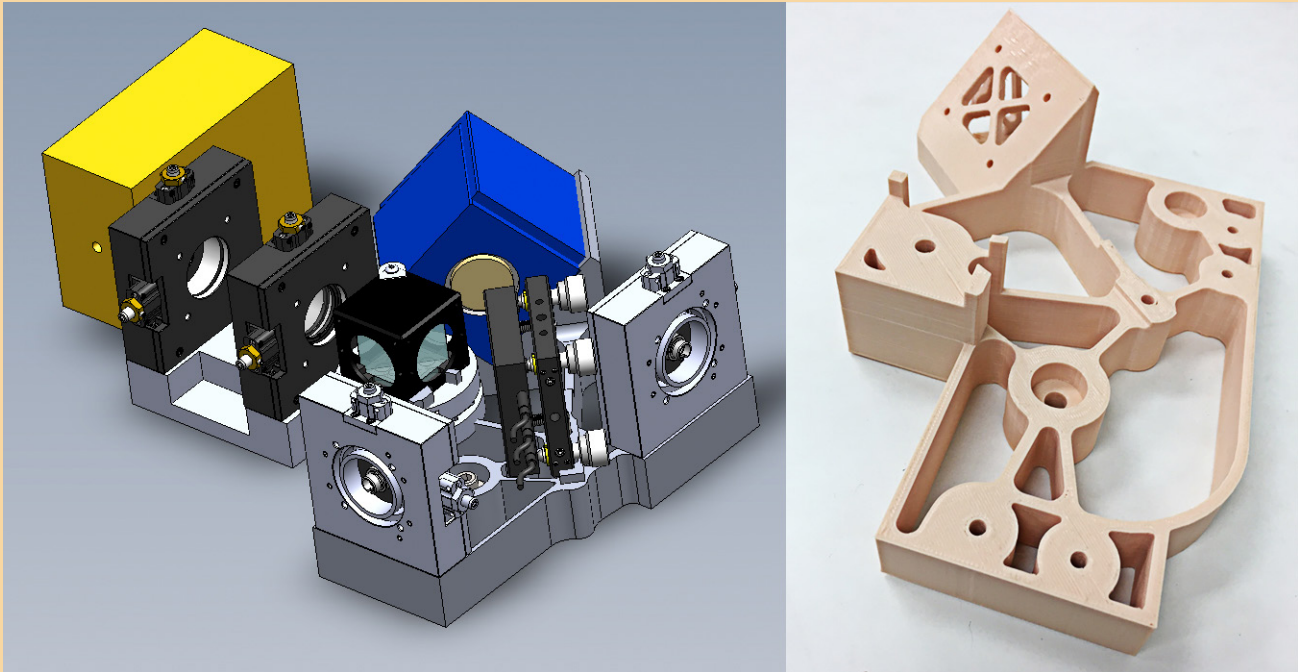


**Fig. 4.** We fabricated a 3D-printed compact version of the DWS bench with design features that allow use of the quadrant photoreceivers made by DLR for GRACE Follow-On.

We are grateful to our German partners on GRACE Follow-On for lending us EM quadrant photoreceivers from GRACE Follow-On for this work. These were lent by STI and AEI; and designed, built, and tested by DLR Adlershof. There are two primary benefits to these photoreceivers compared to the LISA-designed units we had originally intended to use for this work:

1. They are designed to work with the Relative Intensity Noise (RIN) characteristic of the flight lasers used on LISA Pathfinder (LPF) and GRACE Follow-On.
2. These are high-fidelity EMs, and as such represent a more mature design than the LISA photoreceivers we built earlier during our technology development.

The diodes themselves are identical and the noise performance nearly identical. The EM units were built with a custom mechanical interface for integration to the GRACE Follow-On optical bench; we have built a simple mechanical adapter that allows us to incorporate the imaging lens to the mechanical interface and to the photoreceiver, so we can use it in our test bed (Fig. 5). In addition to the photoreceiver front end shown in the figure, there is also back-end amplification and filtering designed to match directly to the LRP phasemeter. We need to complete a realignment of the test bed due to the move, and anticipate using our legacy hardware for much of that work before using the EM hardware.

We are also considering using the GRACE Follow-On EM and flight-spares lasers from Tesat in our test bed once we have it operational again. This provides the most representative laser frequency noise and has the appropriate relaxation oscillation frequency compared to the commercial lasers in our current test bed. The commercial lasers have much higher output power, most of which gets thrown away, so the Tesat lasers, with only 8% the output power of our commercial lasers, may be appropriate. This will be considered further once the low-light design is more mature. The hardware is now all in the same lab, so it should be quite straightforward to implement this if it makes sense.

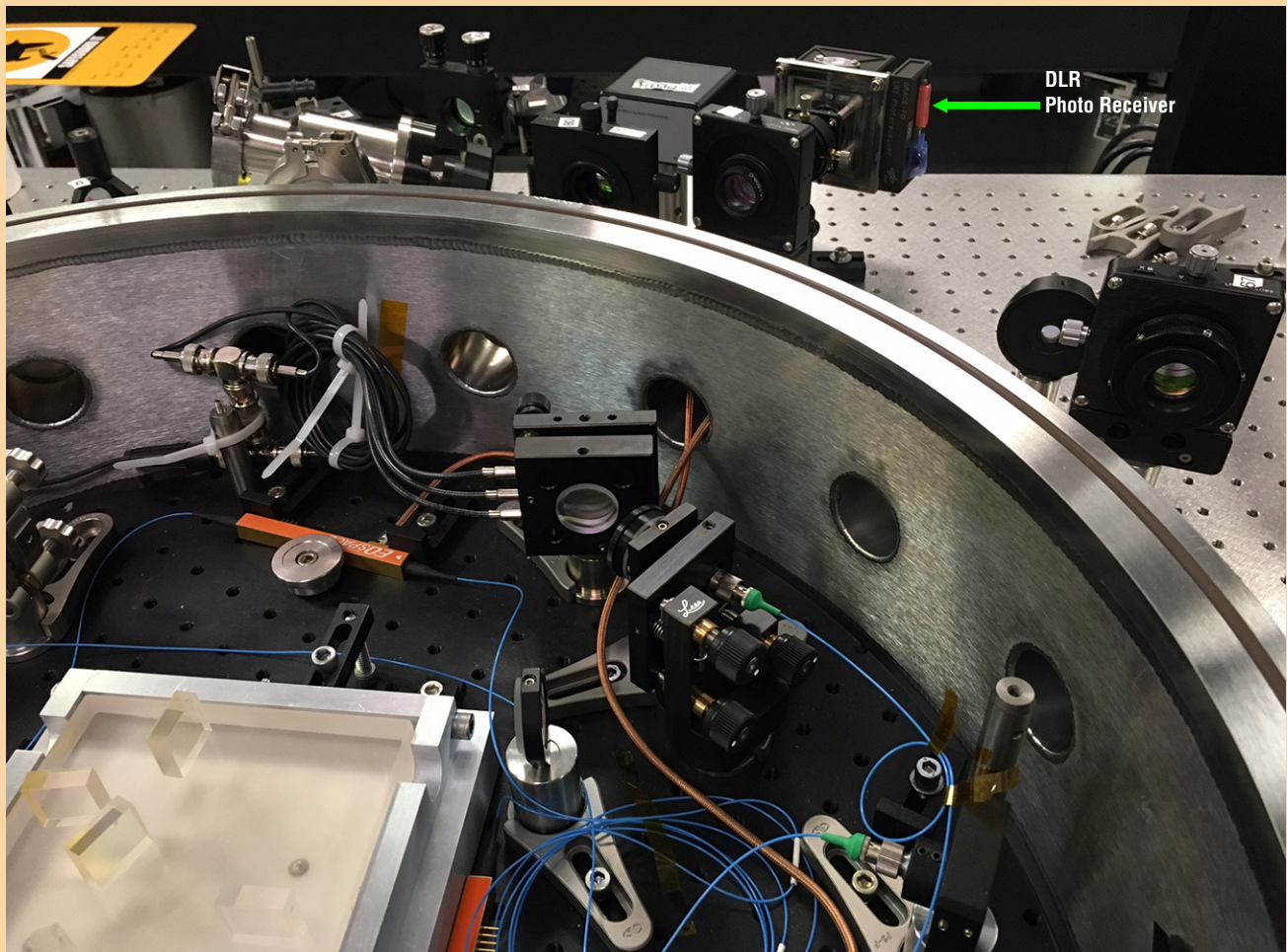


**Fig. 5.** We have prepared the DLR quadrant photoreceiver for use in our test bed. These photoreceivers have similar specifications to the LISA-developed quadrant photoreceivers but with more-appropriate filtering of RIN in the laser. These EM photoreceivers were lent to us by our German partners at STI and AEI, with the photoreceivers designed, built, and tested at DLR Adlershof.

## Path Forward

Incorporating the EMs into our LISA phase-measurement test bed, modified to provide low-visibility signals, will advance the GW technology development, just as it was instrumental in seeding the application to Earth Science.

GRACE Follow-On is scheduled to launch in late 2017. As of this writing, the LRI hardware has been integrated onto Spacecraft 1 at Airbus Defense and Space, and LRI hardware for Spacecraft 2 is currently being integrated. As our LRI work for the mission winds down, we are restarting our SAT efforts, building on our LRI work. Our LISA test bed and LRI laboratories at JPL have been combined, continuing the synergy of technology development for both missions.

For additional information, contact William Klipstein: [bill.klipstein@jpl.nasa.gov](mailto:bill.klipstein@jpl.nasa.gov)





# Telescopes for Space-Based Gravitational-Wave Observatories

Prepared by: Jeffrey Livas (NASA/GSFC)

## Summary

Telescope development for gravitational-wave (GW) detection began in Fiscal Year (FY) 2012 with a funding award from the Physics of the Cosmos (PCOS) Program. It was funded until FY 2015 with a two-year Strategic Astrophysics Technology (SAT) grant plus a no-cost extension. A follow-on SAT grant was awarded in FY 2015 to continue work through FY 2017.

The goal is to develop a telescope suitable for precision metrology for a space-based GW observatory [1-4], where the application is to measure the separation of two spacecraft with a precision of  $10^{-11}$  m/ $\sqrt{\text{Hz}}$  (10 pm/ $\sqrt{\text{Hz}}$ ) over several million kilometers. The telescope technology study effort has developed a set of suitable requirements for the GW metrology application and will investigate the two key design challenges, dimensional stability and scattered-light performance; with modeling, analysis, and experiments. We have adopted the evolved Laser Interferometer Space Antenna (eLISA) [3] as the reference mission.

The work is supported by a team of engineers from the NASA Goddard Space Flight Center (GSFC) Optics Branch; a mechanical engineer; and a postdoctoral fellow, Shannon Sankar, currently a scientist with the Center for Research and Exploration in Space Science & Technology/Universities Space Research Association (CRESST/USRA) (Table 1).

Name	Expertise	NASA/GSFC Code
Jeff Livas	PI	663
Peter Blake	Mirror fabrication	551
Joseph Howard	Optical designer	551
Shannon Sankar	Stray light measurement	663
Lenward Seals	Stray light	551
Ron Shiri	Electro-magnetic (EM) modeling	551
Garrett West	Optical design	551
Justin Ward	Mechanical Engineering	540/Newton

**Table 1.** The eLISA Prototype Telescope Team.

The most significant accomplishment of the past year is the preliminary testing of a prototype telescope that we plan to use to validate our scattered-light model. A summary of the telescope requirements, design, and results has been published [5].

## Background

The telescope technology development targets the requirements for displacement measurement for space-based GW detection. GWs are generated by any mass distribution with a time-changing quadrupole moment [6]. The simplest example is a pair of gravitationally bound masses orbiting around a common center of mass. The efficient generation of GWs requires large compact objects moving at a large fraction of the speed of light. The canonical source is a pair of million-solar-mass black holes colliding. It is believed that black holes of this size are located at the centers of galaxies and co-evolve with them. Therefore, this type of source represents collisions of pairs of galaxies, one of the ways large-scale structure is formed in the universe. The estimated event rate is between 10 and 100 mergers per year, i.e., from once per month to twice per week.

In February 2016, the ground-based Laser Interferometer Gravitational-Wave Observatory (LIGO) network of GW detectors announced the detection of a merging pair of 30-solar-mass black holes. In June, LIGO announced detection of a pair of approximately 10-solar-mass black holes merging. These two detections confirm in spectacular fashion the basic existence of these sources. The million-solar-mass black holes of the centers of galaxies move more slowly and can only be seen from space.

LISA addresses a number of science goals [7-9] and was specifically endorsed by the 2010 Decadal Survey, “*New Worlds, New Horizons in Astronomy and Astrophysics*” (NWNH), as the second-priority large-scale space mission (third priority overall: NWNH, Table ES.5, p. 8) for three specific reasons:

- Measurements of black-hole mass and spin will be important for understanding the significance of mergers in the building of galaxies;
- Detection of signals from stellar-mass compact stellar remnants as they orbit and fall into massive black holes would provide exquisitely precise tests of Einstein’s theory of gravity; and
- Potential for discovery of waves from unanticipated or exotic sources, such as backgrounds produced during the earliest moments of the universe or cusps associated with cosmic strings.

Examples of other expected science returns are the study of galactic populations of binary stars [10] and precision determination of cosmological distances in a manner independent from EM measurements [11].

The function of the telescope for the baseline LISA GW observatory is to serve as a precision beam expander to deliver optical power efficiently from one spacecraft to another [12]. The telescope design for a space-based GW mission is based on a near-diffraction-limited classical Cassegrain-style reflecting optical system. However, since the application is precision-displacement measurement rather than image formation, the normal requirements for high-quality image formation must be augmented by two challenges that require development:

1. The requirement for picometer-level optical-path-length dimensional stability through the telescope in the presence of both axial and transverse temperature gradients.
2. The requirement for low scattered-light levels. Scattered-light levels must be extremely low because the distance measurement uses interferometric techniques that are very sensitive to low light levels and because the telescope must simultaneously transmit a 1W beam and receive a 100 pW beam.

Typical imaging applications do not have these additional requirements.

The long-term goal of this telescope technology-development effort is to make a prototype telescope that meets the basic requirements for a space-based GW observatory and bring it to Technology Readiness Level (TRL) 5-6 in time to be a serious candidate for a mission within the European Space Agency (ESA) Cosmic Vision program L3 opportunity. As of 2016, the best indication we have from ESA is for the technology to be ready by 2019 (see next section), which requires sustained development for the telescope. The ground-based detections announced by LIGO have had the effect of renewed interest in the community, and there is some discussion of moving earlier the launch date for the L3 Mission Opportunity, which is funded in parallel with the L2 opportunity. The immediate goal of the telescope development as currently funded will result in a TRL-3 prototype that can be used to validate a model of the scattered-light performance of the complete telescope and relate it to the properties of the individual mirrors. A second prototype is under development to test dimensional stability with flight-like materials and mirror mounts. Additional work, not currently funded, will be required to reach TRL 4 and then 5.

## Objectives and Milestones

### Overall Objectives in the Context of the International Community

Although the situation is both uncertain and fluid, Fig. 1 shows one possible timeline for development activities for an ESA-led mission. Activities in Europe (top section) and the US (center section, gray background) are shown separately. Shown is the launch and mission of the LISA Pathfinder (LPF) technology demonstration mission, and development activities associated with ESA's Cosmic Vision program L2 opportunity. Not shown are activities associated with the Cosmic Vision L1 mission, JUPITER ICy moons Explorer (JUICE), scheduled for a 2022 launch. The two discoveries of GWs by the ground-based LIGO/Virgo network are shown at the end of 2015. Pulsar timing arrays such as the North American Nanohertz Observatory for Gravitational waves (NANOGrav) may discover signals before the end of the decade. These discoveries have already started to change the scientific landscape and context for a space-based GW mission.

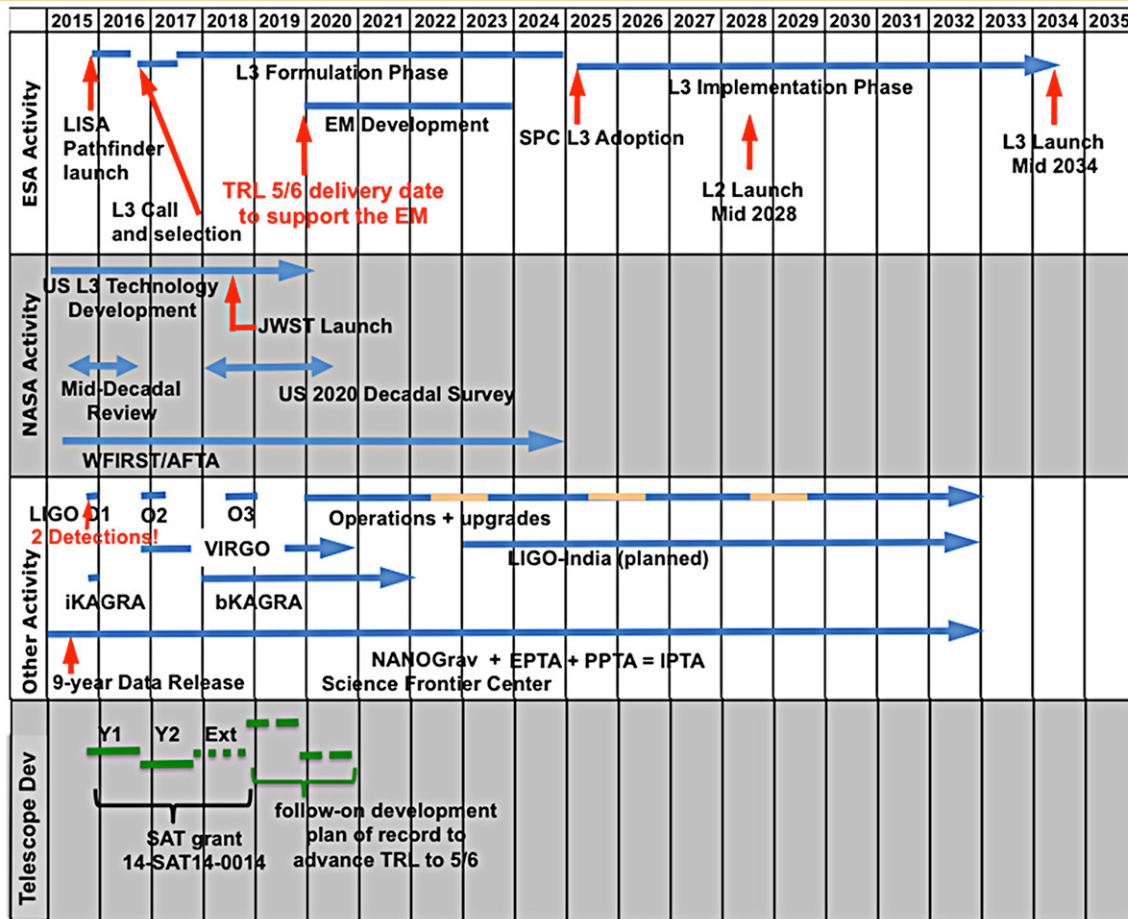


**Fig. 1.** A possible timeline for an ESA-led mission as part of the Cosmic Vision L3 Opportunity showing work in the US (middle section) and Europe (top section). Two discoveries during the first LIGO science operations run, O1, in 2015 and 2016 are shown. The call for the L3 mission concepts is now expected by the end of 2016. Preliminary results from LISA Pathfinder have been released and show that the gravitational reference system (GRS) meets LISA specifications (SPC, Science Programme Committee; KAGRA, Kamioka GRAvitational-wave telescope; PTA, Pulsar Timing Array).

The “Gravitational Universe” was selected as the science theme for ESA’s third large-class mission for the Cosmic Vision Program. With a nominal launch date in 2034, mission selection would nominally occur in 2022. However, ESA established a special committee, the Gravitational Observatory Advisory Team (GOAT) [13], which submitted a report to ESA on March 28, 2016. ESA also recently indicated it has technology development funding available and may select a mission by the end of 2016, with an engineering-model development program beginning in 2020. Therefore, technologies to be considered for the engineering model need to be at TRL 5-6 by the end of 2019. We have adopted this timeline as a working schedule for now.



In this context, the objective of this work over the next few years is to advance the knowledge needed to build a telescope meeting the requirements, so that the US can be a credible international partner for an ESA-led mission, as well as providing a compelling candidate for consideration in the next US Decadal Survey.

### **Objectives and Milestones Specific to Telescope Technology Development**

The tasks and milestones specific to the work in progress are summarized in Fig. 2. Two main activities are currently occurring in parallel: scattered-light testing of the first prototype, and design and procurement of the second prototype. Specific tasks that have been added for the second prototype:

- Second prototype telescope procurement – originally planned for early Jan 2016, but now planned for Aug 2016;
- Preparation for dimensional-stability testing at the University of Florida;
- Stray-light testing of the second telescope; and
- Dimensional-stability testing of the second telescope.

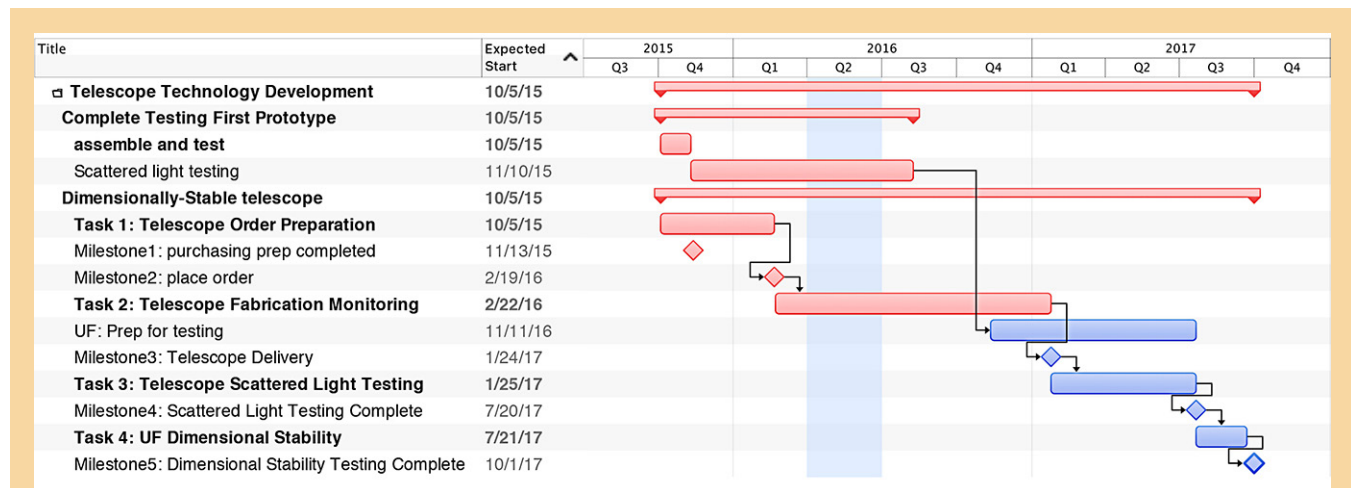


**Fig. 2.** Key project tasks and milestones with an emphasis on the procurement and testing of the second version of the telescope prototype.

Overall, the work has been delayed by approximately six months, but with a no-cost extension, funding should be sufficient to accomplish Task 4, dimensional stability. The stability has already been demonstrated with an on-axis telescope metering structure [14], but still needs a full demonstration with a complete off-axis telescope including optics.

## **Progress and Accomplishments**

### **Previous Accomplishments**

The major accomplishment during 2012-2013 was to complete a study of the telescope design with an industrial contractor. The study included a complete thermal, optical, and a partial mechanical analysis of two implementations – an on-axis design and an off-axis design, and two material systems – carbon-fiber composite and silicon carbide. The study contractor was also required to develop plans for manufacturing and verification testing of these designs. The main results and recommendations are summarized below.

- An on-axis design does not meet the stray-light requirement, so use an off-axis design (on- vs. off-axis manufacturing complexity is similar);
- Use silicon carbide to avoid the unknown effects on dimensional stability from water absorption and subsequent out-gassing with composite materials; and
- The estimate for a ground prototype was a 16-month delivery with a cost of \$2.5M, including:
  - \$1.5M recurring engineering;
  - \$0.26M non-recurring engineering;
  - \$0.43M testing; and
  - \$0.22M focus mechanism.

After the study concluded on April 2013, we chose to concentrate on developing and validating a scattered-light model due to limitations in time and funding. This amounts to a redefinition of Key Milestone #2 (Table 2). We chose to investigate scattering because we had previously investigated silicon carbide for the metering structure and showed it can be stable enough. We therefore fabricated the structure of the telescope out of conventional low-coefficient-of-thermal-expansion (CTE) materials instead of the more expensive silicon carbide.

Year	Milestone	Date	Milestone Description	Redefinition	New Date
FY 2013	1	9/13	Stray light measurement capability	No redefinition – achieved; demonstrated dynamic range of $10^{-10}$	Achieved
FY 2014	2	3/14	Demonstration of scattered-light performance of $<10^{-10}$ of transmit power	Develop and validate a scattered-light model	9/16
FY 2014	3	9/14	Demonstration of optical-path-length stability	Not possible – materials and construction of prototype that could be environmentally tested too expensive	Projected 10/17

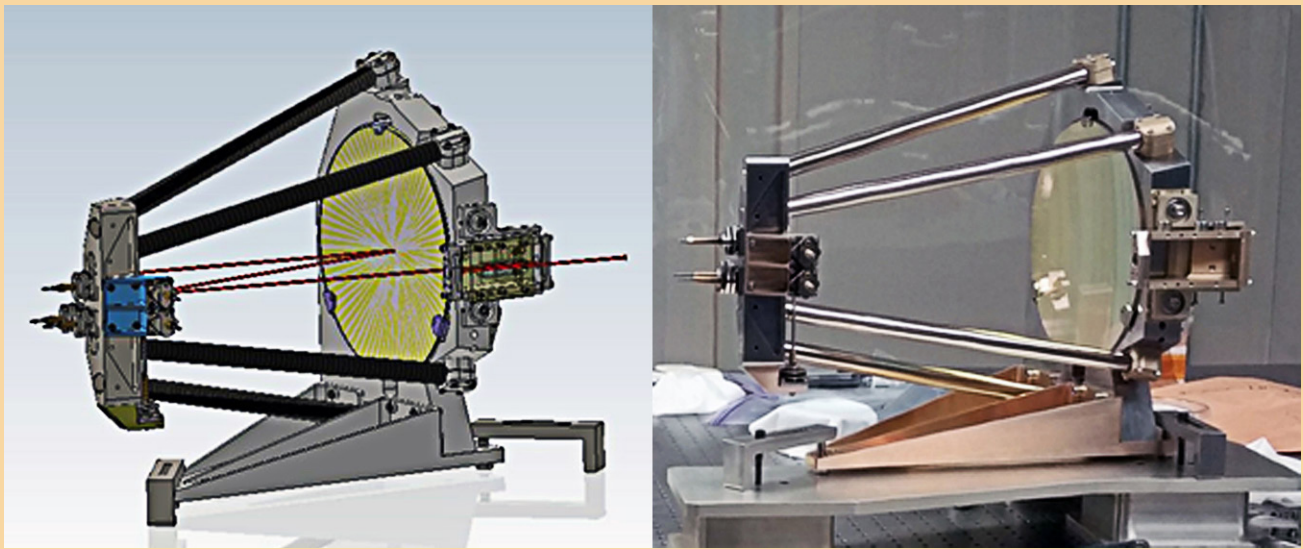
**Table 2.** Key milestones as redefined. No change from 2014.

We modified the telescope design from the one developed in the study, simplifying it while retaining its essential features. We then designed the mirrors for the simplified telescope design. We ordered a complete set of mirrors to build a prototype, as well as several pairs of M3 and M4, the two mirrors the model shows are the largest sources of scattered light. The idea is to try different combinations of surface roughness and coatings to better understand how to achieve the scattered-light requirement and demonstrate that we understand the physics.

We were able to find a vendor who agreed to build a complete prototype telescope to meet our requirements at room temperature, and held a kick-off meeting on June 19, 2014. We supplied a set of mirrors as Government-Furnished Equipment (GFE). The Critical Design Review (CDR) was held on October 30, 2014, and the telescope was delivered to GSFC on June 5, 2015.

### **Recent Accomplishments**

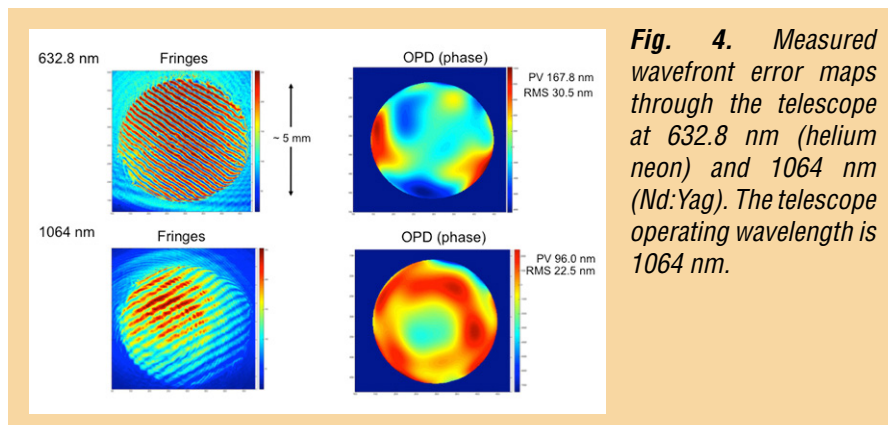
Figure 3 shows the telescope, a 4-mirror afocal design with a 200-mm-diameter primary, and a 5-mm collimated output beam. The left panel shows the path of the central ray through the telescope. The right panel shows a photo of the telescope as it was finally aligned in the vendor's clean facility.



**Fig. 3.** Prototype telescope. Left: Drawing of the telescope with the central, or “gut” ray’s path through the telescope indicated by the solid brown line. The secondary mirror is in the blue mount to the left of the primary. Right: Photo of the telescope as aligned in the vendor’s clean room.

The telescope was installed in the Laser Communication Relay Demonstration (LCRD) clean room, where we arranged to share the space through the end of the calendar year. The immediate next step was to re-assemble and re-align the telescope. The M3/M4 assembly was relatively easy to align with the alignment jig supplied by the vendor, and we were able to recover the coarse alignment of the M1 and M2 pair using a Point-Source Microscope (PSM).

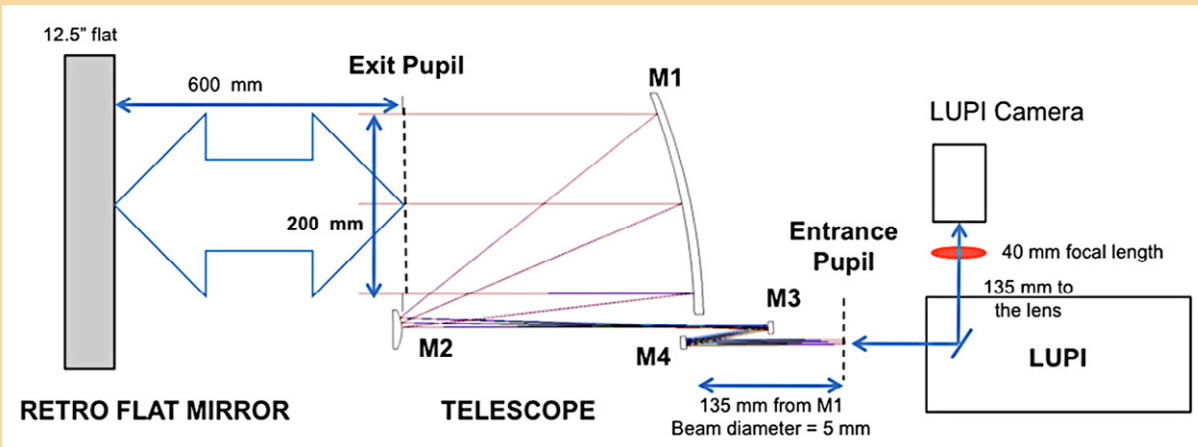
Final alignment was accomplished with a test setup based on a Laser Unequal Path-length Interferometer (LUPI) and a large auto-collimating flat in a double-pass configuration. Figure 4 shows the results. The telescope meets specifications at both wavelengths.



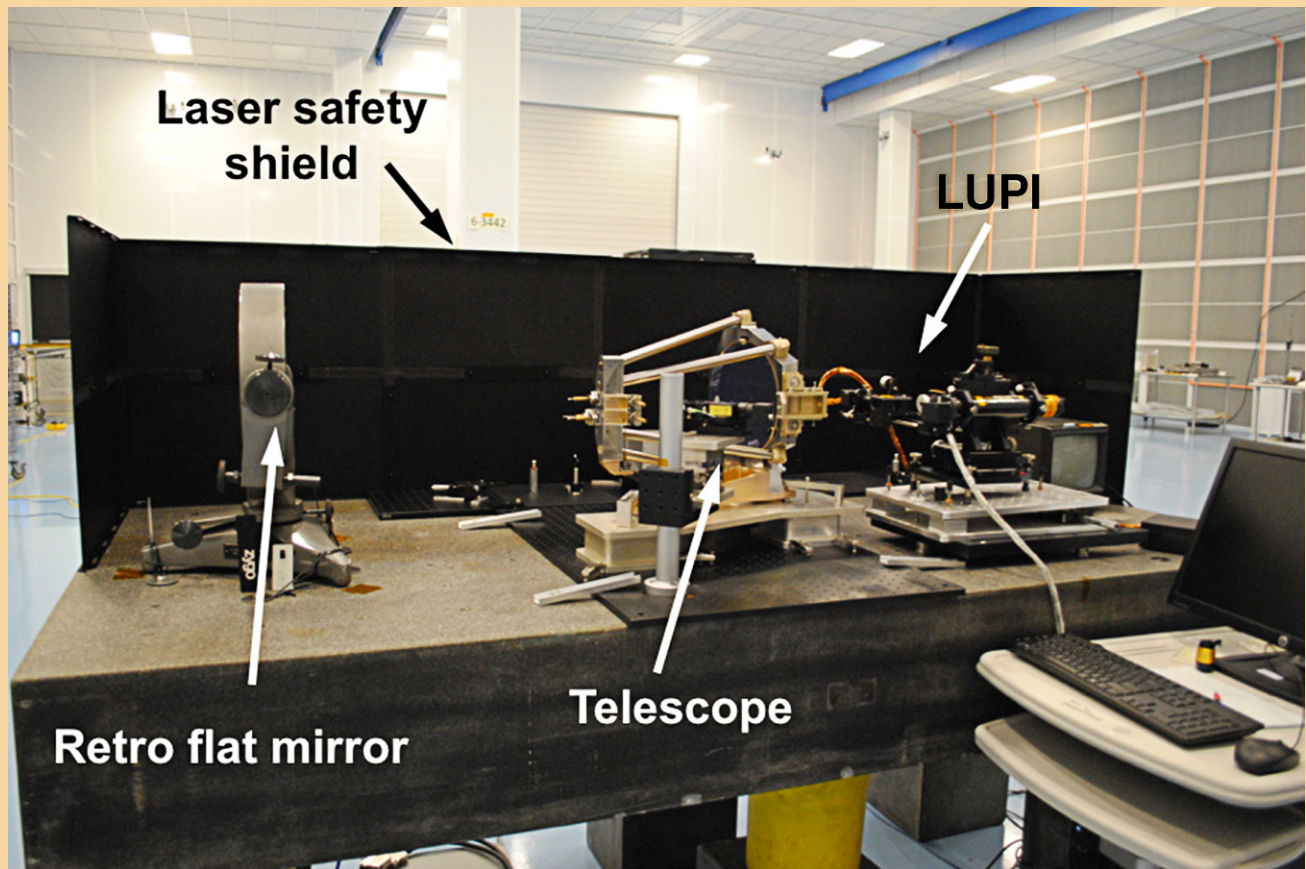
**Fig. 4.** Measured wavefront error maps through the telescope at 632.8 nm (helium neon) and 1064 nm (Nd:Yag). The telescope operating wavelength is 1064 nm.

Figure 5 shows the optical layout with the LUPI on the lower right hand side injecting a collimated beam into the 5-mm entrance pupil of the telescope. A 200-mm collimated beam is reflected from a 318-mm-diameter flat mirror (12.5”) and re-enters the LUPI. Figure 6 shows a photograph of the test setup as installed in the clean room.



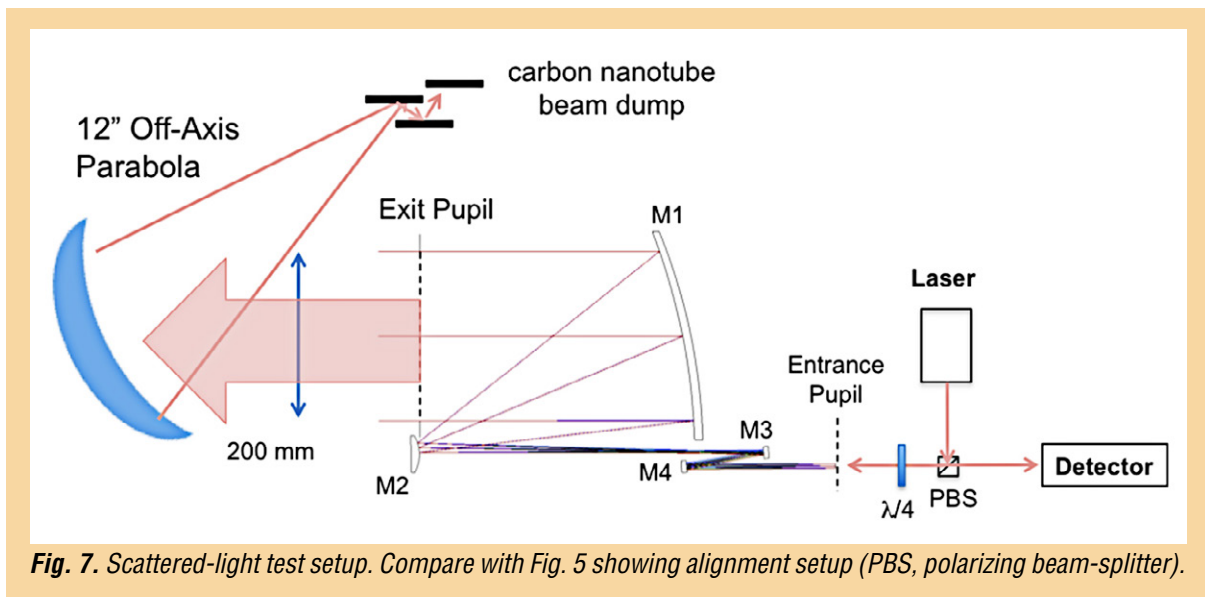


**Fig. 5.** Layout of the alignment and test setup for the telescope. A double-pass test with an auto-collimating flat allows the use of a LUPI with a 5-mm beam to test the full 200-mm aperture telescope.



**Fig. 6.** Photograph of the test setup in the LCRD cleanroom. Setup is shown schematically in Fig. 5.

In April, the LCRD project needed more space, and we were able to relocate to the Advanced Interferometry and Metrology (AIM) Laboratory cleanroom. We have just reassembled the test bed in the AIM laboratory, realigned the telescope, and modified the test setup slightly as shown in Fig. 7. The main difference between the setup in Figs. 5 and 7 is that instead of auto-collimating the light transmitted through the telescope back on itself, we direct it off-axis to a beam dump. Then, the only light coming back into the detector should be that scattered from the telescope.



Before the move to the AIM Lab, we found rough agreement between a scattered-light model and measurements of the total integrated scatter. This is a good start, but we still need to verify scattering into the correct solid angle at the receiver, as well as the distribution of scattering among the different mirrors. Work is now proceeding to get back to the same level of sensitivity to scattered light that we had in the LCRD cleanroom.

As part of the scattered-light testing, we collaborated with Gari Billingsley and Liyuan Zhang from the LIGO project at Caltech to make some measurements of the scattered light from the M3 mirror. Their preliminary results are shown in Fig. 8. We need to compare these measurements against our model in detail, but one immediate conclusion is that the gold coatings, shown in the top red trace, scatter much more light than the ion-beam-sputtered (IBS) coatings. These measurements are part of the verification process for the model. We would like to be able to relate the system-level performance of the telescope to the individual mirror properties.

Scattered-light suppression work was augmented with funding received by Ron Shiri through the GSFC Internal Research and Development (IRAD) program for development of partially

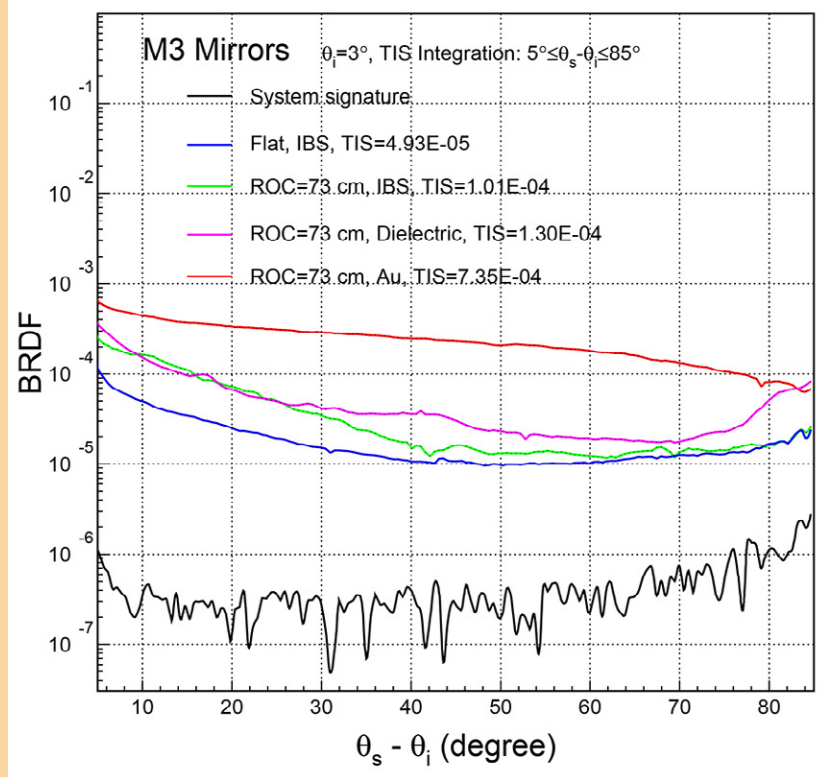


**Fig. 8. Scattered-light measurements from M3.** Data courtesy of Gari Billingsley and Liyuan Zhang, LIGO Caltech (BRDF, Bidirectional Reflectance Distribution Function; TIS, Total Integrated Scatter; ROC, Radius of Curvature).

transparent petaled masks. This funding enabled Ron to engage with the University of Delaware for fabrication of partially transparent masks. Fabrication methods have been tested and a patent application filed [15, 16].

The purpose of this work with masks is risk reduction. Successful implementation of these masks may allow us to adopt an on-axis telescope design, which may be less expensive to build and better suited to the application's environmental requirements compared to an off-axis design. The same design techniques can be applied to coronagraph applications, which are currently proposed for exoplanet missions.

## Path Forward

The key milestones for the project originally proposed for the FY 2012 SAT grant are shown in Table 2 as redefined. The first milestone, demonstrating the ability to detect low levels of scattered light, was successfully accomplished in the summer of 2013.

The second milestone, demonstrating low-scattered-light performance with a prototype telescope, is still in progress. Our model of the telescope predicts that 97% of the light scattered from the telescope should be from the two small mirrors M3 and M4, and we are trying to verify this is correct. This work was described in the previous section.

The third milestone is to demonstrate the optical-path-length stability requirement. It is not necessary to develop the path-length-stability measurement capability because we plan to take advantage of the capability already developed for measuring a silicon carbide spacer at the University of Florida [14, 17, 18]. In practice, some work will be needed to adapt the existing setup to a real telescope with optics instead of just a metering structure, and to improve the temperature-measurement instrumentation, but the basic capability exists. A second iteration of the prototype telescope with more flight-like materials will be required to demonstrate dimensional stability, and the work has been funded with an SAT grant beginning in FY 2015.

Figure 9 shows the optical design that has been developed for the second prototype. The design is based on the first prototype, but one of the key insights from the scattered-light modeling was that although the mirrors all scatter light into a hemisphere, the M3 and M4 mirrors contribute most of the scattered light on the detector because they focus the beam. The optical design for the Prototype 2.0 makes M3 a flat so that it has no focusing properties at all. The optical correction for the loss of the M3 focusing power has been made on the primary mirror, where the added complexity is relatively easy to fabricate and does not contribute to stray light on the detector. A flat mirror can also be polished extremely flat, so in principle this design takes M3 out of the scattered light budget. We plan to fabricate and test this.

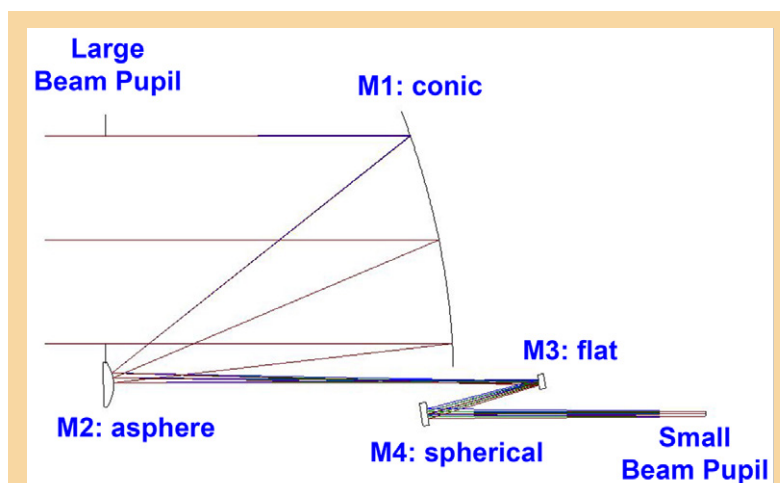


**Fig. 9.** Prototype Telescope 2.0 optical design. This design is based on the previous prototype, but includes some insight from scattered-light modeling and testing.



An important extension of this work is to examine the possibility of including a small moving mirror as part of the design. This design extension is referred to as “in-field pointing,” which allows the telescope in principle to accommodate a large change ( $\pm 1^\circ$ ) in the line-of-sight of the input beam without physically moving the telescope. The current baseline design has the telescope mounted as a complete assembly with the optical bench and the gravitational reference mass so the entire assembly can be moved on a pivot. Preliminary work indicates that the basic design with a small steerable mirror may be optically possible, but that it may have implications on scattered-light performance. This is a system-level aspect of the telescope design that no one else has investigated, and has the potential to be a show-stopper for this concept. As resources permit, we will evaluate the in-field pointing concept and its implications for scattered light to determine if it is feasible or not.

## Acknowledgements

The author would like to thank P. Bender, G. Mueller, J. Sanjuan, A. Spector, R. Stebbins, the members of the GW Study Team and eLISA Telescope Team for advice, support, and stimulating discussions.

## References

- [1] P. Bender, K. Danzmann, and LISA Study Team, “*LISA for the Detection and Observation of Gravitational Waves*,” Max-Planck-Institut für Quantenoptik, Garching Technical Report No. MPQ233 (1998)
- [2] “*LISA Unveiling a Hidden Universe Assessment Study Report*,” (Yellow Book), ESA/SRE 3 (2011)
- [3] P. Amaro-Seoane et al., “*The Gravitational Universe*,” eLISA L2 White Paper
- [4] “*Gravitational-Wave Mission Concept Study Final Report*” (2012)
- [5] J. Livas, P. Arsenovic, J. Crow, P. Hill, J. Howard, L. Seals, and R.S. Shiri, “*Telescopes for Space-based Gravitational Wave Missions*,” Opt. Eng. **53**, 9, 091811 (2013). doi: 10.1117/1.OE.52.9.091811
- [6] B.F. Schutz, “*Gravitational waves on the back of an envelope*,” Am. J. Phys. **52**, 412 (1984)
- [7] P. Amaro-Seoane et al., “*Low-frequency gravitational-wave science with eLISA/NGO*,” Class. Quantum Grav. **29**, 12, 124016 (2012)
- [8] P. Amaro-Seoane et al., “*Intermediate and extreme mass-ratio inspiral astrophysics, science applications, and detection using LISA*,” Class. Quantum Grav. **24**, 17 (2007)
- [9] A. Stroeer and A. Vecchio, “*The LISA verification binaries*,” Class. Quantum Grav. **23** S809-S817 (2006)
- [10] S. Nissanke et al., “*Gravitational-wave emission from compact Galactic binaries*,” Astrophys. J. **758**, 131 (2012)
- [11] C. Cutler and D.E. Holz, “*Ultra-high precision cosmology from gravitational waves*,” Phys. Rev. D **80**, 104009 (2009)
- [12] O. Jennrich, “*LISA technology and instrumentation*,” Class. Quantum Grav. **26**, 15, 153001 (2009)
- [13] ESA “[Gravitational Observatory Advisory Team \(GOAT\) Final Report](#)” (2016)
- [14] J. Sanjuan et al., “*Note: Silicon carbide telescope dimensional stability for space-based gravitational wave detectors*,” Rev. Sci. Instrum. **83**, 11, 116107 (2012)
- [15] R.S. Shiri et al., “[Fabrication of petal-shaped masks for suppression of the on-axis Poisson spot in telescope systems](#),” Rev. Sci. Instrum. **87**, 043112 (2016)
- [16] R.S. Shiri and J. Livas, “*Design and Fabrication of Partially Transparent Petaled Mask or Occulter Using Grayscale Lithography*,” US Patent application GSC-17289-1, filed May 25, 2016
- [17] J. Sanjuan et al., “[Carbon fiber reinforced polymer dimensional stability investigations for use on the laser interferometer space antenna mission telescope](#),” Rev. Sci. Instrum. **82**, 12, 124501, DOI: 10.1063/1.3662470 (2011)
- [18] A. Preston, “*Stability of materials for use in space-based interferometric missions*,” Ph.D. Dissertation, University of Florida (2010)

For additional information, contact Jeffrey Livas: [Jeffrey.Livas@nasa.gov](mailto:Jeffrey.Livas@nasa.gov)



# Directly Deposited Optical-Blocking Filters for Imaging X-ray Detectors

Prepared by: Mark Bautz (PI; MIT Kavli Institute for Astrophysics & Space Research, MKI); S. Kissel (MKI); and K. Ryu and V. Suntharalingam (MIT Lincoln Laboratory), with special thanks to R. Masterson and the MIT Space Sciences Laboratory's REXIS team.

## Summary

We aim to raise the Technology Readiness Level (TRL) of enhanced charge-coupled-device (CCD) detectors capable of meeting the requirements of X-ray grating spectrometers (XGS) and wide-field X-ray imaging instruments for small, medium, and large missions. Because they are made of silicon, all X-ray CCDs require blocking filters to prevent corruption of the X-ray signal by out-of-band, mainly optical and near-infrared (near-IR) radiation. We endeavor to replace the fragile, extremely thin, free-standing blocking filter that is current standard practice with a much more robust filter deposited directly on the detector surface.

High-performance, back-illuminated CCDs have flown with free-standing filters (e.g., one of our detectors on Suzaku) and other, relatively low-performance CCDs with directly deposited filters have flown (e.g., on the X-ray Multi-mirror Mission-Newton, XMM-Newton Reflection Grating Spectrometer, RGS). However, a high-performance, back-illuminated CCD with a directly deposited filter has not yet been demonstrated. Our effort will be the first to show such a filter can be deposited on an X-ray CCD that meets the requirements of a variety of contemplated future instruments.

This Strategic Astrophysics Technology (SAT) program, a collaboration between the MKI and MIT Lincoln Laboratory, began on July 1, 2012. The program is currently scheduled to end June 30, 2017.

## Background

The past two decades have brought extraordinary progress in X-ray astronomy, in large measure as a result of unprecedented improvements in X-ray imaging and grating spectroscopy. Beginning with the launch of the Advanced Satellite for Cosmology and Astrophysics (ASCA) in 1993, and continuing to the present, concurrent operation of Chandra, XMM-Newton, Swift, and Suzaku, much of this success has been enabled by X-ray photon-counting CCDs. CCDs will likely remain essential to many X-ray instruments for some time to come. In fact, the Astrosat mission, launched just last year, and Spektrum-Roentgen Gamma, scheduled to launch early in 2017, both feature these detectors. Moreover, a number of future mission concepts include instruments relying on CCDs or other silicon-based X-ray imagers. Such instruments address a broad range of important scientific objectives. For example, as noted recently in the X-ray Mission Concepts Study Report (XCSR) commissioned by NASA's Program Office for the Physics of the Cosmos (PCOS) [1], several high-priority scientific questions identified by the 2010 Decadal Survey, "New Worlds, New Horizons in Astronomy and Astrophysics" (NWNH) [2] are best addressed by an XGS, which requires large-format X-ray imaging detectors. Specific science goals for an XGS and a Wide-Field Imager (WFI) are discussed in the report of the X-ray Community Science Team [1] and summarized in Table 1. The report notes an XGS could be deployed either alongside an X-ray micro-calorimeter on a Probe-scale mission, or as the sole instrument in a more modest, dedicated mission. XGS technology has therefore been identified as a Priority 1 (highest-priority) need in the 2012 PCOS Program Annual Technology Report (PATR) [3]. Both an XGS and a silicon-based, high-definition X-ray imager are key instruments for the X-ray Surveyor, a strategic mission concept identified as a priority by the NASA Astrophysics Roadmap "Enduring Quests, Daring Visions" [4], and now under study at NASA's Marshall Space Flight Center (MSFC) [5].

Science Question	Measurement	Instrument
How does large-scale structure evolve?	Find and characterize the missing baryons via high-resolution absorption-line spectroscopy of the Warm-Hot Intergalactic Medium (WHIM)	XGS
How does matter behave at high density?	Measure the equation-of-state of neutron stars through spectroscopy	XGS
How are black holes connected to large-scale structure?	Determine energetics and mass flows in Active-Galactic-Nuclei (AGN) outflows; probe hot galaxy halos via absorption spectroscopy	XGS
When did the first galaxies emerge and what were they like?	Identify high-redshift galaxies via Gamma-Ray Bursts (GRBs)	WFI
What new discoveries await in the time domain?	Monitor the entire sky with high sensitivity to find and study gravitational-wave sources and other transients	WFI

**Table 1.** High-priority science drivers for future instruments featuring large-format, imaging X-ray detectors (adapted from PCOS X-ray Mission Concepts Study Report [1]). Directly deposited optical blocking filters (OBFs) will improve performance and reliability, while reducing cost and risk of instruments addressing these questions.

Large-format, X-ray imaging detectors are also required for many missions envisaged for the Explorer program, which NWNH deemed “*a crown jewel of NASA space science*.” For example, an Explorer XGS has been proposed for a focused study of the cycles of baryons in and out of galaxies, and their role in galaxy evolution [6]. Other future Explorers will exploit the power of rapid-response X-ray imaging, so clearly demonstrated by Swift, but with much wider fields of view. As noted in [7], an X-ray WFI on an agile spacecraft can address with unprecedented sensitivity a variety of important science objectives ranging from the nature of the first galaxies to high-energy, time-domain astrophysics. An especially exciting prospect is identification of sources that may be detected by ground-based gravitational-wave observatories later in this decade [8, 9].

Our program aims to raise the TRL of advanced OBF technology required for these instruments. If successful, our effort will improve instrument sensitivity, robustness, and reliability. At the same time, it will reduce mass, complexity, risk, and cost. Our approach is to replace the fragile, free-standing, optical-blocking membrane of current practice with a filter deposited directly on the detector surface. A directly deposited filter can be thinner than a free-standing one, improving instrument sensitivity. Moreover, directly deposited filters do not require the heavy, complex, and expensive vacuum housings used in current instruments, and are of course much more robust than free-standing filters. The key challenge for our program is to demonstrate that blocking filters can be applied directly to the sensitive entrance surfaces of modern CCD detectors without compromising spectroscopic resolution.

To minimize cost, our program uses existing stocks of engineering-grade detectors produced for past programs at MIT Lincoln Laboratory. We apply so-called ‘back-illumination’ processing to these detectors, and then use coating facilities at Lincoln to apply blocking filters. X-ray and optical performance-testing is then conducted at MKI. We have also joined forces with REgolith X-Ray Imaging Spectrometer (REXIS), an MIT student instrument for NASA’s Origins Spectral Interpretation Resource Identification Security – Regolith Explorer (OSIRIS-REx) mission, to incorporate directly deposited blocking-filter technology into a flight program.

## Objectives and Milestones

Silicon X-ray imaging detectors require blocking filters to prevent ambient visible and ultraviolet (UV) background light from adding noise and degrading X-ray spectral resolution. As noted above, most such detectors flown to date have used fragile, free-standing filters comprised of thin plastic substrates coated with aluminum. Free-standing filters usually must be protected from ground-handling and launch acoustic loads using heavy vacuum enclosures equipped with complex door mechanisms. This



project aims to show that adequate OBFs can be deposited directly on a detector, eliminating the need for fragile, freestanding filters. To the extent they eliminate plastic films, such filters could also improve soft X-ray ( $E < 1$  keV) detection efficiency.

A key challenge in this project is to demonstrate directly deposited OBFs provide the requisite optical blocking performance without compromising the spectral resolution of the detectors in the soft band. The latter depends critically on the electric fields present just inside the entrance surface of the detector, and these fields in turn require precisely controlled implant-density profiles. Our aim is to deposit blocking filters in such a way that the surface fields are unaffected by the deposition process or the filter itself. A secondary objective is to demonstrate such filters are sufficiently robust to survive the repeated thermal cycling any such detector is likely to experience.

Originally, we planned to complete the following four tasks:

***Task 1: Select and thin existing CCID41 wafers and apply backside treatment***

The target detectors for this project (Lincoln Laboratory model CCID41, used in Suzaku) were stored in wafer form as front-illuminated (FI) devices (typically four to a wafer). We identify functional devices using wafer-probe equipment. We then subject selected wafers to a custom, backside treatment process, involving wafer thinning and molecular-beam-epitaxy (MBE) passivation, which has already been shown to provide good X-ray results. Selected back-illuminated (BI) devices are packaged (removed from the wafer and installed in test packages) for subsequent test at MKI.

***Task 2: Establish baseline X-ray performance***

We use established X-ray characterization facilities and procedures at MKI to verify suitable X-ray performance of the BI (but uncoated) devices.

***Task 3: Apply filters and characterize filter-equipped devices***

We use established thin-film deposition facilities at MIT Lincoln Laboratory to deposit aluminum blocking layers, and then package and test the filter-equipped devices. Filters are applied at the wafer level, with control areas masked to allow direct comparison of filtered and unfiltered areas of each device. We contemplate three cycles of filter deposition and test (one wafer per cycle), applying a relatively thick filter in the first cycle, and then continuing, after successful test, to progressively thinner filters. In so doing, we span the range of filter thicknesses required by future instruments. All filters will be capped with a 10-nm  $\text{Al}_2\text{O}_3$  layer to improve robustness and provide UV blocking. Both optical rejection and X-ray spectral resolution will be measured in the characterization protocol.

***Task 4: Test robustness and stability***

To verify coating temporal stability and robustness to the repeated thermal cycling experienced by CCD detectors during instrument development and test, we will perform thermal cycling and long-term (6-8-month) stability measurements.

Soon after program start, we decided to alter the sequence of the program for two reasons. First, we discovered that a number of BI devices were already available at MIT Lincoln. To make best use of these, we needed to develop a filter deposition process that would accommodate individual chips as well as full wafers. Second, we learned that the MIT team developing REXIS wished to fly X-ray CCDs with directly deposited blocking filters. We decided to collaborate with REXIS because by doing so we gain the opportunity to demonstrate much higher TRL for our process than we could achieve in our original program. The REXIS flight instrument was integrated into OSIRIS-REx in January, and launched on September 2016. Although this collaboration has entailed some re-planning, we expect to achieve our objectives as scheduled.

Major milestones and our progress in achieving them are summarized in Table 2. We describe our progress in more detail in the following section.

Milestone at completion of:	Success Criteria	Status as of June 2016
1. BI processing	Wafer-probe testing of BI wafers shows: <ul style="list-style-type: none"> <li>• <math>\geq 3</math> wafers with functional devices</li> <li>• <math>\geq 10</math> functional devices total</li> </ul>	<ul style="list-style-type: none"> <li>• Twelve FI wafers processed, yielding 33 devices with at least some functionality, of which eight are allocated to REXIS</li> <li>• Ten other functional BI devices identified as single chips</li> </ul>
2. X-ray test of baseline BI device	X-ray performance demonstrated per protocol specified in proposal	<ul style="list-style-type: none"> <li>• Complete; X-ray performance supports program objectives</li> </ul>
3. 1 <sup>st</sup> device with thickest directly deposited filter	Packaged device delivered to MKI	<ul style="list-style-type: none"> <li>• Complete (220-nm-Al OBF)</li> </ul>
4. X-ray and optical testing of device with thickest filter	X-ray and optical tests done per protocol specified in proposal	<ul style="list-style-type: none"> <li>• Complete; three devices with 220-nm OBF characterized</li> </ul>
5. X-ray and optical testing of device with thinnest filter	X-ray and optical tests done per protocol specified in proposal	<ul style="list-style-type: none"> <li>• Complete; one device with 100-nm OBF and two with 70-nm OBF characterized</li> </ul>
6. Long-term stability test	X-ray and optical tests done per protocol specified in proposal	<ul style="list-style-type: none"> <li>• In progress: 8 months of planned 12-month test completed</li> </ul>
7. Thermal cycle test	X-ray and optical tests done per protocol specified in proposal	<ul style="list-style-type: none"> <li>• Thermal vacuum (TVAC) X-ray testing of REXIS flight unit completed</li> <li>• Post-TVAC optical characterization of REXIS engineering unit planned</li> </ul>

**Table 2.** Project milestones and status.

## Progress and Accomplishments

At the completion of the fourth year of our project, we have developed an OBF-deposition process and thoroughly characterized X-ray and optical performance of BI CCDs with OBFs of a range of thicknesses (220-, 100-, and 70-nm Al) as specified in Milestones 1-7 in Table 2. Our principal results may be summarized as follows.

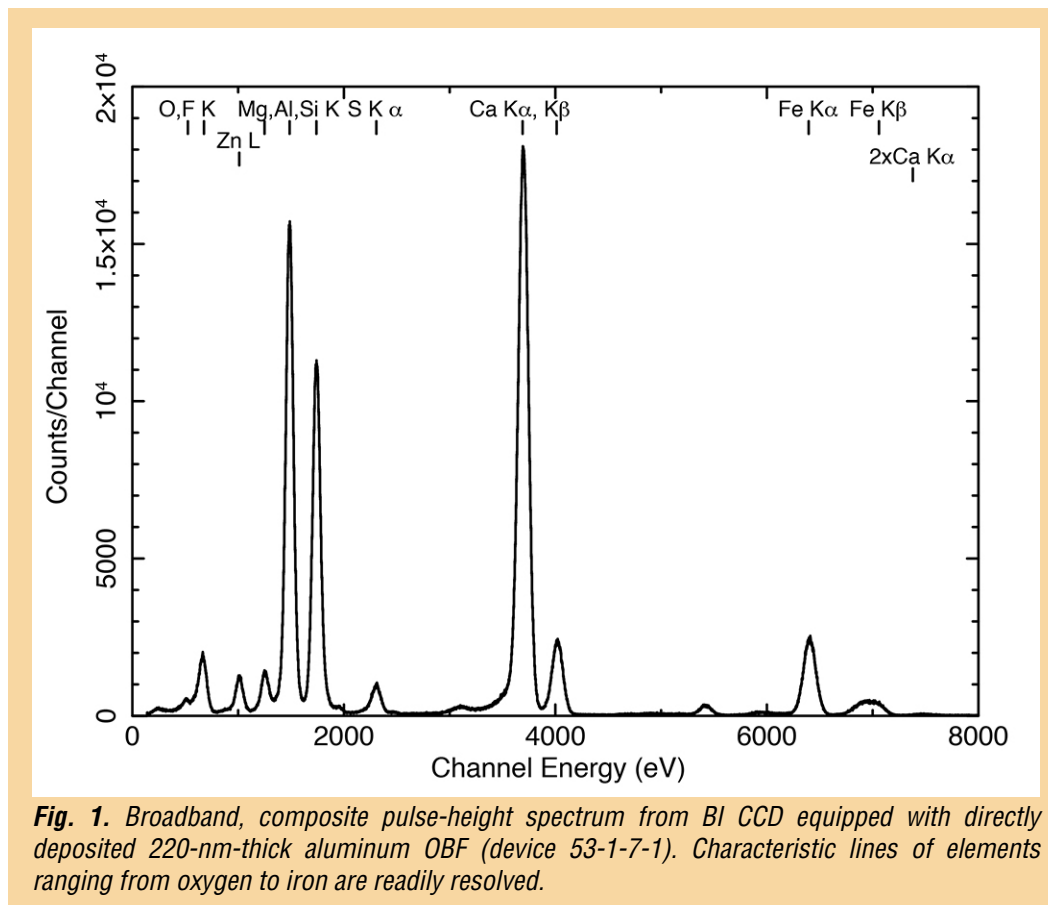
1. We demonstrated that it is feasible to deposit effective aluminum OBFs directly on high-performance BI CCDs with at most modest effect on X-ray spectral resolution.
2. The measured X-ray transmission of these OBFs is consistent with theoretical expectations.
3. The measured visible/near-IR transmission of these OBFs is consistent with the expected level of attenuation over most of the filter area, but higher than expected transmission is observed in a small fraction of pixels. The pixels exhibiting these so-called “pinholes” can have sensitivity to visible light that is  $10\times$  to  $1000\times$  theoretical expectations. We have evidence these pinholes are produced by irregularities on the detector surface. These irregularities, each extending over at most a few hundredths of a square micron of detector surface, seem to cause small breaks in the aluminum blocking layer. The irregularities in turn may be caused either by intrinsic roughness of the CCD surface or by sub-micron particulate contamination. The fraction of pixels exhibiting these pinholes can be reduced to 1% or less by (i) minimizing the density of sub-micron particles on the detector surface before aluminization and (ii) suitably orienting the detectors relative to the aluminum source during OBF deposition.
4. For very demanding optical blocking applications, requiring visible/IR-band attenuation factors greater than  $10^6$ , we found that it may be necessary to take additional steps to prevent light from entering the detector through its sidewalls and through the adhesive layer that affixes the detector to its package. We developed methods for doing this for the REXIS instrument.

5. Interim results from our planned long-term stability tests show no change in visible/IR-blocking performance of a directly deposited OBF after eight months of storage in a lab environment.
6. The REXIS flight instrument, containing CCDs with directly deposited blocking filters, has successfully completed vibration and TVAC testing. Satisfactory X-ray performance was observed throughout these tests, but it has not been possible to monitor the post-test optical performance of the REXIS OBFs. In the coming year, we plan to repeat vibration and TVAC testing of the REXIS engineering unit, including comprehensive post-environmental performance testing, to confirm OBF performance and demonstrate that we have achieved TRL 6.

We discuss each of these results in turn.

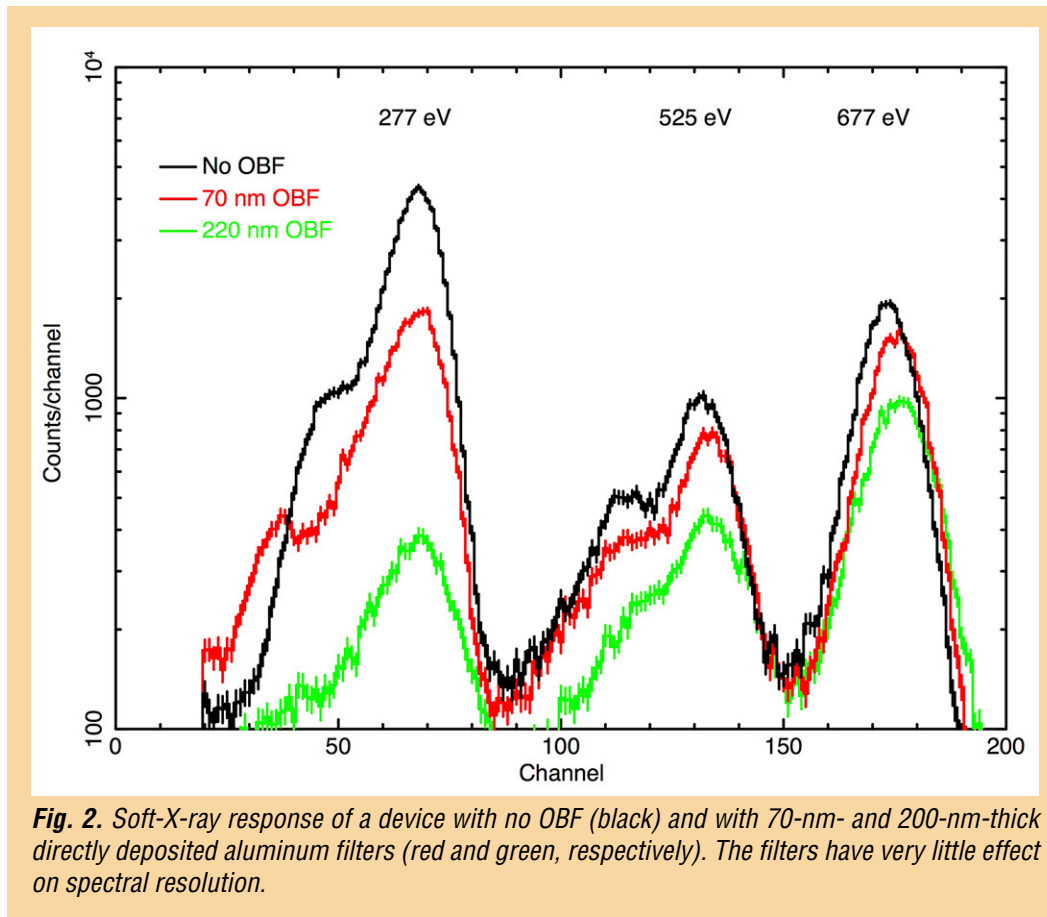
### **1. Soft X-ray spectral resolution with directly deposited blocking filters**

Soft X rays (with energies below 1 keV) are photo-electrically absorbed within  $\sim 1 \mu\text{m}$  of the entrance surface of a silicon detector, so good X-ray spectral resolution requires efficient collection of photoelectrons generated in this region. Precise doping of the entrance ('back') surface of the detector is necessary to produce the internal electric fields required to achieve this. We aimed to determine whether a metal OBF layer deposited directly on this surface would affect the spectral resolution of an X-ray CCD detector. Figure 1 shows a broadband, multi-line, pulse-height spectrum obtained from a BI CCD with a directly deposited, 220-nm-thick OBF. The spectrum shows that such a detector (similar to those installed on REXIS) can readily resolve characteristic lines of elements ranging from oxygen to iron.





How does a directly deposited OBF affect CCD spectral resolution at very soft ( $E < 1$  keV) energies? Figure 2 addresses this question by comparing pulse-height spectra from three representative devices. The back surfaces of all of these detectors were treated with MIT Lincoln Laboratory's MBE process. One device has no OBF, and the other two have directly deposited aluminum OBFs with thicknesses of 70 nm and 220 nm, respectively. Identical exposure times to the same radioactive X-ray source were used to obtain the spectra. The source produces characteristic lines of C-K, V-L, O-K, and F-K, with energies ranging from 277 eV to 677 eV. As expected, X-ray absorption in the filters reduces the amplitudes of the lower-energy peaks. Figure 3 compares peak widths (full-width at half-maximum, FWHM) measured for different spatial regions, called quadrants, on each device. Each device quadrant has a dedicated on-chip amplifier. These are engineering-grade devices, so the noise levels, and thus the expected peak widths, differ from quadrant to quadrant. The points in Fig. 3 for the unfiltered ('no-OBF') and '220-nm OBF' cases show the mean, minimum, and maximum of three device quadrants in each configuration. The 70-nm OBF points show results for a single quadrant. The means of the unfiltered and 220-nm configurations are closer than the quadrant-to-quadrant scatter within each configuration, and the single quadrant measurements available from the device with the 70-nm OBF are marginally better than any of the quadrants on the other two devices at all three energies. Thus, we find no evidence that the directly deposited OBF compromises the soft X-ray FWHM of these detectors.



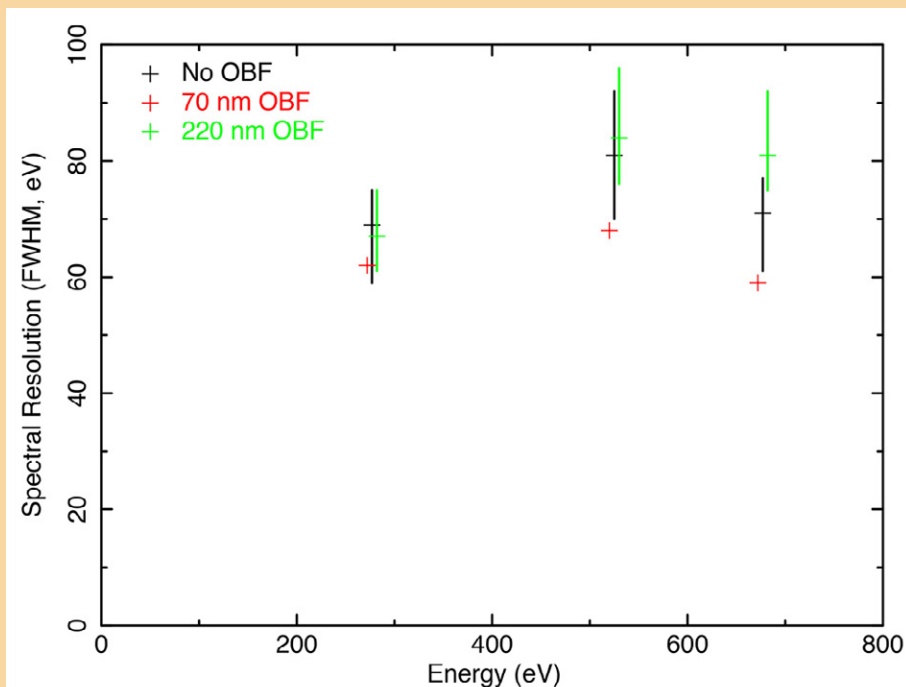


**Fig. 3.** Spectral resolution (FWHM) of devices with No OBF (black), 70-nm-aluminum OBF (red), and 220-nm-aluminum OBF (green). “No OBF” and “220-nm OBF” points show mean, minimum, and maximum FWHM measured for three independent CCD quadrants in each configuration; 70-nm points show measurements for a single CCD quadrant. The OBFs have no clear effect on spectral resolution. Energy coordinates have been displaced slightly to show the ranges in FWHM clearly.

Returning to Fig. 2, it is clear that the shape of the spectral redistribution function of all devices degrades to some extent at the lowest energies. At 677 eV, the response function is quite symmetrical for all three devices. Near 500 eV, the blend of vanadium-L and oxygen K lines produced by the source is evident, and this blend makes it difficult to assess the shape of the response function there. The responses of all three devices at 277 eV show a clear low-energy shoulder. The ratio of main-peak to shoulder amplitudes (about 5:1) is about the same for all devices, suggesting that the shoulder is due neither to the source spectrum nor to the presence of the OBF. We hypothesize the tail is a consequence of the relatively thick (20 nm) p<sup>+</sup> MBE layer applied in fabricating these devices. About 15% of the incident photons at this energy will be absorbed in the MBE layer. A thinner MBE layer might thus be expected to provide better charge collection for very soft X-ray photons. We find no evidence that the shape of the response function is affected by the presence of the OBF.

## 2. X-ray transmission of OBFs

Measured X-ray transmission of a 70-nm-thick OBF is compared to expectations in Fig. 4, with generally good agreement. The data were obtained from a device (53-1-4-2) on which only part of the detector was covered by the OBF. Both covered and uncovered regions were exposed to a multi-line source like the one used to produce the spectra in Fig. 1, and transmission was determined from the line fluxes measured in the two regions. The red circles show measurements obtained by fitting Gaussian profiles to the data. Green crosses show fluxes obtained by summing over a spectral region within  $\pm 3$  standard deviations of line centers. The two methods agree reasonably well, except at the very lowest energy measured (183 eV) where the line profiles are distinctly non-Gaussian. Similarly, good agreement between measurements and expectations is obtained with 200-nm OBFs (see [10] for details).

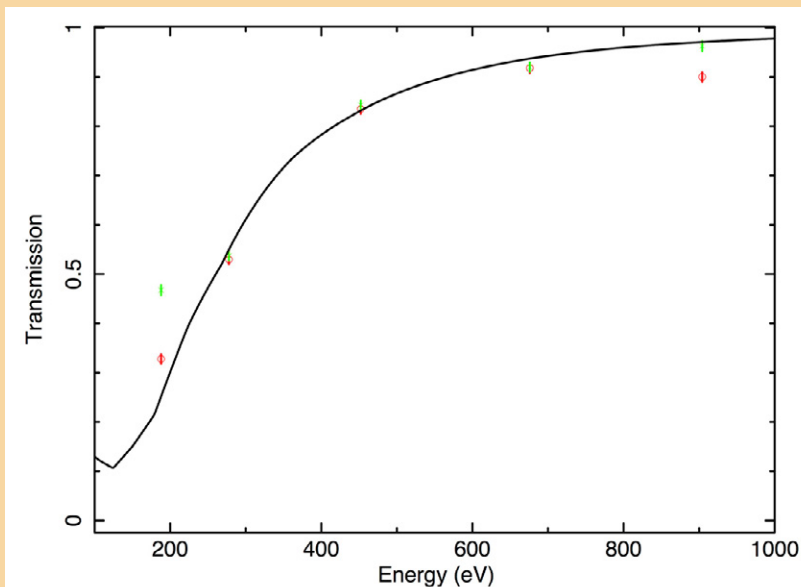


**Fig. 4.** Measured (points) and modeled (curve) X-ray transmission of 70-nm-thick aluminum OBF. Red and green points obtained with different X-ray measurement methods discussed in the text.

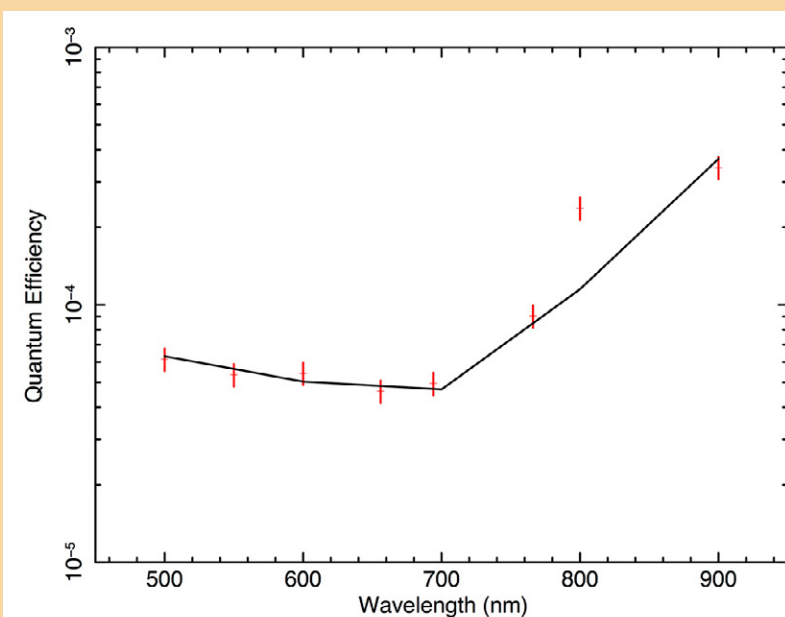


**Fig. 5.** Visible/near-IR QE of a CCD with a directly deposited blocking filter. Nominal filter thickness is 70 nm. The points are measured values; the line is a simple model of a 63-nm-thick OBF. Note: data from device 53-1-4-2.

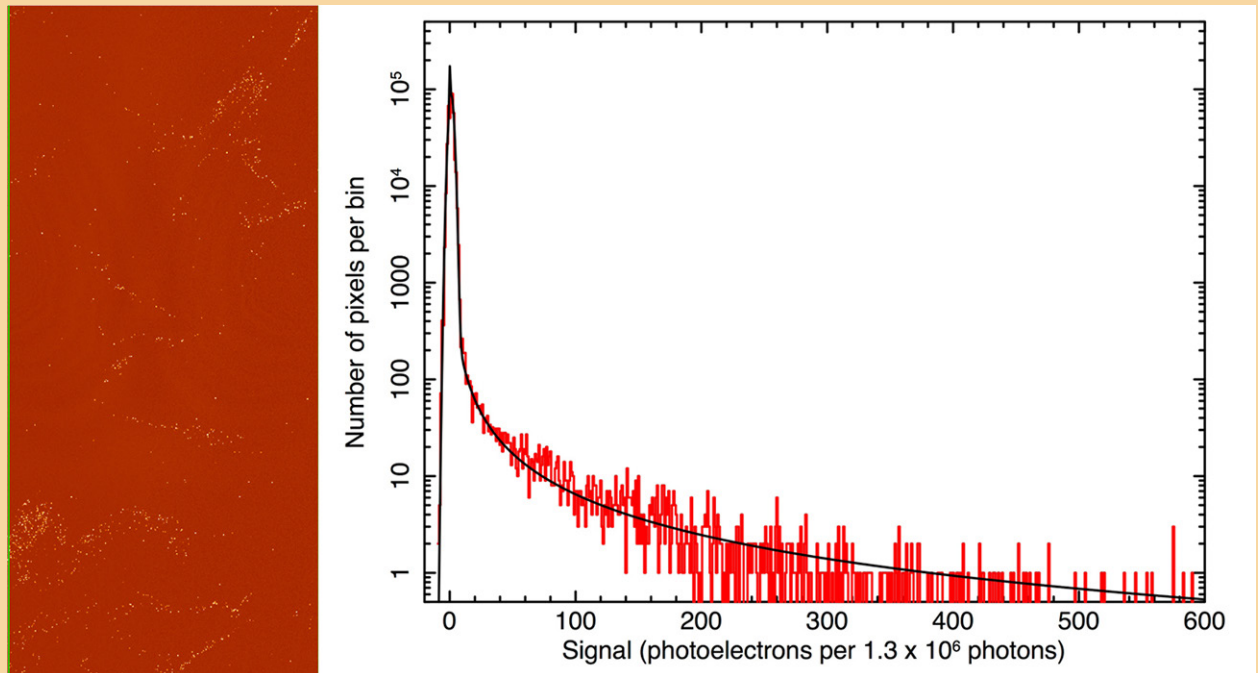
### 3. Visible/near-IR transmission of directly deposited OBFs

Figure 5 shows the measured visible-band quantum efficiency (QE) of a device with a directly deposited blocking filter with a nominal thickness of 70 nm. The measurements agree reasonably well with a simple model of an aluminum layer over a thick silicon substrate. The aluminum thickness in the model has been adjusted to 63 nm to fit the data. The model assumes perfect internal CCD QE, which is certainly an overestimate redward of 600 nm, as the (thinned) detector's sensitive volume (depletion region) is nominally 45 microns thick. A more sophisticated model, incorporating an accurate treatment of the internal detector efficiency, is clearly required to represent the data in the near-IR spectral band. The present results may indicate the OBF is somewhat more transparent in this spectral band than the simple model predicts.

Visible-band, flat-field exposures with both 220-nm-thick and 70-nm-thick OBFs show “pinhole-like” regions of relatively high transmission, as shown in Fig. 6. The image on the left shows pinholes in a 220-nm-thick OBF. The device was exposed to a fluence of  $1.3 \times 10^6$  photons/pixel at 800 nm. A histogram of the 440,000 pixel amplitudes in the image is shown in the right panel. The theoretically expected transmission of this OBF is less than  $10^{-9}$ , so if the OBF was perfect, all pixels would have zero amplitude, modulo the readout noise with root-mean-square (rms)

width of a few electrons. The histogram shows that 99% of pixels are in fact consistent with zero amplitude, and about 1% of pixels are affected by pinholes with transmission ranging from about  $10^{-6}$  to as high as  $5 \times 10^{-4}$ .





**Fig. 6.** Left: Image obtained using CCD with a 220-nm-thick OBF illuminated with  $1.3 \times 10^6$  photons/pixel of 800-nm light. Pinholes (white spots) are evident. Right: Histogram of amplitudes of the 440,000 pixels in the image on the left. While 99% of pixels are in the peak, consistent with zero amplitude, about 1% of pixels show transmission greater than  $10^{-6}$ .

As discussed in detail in [10], we believe the pinholes are caused by surface irregularities present on the detector surface before the OBF is deposited. Several lines of evidence support this explanation. First, test coatings on quartz substrates do not show pinholes. Second, as shown in Fig. 7, scanning electron micrographs of deposited OBFs show texture with sizes ( $< 100$  nm) and spatial density consistent with the observed number and transmission of pinholes. Third, the number of pinholes is dramatically reduced if an optically transparent, 1- $\mu$ m-thick layer of photoresist is deposited on the detector surface before the aluminum OBF layer. Although such an interlayer is opaque to soft X rays and so could not be used on an X-ray sensor, this result does suggest there are no fundamental limitations to fabrication of a pinhole-free, directly deposited OBF.

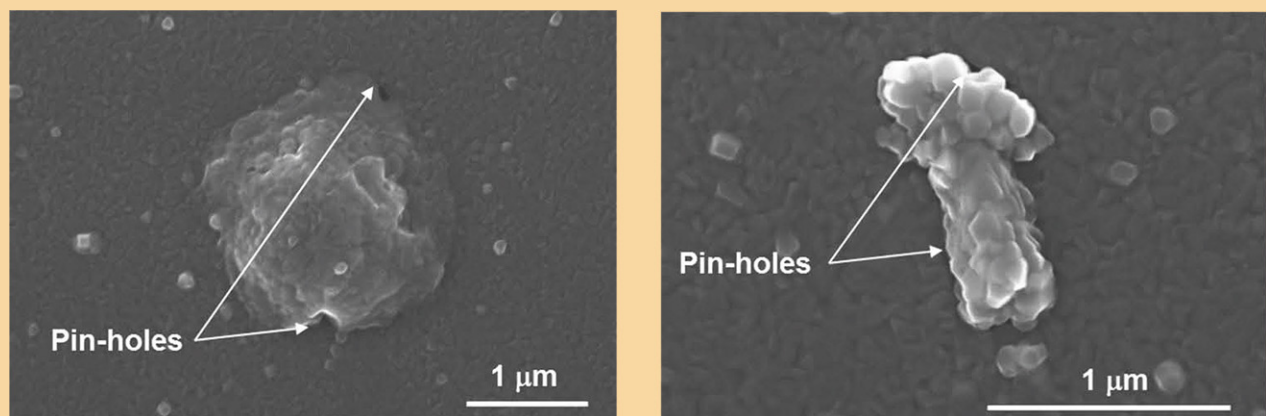


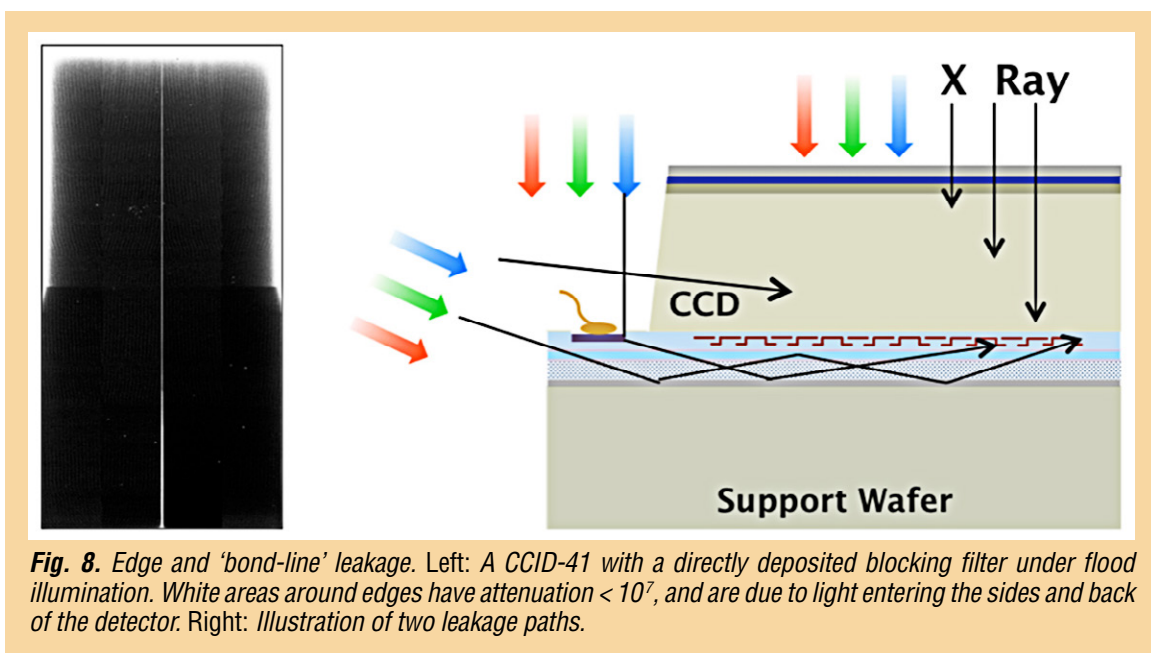
**Fig. 7.** Scanning electron micrograph images of an OBF directly deposited on the surface of a CCD.

Indeed, our success in reducing the pinhole fraction to less than 1%\* for REXIS OBFs is further evidence in favor of this explanation for the origin of pinholes. Two measures in particular have proven effective. First, the interior surfaces of the coating chamber were aluminized after cleaning, to minimize particulate contamination originating in the chamber walls. Second, the deposition geometry was changed so that the incident aluminum atoms approach the detector surface at about  $45^\circ$  to the surface normal. The detector rotates about its surface normal during this process. This ‘angled-deposition’ allows the aluminum to cover the vertical sides as well as the tops of residual surface irregularities, and thus reduces the number of pinholes.

#### 4. Detector sidewall and bond-line leakage paths

The thickest OBF layers we tested, with 220 nm of aluminum, have a theoretical attenuation well in excess of a factor of  $10^9$ . The REXIS instrument, which will map fluorescent X-ray emission from the sunlit surface of asteroid RQ36, requires substantial optical blocking and is equipped with filters of this thickness. Our evaluation of directly deposited OBFs of this thickness revealed that to achieve very large attenuation (greater than  $\sim 10^6$ ), one must block not only the light entering the entrance surface of the detector, but also light entering its thin side walls and even its mounting surface.

The effect and location of these leakage paths are illustrated in Fig. 8. The left panel shows a grayscale image obtained by illuminating a CCD with a 220-nm-thick OBF. The white areas around the edges of the device have an attenuation factor of  $10^7$  or less. The right panel shows two leakage paths responsible for this effect. Light can enter the photosensitive regions of the device through its thin ( $45\text{-}\mu\text{m}$ -thick) sidewalls. Light can also penetrate the thin ( $\sim 10\text{-}\mu\text{m}$ -thick) epoxy bond-line that attaches the CCD to the (photo-insensitive) silicon support wafer. A third leakage path, similar to the second but not shown in the figure, runs through a second, thicker epoxy bond-line that attaches the support wafer to the detector package, through the support wafer and into the detector from below. This third leakage path transmits mainly near-IR radiation to which the support wafer is relatively transparent.



\* Specifically, the mean fraction of pixels with optical density less than 7 (i.e., with pinholes) in 220-nm-thick OBFs in the 12 best REXIS flight devices is 0.76%; the rms pinhole fraction in this sample is 0.45%. An anomalous 13<sup>th</sup> device showed a pinhole fraction of 4.1%.

Leakage through the two paths shown in Fig. 8 was reduced to levels acceptable to REXIS by depositing an additional 100 nm of aluminum using the angled-deposition geometry described above. This coating covers the detector sidewalls and the bond-line between the detector and the support wafer. In addition, the REXIS team qualified two effective countermeasures against bond-line leakage at the bottom of the support wafer. One method was to coat the bottom of the support wafer with black paint, using a suitable adhesion promoter. The other method was to deposit a 300-nm-thick aluminum layer on the bottom surface of the support wafer. REXIS has adopted the latter approach because it permits a flatter surface coating that can be applied more quickly.

### 5. Long-term stability of directly deposited OBFs

The final task in our original program is to evaluate the long-term stability of directly deposited OBFs. We began this process in September 2014 with a baseline evaluation of device 53-1-17-2, which is equipped with a 100-nm-thick OBF. We have monitored this device over a period of eight months and

did not detect any significant change in OBF performance. In particular, Fig. 9 compares pinhole maps obtained for this device before and after eight months of laboratory storage. The images have been scaled to correct for light-source-intensity differences so that the mean of the amplitudes of a set of randomly selected pinhole pixels is the same in both images. To date, we find no evidence for change over time in the optical blocking properties of this OBF. We plan to extend this stability test to two years.

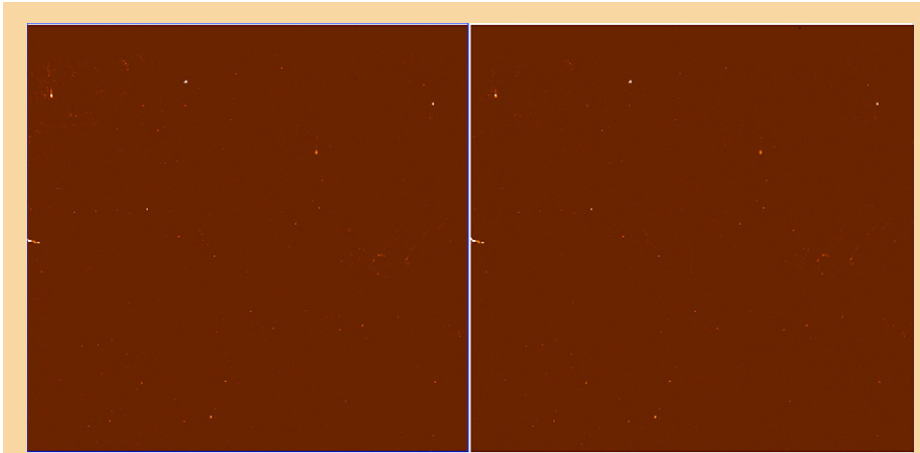


**Fig. 9.** Pinhole maps of a randomly chosen  $400 \times 400$  pixel section of CCD 53-1-17-2 equipped with a 100-nm-thick directly deposited aluminum OBF, obtained in September 2014 (left) and June 2015 (right). These images demonstrate the stability of the OBF over an eight-month period of laboratory storage.

### 6. Thermal testing of directly deposited OBFs with REXIS

As noted above, the OBF technology discussed here has been incorporated into the REXIS instrument for the OSIRIS-REx mission. Our collaboration with REXIS affords us the opportunity to subject OBF-equipped CCDs to realistic environmental testing, and achieve our final project goal (milestone 7 in Table 2). The REXIS flight instrument has successfully completed environmental testing and is now installed on the spacecraft. Temperature profiles during part of spacecraft TVAC testing are illustrated in Fig. 10. Although REXIS has completed environmental testing with successful X-ray performance, it was not possible to verify the post-test visible-band performance characteristics of its OBFs to achieve our final project milestone. Our plan for doing so is described briefly below.

## Path Forward

REXIS provides us with a path to demonstrating that our technology has reached TRL 6, exceeding our goals. To do so, we must at a minimum demonstrate that the performance characteristics of directly deposited OBFs are robust when subjected to realistic space environments.



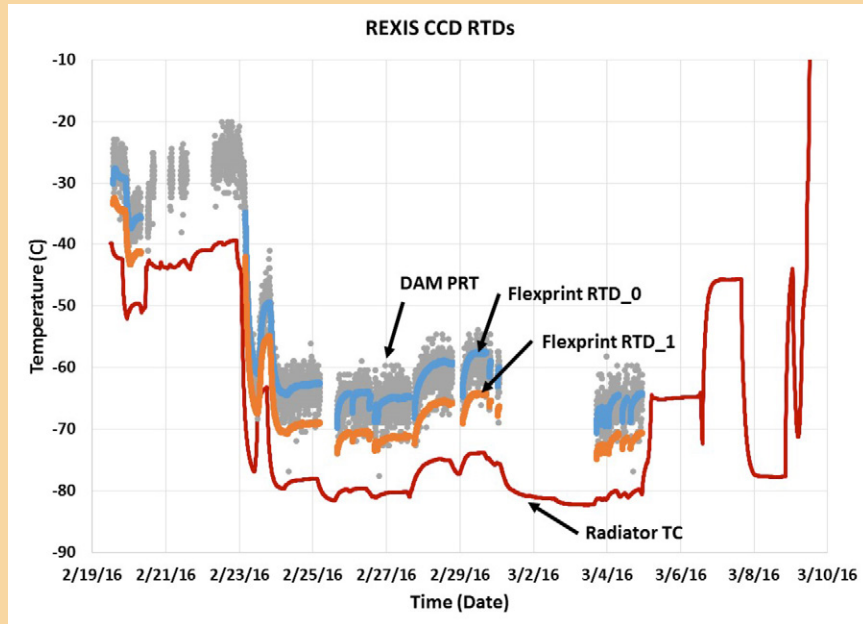


**Fig. 10.** Temperature histories of OBF-equipped REXIS focal plane and other REXIS test points during OSIRIS-REx spacecraft thermal vacuum testing. Temperatures of the focal plane radiator (red), CCD flexprint (orange and blue; RTD, resistance temperature detector), and detector assembly module (Detector Assembly Mount, DAM; grey) exterior are shown (PRT, platinum resistance thermometer; TC, thermocouple). Courtesy of MIT Space Sciences Laboratory.

In the coming academic year we therefore plan to repeat vibration and TVAC testing with the REXIS engineering model DAM (Fig. 11), including visible and X-ray OBF performance characterization before and after exposure to REXIS test environments. This work will be carried out by two students in MIT's undergraduate research opportunities program (UROP) under the direction of the REXIS program manager and with the guidance of MKI scientific staff. Success in these tests will demonstrate that our technology is at TRL 6.

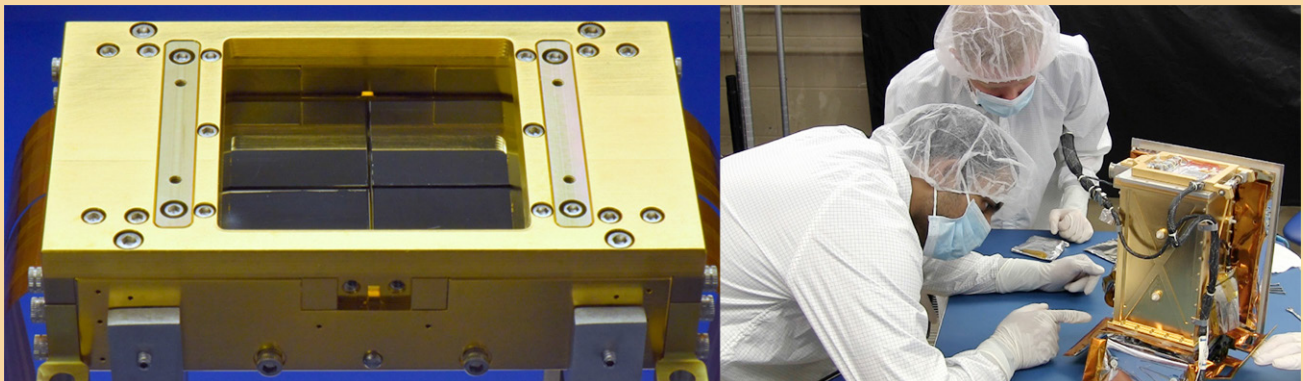


**Fig. 11.** Left: The REXIS DAM features four MIT/Lincoln CCDs, each with a directly deposited OBF. The total active area of the detectors is about 5 cm × 5 cm. Right: Students preparing the REXIS instrument for environmental testing. We plan a UROP project using REXIS engineering model hardware to demonstrate that directly deposited OBF technology is at TRL 6. Images courtesy of MIT Lincoln Laboratory and MIT Space Sciences Laboratory.

We also plan to continue the long-term stability test (milestone 6 in Table 2) through a total duration of two years, and conclude thermal testing (milestone 7 in Table 2).

## References

- [1] X-ray Community Science Team, X-ray Science Support Team, and X-ray Engineering Support Team, “*X-ray Mission Concepts Study Report*” (2012)
- [2] National Academy of Science, Board on Physics and Astronomy, “*New Worlds, New Horizons in Astronomy and Astrophysics*” (2010)
- [3] NASA Physics of the Cosmos Program Office, “*NASA Physics of the Cosmos Program Annual Technology Report*” (2012)
- [4] NASA Astrophysics Roadmap Team, C. Kouveliotou, Chair, “*Enduring Quests, Daring Visions: NASA Astrophysics in the Next Three Decades*” (2013)
- [5] M. Weisskopf et al., “*Beyond Chandra – The X-ray Surveyor*,” Proc. SPIE 1505.00814 (2015)
- [6] R. Smith et al., “*Arcus: an ISS-attached high-resolution X-ray grating spectrometer*,” Proc. SPIE **9144**, id. 9144Y, (2014)
- [7] N. Gehrels, S. Barthelmy, and J. Cannizzo, “*Time-Domain Astronomy with Swift, Fermi and Lobster*,” Proc. IAU, **Vol. 285**, pp. 41-46, (2012)
- [8] Laser Interferometer Gravitational-wave Observatory (LIGO) Scientific Collaboration, “*Predictions for the rates of compact binary coalescences observable by ground-based gravitational-wave detectors*,” Classical and Quantum Gravity, **Vol. 27**, p. 173001, (2010)
- [9] B.D. Metzger and E. Berger, “*What is the Most Promising Electromagnetic Counterpart of a Neutron Star Binary Merger?*” Astrophysical Journal, **Vol. 746**, p. 48, (2012)
- [10] K. Ryu et al., “*Development of CCDs for REXIS on OSIRIS-REx*,” Proc. SPIE **9144**, 91444O-1 (2014)

For additional information, contact Mark Bautz: [mwb@space.mit.edu](mailto:mwb@space.mit.edu)



# Fast Event Recognition for the Athena Wide-Field Imager

Prepared by: David N. Burrows (PSU)

## Summary

High-throughput X-ray missions of the future, including proposed missions like the Arcus Medium-class Explorer (MIDEX) mission that will be proposed later this year, the European Space Agency (ESA) Advanced Telescope for High ENergy Astrophysics (Athena) mission, and the notional X-ray Surveyor (XRS) mission, will use detectors with very high readout speeds that are too fast for software event recognition. Under this Strategic Astrophysics Technology (SAT) program, we are developing a high-speed Event Recognition Processor (ERP), running on a field-programmable gate array (FPGA). The purpose of this project is to advance the ERP from Technology Readiness Level (TRL) 3 to at least 4.

## Background

For the past two decades, the state-of-the-art detector for X-ray astronomy missions has been the CCD detector. X-ray CCD instruments use a technique of “event recognition” to read images, scan them for X-ray events, and telemeter only X-ray events; compressing the data rate from these instruments by more than a factor of 500. These algorithms are well-proven in flight and have been shown to produce data quality indistinguishable from laboratory analysis of full CCD images [1, 2].

## Objectives and Milestones

### *Technical Approach and Methodology*

The primary objectives of this proposal are to design and build a prototype breadboard version of a high-speed ERP, and to advance the design to TRL 4. This board must extract X-ray events from the high-speed data stream from a CCD or Active Pixel Sensor (APS); in other words, it performs event recognition and data compression. The existence of high-speed, radiation-tolerant FPGAs makes this feasible. During Phase A of our Joint Astrophysics Nascent Universe Satellite (JANUS) proposal, we developed a preliminary design concept for this circuitry that is at TRL 3. Over the past year, we have implemented our event recognition algorithms on a low-fidelity breadboard ERP. We are now building a higher-fidelity ERP with on-board memory in order to demonstrate basic functionality and high-speed operation in our laboratory to achieve TRL 4.

### *Event Recognition*

Most pixel data obtained with a CCD or APS are “empty,” containing only read noise (Fig. 1). Reducing the data to fit satellite telemetry bandwidth requires extracting candidate X-ray signals from this data stream, a process we refer to as “event recognition,” and passing them to the flight software for characterization and transmission to the ground. The spatial distribution of charge generated by X-ray interactions has characteristic features: charge is usually deposited in 1–4 pixels, depending on exactly where the photon lands within the pixel [3]. For example, if a photon hits near a pixel boundary, the charge cloud produced in the detector will be split between the adjacent pixels (Fig. 1). By contrast, background events due to charged-particle interactions in the detector tend to deposit large amounts of charge across many adjacent pixels (Fig. 2). Thus, classifying the “morphology” of an event allows it to be interpreted with high confidence as either an X-ray or background event [4]. Amplitude windows provide a second powerful discriminator, since charged particles deposit charge packets in the deep depletion region of an active pixel detector that are much larger than those produced by X-rays in the instrument bandpass. These techniques have been used for several decades, achieving charged-particle rejection efficiencies of order 99.9% in X-ray CCD data [4 – 8]. Because they depend primarily on photoelectric absorption in pixelated silicon detectors, the same techniques apply to active pixel detectors.



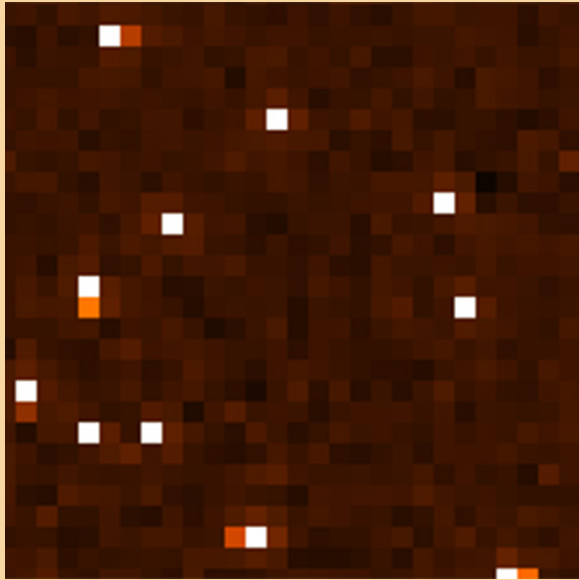


**Fig. 1.** Small portion of a single frame of ground-test data from hybrid CMOS detectors developed by PSU, where color indicates the signal in each pixel. Most pixels show read noise (dark red/black). A few isolated bright pixels (white) represent X-ray events depositing their energy into single pixels. Several events are also seen in which the charge is spread into adjacent pixels, indicating the photon was absorbed near a pixel boundary [3].

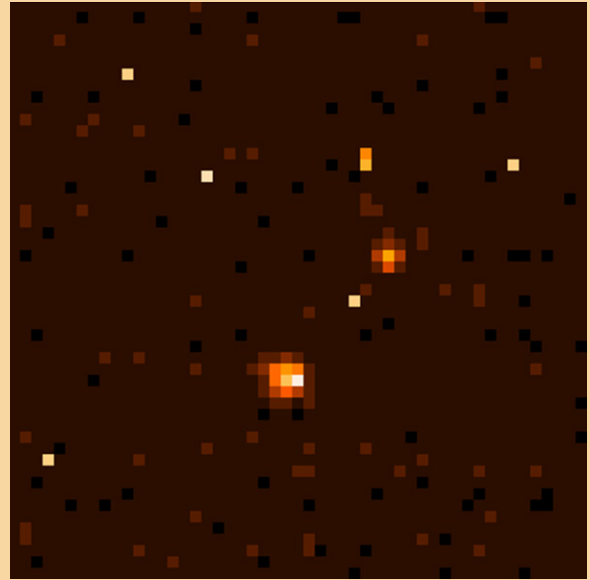


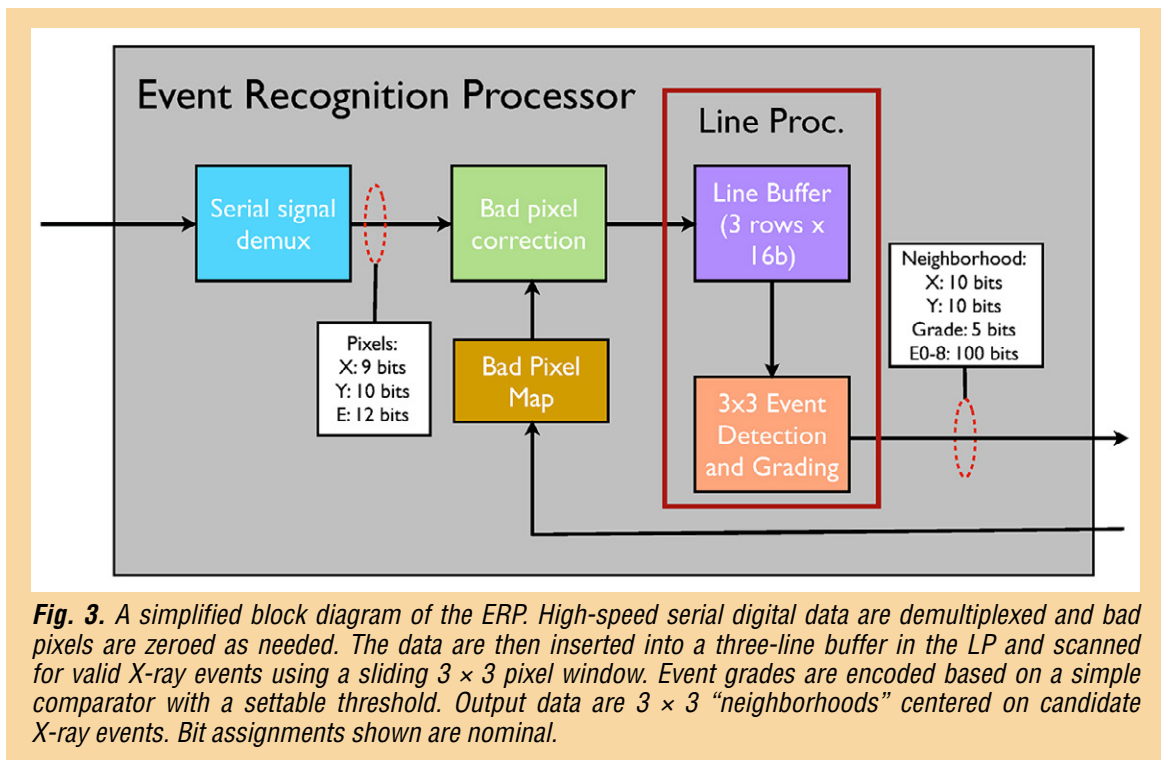
**Fig. 2.** Small portion of a single frame of flight data from the Swift X-Ray Telescope (XRT) CCD. Most pixels show read noise. A few isolated bright pixels (white/yellow) represent X-ray events depositing their energy into one or two pixels. Two broad, "blobby" events are from cosmic-ray interactions in the detector, which produce wide charge clouds, easily distinguished from X rays.

### **ERP Concept**

The ERP is an FPGA-based board that performs high-speed processing of CCD or active-pixel frames and identifies candidate X-ray events. A block diagram of the main functions of the ERP is shown in Fig. 3. The ERP consists of a high-speed data capture and demultiplexing block, masking of bad pixels, event detection and grading (event recognition), and an output buffer (not shown). A full-scale ERP must be able to combine data from multiple readout channels. The required logic is very similar to that which we designed for JANUS and updated for the International X-ray Observatory (IXO) Wide-Field Imager. Under this grant, we will implement a single-channel version of the ERP to test our ability to process data accurately at speeds approaching those required by future instruments, including the Athena Wide-Field Imager (WFI).

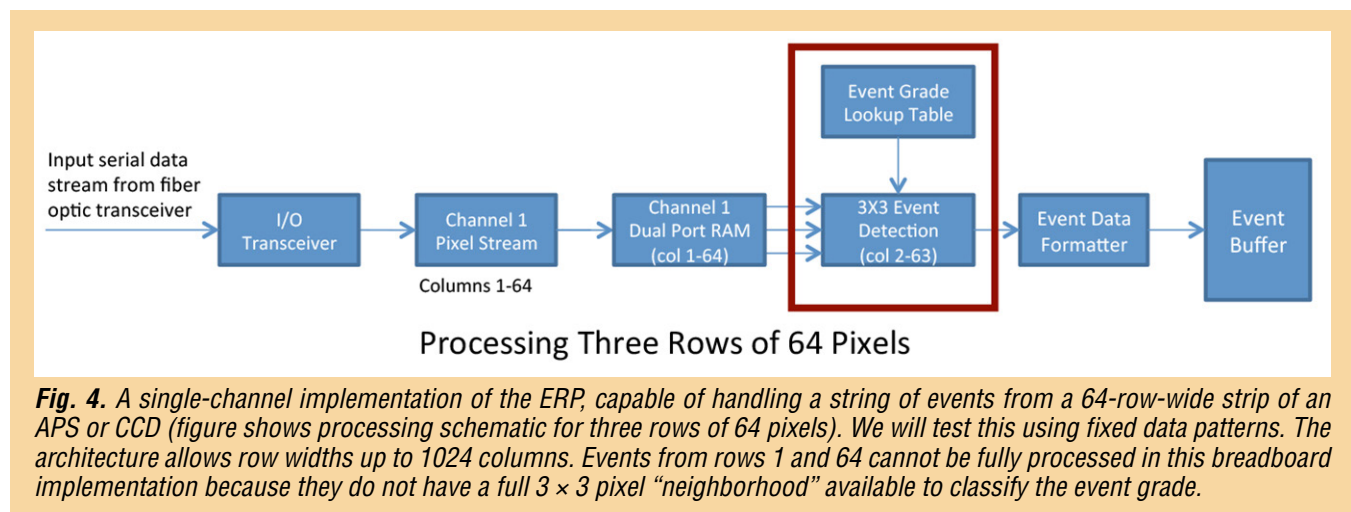
### **Implementation of a Single-Channel ERP**

The heart of the ERP is the Line Processor (LP), as shown in Fig. 3. The LP accomplishes the event recognition task through signal processing and pattern matching. The input data have already had any necessary bias and gain corrections applied and have been demultiplexed to determine the (X, Y) location and signal value of each pixel. The data are temporarily stored in high-speed FPGA memory. A sliding  $3 \times 3$  window is then virtually scanned across the three-row pixel buffer and each  $3 \times 3$  "neighborhood" is searched for a local maximum (that exceeds an adjustable threshold) in the central pixel. When one is found, this pixel is identified as a possible X-ray event, and the event is graded, using an uploadable lookup table to assign event grades. The event is then formatted and passed to the output telemetry stream as a  $3 \times 3$  "neighborhood" or as an X-ray with position, energy (E), and grade (depending on the instrument telemetry mode).



The basic processing implied in the previous sentence has been implemented in software by all three of our groups (PSU in our laboratory CCD and CMOS cameras on the Satellite de Aplicaciones Cientificas-B, SAC-B, and the Swift X-ray Telescope; MIT on the Advanced Satellite for Cosmology and Astrophysics, ASCA, Chandra, and Suzaku; and SAO in their laboratory CMOS cameras). Various event-grading schemes have been used in previous missions, ranging from the ASCA grades (0-7) to the Chandra Advanced CCD Imaging Spectrometer (ACIS) system, in which a bit is assigned to each of the eight surrounding pixels in a  $3 \times 3$  neighborhood, resulting in grades from 0 to 255. We will use the ACIS system internally, optionally converting to the Swift system for output data.

For this project, we will implement the single-channel ERP shown in Fig. 4. This will provide a proof-of-concept for hardware implementation of the critical function of this board, identification, and grading of X-ray events in a data stream. TRL 4 testing will be done at simulated data rates ranging from 1200 kilobits per second (kbps), the speed of the Swift software implementation, to 1 gigabyte per second (GBps).



The ERP will be implemented on a Xilinx Virtex-5 (V5) FPGA. The Virtex-5 OpenSPARC Evaluation Platform (Fig. 5) is a PCI Express board (equivalent to the Xilinx ML509 board) that facilitates development and testing of the FPGA in a host PC. This board allows us to test the most critical portions of the design at a variety of operating speeds in a simple, convenient test environment, with minimal development costs. We have used it successfully to test the design of the LP.

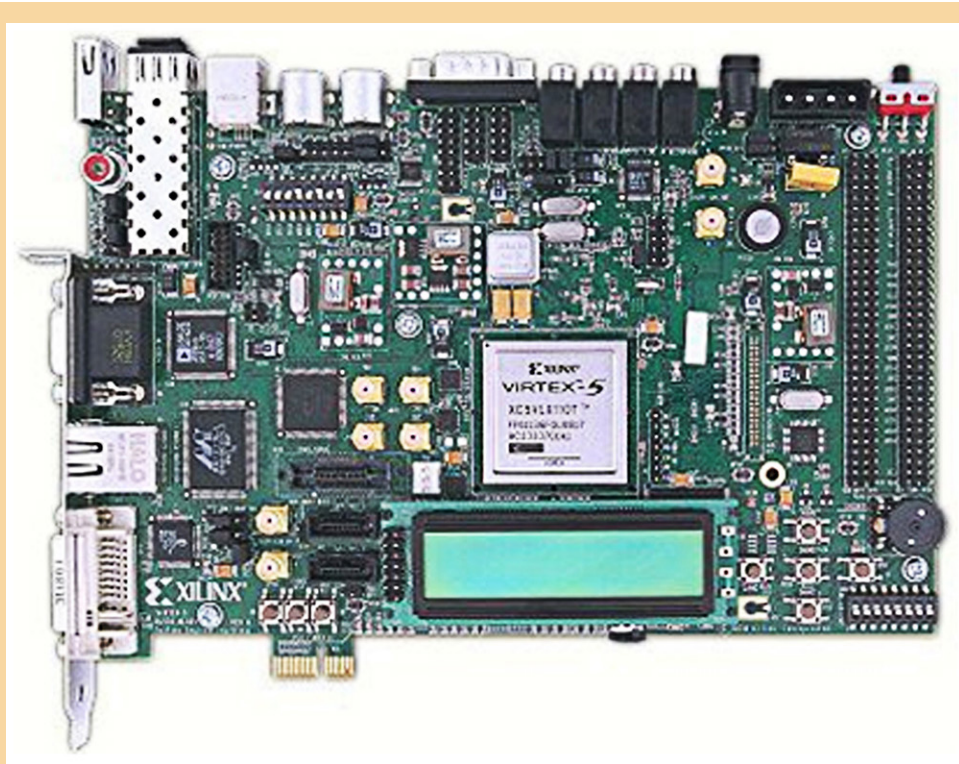


**Fig. 5.** The Virtex-5 OpenSPARC Evaluation Platform is specifically designed to be a flexible development board for testing high-speed Virtex-5-class FPGAs.

We are now moving on to implement and test the complete single-channel ERP block (Fig. 4), capable of handling data from a  $64 \times 64$  detector (or a 64-column segment of a larger detector of up to 3072 pixels width). This gives us a reasonable image size on which to test the algorithms against input test patterns, and will also allow us to perform tests on a real APS in our laboratory once the tests using simulated data are complete. However, the architecture will allow expansion up to 1024-row-high devices. In laboratory tests using the LP, we have demonstrated that speeds of  $> 1$  GBps can be achieved by implementing eight of these channels in parallel, and that the V5 processor has sufficient resources to implement this design. However, this full single-channel ERP block cannot be tested on the demo board because of insufficient memory resources. We have therefore designed a custom circuit board implementation, which we are currently fabricating for full single-channel tests later this summer and fall.

## Progress and Accomplishments

### Task List

This effort extends over two years (Fig. 6). In the first year, the work focused on implementing the LP design in the FPGA and testing the basic event-detection logic on a simple single-channel segment. This work was performed jointly by the PSU Department of Astronomy and Astrophysics and the PSU Applied Research Laboratory. MIT and SAO participated throughout the project via monthly telecons, and both institutions contributed to design reviews held at PSU in November 2015 and April 2016.



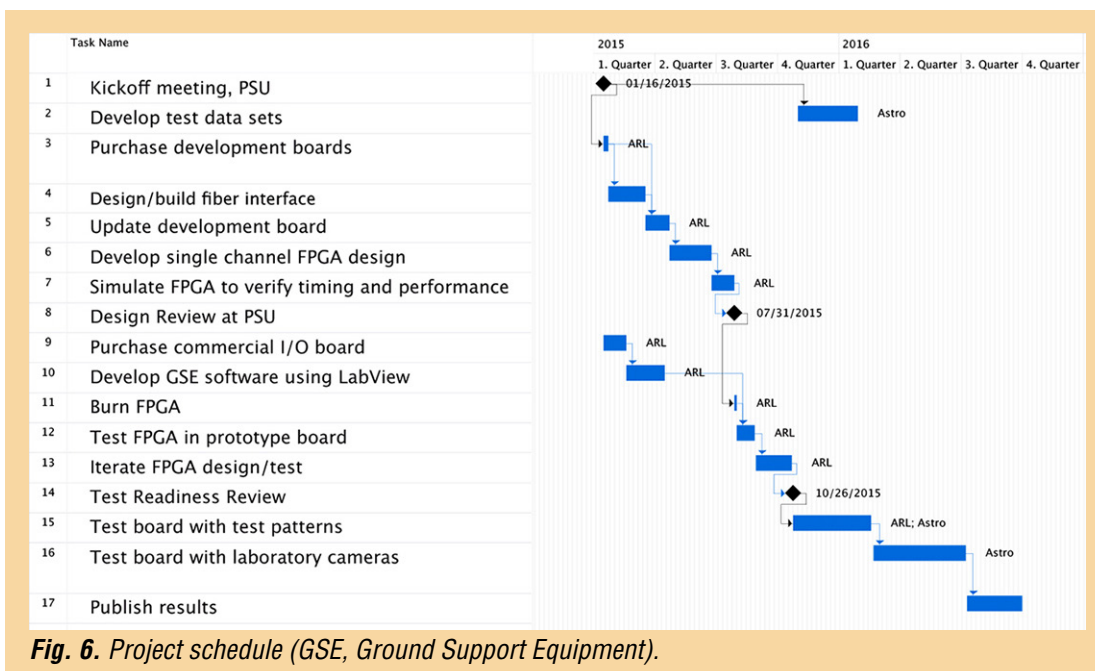


Fig. 6. Project schedule (GSE, Ground Support Equipment).

### Progress to Date

Here is the state of progress to date by task number:

- Tasks 1, 2, 3, 6, 7, 8, 9, and 10 are complete.
- Task 4 has been deferred indefinitely, but may be undertaken if time and resources allow.
- Tasks 5, 11, and 12 are currently underway.

### Path Forward

We expect to have the prototype board built by the end of June 2016. Testing of the ERP will take place over the remainder of this summer. We expect to hold a TRL review with the Physics of the Cosmos (PCOS) Program Office in October or November of 2016.

### References

- [1] L.J. Cawley et al., "CCD x-ray detectors: on-board data processing," in O.H.W. Siegmund and J.V. Vallerga (eds.), EUV, X-Ray, and Gamma-Ray Instr. for Astr. VI, **2518** SPIE Conf. Series, 179–187 (1995)
- [2] J.E. Hill et al., "Readout modes and automated operation of the Swift X-ray Telescope," in K.A. Flanagan and O.H.W. Siegmund (eds.), X-Ray and Gamma-Ray Instr. for Astr. XIII, **5165** SPIE Conf. Series, 217–231 (2004)
- [3] J. Hiraga et al., "Subpixel Spatial Resolution of the X-Ray Charge-Coupled Device Based on the Charge Cloud Shape," Japanese Journal of Applied Physics, **40**, 1493 (2001)
- [4] D.H. Lumb and A.D. Holland, "Event recognition techniques in CCD X-ray detectors for astronomy," Nuclear Instruments and Methods in Physics Research A, **273**, 696 (1988)
- [5] D.H. Lumb and A.D. Holland, "Background rejection techniques in CCD X-ray detectors for astronomy," IEEE Transactions on Nuclear Science, **35**, 534 (1988)
- [6] D.H. Lumb, "Particle background in CCD detectors," in O.H.W. Siegmund (ed.), EUV, X-Ray, and Gamma-Ray Instr. for Astr. IV, **2006** SPIE Conf. Series, 300–306 (1993)
- [7] A. Owens and K.J. McCarthy, "Energy deposition in X-ray CCDs and charged particle discrimination," Nuclear Instruments and Methods in Physics Research A, **366**, 148 (1995)
- [8] J.A. Mendenhall and D.N. Burrows, "CCD Sounding Rocket Observation of the High-Latitude Soft X-Ray Background," Astrophys. J., **563**, 716 (2001)

For additional information, contact David Burrows: [burrows@astro.psu.edu](mailto:burrows@astro.psu.edu)



# Providing Enabling and Enhancing Technologies for a Demonstration Model of the Athena X-IFU

Prepared by: Caroline Kilbourne (PI; NASA/GSFC); Simon Bandler, James Chervenak, and Stephen Smith (NASA/GSFC); Joel Ullom and W. Bertrand Doriese (NIST); and Kent Irwin (Stanford University)

## Summary

On June 27, 2014, the European Space Agency (ESA) announced its selection of the Advanced Telescope for High-ENergy Astrophysics (Athena) mission concept to study the science theme the “Hot and Energetic Universe.” The theme aims to address two important astrophysical questions [1]:

1. How does ordinary matter assemble into large-scale structures?
2. How do black holes grow and shape the universe?

One of the two instruments for this mission, the X-ray Integral Field Unit (X-IFU), is a high-resolution imaging X-ray spectrometer. The use of Transition Edge Sensor (TES) microcalorimeters, originally pioneered by our collaboration and under development in our Strategic Astrophysics Technology (SAT) program, is currently assumed for this instrument [2]. Both NASA and the X-IFU Principal Investigator (PI), Dr. Didier Barret, had previously communicated interest in designating the X-IFU microcalorimeter array as one of NASA’s principal contributions to Athena, with ESA’s concurrence. As a consequence, this collaboration submitted a new SAT proposal to cover our contribution to X-IFU technology development in fiscal years (FYs) 2016 and 2017. Our US collaboration is recognized as part of the Athena proto-consortium and is responsible for providing the baseline TES array technology, and our time-division-multiplexed (TDM) [3] readout technology is currently viewed as a backup to the European-developed frequency-domain multiplexing (FDM) [4]. The current program has been supported by the SAT program since 2013, and is the work of a collaboration between our research groups at GSFC (PI C. Kilbourne); National Institute of Standards and Technology (NIST), Boulder (lead J. Ullom); and Stanford University (lead K. Irwin). These groups have been collaborating on microcalorimeter spectrometer technology development since 1998, with the primary goal of advancing the integrated detector-TDM system to a strong demonstration of Technology Readiness Level (TRL) 5. Since the reference design for the X-IFU is based on FDM of the signals from the nearly 4000 TES pixels of the focal-plane array, primary demonstration models will incorporate this scheme. In addition to fully supporting these primary demonstrations, we are also developing a parallel demonstration model using TDM. TDM is more advanced than FDM, so developing it as a backup option provides important risk reduction for the X-IFU development schedule. We are also developing code-division multiplexing (CDM), which promises better performance while making use of most of the same readout architecture as TDM.

Additional objectives of this program are focused on demonstrating enhanced array technologies for Athena/X-IFU such as ‘hybrid’ arrays, where different pixel designs are integrated on a single detector die. For example, a high count-rate sub-array for point source observations could be integrated on the same chip as a main array optimized for extended source observations. The project also includes development of critical technologies needed for the thermal, electrical, and mechanical integration of the detector and readout components into the focal-plane assembly. We are also developing large-scale testing platforms and assemblies that are essential for screening full-scale arrays and for large-scale multiplexed demonstrations.

## Background

The X-IFU [1, 2] will be an extremely powerful instrument that will capitalize on four decades of technology development to create an instrument that simultaneously provides high spatial and spectral resolution. The instrument is very similar to the X-ray Microcalorimeter Spectrometer (XMS) envisioned for the International X-ray Observatory (IXO) mission, which was highly endorsed scientifically in the 2010 National Research Council Decadal Survey, “*New Worlds, New Horizons in Astronomy and Astrophysics*” (NWNH). For the first time, astrophysicists will have a spectral resolving power of  $\sim 2500$  over the most diagnostically rich part of the X-ray band with up to 5-arcsec spatial resolution. With the very high collecting area of  $2 \text{ m}^2$  and 2.5 eV energy resolution projected for the X-IFU, a wide range of celestial high-energy sources will be available for detailed analysis out to a redshift of 2.

The reference detector technology we have been developing consists of Mo/Au TES thermometers (operated at  $< 0.1 \text{ K}$ ) with close-packed Bi/Au thermalizing X-ray absorbers on a 0.25-0.3 mm pitch. In our baseline TDM concept [3], outputs from the dedicated input Superconducting QUantum Interference Devices (SQUIDs) of individual TES pixels are coupled to a single amplifier, and multiplexing is achieved by sequential switching of these input SQUIDs. Under the previous program, we made substantial progress that is relevant for X-IFU. The integrated detector-TDM system reached TRL 4 in March 2008 with the successful demonstration [5] of multiplexed (2 columns  $\times$  8 rows) readout of 16 different pixels. We then defined the following milestone as necessary for achieving TRL 5: “*Demonstrate multiplexed (3 columns  $\times$  16 rows) readout of 48 different flight-like pixels. The pixels shall be placed on a 0.25-mm pitch in a  $32 \times 32$  (or greater) array, and more than 95% of pixels must achieve better than 3 eV resolution at 6 keV, using an analysis method consistent with the requirement of 80% live-time at an X-ray rate of 50/s/pixel.*”

Fulfilling this milestone is consistent with the requirements for TRL 5 because the full detector requirements (as previously defined) would be demonstrated at the detector/readout subsystem level though on a smaller scale. Note that the multiplexing factor is not a performance requirement, but rather an accommodation requirement that comes out of the system design. For Athena-L1 it was 16 channels per multiplexer, for Constellation-X it was 32, and now for Athena-L2 it is 40.

The other related technology we are developing is CDM, a switched-multiplexing system like TDM. In TDM, only one TES channel is on at a time, whereas in CDM all channels are always on, but switched in polarity according to a matrix of combinations, thus avoiding the aliased noise of TDM. CDM is compatible with the TDM infrastructure, but provides increased design margin. In FDM, the TESs are biased with AC signals of different frequencies, acting as carriers for the slower thermal signals.

The X-IFU requirements are currently being refined, and ESA has yet to define the formal X-IFU TRL-5/6 requirement. The X-IFU project managers intend that the team produce a very-high-fidelity demonstration model (DM). The primary goal of the DM instrument is to provide a system-level demonstration of critical technologies, and in particular to characterize a prototype X-IFU focal-plane assembly (FPA) in a prototype X-IFU cryostat. DM development is thus expected to contribute to the demonstration of maturity (at TRL 5) and instrument development, but will not demonstrate the instrument design. Within the FPA development program, the DM FPA is also the first system demonstration in which the parallel development programs for the detector and its readout, the anti-coincidence detector and its readout, and the FPA shielding and suspension technologies are integrated, and the only such system demonstration before the instrument’s TRL 5 demonstration.

The baseline instrument design concept will be defined in Phase A (2016-2017) and further developed in Phase B1 (2018-2020), with the design of the next instrument model, the engineering model (EM), a product of Phase B. In support of this instrument development, the FPA DM program includes technology development in parallel with the DM FPA to demonstrate critical components and sub-assemblies required for an EM FPA in Phase B, and as part of the FPA TRL 5 demonstration.



The X-IFU DM requires a detector array in a preliminary flight design, meeting the requirements determined by the noise budget. The baseline is a standard GSFC kilo-pixel array and Space Research Organization Netherlands (SRON) FDM readout. Thus, no new detector design needs to be developed for this demonstration. Though the full requirements are still being finalized, the detector array and readout would be expected to achieve performance commensurate with an energy resolution of 3 eV in a 2-column by 40-row FDM configuration using an analysis method consistent with the requirement of 80% live-time at an X-ray rate of 20/s/pixel. This is a very similar requirement to our TRL 5 definition quoted above.

As presently envisaged, the X-IFU flight array will be a uniform array of  $\sim 4000$  pixels on a 0.26-mm pitch. This is referred to as the uniform large-pixel-array (LPA) configuration and is the simplest array implementation scheme. However, an enhanced ‘hybrid’ array configuration that includes an  $18 \times 18$  small-pixel array (SPA) in the center of the LPA is also under serious consideration. This SPA would provide a 10 $\times$  increase in count-rate capability for point-source observations while reducing the speed requirements of the pixels in the main part of the array. Such pixels can be optimized for either high count-rate capability with high dynamic range or, alternatively, higher energy resolution at reduced dynamic range [6, 7]. We have been supporting X-IFU trade studies of these array configurations and provided baseline pixel properties that are being used for end-to-end science simulations and dimensioning of the readout architecture.

## Progress and Accomplishments

### *Multiplexed Readout of Large-Format Arrays*

A standard GSFC  $32 \times 32$  TES array [8] is shown in Fig. 1. The pixels are on a 0.25-mm pitch. All pixels are wired out to the edge of the array, but on these test devices only 256 of the pixels (25%) are wired to bond pads around the circumference of the silicon carrier wafer. This array format, which is also the baseline DM array configuration, will be used to complete our own TRL-5 demonstration as defined in the previous program.

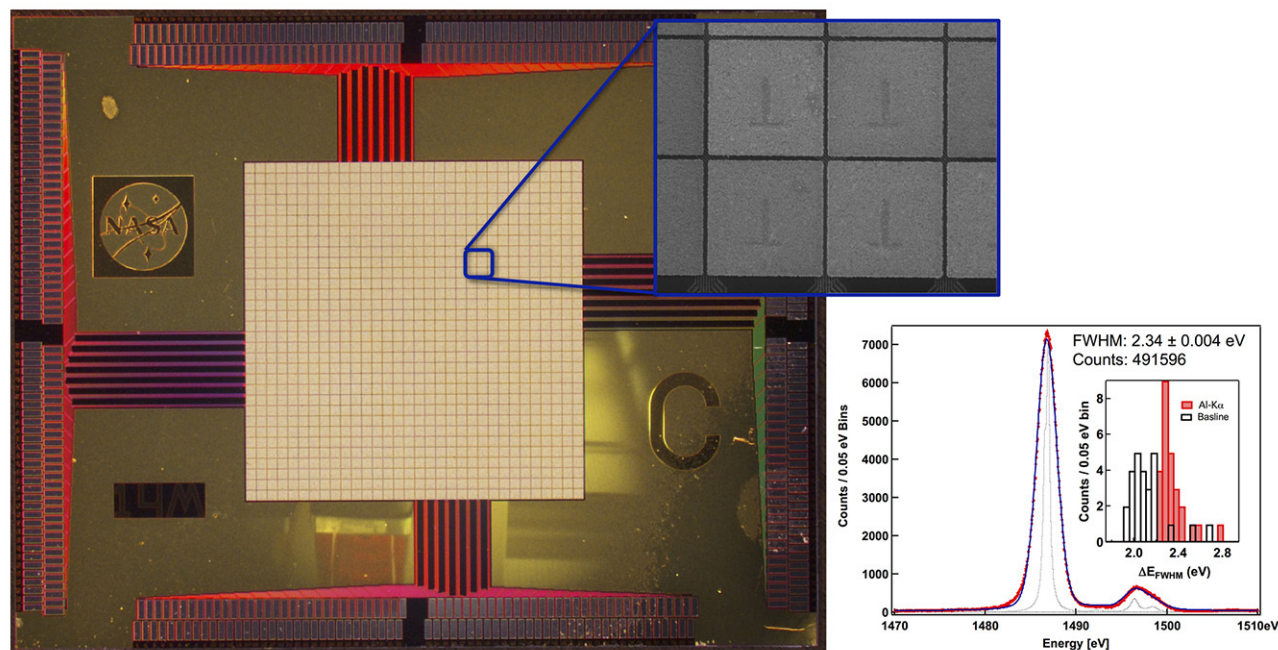


**Fig. 1.** A  $32 \times 32$  array of close-packed X-ray microcalorimeters. Only the X-ray absorbers are visible; they are composed of a 1.5- $\mu\text{m}$  thick layer of gold and a 3.0- $\mu\text{m}$  thick layer of bismuth. The absorbers are 0.242 mm  $\times$  0.242 mm in size, on a 0.25-mm pitch. Inset shows a scanning electron microscope image of four pixels within the array. The absorbers are cantilevered above TES sensors, with the wiring in-between pixels. The inverted ‘T’ image imprinted on each absorber is the region where the absorbers are supported by the substrate, making contact with the TES. Also shown is a combined spectrum from a  $1 \times 32$  row TDM measurement of Al-K $\alpha$ , with an inset showing the resolution distributions.

The main goals of TDM development have been to lower row-switching time and system readout noise. Significant improvements have been made throughout the multiplexer system, including:

- Room-temperature amplifier for  $> 20$  MHz bandwidth (increased from  $\sim 2$  MHz);
- Hardware and firmware upgrades enabling 32 bits of data to be streamed in 16 master-clock cycles;
- New multiplexer (mux) chips utilizing “Zappe-style” [9, 10] flux-actuated switches enabling reduced intrinsic flux noise of  $0.19 \mu_0/\sqrt{\text{Hz}}$ ;
- Increased frequencies of bandwidth-limiting poles in the system, enabling 160-ns row switching times; and
- Factor-10 crosstalk reduction between feedback loop and input circuit vs. previous designs.

These improvements more than satisfy the combined requirements for row-switching time and noise, and have been used in a breakthrough 32-row TDM demonstration at NIST achieving  $2.55 \pm 0.01$  eV average energy resolution at 6 keV in a single column [11]. Figure 2 shows the 30 individual spectra obtained around 6 keV (two detectors were non-operational). The detector used was a NIST development array with 2.4-eV intrinsic resolution and a maximum slew rate of 0.21 A/s, but the readout is suitable for the target array design of  $< 2$  eV intrinsic resolution and twice the slew rate.

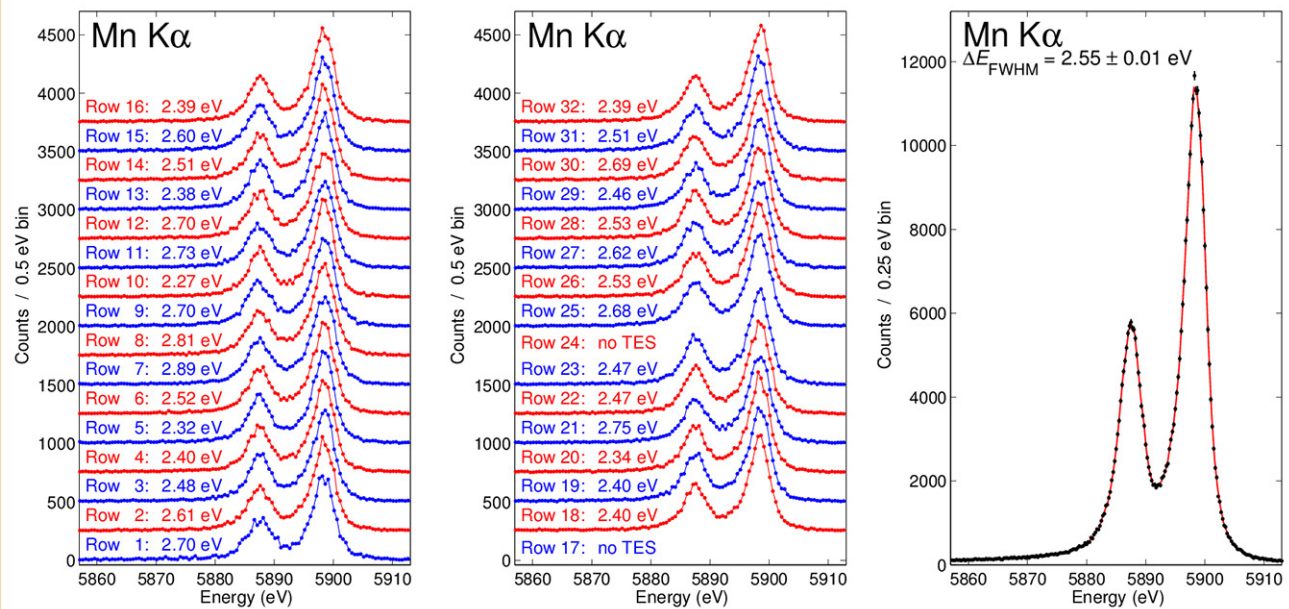


**Fig. 2.** Left and center: Spectra from 30 TES pixels (and two empty channels) read out through a 32-row TDM column. Each spectrum is labeled by its row number and the full width at half-maximum (FWHM) resolution attained in the Mn K $\alpha$  complex. Right: In the combined spectrum, the measured energy resolution is 2.55 eV. The row-switching time was 160 ns, meaning the frame time was 5  $\mu$ s.

The test platform at GSFC uses an eight-column FPA configured with multiplexer chips and second-stage SQUID amplifiers of different designs. This mixed configuration enables direct comparison of important performance metrics such as noise, crosstalk, and bandwidth for the different SQUID multiplexing architectures under consideration. Because of the differences, however, rows cannot be addressed simultaneously in multiple columns, limiting our initial results to a single column. Furthermore, the particular  $32 \times 32$  TES array used for these measurements exhibited some non-ideal characteristics, including lower-than-targeted  $T_c$  ( $\sim 82$  mK) and a larger-than-standard  $T_c$  gradient across the array. These effects resulted in non-uniformity across the array and decreased detector linearity with respect to energy [8].



Despite these less-than-ideal characteristics, excellent performance has been achieved. Of particular note is a 32-row TDM demonstration at 1.5 keV, in which we achieved  $2.34 \pm 0.1$  eV (Fig. 1). For the same system and detector, the resolution at 6 keV was 3.3 eV, consistent with the non-linearity of the particular detector. We have almost completed converting the present multi-configuration test platform to a uniform configuration with optimal mux chips, second stage SQUID amplifiers, and room-temperature electronics, and will complete this demonstration in platforms at both GSFC and NIST before the end of FY 2016.

### ***Flux-Actuated, 32-Channel CDM Multiplexer Chips***

Our new CDM SQUID multiplexer chips use the same Zappe-style flux-actuated switches as described above. Here, each SQ1 is a six-element series array. As expected, more elements improve noise performance: here the full system noise is  $0.17 \mu_0/\sqrt{\text{Hz}}$ . A CDM chip of this flux-switched architecture was recently used in a successful 32-channel demonstration. The combined spectrum from the 30 TESs connected to the readout had a resolution of  $2.77 \pm 0.02$  eV FWHM at 6 keV [12]. The raw and demodulated CDM signals are also shown in Fig. 3.

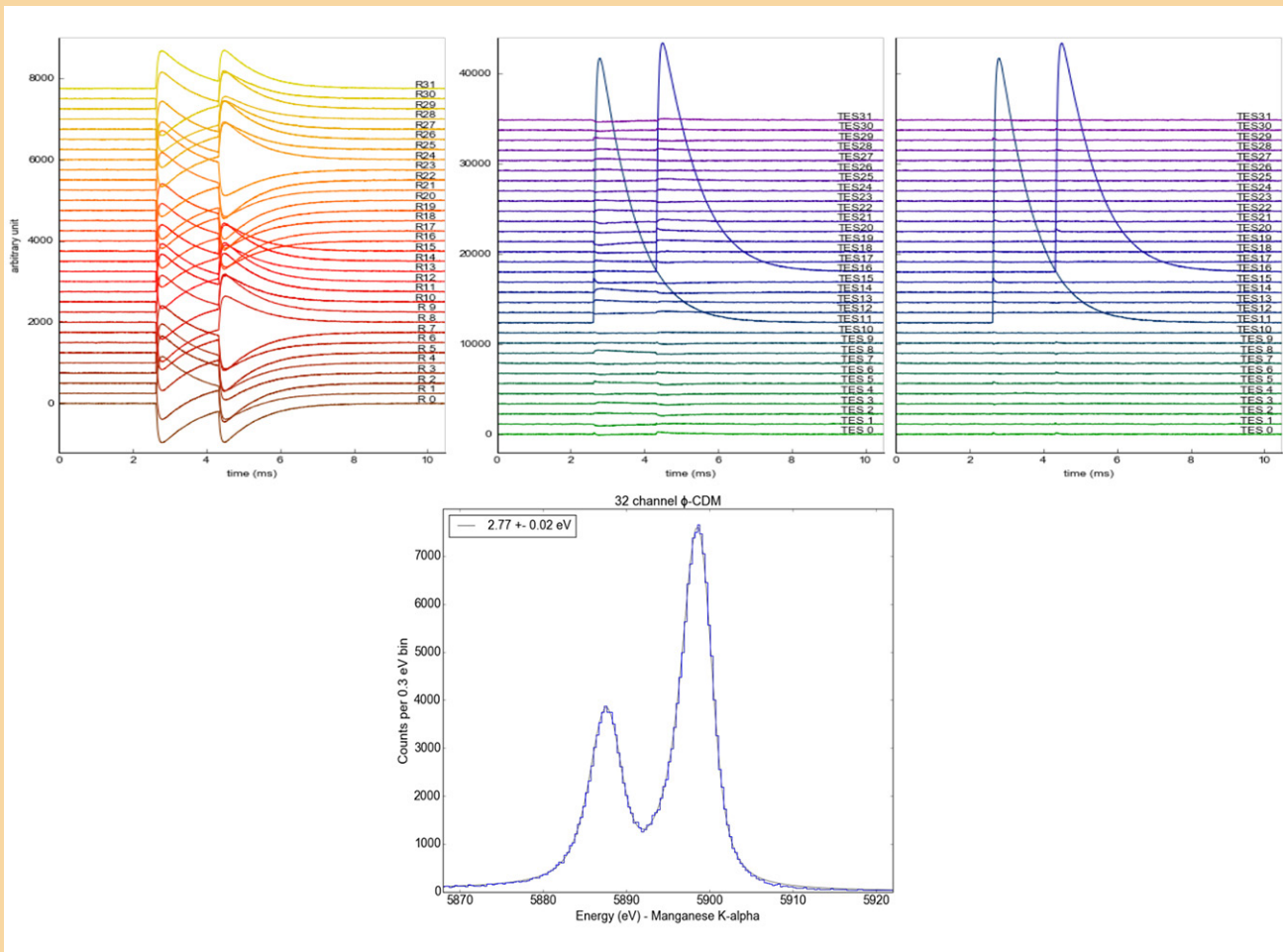


**Fig. 3.** Upper left: Raw TES pulses from 32-row CDM demonstration. Upper center and right: Demodulated TES pulses from 32-row CDM demonstration with two X-ray events arriving 2 ms apart in different pixels. The data are demodulated assuming an idealized demodulation matrix where all couplings are equal to 1 (center). Departures from ideal coupling due to fabrication non-uniformity and other on-chip sources of crosstalk are on the order of a few percent and cause spurious signals in all detectors. Using a correction to the ideal matrix, we reduced crosstalk to less than 0.1%. Bottom: The combined spectrum from the 32-channel CDM demonstration with 30 TESs connected.



### ***Development of Large-Scale Array and Readout Capability***

We are developing two identical  $^3\text{He}$ -backed Adiabatic Demagnetization Refrigerator (ADR) demonstration platforms to instrument a full kilo-pixel-scale TDM/CDM array for technology demonstration and device characterization. One of these systems will be at NIST and one at GSFC. Two systems are essential because we will be testing multiple array types (uniform arrays and hybrid arrays) with multiple readouts (TDM and CDM). These ADRs are being procured and will be received later this year. Figure 4 shows a computer-aided design (CAD) schematic of the new ADR and a close-up of the new 50 mK ‘Snout’ FPA. This system is a scaled-up version of the successful 256-pixel Snout presently used in both NIST and GSFC platforms. This architecture is being dimensioned for 40-row  $\times$  24-column TDM/CDM, enabling 960-pixel characterization and multiplexed-technology demonstrations. The detector chip will sit atop the Snout, with flexible interconnects to the two sets of 80-pixel multiplexer and Nyquist chips (four columns) on each of the six side panels. Final versions of the new multiplexer and Nyquist chips are currently being designed. The new chips will implement iterations on existing designs, incorporating geometric optimizations to reduce on-chip crosstalk sources to negligible levels.

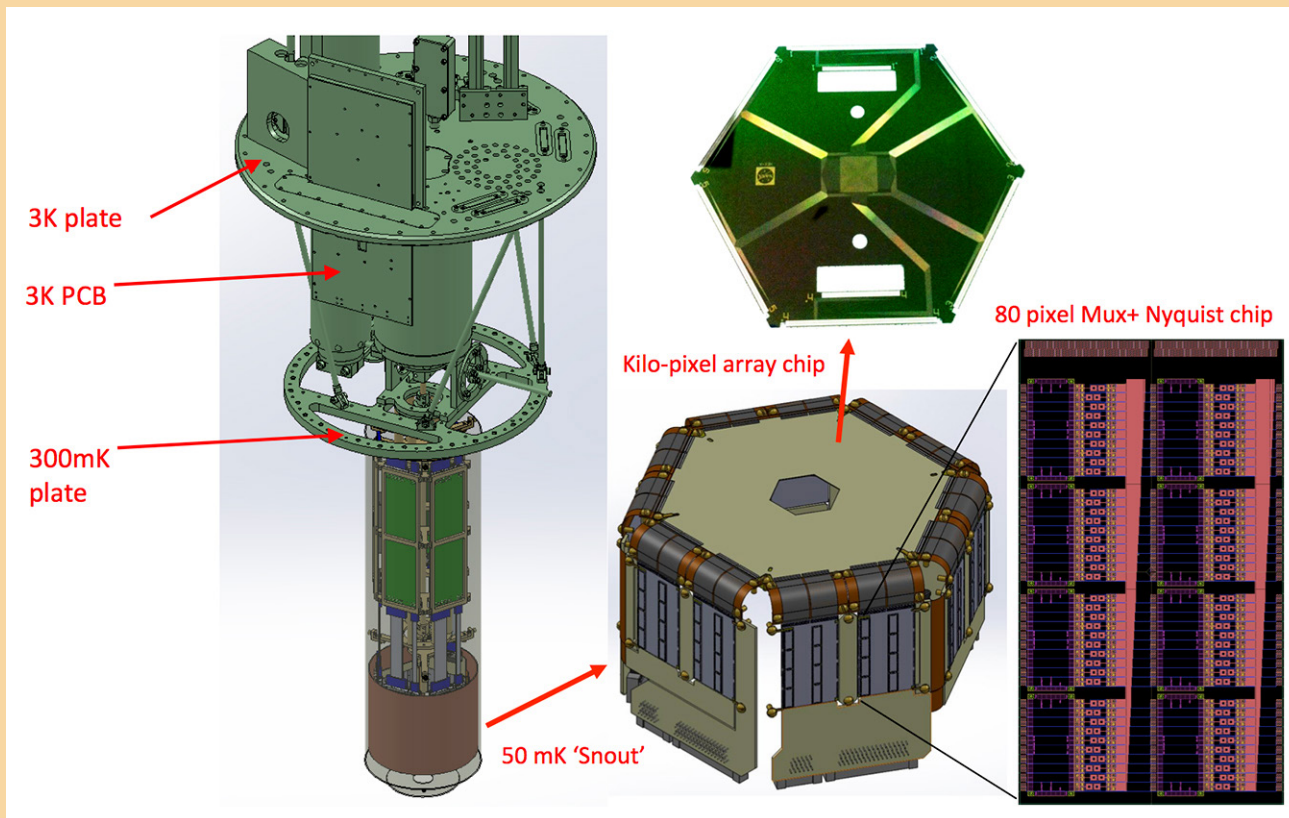


**Fig. 4.** Left: CAD of new laboratory test platform for kilo-pixel array characterization and TDM/CDM demonstrations. Bottom right: CAD sketch of new 40-row  $\times$  24-column 50 mK ‘Snout’ and the new  $2 \times 80$ -pixel Nyquist and multiplexer chips that will populate the six panels. Top Right: Photograph of prototype, fully wired, kilo-pixel array chip with 1024 bond-pad pairs, all TESs, and an additional 128 bond-pads routed to rectangular holes which could be used to incorporate a second array. The size is 72 mm corner-to-corner (opposite vertices). The circular holes are for use with an earlier design of the kinematic mounting.

We have also designed kinematic mounts that can incorporate two detector arrays and an anti-coincidence detector on three separate levels. A first mechanical model (used for fit-checks and verifying the assembly process) has been fabricated. A second iteration using the design materials will be produced. A mechanical model of a full-scale array chip (with perimeter long enough to accommodate pads for all channels) has also been produced and will be iterated to accommodate the mount design. Other ongoing supporting activities taking place include development of “around-the-corner” flexible interconnects and investigation of bump-bonded connections to the TES wafer.

The TDM/CDM interface between detector and readout/bias circuit component is very different from that of FDM. Any large, Athena-scale, demonstration array will need to be characterized using both DC-biased (TDM/CDM) measurements, which will be wire-bonded to flexible interconnects, and AC-biased (FDM) measurements, which will be inductively coil-coupled to the readout components. We are developing wafers of the size, shape, and layout required for future kilo-pixel testing of the X-IFU arrays. We are converging on a wafer-layout solution that will incorporate DC-biased pixels in three sectors of a hexagonal wafer and AC-biased pixels in the other three sectors. This layout concept is shown in Fig. 5. We have also completed a prototype wiring layout for a full-sized X-IFU hybrid array (Fig. 5). The fully wired array consists of 3476 large pixels on a 0.26-mm pitch with an  $18 \times 18$  SPA on a  $155.5\text{-}\mu\text{m}$  pitch in the center. To wire all pixels to the edge of the array, there are up to 20 wire pairs (on a  $4\text{-}\mu\text{m}$  pitch) per  $82\text{-}\mu\text{m}$ -wide muntin between pixel pairs.

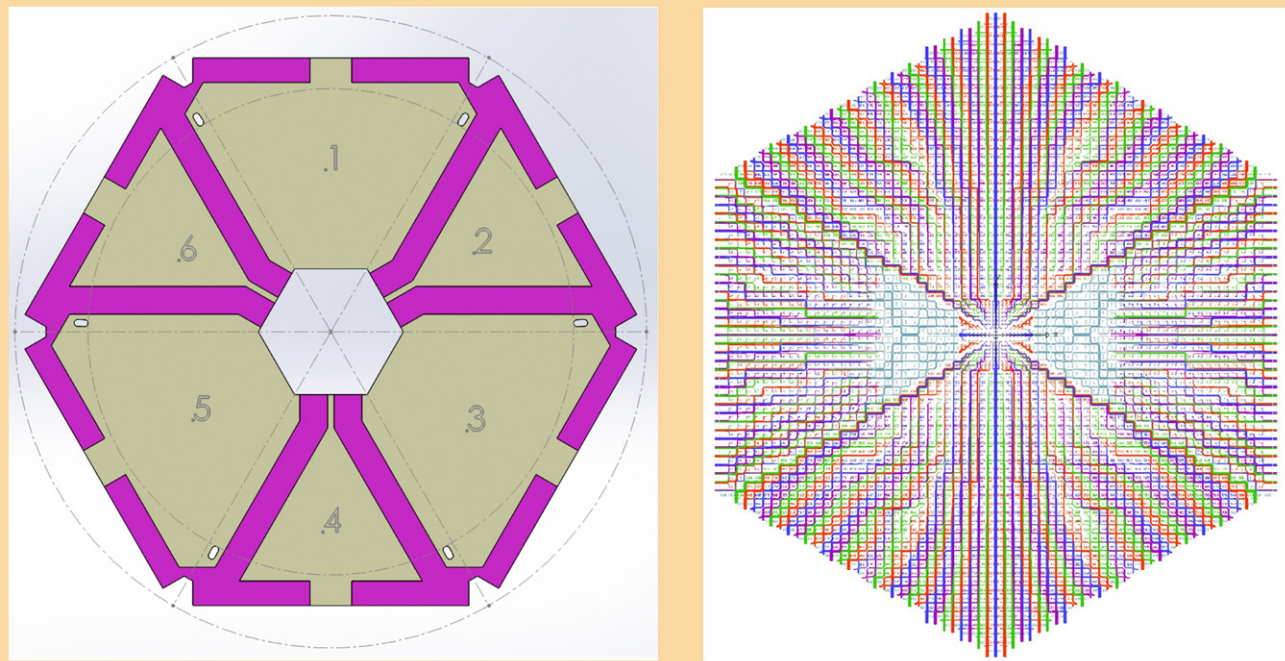


**Fig. 5.** Left: Wafer layout for kilo-pixel level testing/demonstrations. The TES array is the center hexagon. The wiring for DC-biased pixels will be routed through the sectors labeled 2, 4, and 6 to bond pads on all six edges. Transformer coils for AC-biased pixels will be in the centers of sectors 1, 3, and 5. Right: Complete wiring layout of hybrid array consisting of 3476 large pixels on a 0.26-mm pitch and an  $18 \times 18$  array of small pixels on a  $115.5\text{-}\mu\text{m}$  pitch. All pixels are wired out to the edge of the array.

### Hybrid Array Development

As an alternative to the X-IFU baseline array of identical pixel types, a hybrid array of two different pixel types is presently under study. To implement a ‘hybrid’ array of different detector optimizations on a single die, several new fabrication-processing steps must be developed and demonstrated. For example, the presently envisaged hybrid array configuration consists of an LPA with Au/Bi absorber



surrounding a high-count-rate SPA with Au absorber. The different absorber compositions are required to independently optimize device heat capacity while maintaining the required quantum efficiency in both pixel types. We have developed new processing steps and now demonstrated the ability to fabricate two different absorber compositions in different parts of a single array. Since Bi and Au etch at different ion-milling rates, additional processing steps are being developed to enable uniform 4- $\mu\text{m}$  gaps between the absorbers over all parts of the array to achieve the X-IFU fill factor requirement. Figure 6 shows a scanning electron micrograph (SEM) of a hybrid array consisting of an all-Au absorber in the central region of small pixels and a composite Au/Bi absorber in the surrounding main array.

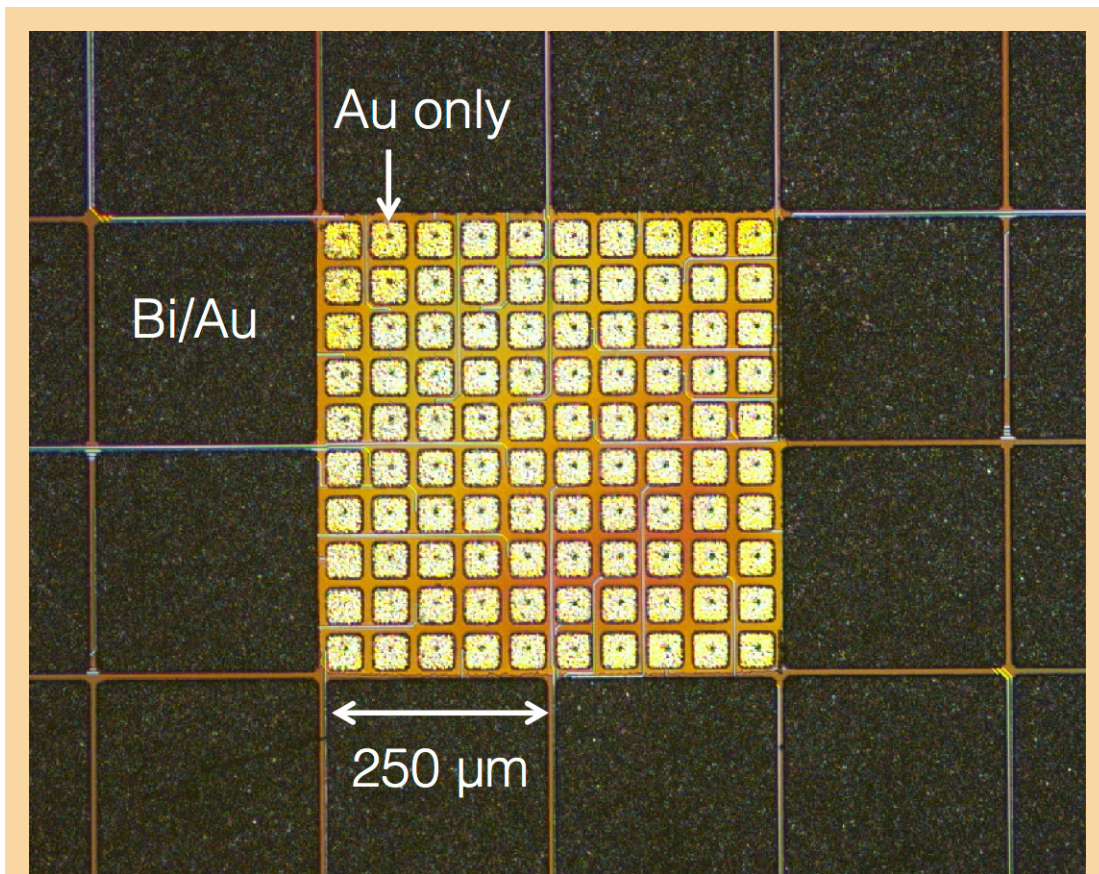


**Fig. 6.** SEM image of an example of a kilo-pixel hybrid array consisting of a  $10 \times 10$  array of small-pixel TESs with Au absorbers (50- $\mu\text{m}$  pitch) surrounded by an array of larger pixels with composite Au/Bi absorbers (250- $\mu\text{m}$  pitch). This is similar to that proposed for the Athena X-IFU.

We have begun test depositions in the newly installed electron-beam evaporation tool that will be used for dedicated TES Mo/Au depositions. Due to the specific design of the system, variations of important process parameters such as film thickness and wafer temperature across each wafer and from wafer to wafer are set to be less than 2%. Initial depositions suggest we can achieve the target of < 2-mK bilayer  $T_c$  uniformity over a full Athena-scale array. This new custom tool will produce seven-device bilayer wafers and a witness wafer (used for diagnostic  $T_c$  checks) in a single deposition run without breaking vacuum, and is essential for achieving the required array-scale uniformity and wafer-to-wafer reproducibility. Refinement of the critical deposition processes will continue and the first product devices are expected in late FY 2016 or early FY 2017.



## Path Forward

Given a detector of suitable  $T_c$  and heat sinking, our recent improvements in TDM architecture are sufficient to complete a 32-row demonstration, more than satisfying the previously defined milestone. This remains a highly relevant metric for demonstrating TRL 5 for the backup technology, and is commensurate with the main DM objectives using the baseline FDM readout. Beyond this, our focus is on developing full scale Athena arrays (uniform and hybrid), and designing the testing infrastructure to characterize these arrays and provide additional large-scale technology demonstrations.

Because the baseline X-IFU FDM readout applies an AC bias to the TES thermometers, we also need to characterize and optimize TES performance under AC bias. There has previously only been a single GSFC array tested under AC bias at SRON, under the IXO framework. We have now delivered a new test array with different pixel geometries, and GSFC scientists have visited SRON to participate in testing and data interpretation. By the end of FY 2016, we will have delivered a second array of uniform pixels of preferred geometry for FDM demonstrations; and in the early part of FY 2017, we anticipate delivering the first uniform kilo-pixel-scale array for DM integration and testing. We are about to start our own AC-biased pixel tests at GSFC and at NIST. This single-pixel AC-bias research is the main component of the related program in which our collaboration is engaged (PI J. Ullom, “Technology Development for an AC-Multiplexed Calorimeter for Athena”). That effort is merging with our overall effort to support these early technology demonstrations for the X-IFU.

## References

- [1] K. Nandra et al., “*Athena, the Advanced Telescope for High ENergy Astrophysics*,” a mission proposal submitted to ESA’s L2 large mission opportunity, recently accepted (2014)
- [2] D. Barret et al., “*The Hot and Energetic Universe: The X-ray Integral Field Unit (X-IFU) for Athena+*,” astro-ph arXiv:1308.6784 (2013)
- [3] J.A. Chervenak et al., “*Superconducting multiplexer for arrays of transition edge sensors*,” Appl. Phys. Lett., **74**, 4043-4045 (1999)
- [4] R. den Hartog et al., “*Baseband Feedback for Frequency-Domain-Multiplexed Readout of TES X-ray Detectors*,” AIP Conf. Proc. **1185**, 261-264 (2009)
- [5] C.A. Kilbourne et al., “*Multiplexed readout of uniform arrays of TES X-ray microcalorimeters suitable for Constellation-X*,” Proc. SPIE **7011**, 701104 (2008)
- [6] S.J. Smith et al., “*Small Pitch Transition-Edge Sensors with Broadband High Spectral Resolution for Solar Physics*,” J. Low Temp. Phys., **167**, 168-175 (2012)
- [7] S.R. Bandler et al., “*Advances in Small Pixel TES-Based X-Ray Microcalorimeter Arrays for Solar Physics and Astrophysics*,” IEEE Trans on Appl. Sup., **23** (3), 2100705 (2013)
- [8] S.J. Smith et al., “*Uniformity of Kilo-Pixel Arrays of Transition-Edge Sensors for X-ray Astronomy*,” IEEE Trans. Appl. Supercon., **25**, 2100505 (2015)
- [9] H.H. Zappe, “*Josephson quantum interference computer devices*,” IEEE Trans. on Magnetics, **13**, 41-47 (1977)
- [10] J. Beyer and D. Drung, “*A SQUID multiplexer with superconducting-to-normal conducting switches*,” Superconductor Sci. and Technol., **21**, 105022 (2008)
- [11] W.B. Doriese et al., “*Developments in Time-Division Multiplexing of X-ray Transition-Edge Sensors*,” J. Low Temp. Phys., DOI 10.1007/s10909-015-1373-z (published online Dec 2015)
- [12] K.M. Morgan et al., “*Code-division-multiplexed readout of large arrays of TES microcalorimeters*,” in preparation; to be submitted to Appl. Phys. Lett. (2016)

For additional information, contact Caroline Kilbourne: [caroline.a.kilbourne@nasa.gov](mailto:caroline.a.kilbourne@nasa.gov)



# Reflection Grating Modules: Alignment and Testing

Prepared by: Randall L. McEntaffer (PSU)

## Summary

The science requirements for future soft X-ray spectroscopy missions drive the instrumentation requirements for spectral resolving power and spectrograph effective area. Key science goals that address the physical properties and distribution of hot matter in the universe can be realized with diffraction-grating-based spectrographs in a range of platforms from Explorers to Probes to large missions. The majority of spectral features from astrophysical plasmas at temperatures  $>10^6$  K occur in the soft X-ray regime, below 2 keV, where diffraction gratings can provide the instrument performance required for these science goals. A sustained program of grating technology development is necessary to qualify these spectrographs for future flight opportunities.

This document details the results from a Strategic Astrophysics Technology (SAT) program with a period of performance spanning calendar years 2015 and 2016. These developments leverage heavily from associated NASA programs including:

1. A previous SAT program, “Off-plane Grating Arrays for Future Missions,” that performed the initial trade studies necessary to identify grating fabrication, alignment, and testing techniques.
2. An ongoing Roman Technology Fellowship (RTF) dedicated to developing fabrication methodologies for reflection gratings.
3. A current Astrophysics Research and Analysis (APRA) grant for suborbital flight of a reflection-grating-based spectrograph.

The progress made during these programs [1-7] has enabled the current SAT to concentrate on the developments needed in the areas of grating alignment and performance testing. Collaborations with NASA’s MSFC and GSFC provided critical support for this SAT. Colleagues at GSFC provided an X-ray telescope for use during grating performance testing, while MSFC is providing testing facilities and support at their Stray Light Facility (SLF) X-ray beamline. The ultimate goal of this project is to populate and qualify a flight-like grating module with several large-format, high-fidelity gratings to create a spectrograph subsystem that is ready for incorporation into the next spectroscopic X-ray observatory.

This is the second report during this project and therefore shares the same Background and similar milestones as the 2015 Physics of the Cosmos (PCOS) Program Annual Technology Report (PATR) [8]. Subsequently, a description of the most recent developments in grating alignment and testing is given.

## Background

The purpose of this study is to advance high-throughput, high-spectral-resolving-power, X-ray spectroscopy and its application in future NASA missions. Specifically, the project will concentrate on improving the Technology Readiness Level (TRL) of off-plane reflection-grating spectroscopy for soft X rays (0.2 – 2.0 keV). This technology has applications in a variety of NASA missions from suborbital rockets to Explorer-class missions to large observatories. An Off-Plane X-ray Grating Spectrograph (OP-XGS) was included in the instrument suite for the International X-ray Observatory (IXO) during the last Decadal Survey, which spurred many follow-on studies [9] including mission concepts such as the Advanced X-ray Spectroscopic Imaging Observatory (AXSIO), the Notional X-ray Grating Spectrometer (N-XGS), and the Square Meter Arcsecond Resolution Telescope for X rays (SMART-X). Currently, an OP-XGS forms the backbone of an Explorer mission concept, Arcus, submitted in response to the 2014 Explorer Announcement of Opportunity (AO) [10], and is included as a spectrometer concept for the X-ray Surveyor large mission concept [11]. Progress made during the development of the OP-XGS was detailed in the four previous PATRs of the PCOS Program. The PCOS Program identified X-ray reflection gratings

as a critical technology for development in this decade to address X-ray science goals. In this role, we also contributed a development roadmap detailing the efforts and milestones needed to advance the OP-XGS to flight readiness, incorporated into the most recent X-ray Technology Development Roadmap (TDR).

Soft X-ray grating spectrometers with high throughput and high spectral resolving power can address many top science questions such as:

- What controls the mass-energy-chemical cycles within galaxies?
- How do baryons cycle in and out of galaxies, and what do they do while they are there?
- What are the flows of matter and energy in the circumgalactic medium?
- How do black holes work and influence their surroundings?
- How do massive stars end their lives?
- What controls the masses, spins, and radii of compact stellar remnants?

These science questions can be addressed with high-quality X-ray spectra as specifically stated in the 2010 Decadal Survey, “New Worlds, New Horizons in Astronomy and Astrophysics” (NWNH). At the lowest energies, the most efficient method of obtaining high spectral resolving power is grating spectrometers.

To achieve these science goals, a grating spectrograph must be capable of producing spectral resolving powers ( $\lambda/\delta\lambda$ ) better than 1500, with high throughput over the soft X-ray energy band. The major limiting factor is meeting the spectral-resolving-power requirement. In the context of off-plane reflection gratings, this requires customization of the groove profile to obtain blazed facets with high groove density that varies along the groove direction. In a parallel RTF effort, we are developing a new fabrication method using common lithographic techniques borrowed from the semiconductor industry. Electron-beam (e-beam) lithography enables tight control over the groove profile during recording, while various etching steps can be used to shape the facets to the desired blaze. An optimal groove profile will limit any grating-induced aberrations to the telescope focus while maximizing throughput and resolving power over our wavelength band-of-interest. We have used gratings fabricated during the RTF in the current SAT study to populate our grating modules. The design of the grating module has gone through several iterations during the previous SAT program. This design has been refined through testing and analysis leveraged from the APRA program and concept mission studies. In the course of our current SAT, we have implemented this design to house our gratings. During module population, alignment tolerances must be met so that every spectrum from every grating overlaps at the focal plane with limited alignment-induced distortion. We have previously analyzed our alignment tolerances, assessed required metrology, and developed a concept alignment methodology. Over the past year, we implemented these techniques to produce an aligned module of gratings, and undertook associated performance testing. Therefore, we are well on our way to achieving the two main paths of our development plan:

- Implementation of our alignment methodology; and
- Performance-testing of aligned modules.

## Objectives and Milestones

High diffraction efficiency and high spectral resolving power have been demonstrated for off-plane reflection gratings. Prototype gratings have been shown to place > 40% of incident light into diffracted orders [1, 12] while also achieving spectral resolving powers > 3000 in the soft X-ray band. These demonstrations place off-plane gratings at TRL 4, as recently vetted by the PCOS Program. The Program has also agreed with our proposed path toward TRL 5.

While single prototype gratings have proven the capability of the off-plane design, aligned arrays of large-format, blazed gratings need to be fabricated and tested to prove the technology for flight missions. A program of grating fabrication, alignment, and performance/environmental testing is necessary to bridge the current technology gap and achieve flight readiness.



Several of the milestones needed to achieve our goals for this SAT have been accomplished over the past year. Here we outline some of the major milestones achieved, as well as those remaining for the calendar year:

1. Install alignment fixtures and metrology in the lab – completed 3<sup>rd</sup> quarter of 2015.
2. Align multiple grating substrates into mount – completed 4<sup>th</sup> quarter of 2015.
3. Improve grating mounting and alignment methodology, informed by initial alignment results – completed 4<sup>th</sup> quarter 2015/1<sup>st</sup> quarter of 2016.
4. Design and fabricate high-fidelity grating mount – completed 1<sup>st</sup> quarter of 2016.
5. Implement alignment improvements – completed 1<sup>st</sup> quarter of 2016.
6. Receive large-format gratings from RTF program – completed 2<sup>nd</sup> quarter of 2016.
7. Align multiple large-format gratings into mount – completed 2<sup>nd</sup> quarter of 2016.
8. Carry out performance and environmental testing of a high-fidelity module of aligned, large-format gratings – completed 2<sup>nd</sup> quarter of 2016.
9. Analyze results – planned for 3<sup>rd</sup> quarter of 2016.
10. Publish results – planned for 4<sup>th</sup> quarter of 2016.

Highlights of the results accomplished in the completion of these milestones are summarized below.

## Progress and Accomplishments

The progress made during this SAT was enabled by advancements in the grating fabrication studies of the RTF program, as well as the system-level studies of the associated APRA program and Arcus Explorer mission concept. Our grating fabrication method developed over the course of this SAT, which resulted in our ability to fabricate large-format, flight-like gratings (Fig. 1). These gratings are large format (75 mm × 96 mm × 0.5 mm), blazed (54.7° facet angle), variable line spaced (8× periods from 158.25 nm – 160 nm in 0.25-nm steps), coated (15-nm Au with 5-nm Cr binding layer), and replicated onto flat (<1 μm peak-to-valley flatness over 80-mm diameter) fused-silica substrates. Realization of these large-format gratings has enabled our goal of aligning and populating a flight-like module.

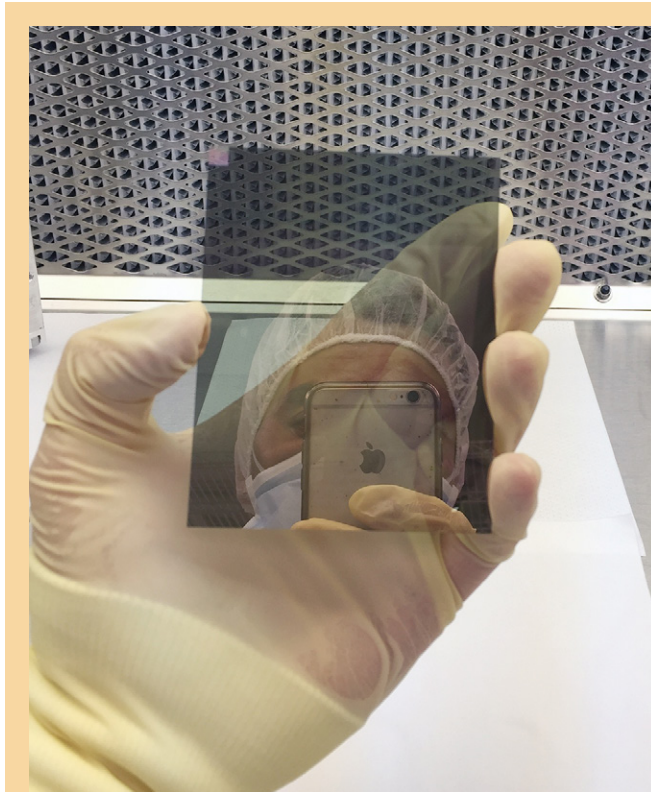


**Fig. 1.** A full-format, off-plane, X-ray reflection grating. The grating measures 75 mm × 96 mm in grooved area and is replicated onto a fused-silica substrate. The coating is 5-nm Cr under 15-nm Au. A 5 mm × 5 mm area in the top left, with a noticeable optical diffraction grating, is used for alignment purposes.

During our grating fabrication efforts, we also performance-tested the blazed profile for diffraction efficiency. These tests were carried out at the Advanced Light Source at Lawrence Berkeley National Laboratory (LBNL) in collaboration with Eric Gullikson. The tested grating measured 10 mm × 30 mm × 0.5 mm and was etched into a silicon wafer in collaboration with Dmitriy Voronov at LBNL. The profile was blazed at 54.7° and variable-line-spaced with a period change from 160 nm to 159.75 nm. The sample was coated with 5-nm Cr and 30-nm Au prior to testing.

The diffraction efficiencies of the blazed off-plane grating are shown in Fig. 2 for orders measured between 0.5 keV and 1.0 keV. The sum of absolute efficiencies (includes Au reflectivity) in diffracted orders 5-8 is greater than 35%. This is the highest diffraction efficiency measured to date for a blazed grating and is an important result, as it shows that gratings such as these can achieve performance goals necessary for future spectrographs. Due to our current fabrication method, the tested grating exhibited a plateau at the top of the groove that measured ~35 nm. This plateau placed flux into zero and lower orders as opposed to orders close to the blaze. We understand how to limit this effect and, if successful, could achieve ~50% diffraction efficiency (see black dash-dot line in Fig. 2).

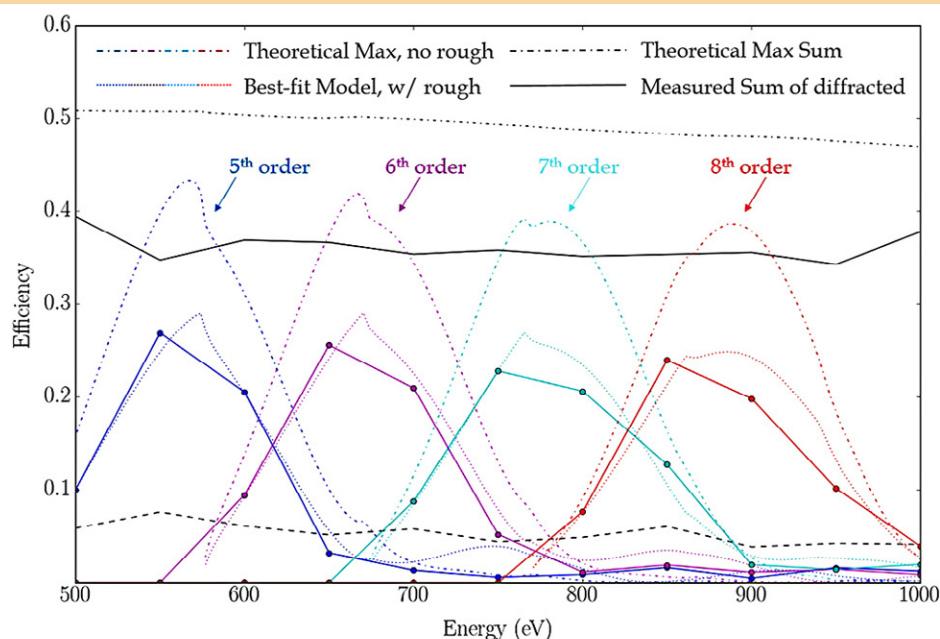


**Fig. 2.** Diffraction efficiencies for a blazed off-plane grating. The data points mark the measured efficiency values in 50-eV increments and are connected by solid lines. The dotted line shows best-fit models generated by PCGrate and includes roughness. The dash-dot lines show theoretical model efficiencies for this blaze ignoring roughness and the 35-nm groove plateau. The black lines show sum of diffracted order efficiencies for the theoretical maximum (dash-dot) and the measured data (solid).

Our alignment developments paralleled our large-format grating production. A picture of our early alignment setup is shown in Fig. 3. We initially aligned two Au-coated fused-silica substrates (no grating surface) in an attempt to learn how to debug the system and learn about shortcomings and develop possible improvements to our module design, alignment metrology, and methodology. We performed this exercise on two separate modules that contained two optics each. We also vibration-tested these modules to 12.1-g root-mean-square (rms) in three axes with a ¼-g sine sweep. One module failed vibration testing due to a poor epoxy joint which was remedied in the second module that survived the test. This gave us confidence in our module design and bonding procedures and enabled design of our high-fidelity module. These activities also allowed us to assess our metrology and determine our control in each of the six degrees of freedom. We recognized that we were dependent on environmental variables and implemented a temperature control system (not shown in Fig. 3). We also implemented additional metrology, including laser distance-meters to monitor the position of the grating module during actuation.

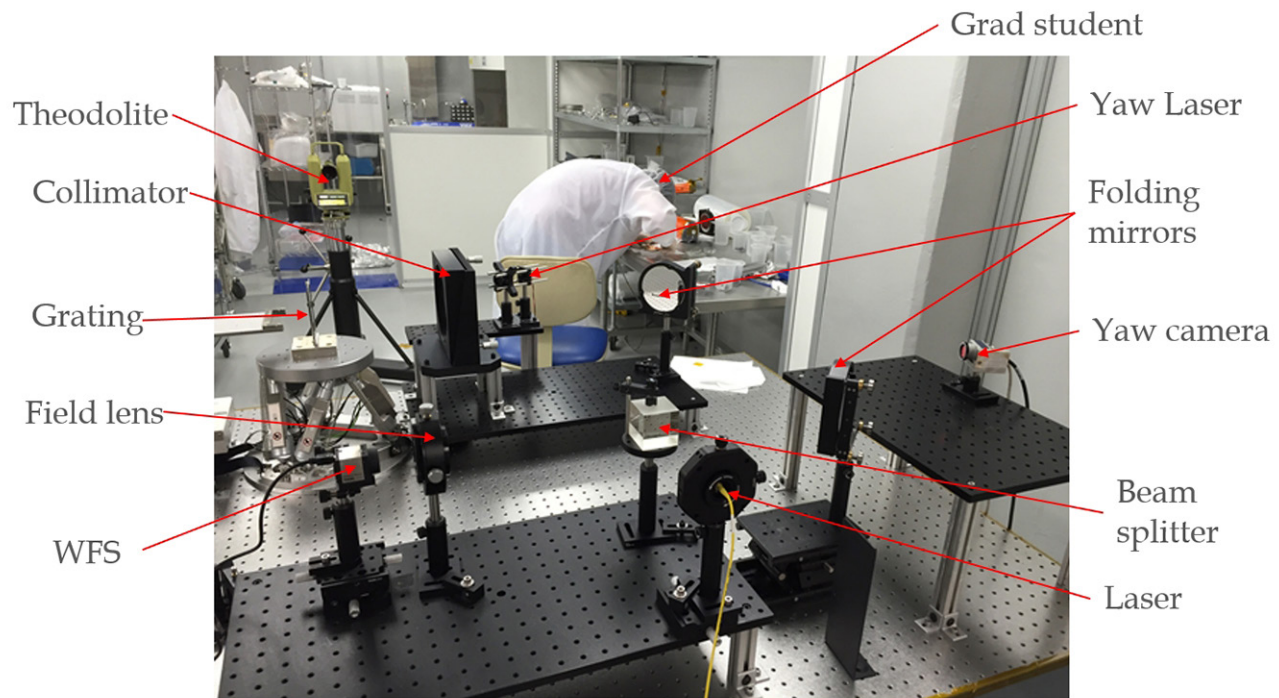


**Fig. 3.** The off-plane reflection grating alignment setup. A spherically diverging laser is passed off the grating surface and back through the system to a wavefront sensor (WFS) to measure pitch and roll on the grating. A yaw laser and camera sample the optical diffraction grating written into the grating profile (Fig. 1) to measure yaw. The position of the grating is controlled by a hexapod. The grating module is indexed using an independent stage stack (not shown) and the module is referenced using a theodolite.

Given the results of our preliminary testing, we updated the alignment system and module design to produce a high-fidelity, flight-like grating module. This module is made from Invar and holds onto the grating with a clip-and-pin system [13]. The assembly of four aligned, large-format gratings is shown in Fig. 4. These gratings are aligned to be parallel to one another given that our X-ray test setup consists of a single mirror shell [14]. In this way, we can scan the individual gratings across the single telescope beam and watch the position of the spectrum at the focal plane to assess our achieved alignment. We recently carried out this testing at MSFC. These tests included a vibration test between X-ray verification tests. The module was vibrated at the NASA general environmental verification standard (GEVS) levels and survived qualification at 14.1g rms in three axes. Preliminary X-ray data from the MSFC tests are shown in Fig. 5. The top half of the image shows the line spread function of 3<sup>rd</sup> order Al K $\alpha$  prior to vibration testing, while the bottom half shows the same lines after testing. The four smaller images are the line-spread functions resulting from each of the four aligned gratings while the larger image shows their superposition. Qualitatively, a gross misalignment is not obvious. Detailed analysis of these lines over the range of testing parameters is necessary to discern the actual alignment achieved. The analysis of these data is ongoing, and will be published later in the year [15]. This analysis will concentrate on verifying the accuracy of our alignment pre-vibration along with verification that this alignment held post-vibration. These verifications will satisfy our requirements for TRL 5.



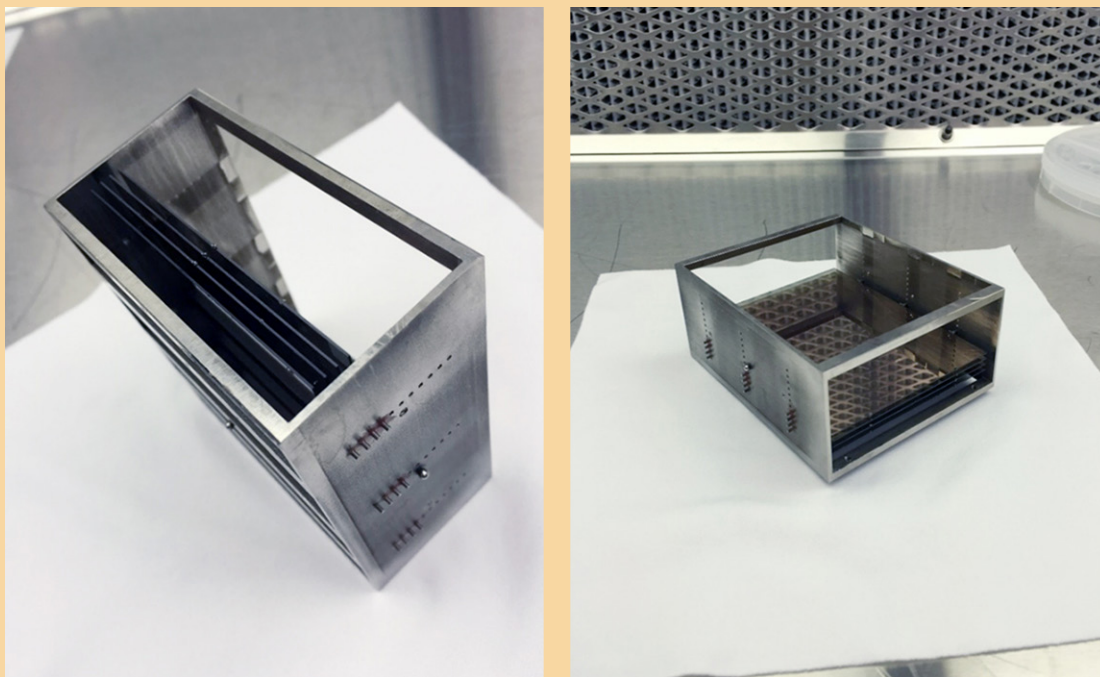


**Fig. 4.** Two views of a high-fidelity, aligned module of full-format, off-plane diffraction gratings. The module measures 83 mm × 99 mm × 45 mm.

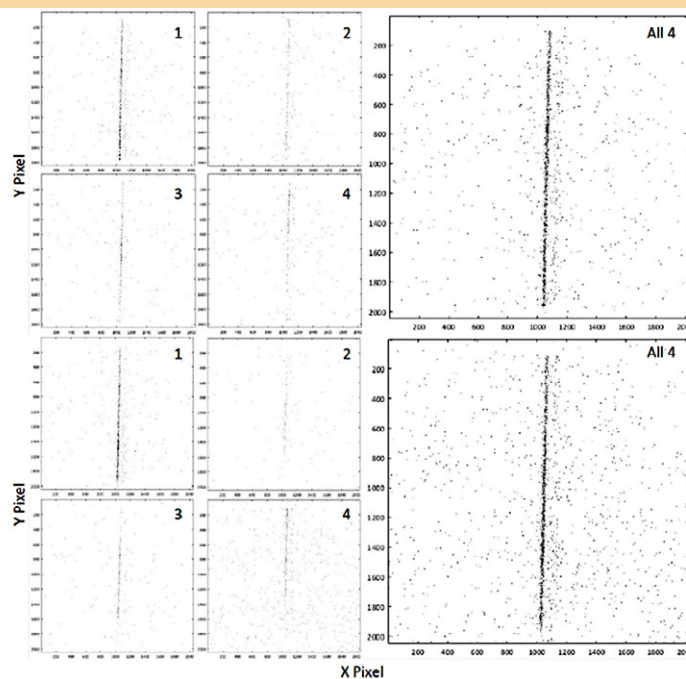


**Fig. 5.** Top Left: Line-spread function from 3<sup>rd</sup> order Al  $K\alpha$  from each of the four aligned gratings prior to vibration testing. Top Right: Combined line-spread functions of all four gratings prior to vibration testing. Bottom Left: The same line-spread functions after vibration testing. Bottom Right: Combined line-spread functions of all four gratings after vibration testing.

## Path Forward

Most of the goals for this SAT program have been fulfilled. The final large effort involves in-depth analysis of the X-ray test data. These results, along with a description of our alignment methodology, will be published later in the year. The findings will be reported to the TRL vetting board in the hope of achieving TRL 5 for off-plane reflection gratings, the ultimate goal of this SAT.

This work has elucidated several areas that could use further study. These studies would assist in fabrication and alignment, with the goal of maximizing effective area and spectral resolving power. There is ample parameter space that has yet to be realized, yet could be critical for achieving performance that would likely be necessary for future large X-ray missions. Examples include the study of larger grating formats. Larger gratings increase the effective area per grating, easing alignment. This will also potentially allow for thicker gratings, which will be easier to produce with a flat figure. Another example is a stress study. We would like to understand more fully the stress induced during the imprint process and the reflection coating process. The latter can also be studied as a function of material in order to concurrently optimize reflectivity. Another example is a study of the optimal groove profile. The groove density can easily be increased by a factor of two (which also increases dispersion, and hence resolution), but we do not understand the limit and possible effects these densities may cause down the fabrication line. We can also create finer period changes with higher-fidelity variable line spacing, but again, do not understand the limits. The blaze angle can also be tuned, but we do not yet understand if there is a substantial difference between the creation of very shallow blaze angles and very steep ones. Finally, we would like to understand groove-profile roughness and how this carries forward from substrate to final reflective coating. This is a multi-step process that would require a dedicated study, yet could substantially increase diffraction efficiency.

## References

- [1] R.L. McEntaffer, C. DeRoo, T. Schultz, B. Gantner, J. Tutt, A. Holland, S. O'Dell, J. Gaskin, J. Kolodziejczak, W.W. Zhang, K.-W. Chan, M. Biskach, R. McClelland, D. Iazikov, X. Wang, and L. Koecher, "*First results from a next-generation off-plane X-ray diffraction grating*," *Experimental Astronomy*, **36**, 389 (2013)
- [2] R. Allured and R.L. McEntaffer, "*Analytical Alignment Tolerances for Off-Plane Reflection Grating Spectroscopy*," *Experimental Astronomy*, **36**, 661 (2013)
- [3] R. Allured, B.D. Donovan, and R.L. McEntaffer, "*Alignment Tolerances for Off-Plane Reflection Grating Spectrometry: Theoretical Calculations and Laboratory Techniques*," *Proc. SPIE*, **8861**, 88611C (2013)
- [4] C. DeRoo, R.L. McEntaffer, T. Schultz, W.W. Zhang, N.J. Murray, S.L. O'Dell, and W. Cash, "*Pushing the boundaries of X-ray grating spectroscopy in a suborbital rocket*," *Proc. SPIE*, **8861**, 88611B (2013)
- [5] H. Marlowe et al., "*Performance Testing of an Off-plane Reflection Grating and Silicon Pore Optic Spectrograph at PANTER*," *J. Astro. Tele., Inst., and Sys.*, **1**, 045004 (2015)
- [6] R. Allured, B. Donovan, C. DeRoo, H. Marlowe, R.L. McEntaffer, J. Tutt, P. Cheimets, E. Hertz, R.K. Smith, V. Burwitz, G. Hartner, and B. Menz, "*Optical and x-ray alignment approaches for off-plane reflection gratings*," *Proc. SPIE*, **9603**, 960315 (2015)
- [7] C. DeRoo et al., "*Line Spread Functions of Blazed Off-Plane Gratings Operated in the Littrow Mounting*," *J. Astro. Tele., Inst., and Sys.*, accepted for publication (2016)
- [8] National Aeronautics and Space Administration, *Physics of the Cosmos Program Annual Technology Report*, REP. NO. 440-RPT-0016 (2015)
- [9] M.W. Bautz, W.C. Cash, J.E. Davis, R.K. Heilmann, D.P. Huenemoerder, M.L. Schattenburg, R.L. McEntaffer, R.K. Smith, S.J. Wolk, W.W. Zhang, S.P. Jordan, and C.F. Lillie, "*Concepts for high-performance soft X-ray grating spectroscopy in a moderate-scale mission*," *Proc. SPIE*, **8443**, 844315 (2012)

- [10] R.K.Smith et al., “*Arcus: an ISS-attached high-resolution X-ray gratings spectrometer*,” Proc. SPIE, **9144**, 91444Y (2014)
- [11] J.A. Gaskin et al., “*The X-ray Surveyor Mission: a concept study*,” Proc. SPIE, **9601**, 96010J (2015)
- [12] C. DeRoo et al., “*Diffraction efficiencies of Blazed Off-Plane Gratings Operated in the Littrow Mounting*,” Applied Optics, in preparation (2016)
- [13] K.-W. Chan et al., “*Aligning, bonding, and testing mirrors for lightweight X-ray telescopes*,” Proc. SPIE, **9603**, 96030Z (2015)
- [14] J.H. Tutt et al., “*Alignment of off-plane reflection gratings using optical light*,” J. Astro. Instr., in preparation (2016)
- [15] B. Donovan et al., “*X-ray and environmental testing of an aligned off-plane grating module*,” in preparation (2016)

For additional information, contact Randall McEntaffer: [rlm90@psu.edu](mailto:rlm90@psu.edu)





# Development of 0.5-Arcsecond Adjustable Grazing-Incidence X-ray Mirrors for the SMART-X Mission Concept

Prepared by: Paul B. Reid (PI; SAO) and Eric Schwartz (SAO)

## Summary

*“Development of 0.5-Arcsecond Adjustable Grazing Incidence X-ray Mirrors for the SMART-X Mission Concept,”* NASA Contract NNX15AC44G, is a Strategic Astrophysics Technology (SAT) program that began in February 2015 and is scheduled to run through the end of calendar year (CY) 2016. This program follows an earlier Astrophysics Research and Analysis (APRA) project on the development of adjustable X-ray optics. The program seeks to develop a modular, highly nested grazing-incidence X-ray mirror assembly composed of bimorph adjustable X-ray mirror segments to achieve 0.5-arcsec imaging while also achieving extremely lightweight mirror assembly mass-per-unit-effective-area (e.g.,  $< 500 \text{ kg/m}^2$  effective area, compared to  $\sim 16,000 \text{ kg/m}^2$  for Chandra). Also included in this report is our APRA program *“Adjustable grazing incidence X-ray optics with 0.5 arc second resolution,”* NASA Contract NNX13AD46G. This program is for the development of the adjustable X-ray mirror segments themselves, but the two programs are completely complementary and linked, as development of mirror technology must include the adjustable optics component; as well as the fabrication of test mirrors, their alignment, mounting, and control technology. Funding for the APRA is exhausted as of June 2016. Our technology will enable large-area, high-resolution imaging X-ray telescope mission concepts such as the Square Meter Arc-second Resolution Telescope for X rays (SMART-X) [1], or equivalently, the 2013 NASA Astrophysics Roadmap committee-recommended X-ray Surveyor (XRS) [2] mission concept. The XRS will study the early universe (growth of structure, merger history of black holes), as well as feedback and evolution of matter and energy.

Our adjustable optics technology eliminates the figure errors and unwanted distortions usually inherent in thin lightweight mirrors. We use a thin (nominally  $1.5 \text{ }\mu\text{m}$ ) film of the piezoelectric material, lead zirconate titanate (PZT), sputtered as a continuous film on the back of thin ( $0.4 \text{ mm}$ ) thermally formed glass Wolter-I mirror segments (a continuous ground electrode is first applied to the back surface). A pattern of independently addressable platinum (Pt) electrodes is deposited on top of the PZT layer, forming individual piezo cells. Applying a low ( $< 10\text{V}$ ) DC voltage between a cell's top electrode and the ground electrode creates an electric field that produces a local strain in the piezo material parallel to the mirror surface. This strain causes localized bending in the mirror, called an influence function. By supplying an optimally chosen voltage to each of the individual cells, one can change the amplitude of each influence function to minimize figure errors in the mirror, thereby improving imaging performance. This allows us to correct mirror figure errors from fabrication, distortions introduced during mounting, and any gravity-release errors. Figure correction is implemented once on the ground during a calibration step after mirror alignment and mounting. Adjusting and correcting the figure of thin mirror segments increases their performance from the 10-arcsec resolution level to 0.5 arcsec. We have shown through simulations improvements from  $\sim 7$  arcsec half-power diameter (HPD) to less than 0.5-arcsec HPD using exemplar-mirror figure data and modeled influence functions [3].

Besides the adjustable optics and XRS teams at the Smithsonian Astrophysical Observatory (SAO), significant contributors to the adjustable optics team are our colleagues at Penn State University (PSU) Materials Research Institute. Prof. Susan Trolier-McKinstry, formerly supported by recently matriculated Dr. Margeaux Wallace, now supported by Dr. Tianning Liu and Julian Walker, develops the PZT processes. Anisotropic Conductive Film (ACF) and ZnO thin-film transistor development is led by Prof. Tom Jackson at PSU, also assisted by Dr. Liu.

The SAT project began at SAO in April 2015, while the APRA project started in February 2013. Progress to date includes performing structural thermal and optical performance (STOP) analyses to examine the performance sensitivity of mirror-assembly temperature control, developing adjustable-mirror-segment technology, developing alignment and mounting technology, reducing mirror complexity via row-column addressing and developing the application of microelectronics industry electrical connectivity, and developing adjustable-mirror-performance monitoring technology that could be used for on-orbit figure correction.

## Background

XRS will be able to address a plethora of important science goals: studies of the growth of supermassive black holes (SMBH) and strong gravity effects; evolution of large-scale structure and detection of the warm-hot interstellar medium (WHIM); and active galactic nuclei (AGN) feedback and cycles of matter and energy. It will be able to carry out surveys to the Chandra deep-field depth over  $10 \text{ deg}^2$ ; study galaxy assembly processes to  $z = 2.5$ ; track the evolution of group-sized objects, including those hosting the first quasars, to  $z = 6$ ; and open new opportunities in the time domain and high-resolution spectroscopy.

Over the past few years, we have developed the concept of the adjustable-optic X-ray telescope. The challenge is to develop a mirror assembly, equivalent to the Chandra High-Resolution Mirror Assembly (HRMA), to a high level of technical readiness over the next several years to provide Chandra-like 0.5-arcsec HPD angular resolution with large effective area. The goal is  $2.3 \text{ m}^2$  at 1 keV, or  $\sim 30$  times that of Chandra, which would be a tremendous increase (a factor-of-four increase in area from Palomar to Keck was considered a breakthrough at the time).

Our baseline plan for SMART-X optics uses slumped-glass mirror segments with deposited piezoelectric actuators energized to correct mirror figure errors from 10-arcsec HPD (achieved for the International X-ray Observatory, IXO; and Advanced X-ray Spectroscopic Imaging Observatory, AXSIO) [4] to better than 0.5-arcsec HPD. The slumped-glass mirror segments developed for IXO/AXSIO represent the current state of the art in lightweight optics. Another approach to develop adjustable X-ray optics simultaneous to our work relied on gluing individual, thick (0.2-mm) ceramic piezoelectric actuators to thin mirrors. This resulted in large ‘print-thru’ errors in the mirror figure [5]. Our approach builds on the mirror development for IXO/AXSIO, in terms of the thermally formed substrates, as well as mirror alignment and mounting. The addition of the piezoelectric layer is essentially just a single process step in the mirror-fabrication process. Our approach resolves the two main problems with lightweight slumped-glass mirrors: (1) it corrects for the low-frequency figure errors that result from a combination of mandrel and thermal-forming errors, and (2) it corrects after the fact for deformations introduced in coating and mounting thin flexible mirrors. In addition, the ability to make an on-orbit correction of mirror figure is critical for telescopes with apertures larger than can be tested with full aperture on the ground (i.e., larger than Chandra).

Our development plan contains several major activities:

1. Development of thin, lightweight slumped-glass adjustable optics, with corrected figure better than 1 arcsec, as demonstrated by X-ray testing of an aligned mounted pair of segments.
2. Flight-like mounting of aligned mirrors in a modular housing that maintains sub-arcsec alignment through the application of launch loads, and after (spacecraft) thermal survival temperature cycling.
3. Connection of control signals and power to the adjustable optics in their flight-like housing, without introducing loads into the mirrors and without losing connection after launch.

We will generate requirements for an adjustable optic mirror assembly capable of achieving 0.5-arcsec HPD. This includes iterative error-budgeting as well as thermal and structural modeling, balancing the difficulty of achieving multiple mirror-assembly requirements.

We will develop, design, and model a flight-like mounting able to support multiple, closely spaced shells of adjustable mirror segments. This will entail structural and thermal modeling to ensure compatibility with system requirements. Subsequently, we will develop hardware to implement and test the designs.

We will explore the use of ACFs for connecting control and power lines to the mirror segment. ACFs are film adhesives with uniformly dispersed conductive particles, several micrometers in diameter, in a low-temperature thermo-setting resin [6-9]. They are used routinely in connecting to LCD and organic LED (OLED) displays and connecting bare chips directly onto glass, because they are extremely thin and allow a high connection density without difficult alignments. They are standard products manufactured by companies such as Hitachi and 3M, among others. We will investigate the deformations introduced into the mirrors by ACFs by measuring the figure of mounted mirrors before and after bonding ACF connections onto the mirror. We will also investigate thermal effects on ACF-induced stresses under temperature changes resulting from the differing coefficients of thermal expansion (CTEs) of the ACF and the mirror segment, and explore the best location structurally to make the connections without degrading mirror effective area, while mitigating attachment-related stresses. Lastly, the ACF connections will be in place before vibro-acoustic and thermal-cycling tests, and we will test for functionality after these environmental tests. This effort comprises about 10% of our budgeted work and will be performed at PSU. Performance testing will be carried out at SAO, and environmental testing at MSFC.

## Objectives and Milestones

SAO began the project in April 2015 and has made good progress against the baseline plan. Figure 1 shows the annotated baseline schedule from our proposal. Thermal modeling and structural analysis have proved to be far more work than originally envisioned. Assembly, test, and alignment activities have also gone more slowly, as we have learned much and modified our approaches accordingly.

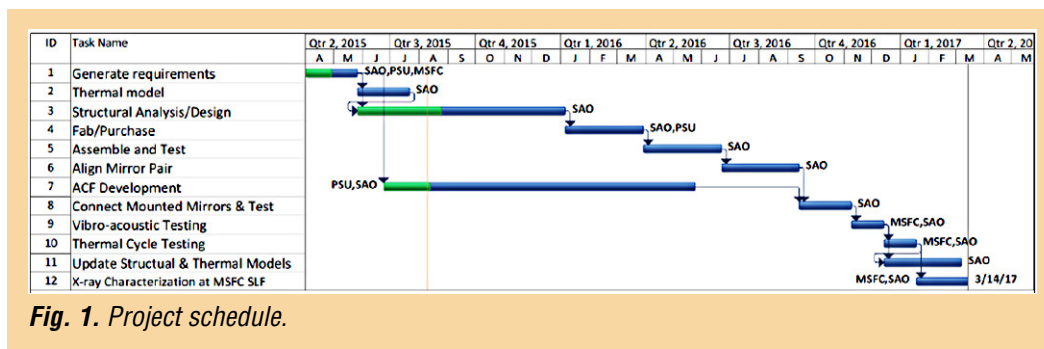


Fig. 1. Project schedule.

## Progress and Accomplishments

Major work has been progressing in the areas of system requirements and finite element modeling. In this earliest phase, we focus on the performance impact of different mounting schemes. A structural model was developed for a mounted pair of mirror segments, and thermal gradients and ambient temperature changes were applied to the mounted mirror segments (Tasks 1, 2, and 3 in Fig. 1). We will compute the sensitivities of imaging performance to on-orbit thermal conditions via ray-tracing of the modeled deformations. Two different mounting configurations are modeled: (1) mirror attachment points on the forward and aft ends, and (2) mirror attachment points on the side edges of the mirror segments. Initially, this study is for a conic mirror shell with a 1-m radius-of-curvature and 400-mm circumferential dimension at its leading edge, with an axial dimension of 200 mm and primary mirror cone angle of 0.025 radians (1.43°). The mirrors are modeled as a (multilayer) stack of materials to reflect the actual, current state of design:

- 0.05- $\mu\text{m}$  Ir X-ray reflective surface layer, sputtered material;
- 0.05- $\mu\text{m}$  Cr coating binder and stress compensation layer, sputtered material;
- 400- $\mu\text{m}$  Corning Eagle glass substrate;



- 0.05- $\mu\text{m}$  Ti sputtered protective layer;
- 0.10- $\mu\text{m}$  Pt sputtered ground electrode;
- 1.5- $\mu\text{m}$  PZT sputtered piezoelectric material; and
- 0.10- $\mu\text{m}$  Pt sputtered top electrode.

We have also modeled the above mirror “stack” with twice the thickness of the Ir and Cr layers. This was done to improve compensation for the thermal stresses introduced on both sides of the mirror due to the different effective CTEs from the coating stacks on the front and back side of the mirror.

The housing is designed to provide a CTE-matched structure in which to mount the mirror. Housing-wall thicknesses are modeled as 6 mm. Properties for the housing used in analysis are based on a near-zero CTE quasi-isotropic M55J/954-3 carbon-fiber/cyanate core with 23.6 ppM/ $^{\circ}\text{C}$  CTE aluminum face-sheets. For 6-mm total thickness, a 4.92-mm composite core with 0.54-mm-thick aluminum face-sheets provides an effective CTE of 3.17 ppM/ $^{\circ}\text{C}$ , which matches the Corning Eagle glass substrate and is within 50 ppB/ $^{\circ}\text{C}$  of the mirrors. For this analysis, the housing is modeled with isotropic properties rather than as a composite laminate structure.

Different mirror-mounting solutions were designed and analyzed for mirror deformations under a  $+1^{\circ}\text{C}$  change in nominal temperature (soak) and  $1^{\circ}\text{C}$  axial, azimuthal, and diametric gradients over the mirror (temperature changes are relative to the conditions at mirror bonding during assembly). The design intent is to support the mirror against rigid body translations and rotations while also providing additional radial constraints to restrain the mirrors against deformations caused by temperature soaks. An example of the mounting and model for a primary mirror is shown in Fig. 2.

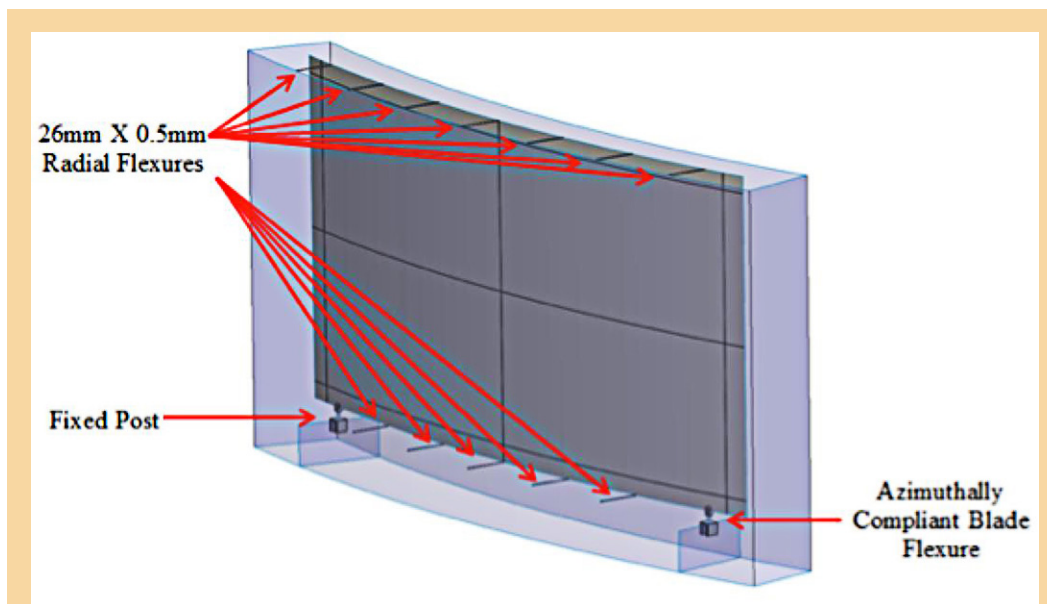
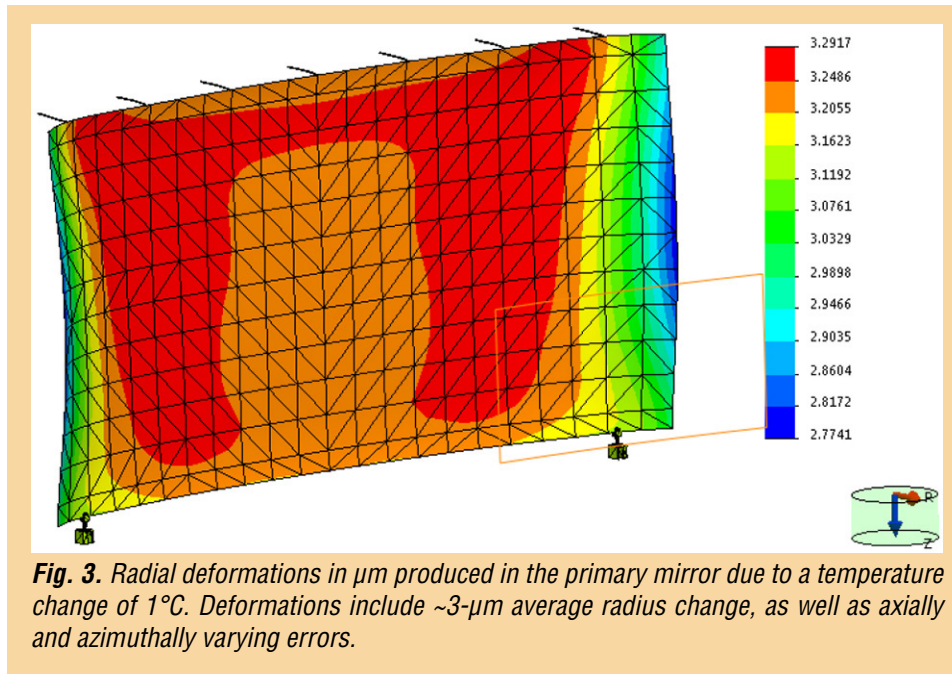


**Fig. 2.** Primary mirror modeled mounting structure. Two fixed supports are used as in SAO's APRA development: 6 degree-of-freedom (dof) fixed support and a tangential flexure (azimuthally compliant blade flexure). Twelve additional radial wire flexures are used (seven at forward end and five at aft end) to provide radial positioning of the mirror edges.

Figure 3 shows the radial figure error due to a  $1^{\circ}\text{C}$  change in ambient temperature for the same mirror. Uniform displacement of the mirror (effectively a change in mirror radius) is included in the figure. Displacement amplitudes range from  $\sim 2.77\text{ }\mu\text{m}$  to  $\sim 3.29\text{ }\mu\text{m}$ . Besides the  $\sim 3\text{-}\mu\text{m}$  change in average radius error, the temperature change introduces  $\sim 0.06\text{-}\mu\text{m}$  root-mean-square (rms) error.



We modeled four different thermal cases for the two different mirror designs:

1. An ambient (or cavity) temperature change of  $1^{\circ}\text{C}$ .
2. An axial gradient of  $5^{\circ}\text{C}/\text{m}$ .
3. A “lateral” gradient of  $2.5^{\circ}\text{C}/\text{m}$ .
4. A radial gradient of  $13^{\circ}\text{C}/\text{m}$ .

The relatively large amplitude gradients are needed because we were modeling a single mirror as a start and the radial cross-section is so small that a large gradient is required to model the result reliably, allowing us to see the sensitivities.

Finite element modeling was repeated for the same thermal conditions for the secondary mirror. Distortion maps of the modeling cases are used as inputs for ray-tracing the various thermal cases. The ray-tracing is also done as a sensitivity test; i.e., we ray-traced exactly the distortions produced from the thermal modeling, without scaling to a more realistic thermal environment. We analyzed the ray-trace results at both at nominal and best focus. Spot diagrams at focus were produced for each case, and rms image diameter and image HPD were calculated. An example of a spot diagram from a single segment pair with a  $+1^{\circ}\text{C}$  cavity temperature change is shown in Fig. 4. Table 1 summarizes the sensitivity to image rms HPD diameter as a function of focal plane position.

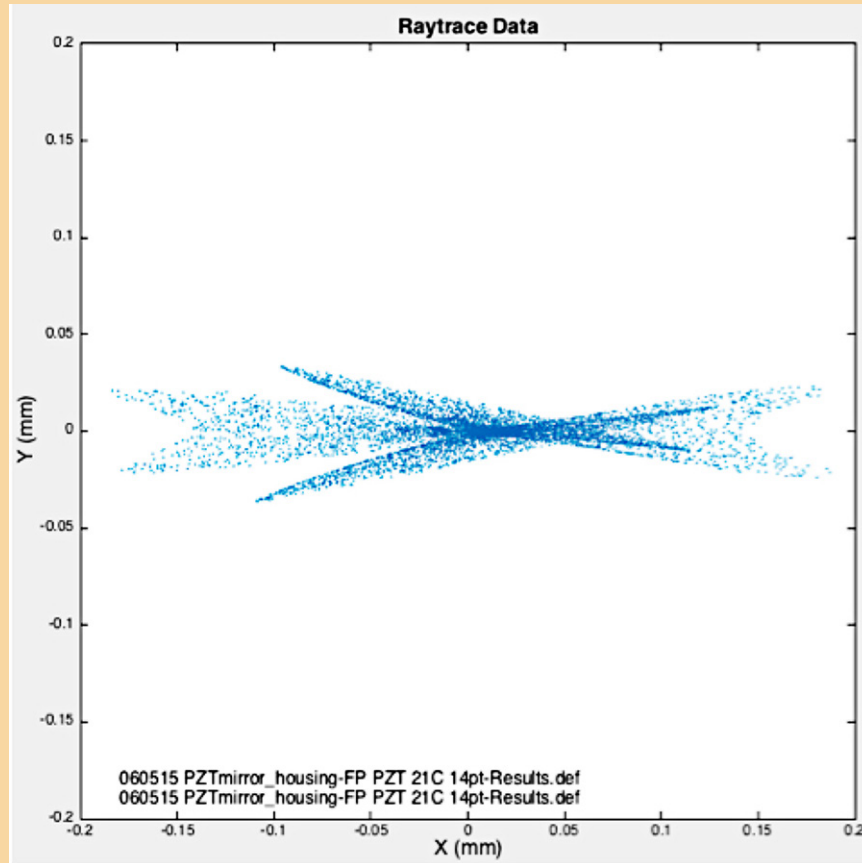


**Fig. 4.** Spot diagram at best focus after ray-tracing a single XRS mirror-segment pair with a  $+1^{\circ}\text{C}$  temperature difference relative to the temperature at mirror alignment and bonding. X and Y coordinates at the best focus plane are in mm, with the optical axis located at the origin. For reference, the plate scale is 0.050 mm per arcsec.

Thermal Case	Best Focus		Nominal Focus	
	rms Diameter (arcsec)	Focus Shift (mm, positive shift = aft of nominal)	rms Diameter (arcsec)	HPD (arcsec)
Radial Gradient $13^{\circ}\text{C}/\text{m}$	3.45	+0.894	3.53	2.18
Azim. Gradient $2.5^{\circ}\text{C}/\text{m}$	0.492	-0.0005	0.50	0.077
Axial Gradient $5^{\circ}\text{C}/\text{m}$	0.721	+0.0846	0.75	0.18
Cavity $+1^{\circ}\text{C}$	1.73	+0.214	1.77	0.34

**Table 1.** Ray-traced sensitivities to thermal environment.

Doubling the X-ray-reflective coating thickness to better balance the effects of cavity temperature change greatly reduces the sensitivity to cavity temperature and azimuthal gradients, but makes little difference in the sensitivity to radial and axial temperature gradients. This is seen by comparing the sensitivities shown in Table 2 with those in Table 1.



Thermal Case	Best Focus		Nominal Focus	
	rms Diameter (arcsec)	Focus Shift (mm, positive shift = aft of nominal)	rms Diameter (arcsec)	HPD (arcsec)
Radial Gradient 13°C/m	3.42	+0.889	3.49	2.22
Azim. Gradient 2.5°C/m	0.090	-0.0014	0.092	0.015
Axial Gradient 5°C/m	0.82	+0.0986	0.86	0.18
Cavity +1°C	0.22	-0.0249	0.34	0.19

**Table 2.** Ray-traced sensitivities to thermal environment using twice the Ir and Cr thicknesses for the X-ray reflective layer.

Finally, we fold these sensitivities in with an XRS mirror-assembly temperature-control system with requirements and performance similar to the Chandra HRMA measured thermal control system performance over its (currently more than) 15-year operation. We use the Chandra system performance as a basis for the XRS because our approach is to make the XRS as similar as possible to Chandra, to minimize cost. The resulting performance impacts for the two mirror design cases, at nominal focus only, are tabulated in Table 3.

Thermal Case	Nominal Ir/Cr Coating Thickness	2× Ir/Cr Coating Thickness
	rms Diameter (arcsec)	rms Diameter (arcsec)
Sun/Earth Gradient $\pm 0.2^\circ\text{C}$	0.054	0.054
Lateral Gradient $\pm 0.2^\circ\text{C}$	0.054	0.054
Axial Gradient $\pm 0.1^\circ\text{C}$	0.017	0.017
Cavity $\pm 0.1^\circ\text{C}$	0.177	0.034

**Table 3.** Estimated imaging errors due to assumed Chandra-like thermal environment, for adjustable X-ray optics with either “nominal” Ir on Cr X-ray-reflective layer thickness (50 nm each layer) or double the Ir and Cr thicknesses. Note the radial and azimuthal gradients are converted to Sun-Earth direction and lateral gradients. We set the contributions of the two gradients as equal to the larger of radial and azimuthal because for some segments a radial gradient will be in the Sun-Earth direction, while for others an azimuthal gradient will be in the Sun-Earth direction (and vice versa). Short of designing and modeling a full mirror assembly (out of scope of this SAT), this is a conservative way to estimate thermal control impacts on imaging performance.

The estimated image error total rms amplitude is 0.194 arcsec for the nominal Ir/Cr thickness and 0.085 arcsec for the doubled thickness case. The latter meets the preliminary allocation of 0.1 arcsec rms diameter for on-orbit thermal effects. Alternatively, with the nominal coating thicknesses, we would need to tighten the cavity temperature tolerances or adjust error-budget allocations. We still plan to examine the sensitivity of thermal deformations for different mounting constraints (i.e., lateral sides versus forward and aft ends, as currently envisioned). Results to date do not include a full mirror assembly design and are therefore preliminary. However, modeling the nominal Ir/Cr thickness and 0.085 arcsec rms for double thickness coating, we see that the two approaches are at least consistent with the allocation to within a factor of two for a Chandra-like thermal control system performance.

Good progress is also being achieved in Task 7, ACF development (Fig. 1). As mentioned above, ACF is a technology allowing high-linear-density, minimal-labor electrical connections from control electronics to the mirror element. We have successfully used ACFs to connect to a test flat mirror with piezoelectric cells controlled via ZnO thin-film transistors (TFT) using row-column addressing. ACF tape is used, wherein no alignment is required between the ACF and the mating electrodes. Because the ACF only conducts down its length and not in the cross direction, the electrical connections are never shorted together. This obviates having to make many individual connections to each mirror. Figure 5 shows a photograph of the ZnO TFT test mirror, installed in its metrology mount and with the ACF connections.

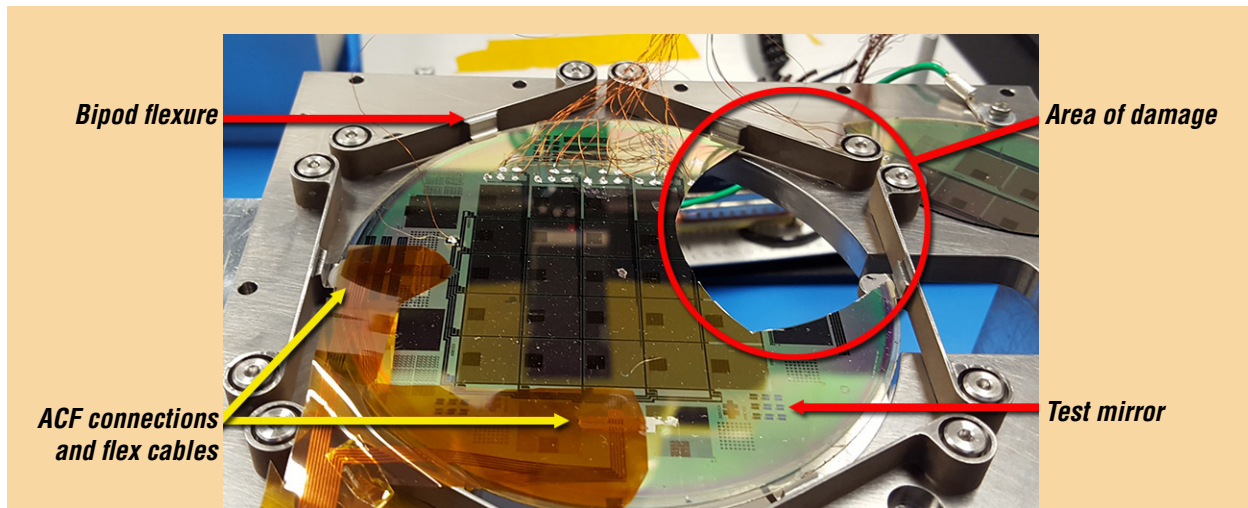


**Fig. 5.** ZnO TFT flat test adjustable mirror, mounted in its six-bipod-flexure metrology mount. ACF connections to the TFTs are made at the ends of the yellow flex cables on the mirror. A handling-procedure error damaged the mirror (note the missing piece of mirror between approximately 1 and 3 o'clock), but this did not impact testing of the undamaged piezoelectric cells on the mirror. Row-column addressing and energizing the piezoelectric cells was achieved through the ACF connections to the mirror.

A handling error damaged the mirror, with a piece breaking off between about 1 o'clock and 3 o'clock. Fortunately, this did not affect testing of the mirror, as the undamaged piezo cells still functioned. Separate power wires were also attached to the mirror cells by bonding to pads and traces directly connected to the individual cell top electrodes (our standard practice). This allowed us to directly power the piezo cells individually and measure influence functions; and then to control the piezo cells through the ACF connections and TFTs with row-column addressing, measure the influence functions, and compare with the previous measurements. While not every TFT functioned perfectly, we were able to control most cells through the ACF and TFTs for the first time, achieving initial success. In addition, wavefront sensor measurements did not reveal any large local deformations in the vicinity of the ACF attachments. This indicates connecting the ACF to a flat mirror, at least, does not produce unacceptably large distortions that might argue against their use.

In the past year, advances were also made in the areas of individual cylindrical mirror mounting and figure control. As part of the High-Fidelity Deterministic Figure Control (HFDFC) experiment, we engaged in mounting a single adjustable mirror to the mirror housing, monitoring its figure as a function of the various mounting steps, wiring the mirror, and then verifying functionality by attempting to control mirror figure errors. Results were mixed due to a variety of problems encountered. The initial test, HFDFC1, revealed several problems. First, after the fact it was found that the lithographic mask used to print the top electrodes and electrical traces was scratched, resulting in a large number of piezo cells (~25%) having open circuits in their 100- $\mu\text{m}$ -wide electrical traces from the top electrode of the cell to the edge of the mirror. Second, we discovered that our wire-bonding approach (for control wires to the electrical contacts on the mirror edges) was both difficult to do operationally, resulting in several non-adjacent piezo cells being electrically shorted together; and introduced stray loads, distorting the mirror. The combination of these errors made it impossible for us to correct mirror figure or to determine the frequency-dependent mirror correction function (the efficiency with which errors of different spatial frequency can be corrected). However, despite this, we did demonstrate our concept works in that we were able to experimentally match predicted introduced figure changes to within the limit of metrology noise, ~0.45 arcsec rms.



The mounted test optic is shown in Fig. 6. The piezoelectric cell electrodes are visible, as are the piezo power wires bonded to the contact pads with conductive epoxy.

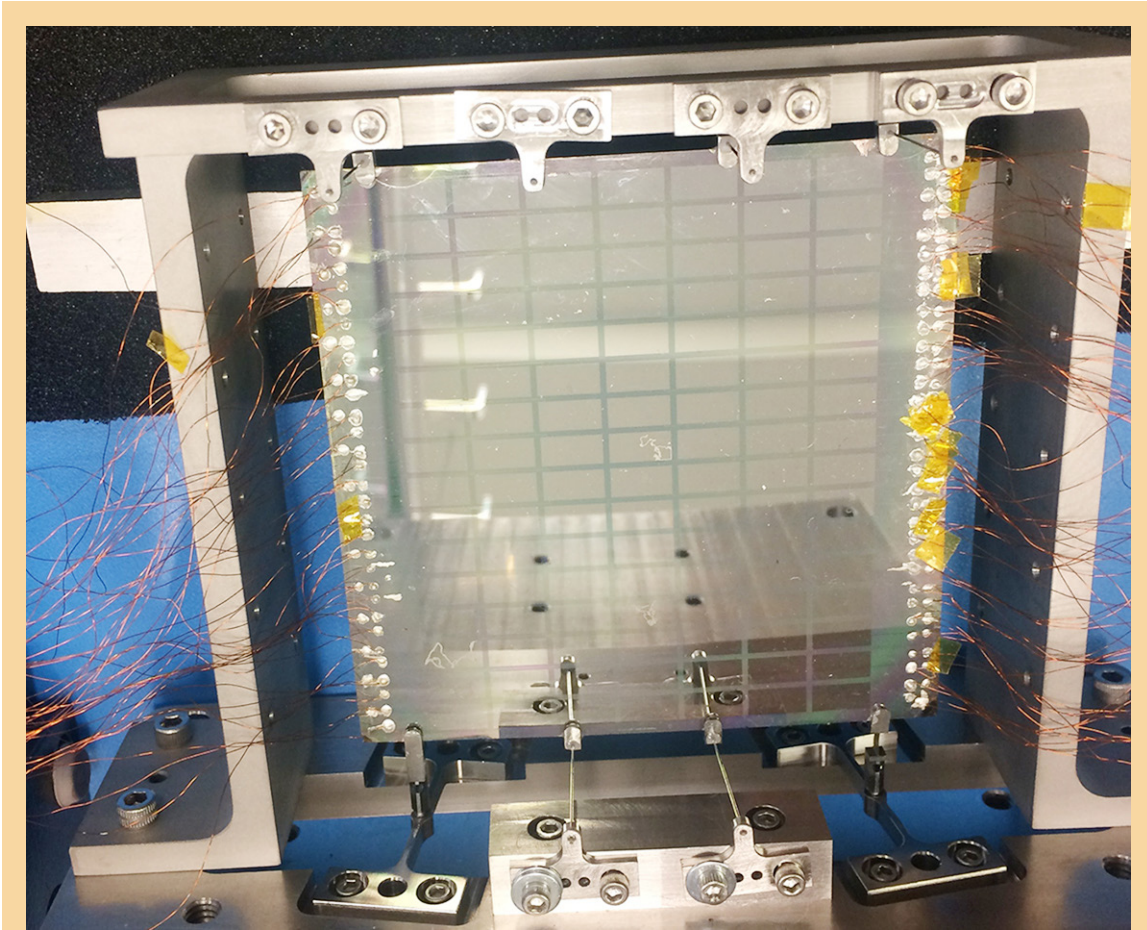


**Fig. 6.** Photograph of back (convex) side of HFDFC1, with the mirror bonded into its housing; 5-mm-axial  $\times$  10-mm-azimuthal piezo cell top electrodes are clearly visible. The mirror is bonded with four wire flexures at the top, two wire flexures at the bottom, as well as a 6-dof post and a 3-dof blade flexure at the bottom. The fine wires epoxied to the electrical contact pads can be seen on either side of the mirror.

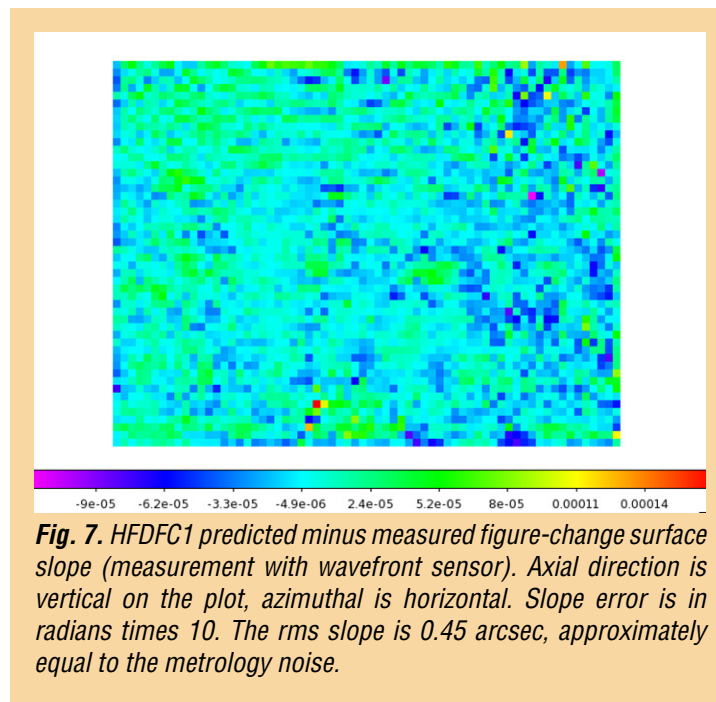
Three lessons learned from this experiment were:

- Attaching wires to the mirror after mounting would be easier than before mounting;
- A better system of wire attachment is needed, as is a different epoxy; and
- Finer-gauge wire should be used, and the wires should be pre-straightened.

All these procedural modifications were incorporated for HFDFC2.

The HFDFC1 results are shown in Fig. 7, where the difference between the predicted residual slope error and the measured residual slope error are plotted. The rms slope difference was 0.45 arcsec, equal to the metrology noise for the experiment.





A second attempt at the HFDFC experiment was undertaken, incorporating the changes described above, but unfortunately we determined during the wiring process that the mirror was cracked. Investigation of the root cause of the failure is ongoing. At present, we believe the crack initiated at a poorly cut edge of the mirror done using a non-representative, but expedient, process. Close review of metrology data taken during the mounting process revealed a pattern of data “drop-outs” that traced the path, and growth, of the crack. Micrographs of the mirror edges revealed sometimes extensive cracking at the edges. To eliminate this problem as a future concern, we initiated a series of glass strength tests to investigate strength as a function of edge condition (i.e., rough-cut edge vs. smooth-cut edge), and the sensitivity of the relative edge strengths to the glass being pre-slumped or post-slumped. We expect this experiment to take much of the summer, at which point we hope to carry out HFDFC3, with smooth edges.

## Path Forward

Several activities are planned, with many already in progress. ACF development on curved (conical) mirrors has begun, focusing on the 220-mm radius of curvature that will be used for X-ray testing planned in early CY 2017. The root-cause investigation into the cracking of HFDFC2 implicated an edge defect. Experiments will begin shortly, after test-fixture fabrication, to investigate the sensitivity of mirror break-strength to edge condition and level of glass annealing (i.e., pre- or post-slumping). A modified mounting procedure will also be employed to reduce the procedural difficulties between mounting and wiring the mirrors. Although ACF is planned for the X-ray test, using conductive-epoxy-bonded wires is the back-up plan should ACF development prove too difficult in the near term. Work continues with MSFC to prepare the necessary hardware for mounting an aligned, bonded, corrected primary/secondary mirror pair in the MSFC Stray Light Facility (SLF) for X-ray testing in CY 2017. This work includes reworking the 6-dof stage in the SLF and refurbishing the Con-X X-ray test thermal control system, as well as establishing X-ray test procedures. This also includes fabrication of an adjustable X-ray mirror assembly “dummy” unit for dry running installation and alignment at MSFC, planned for October/November 2016. Finally, Coherent Optics (formerly Tinsley) of Richmond CA is completing fabrication of an X-ray-test set of primary and secondary mandrels with improved mandrel figure error, suitable for thermal-forming mirrors for X-ray testing.

SAO continues to show strong institutional support for the adjustable X-ray-optics program, providing funds for internal research and development activities in addition to the three-year Leon Van Speybroeck (LVS) Fellowship in X-ray Optics. In the past year, we hired into our science staff our first LVS Fellow, Ryan Allured, who is working about 85% of full time on adjustable X-ray optics programs. In addition, we selected a new LVS Fellow, Casey DeRoo, starting Aug 1, 2016. We also hired a new High Energy Astrophysics Division Program Manager for adjustable X-ray optics programs and XRS. This fills a critical gap that opened when our previous program manager moved laterally within SAO to ground-based-telescope programs. This institutional support has helped us advance technically and reduce overall project risk.

## References

- [1] A. Vikhlinin et al., “*SMART-X: Square Meter Arcsecond Resolution X-ray Telescope*,” SPIE Proc. **8443**, 844316 (2012)
- [2] “*Enduring Quests, Daring Visions*,” 2013 NASA Astrophysics Roadmap (Dec. 2013)
- [3] T. Aldcroft et al., “*Simulating correction of adjustable optics for an X-ray telescope*,” SPIE Proc. **8503**, 85030F (2012)
- [4] W.W. Zhang et al., “*Lightweight and high angular resolution X-ray optics for astronomical missions*,” SPIE Proc. **8147**, 81470K (2011)
- [5] C. Feldman et al., “*The performance of thin shell adaptive optics for high angular resolution X-ray telescopes*,” SPIE Proc. **7803**, 78030N (2010)
- [6] J. Liu, “*Conductive Adhesives for Electronics Packaging*,” Electrochemical, Port Erin, p. 12 (1999)
- [7] S. Ganesan and M. Pecht, “*Lead-free Electronics*,” Wiley, New Jersey, p. 437 (2006)
- [8] W.S. Kwon and K.W. Paik, “*Experimental Analysis of Mechanical and Electrical Characteristics of Metal-Coated Conductive Spheres for Anisotropic Conductive Adhesives (ACAs) Interconnection*,” IEEE Trans. Compon. Packag. Technol. **29**, 3, 528 (2006)
- [9] K.W. Jang et al., “*Material properties of anisotropic conductive films (ACFs) and their flip chip assembly reliability in NAND flash memory applications*,” Microelectron. Reliab. **48**, 1052 (2008)

For additional information, contact Paul Reid: [preid@cfa.harvard.edu](mailto:preid@cfa.harvard.edu)



# Advanced Packaging for Critical-Angle X-ray Transmission Gratings

Prepared by: Mark L. Schattenburg (PI; MIT), Ralf K. Heilmann (MIT), and Alex R. Bruccoleri (Izentis, LLC)

## Summary

Critical-Angle Transmission (CAT) gratings combine the advantages of traditional phase-shifting transmission gratings – e.g., relaxed alignment and figure tolerances, low mass, and transparency at high energies; with the advantages of blazed reflection gratings – e.g., high diffraction efficiency and high resolving power due to utilization of higher diffraction orders. In combination with grazing-incidence X-ray mirrors and CCD detectors, they promise a five- to 10-fold increase in efficiency and a three- to five-fold improvement in resolving power over existing X-ray grating spectrographs [1]. Development of CAT-grating fabrication technology has been supported by NASA under the Strategic Astrophysics Technology (SAT) program since January 2012.

During the past year, NASA support has enabled us to achieve three major breakthroughs: the fabrication of several CAT gratings with record absolute diffraction efficiency  $> 30\%$ ; the extension of the CAT-grating bandpass through metal-coating of the silicon grating bars; and the experimental demonstration of a CAT grating spectrometer with a spectral resolving power  $R = \lambda/\Delta\lambda > 10,000$ , exceeding requirements for all currently posed mission concepts, and quite possibly a world record for grating-based spectroscopy in the soft X-ray band. CAT-grating technology has now been vetted at Technology Readiness Level (TRL) 4.

## Background

Absorption- and emission-line spectroscopy, with the performance made possible by a well-designed CAT X-ray grating spectrometer (CATXGS), will target science objectives concerning the large-scale structure of the universe, cosmic feedback, interstellar and intergalactic media, and stellar accretion. A CATXGS-carrying mission can address the kinematics of galactic outflows, hot gas in galactic halos, black-hole growth, the missing baryons in galaxies and the Warm-Hot Intergalactic Medium, and the effect of X-ray radiation on protoplanetary disks. All of these are high-priority International X-ray Observatory (IXO) science questions described in the 2010 Decadal Survey, “New Worlds, New Horizons in Astronomy and Astrophysics” (NWNH) [2], and are addressed further in the NASA “X-ray Mission Concepts Study Report” [3]. A number of mission concepts submitted in response to NASA Request for Information (RFI) NNH11ZDA018L could be enabled by a CATXGS; these include Advanced X-ray Spectroscopic Imaging Observatory (AXSIO), Astrophysics Experiment for Grating and Imaging Spectroscopy (AEGIS), and Square Meter Arcsecond Resolution Telescope for X rays (SMART-X), as well as the Notional X-ray Grating Spectrometer (N-XGS) studied by the X-ray Community Science Team (CST) [4-6] or future Explorers. Also, an X-ray Surveyor – a mission described in the 2013 “Enduring Quests, Daring Visions” Astrophysics Roadmap [7] – is on a short list of possible mission concepts being studied in preparation for the 2020 Decadal Survey [8]. A core instrument for an X-ray surveyor would be a grating spectrometer, for example one similar to the CATXGS design for SMART-X.

The soft-X-ray band contains many important diagnostic lines (C, N, O, Ne, and Fe ions). Imaging spectroscopy with spectral resolution better than 2 eV has been demonstrated with small transition-edge-sensor-based microcalorimeter arrays, providing resolving power over 3000 above 6 keV. However, toward longer wavelengths, energy-dispersive detectors cannot provide the spectral resolution required to address several of the NWNH high-priority science objectives. The only known technology providing high spectral-resolving power in this band is wavelength-dispersive, diffraction-grating-based spectroscopy.



The technology currently used for grating-based soft-X-ray spectroscopy was developed in the 1980s. The Chandra High-Energy Transmission-Grating Spectrometer (HETGS) carries polyimide-supported gold gratings with no more than 10% diffraction efficiency in the 1-5 nm band, but the whole moveable grating array only weighs about 10 kg. The X-ray Multi-mirror Mission – Newton (XMM-Newton) Reflection Grating Spectrometer (RGS) has more efficient grazing-incidence reflection gratings, but its mass is high (>100 kg) and it has low spectral-resolving power (~300). CAT gratings combine the advantages of the HETGS and RGS gratings, and promise higher diffraction efficiency over a broad band, with a resolving power greater than 3000 for a 10-arcsec Point Spread Function (PSF) telescope. These gratings also offer near-ideal synergy with a calorimeter-based imager, since CAT gratings become increasingly transparent at higher energies. Thus, high-resolution spectroscopy could be performed with a CATXGS in tandem with a calorimeter over the range of ~0.2 to tens of keV on a larger mission such as an X-ray Surveyor. Figures-of-merit for many types of observations, such as the accuracy of line-centroid measurement in absorption-line spectroscopy, could be improved by more than an order of magnitude over Chandra and XMM-Newton. The new patented CAT-grating design relies on the reflection (blazing) of X rays from the sidewalls of free-standing, ultra-high-aspect-ratio, sub-micron-period grating bars at grazing angles below the critical angle for total external reflection. Fabrication combines advanced novel methods and tools from the semiconductor and Micro-Electro-Mechanical Systems (MEMS) industries with patterning and fabrication methods developed at MIT over several decades.

We plan to bring CAT-grating technology to TRL 5 by the end of 2018 to reduce technology risk and cost for future CATXGS-bearing missions before they enter Phase A. We therefore want to demonstrate efficient, large-area (over 30 mm × 30 mm) CAT-grating facets with minimal blockage from support structures. Facets will be mounted to thin and stiff frames, which can then be assembled into grating arrays sized on the order of 1 m<sup>2</sup>.

## Objectives and Milestones

The objective of this project is to demonstrate an aligned array of large-area, high-efficiency CAT gratings with minimal support-structure blockage, providing resolution higher than 3000 in the soft-X-ray band, and maintaining its performance after appropriate vibration, shock, and thermal testing. The array will consist of so-called grating facets mounted to a Grating-Array Structure (GAS). Facets are comprised of a grating membrane, etched from a silicon-on-insulator (SOI) wafer, and a facet frame that holds the membrane.

### *Key project milestones:*

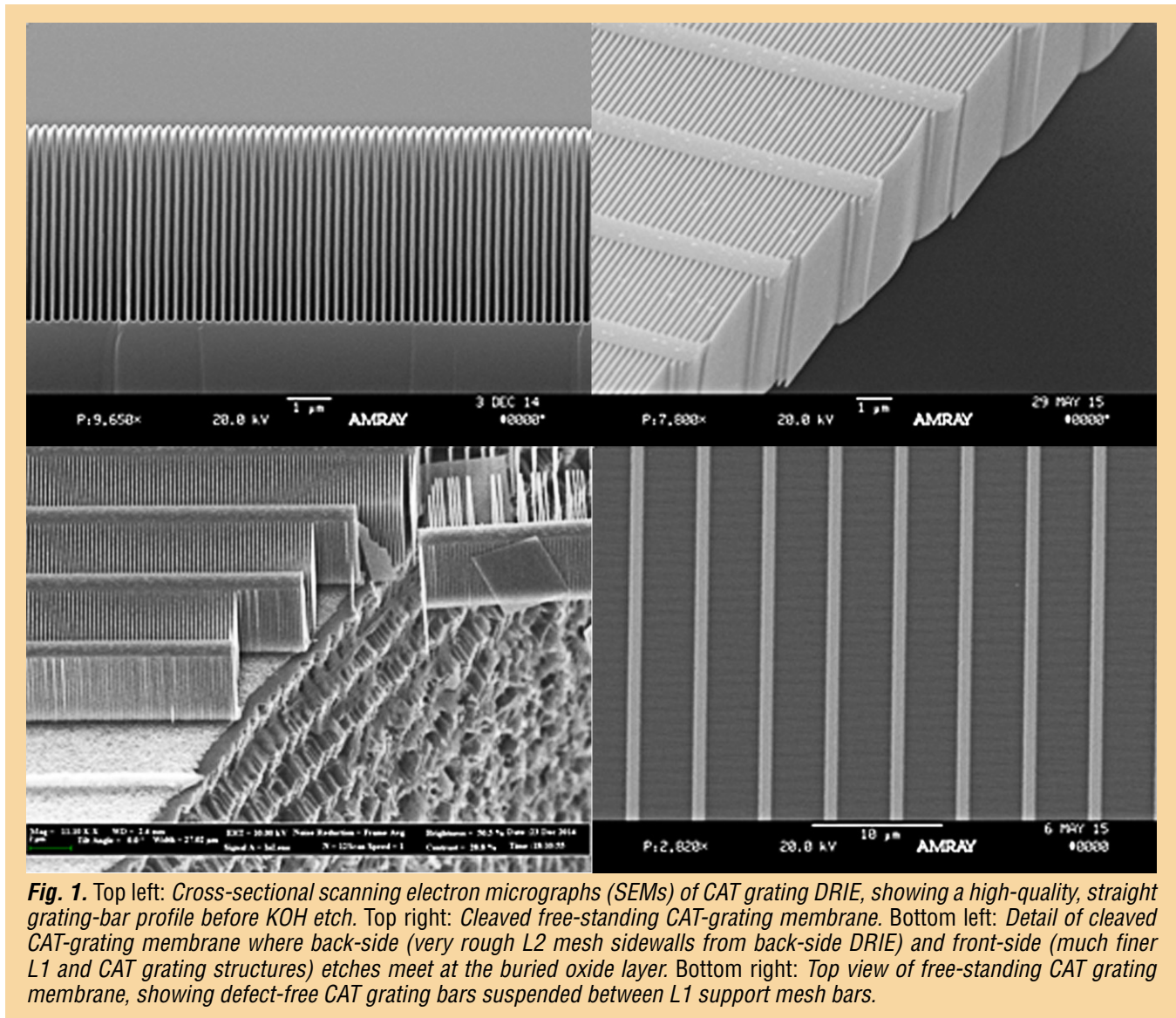
1. Develop silicon lattice-independent anisotropic etch capable of achieving the required aspect ratios for 200-nm-period gratings (Deep Reactive Ion Etch, DRIE, at a University of Michigan tool, completed in 2011).
2. Develop process for free-standing, large-area gratings with hierarchy of low-blockage supports (completed in 2012).
3. Combine (completed in 2013) and optimize (ongoing) dry- and wet-etch processes to obtain smooth grating-bar sidewalls and narrow Level 1 (L1) supports; produce free-standing, large-area gratings with hierarchy of low-blockage supports (demonstrated, improving yield); and test X-ray efficiency (ongoing).
4. Select, acquire, install, and test advanced DRIE tool at MIT (completed in 2014).
5. Demonstrate CAT-grating resolving power in an X-ray imaging system (completed in 2016). Repeat with more than one grating or small array (Calendar Year, CY, 2017/18, in preparation).
6. Develop grating facet/frame design, process for integration of CAT grating membrane and frame, and alignment of facets on a breadboard GAS (Fiscal Year, FY, 2017/18).
7. Environmental and X-ray tests of aligned array of grating facets mounted to GAS (CY 2017/18).

## Progress and Accomplishments

The key challenges in the fabrication of CAT gratings lie in their structure – small grating period (200 nm), small grating duty cycle (~40-nm-wide grating bars with 160-nm spaces between), and large depth (4-6 μm) result in ultra-high aspect ratios (100-150), with nm-smooth sidewalls. In addition, the gratings should not be supported by a membrane, but rather be freestanding. Structures with such an extreme combination of geometrical parameters, or anything similar, have never been made before.

Prior to SAT support, we fabricated small KOH-wet-etched CAT-grating prototypes that met all these requirements, and measured their efficiency at a synchrotron source, demonstrating good agreement with theoretical predictions [9, 10]. Due to their extreme dimensions and the requirement to be freestanding, CAT gratings must be supported by slightly “bulkier” structures. We use a so-called L1 cross-support mesh (period  $\sim 5\text{--}20\ \mu\text{m}$ ), integrated into the SOI device layer, and etched at the same time as the CAT gratings. Unfortunately, the wet-etch that provides the nm-smooth CAT grating sidewalls leads to widening L1 supports with trapezoidal cross sections and unacceptable X-ray blockage.

DRIE is an alternate process that can provide the required etch anisotropy for CAT grating bars and L1 supports simultaneously. To make large-area, freestanding gratings, we also use this process to fabricate a high-throughput hexagonal Level 2 (L2) mesh, etched out of the much thicker ( $\sim 0.5\ \text{mm}$ ) SOI handle layer (Fig. 1). We developed a process that allows us to DRIE the CAT grating bars and the L1 supports out of the thin SOI device layer (front side), stopping on the buried-oxide (BOX) layer; and to subsequently etch the L2 mesh with a high-power DRIE into the back side, again stopping on the BOX layer. The BOX layer is removed with a hydrofluoric acid etch, and the whole structure is critical-point-dried in liquid  $\text{CO}_2$ . We fabricated several  $31\ \text{mm} \times 31\ \text{mm}$  samples with acceptable yield [11].





Unfortunately, DRIE leaves the sidewalls of etched structures with several nm of roughness, detrimental to CAT grating efficiency. In 2012 – 2013, we developed a combined DRIE/KOH approach on bulk silicon that follows DRIE with a relatively short KOH “polishing” step that reduces sidewall roughness, and straightens and thins the grating bar profile [12]. In 2014, we transferred and modified our new process to be compatible with the more delicate double-sided processing on SOI wafers for large-area, freestanding gratings (Fig. 1).

Over the last two years, our process development has accelerated significantly, thanks to a newly acquired dedicated DRIE tool in our lab at MIT, funded through a previous SAT grant. We greatly improved DRIE grating-bar profile control, and we now routinely achieve constant-thickness or slightly retrograde bar profiles (Fig. 1). These improved grating bars survive vastly longer wet-etch (sidewall polishing) times in concentrated KOH, up to 40 minutes, presumably leading to smoother sidewalls and thus higher reflectivity and diffraction efficiency. In the past year, we have produced several gratings with very similar record-high X-ray performance, a tribute to our improved and matured fabrication process [13 – 15].

The resolving power of an X-ray objective transmission-grating spectrometer is usually limited by the optical design, the focusing optics PSF, and the angle of diffraction, but not by the alignment-insensitive transmission gratings. To verify the last point, we recently performed a measurement of resolving power at the NASA MSFC Stray Light Facility (SLF), using the Al  $K\alpha_{1,2}$  lines from an electron bombardment source, and a segmented slumped-glass mirror pair from the Zhang X-ray optics group at the NASA GSFC as the focusing optic. In order to resolve the line shape of the Al  $K\alpha_{1,2}$  pair, we coated a 32-mm-wide CAT grating with a thin layer of platinum, using Atomic Layer Deposition (ALD). The metal coating increased the critical angle and allowed us to measure the Al  $K\alpha_{1,2}$  line shape in 18<sup>th</sup> order, where the lines are much broader than the optic PSF (Fig. 2). Preliminary data analysis shows that our CAT gratings are compatible with a resolving power significantly in excess of  $R = 10,000$  (Fig. 3). This demonstrates that CAT gratings will not degrade the resolving power of spectrometers designed for  $R$  on the order of 5000, such as a CATXGS for the X-ray Surveyor [16].

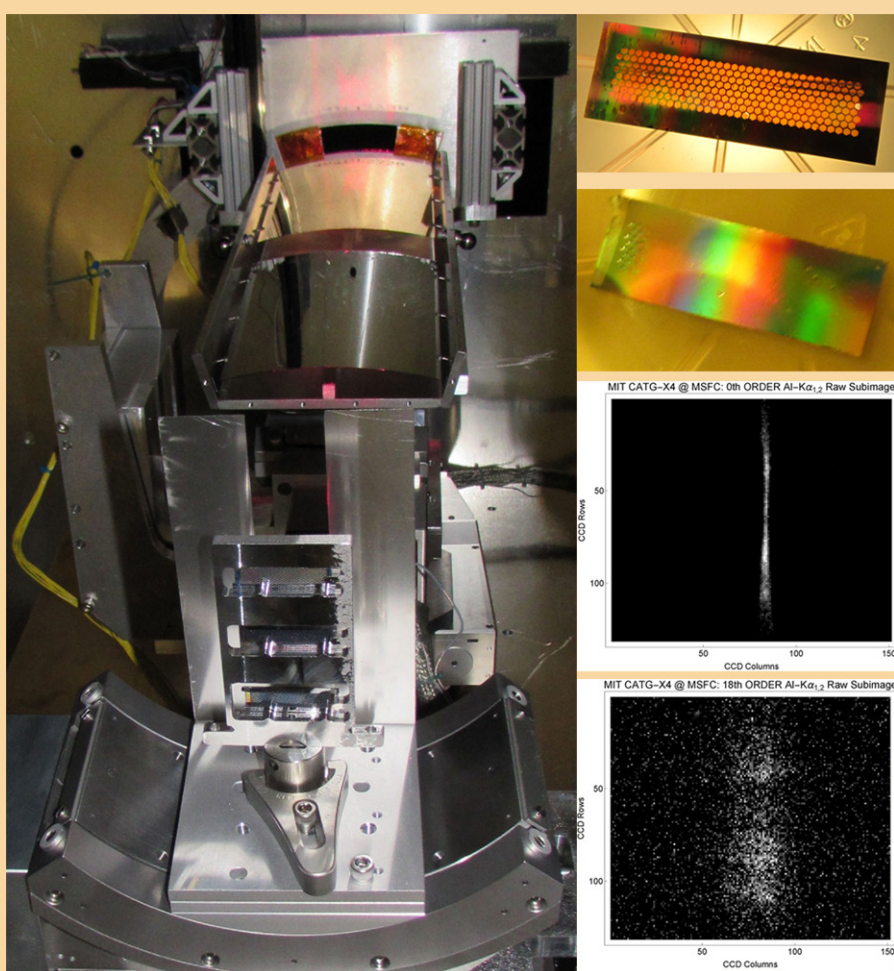


**Fig. 2.** Left: View of the grating mount (bottom) and the GSFC focusing slumped glass mirrors inside the MSFC SLF, looking upstream towards the source. Right, top to bottom: Silicon CAT grating with 32-mm-wide active area; silicon CAT grating of the same size, ALD-coated with a thin layer of platinum; image of the combined mirror and source PSF at the focus (the PSF is narrow in the dispersion direction due to the so-called sub-aperturing effect); image of the 18<sup>th</sup> diffracted order of the Al  $K\alpha_{1,2}$  line pair. Projecting this image onto the dispersion axis leads to Fig. 3.



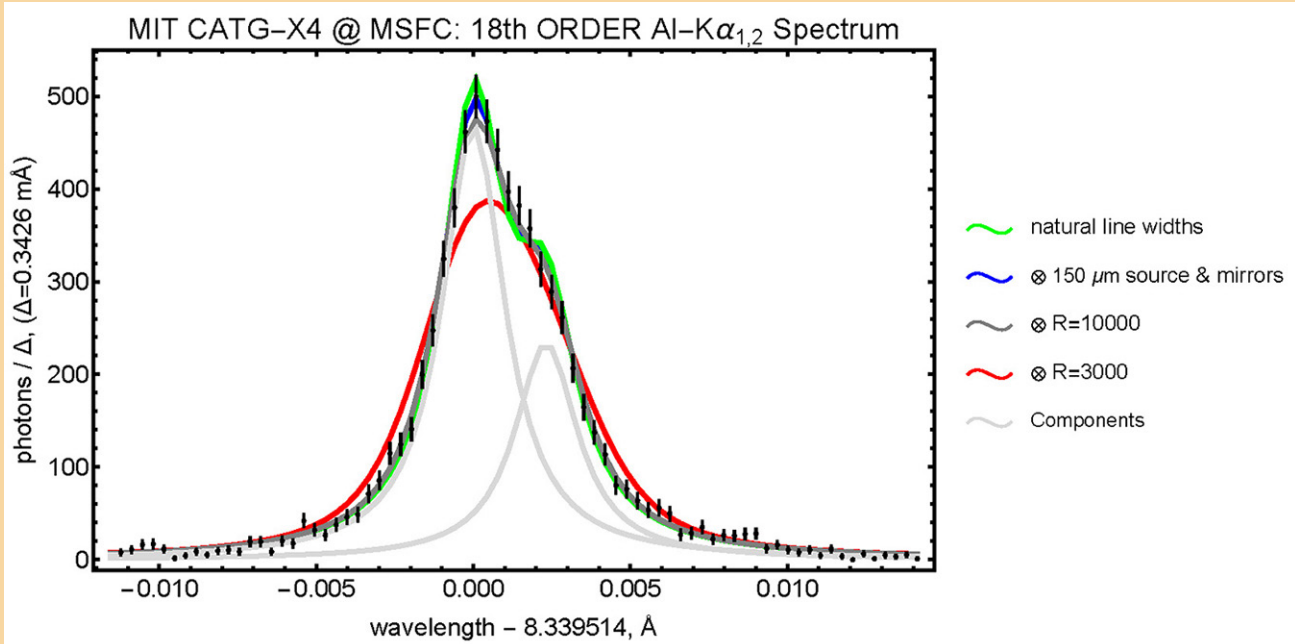


**Fig. 3.** Measured Al  $K\alpha_{1,2}$  spectrum in 18<sup>th</sup> order with 0.15-mm slit. Vertical lines are the error bars around the number of photons in a given bin. Light gray are the two  $K\alpha$  components with their natural Lorentzian widths and green is their sum. Blue is the convolution with the measured source/mirror 1-D line spread function, LSF. Dark gray is the blue curve convolved with broadening due to a Gaussian  $\Delta p/p$  distribution that would limit  $R$  to 10,000. It still falls short at the peak. The red curve also assumes a Gaussian  $\Delta p/p$  distribution, but corresponding to  $R = 3000$ .

Furthermore, the demonstrated ability to conformally ALD-coat the ultra-high-aspect-ratio CAT grating bars with high-electron-density materials opens up a new design space for CAT gratings, extending their band to shorter wavelengths and/or to larger blaze angles and thus higher spectrometer resolving power.

## Path Forward

We are working towards the next TRL, which involves integrating facets and frames, mounting and alignment of a grating array, and environmental and X-ray tests to verify performance, subject to funding:

1. Develop grating facet/frame design, integration process of CAT grating membrane and frame, and alignment of facets on a breadboard GAS (FY 2017/18).
2. Environmental and X-ray tests of aligned array of grating facets mounted to GAS (CY 2017/18).
3. Scale up grating fabrication, frame design, and membrane/frame integration to full size (mission-dependent).

## References

- [1] R.K. Heilmann, J.E. Davis, D. Dewey, M.W. Bautz, R. Foster, A. Bruccoleri, P. Mukherjee, D. Robinson, D.P. Huenemoerder, H.L. Marshall, M.L. Schattenburg, N.S. Schulz, L.J. Guo, A.F. Kaplan, and R.B. Schweickart, “Critical-Angle Transmission Grating Spectrometer for High-Resolution Soft X-Ray Spectroscopy on the International X-Ray Observatory,” Space Telescopes and Instrumentation 2010: Ultraviolet to Gamma Ray, M. Arnaud, S.S. Murray, T. Takahashi (eds.), Proc. SPIE **7732**, 77321J (2010)
- [2] Blandford et al., “New Worlds, New Horizons in Astronomy and Astrophysics,” National Academy of Sciences, (2010)
- [3] “X-ray Mission Concepts Study Report” (2012)

- [4] J.A. Bookbinder, R.K. Smith, S. Bandler, M. Garcia, A. Hornschemeier, R. Petre, and A. Ptak, “*The Advanced X-ray Spectroscopic Imaging Observatory (AXSIO)*,” Proc. SPIE **8443**, Space Telescopes and Instrumentation 2012: Ultraviolet to Gamma Ray, 844317 (2012)
- [5] M.W. Bautz, W.C. Cash, J.E. Davis, R.K. Heilmann, D.P. Huenemoerder, M.L. Schattenburg, R. McEntaffer, R. Smith, S.J. Wolk, W.W. Zhang, S.P. Jordan, and C.F. Lillie, “*Concepts for High-Performance Soft X-Ray Grating Spectroscopy in a Moderate-Scale Mission*,” Space Telescopes and Instrumentation 2012: Ultraviolet to Gamma Ray, T. Takahashi, S.S. Murray, and J.-W. A. den Herder (eds.), Proc. SPIE **8443**, 844315 (2012)
- [6] A. Vikhlinin, P. Reid, H. Tananbaum, D.A. Schwartz, W.R. Forman, C. Jones, J. Bookbinder, V. Cotroneo, S. Trolrier-McKinstry, D. Burrows, M.W. Bautz, R.K. Heilmann, J. Davis, S.R. Bandler, M.C. Weisskopf, and S.S. Murray, “*SMART-X: Square Meter Arcsecond Resolution X-Ray Telescope*,” Space Telescopes and Instrumentation 2012: Ultraviolet to Gamma Ray, T. Takahashi, S.S. Murray, and J.-W. A. den Herder (eds.), Proc. SPIE **8443**, 844316 (2012)
- [7] “*Enduring Quests, Daring Visions*,” Astrophysics Roadmap (2013)
- [8] P. Hertz, “*Planning for the 2020 Decadal Survey: An Astrophysics Division White Paper*” (2015)
- [9] R.K. Heilmann, M. Ahn, E.M. Gullikson, and M.L. Schattenburg, “*Blazed High-Efficiency X-Ray Diffraction via Transmission through Arrays of Nanometer-Scale Mirrors*,” Opt. Express **16**, 8658 (2008)
- [10] R.K. Heilmann, M. Ahn, A. Bruccoleri, C.-H. Chang, E.M. Gullikson, P. Mukherjee, and M.L. Schattenburg, “*Diffraction Efficiency of 200 nm Period Critical-Angle Transmission Gratings in the Soft X-Ray and Extreme Ultraviolet Wavelength Bands*,” Appl. Opt. **50**, 1364-1373 (2011)
- [11] A. Bruccoleri, P. Mukherjee, R.K. Heilmann, J. Yam, M.L. Schattenburg, and F. DiPiazza, “*Fabrication of Nanoscale, High Throughput, High Aspect Ratio Freestanding Gratings*,” J. Vac. Sci. Technol. B **30**, 06FF03 (2012)
- [12] A.R. Bruccoleri, D. Guan, P. Mukherjee, R.K. Heilmann, and M.L. Schattenburg, “*Potassium Hydroxide Polishing of Nanoscale Deep Reactive-Ion Etched Ultrahigh Aspect Ratio Gratings*,” J. Vac. Sci. Technol. B **31**, 06FF02 (2013)
- [13] R.K. Heilmann, A.R. Bruccoleri, D. Guan, and M.L. Schattenburg, “*Fabrication of Large-Area and Low Mass Critical-Angle X-ray Transmission Gratings*,” Proc. SPIE **9144**, Space Telescopes and Instrumentation 2014: Ultraviolet to Gamma Ray, 91441A (2014)
- [14] R.K. Heilmann, A.R. Bruccoleri, and M.L. Schattenburg, “*High-Efficiency Blazed Transmission Gratings for High-Resolution Soft X-ray Spectroscopy*,” Proc. SPIE **9603**, Optics for EUV, X-Ray, and Gamma-Ray Astronomy VII, 960314 (2015)
- [15] A.R. Bruccoleri, R.K. Heilmann, and M.L. Schattenburg, “*Fabrication Process for 200 nm-Pitch Polished Freestanding Ultra-High Aspect-Ratio Gratings*,” submitted to J. Vac. Soc. Technol. B (2016)
- [16] R.K. Heilmann, A.R. Bruccoleri, J. Kolodziejczak, J.A. Gaskin, S.L. O'Dell, R. Bhatia, and M.L. Schattenburg, “*Critical-Angle X-ray Transmission Grating Spectrometer with Extended Bandpass and Resolving Power > 10,000*,” Proc. SPIE **9905**, Space Telescopes and Instrumentation 2016: Ultraviolet to Gamma Ray, 99051X (2016)

For additional information, contact Mark Schattenburg: [marks@space.mit.edu](mailto:marks@space.mit.edu)



# Technology Development for an AC-Multiplexed Calorimeter for Athena

Prepared by: Joel Ullom (PI; NIST/Boulder), Simon Bandler and Caroline Kilbourne (NASA/GSFC), and Kent Irwin (Stanford)

## Summary

We are developing large-format arrays of X-ray microcalorimeters and the associated readout that will enable the next generation of high-resolution X-ray imaging spectrometers for astrophysics. These sensors have very high spectral resolution, quantum efficiency, focal-plane coverage, and count-rate capability, combined with the ability to observe extended sources without spectral degradation. The goal of this program is to advance a readout architecture for an X-ray microcalorimeter imaging spectrometer from Technology Readiness Level (TRL) 3 to 4. The key components are (1) the use of an alternating current (AC) bias for microcalorimeter sensors, and (2) frequency-division multiplexed (FDM) readout. This work is a collaboration between the National Institute of Standards and Technology (NIST), Boulder (PI J. Ullom); NASA/GSFC (lead C. Kilbourne); and Stanford University (lead K. Irwin). The work is supported by the Strategic Astrophysics Technology (SAT) program. It began in Fiscal Year (FY) 2015, and is supported through FY 2016. The scientists in our groups have been collaborating on technology development for an imaging X-ray microcalorimeter spectrometer since 1998. This heritage has focused on Transition Edge Sensor (TES) microcalorimeter arrays with a different readout architecture: direct current (DC) bias and time division multiplexing (TDM).

The landscape for future missions based on microcalorimeter sensors has recently changed with the choice of the Advanced Telescope for High ENergy Astrophysics (Athena) [1] for the European L2 large mission slot. One of the two key instruments for this mission is called the X-ray Integral Field Unit (X-IFU). X-IFU is based on the use of a large array of X-ray microcalorimeters as a high-resolution imaging spectrometer. The use of TES for the X-ray microcalorimeters, originally pioneered by our collaboration, is currently assumed for this instrument [2]. With this choice, the possibility for a near-term US-lead or joint-lead mission such as the International X-ray Observatory (IXO) has now ended. Thus, the aim of our program has shifted toward our collaboration trying to make a significant contribution to Athena's X-IFU.

The primary goal of the current project is to advance the technical readiness of the AC-biased read-out of X-ray microcalorimeters from TRL 3 to 4. This advance requires work on both single TES devices and on small numbers of devices operating together. For single devices, we will compare sensor resolution under AC and DC bias; as well as properties that affect the energy resolution, such as transition shape and noise. Studies of small numbers of devices operating together will allow interaction pathways within the AC readout architecture to be identified and characterized. Interactions between sensors are a potential source of energy-resolution degradation.

## Background

The ability to perform broadband imaging X-ray spectroscopy with high spectral and spatial resolution has been a core capability of recent X-ray satellite mission concepts. Multiplexed microcalorimeter arrays provide this capability. The technology development program we are pursuing is a response to this need and is now directed towards Athena. The science case for developing microcalorimeter technology is that of the universe of extremes, from black holes to large-scale structure. The main goals are structured around three main topics – “black holes and accretion physics,” “cosmic feedback,” and “large-scale structure of the universe.” Underpinning these topics is the study of hot astrophysical plasmas that broadens the scope of this science to virtually all corners of astronomy.



The baseline readout architecture for the X-IFU on Athena is FDM [3], in which the TESs are biased with AC signals of different frequencies, which act as carriers for the slower thermal signals. The AC signals from different TESs are measured by a shared Superconducting-Quantum-Interference-Device (SQUID) current amplifier.

To date, the resolutions achieved using DC-biased TESs have not been reproduced in AC-biased TESs. As of the start of this work, the best results with AC bias are from the Space Research Organization Netherlands (SRON) group, which reported a full-width at half maximum (FWHM) resolution of 3.6 eV at 5.9 keV using transformer coupling to low resistance Mo/Au NASA/GSFC devices [4, 5]. Under DC bias, these same devices yielded 2.3 eV FWHM at 5.9 keV. Since the essential principle of AC bias has been demonstrated, its current TRL is 3. If we succeed in improving AC-biased performance to levels that meet the Athena mission specifications, then we will have increased the TRL of AC bias to 4. Thus, we will initially attempt to advance the TRL for reading out single pixels in large arrays of TESs with AC bias. We will attempt to demonstrate a FWHM energy resolution performance of less than 2.5 eV at 6 keV, and be capable of achieving this energy resolution at an input X-ray count-rate of 50 counts per second, with 80% throughput for the high-resolution events. These results will likely meet the Athena mission requirements.

The behavior of a TES is more complicated than that of a temperature-dependent resistor because of the role of superconductivity. Noise and responsivity depend on both the current and the temperature in the device. Under AC bias, the current is constantly changing even though the temperature is very close to fixed. This current variation is one possible reason why results under AC bias are not as mature as those under DC bias. We will study how the properties of TES devices under AC bias compare to those under DC bias. We will focus on Mo/Au TES thermometers developed at GSFC that are currently the baseline sensor technology for the X-IFU, but will also study other TES designs insofar as these can provide insight into the details of AC bias. This work encompasses both the fundamental physics of TES devices and the role of the readout SQUID and feedback system in determining performance levels.

## Progress and Accomplishments

In order to complete the goals of this program, new measurement setups were needed at both NIST Boulder and GSFC, capable of studying and evaluating the effects of AC bias on the performance of TESs. To broaden the impact and maximize the chances of success, different approaches were pursued at each institution. GSFC pursued an approach that allowed the maximum use of components from European institutes collaborating on the Athena mission. This approach provides the most straightforward path to boosting the collaboration's ability to characterize AC-biased TES. In contrast, the NIST AC-bias measurement setup is designed to maximally separate the contribution of the readout system from that of the TES microcalorimeter in assessments of detector performance, as described below. These two approaches for increasing the measurement capability for AC-biased TESs within the US are augmented by joint FDM measurements with European collaborators that are being carried out at SRON.

All the necessary components for the GSFC measurement platform have been installed and AC-bias studies using FDM are commencing. Some of the major components have been supplied by SRON, including the specialized LC filter chip and the transformer chip. The room-temperature electronics, which include an analog amplifier and digital base-band feedback electronics, were recently delivered and installed. The FDM setup at GSFC will also utilize the same two-stage SQUIDs used by SRON that will be provided by VTT Finland. The wire-routing boards and the cryogenic mount have been fabricated and integrated into the cryostat (Fig. 1).

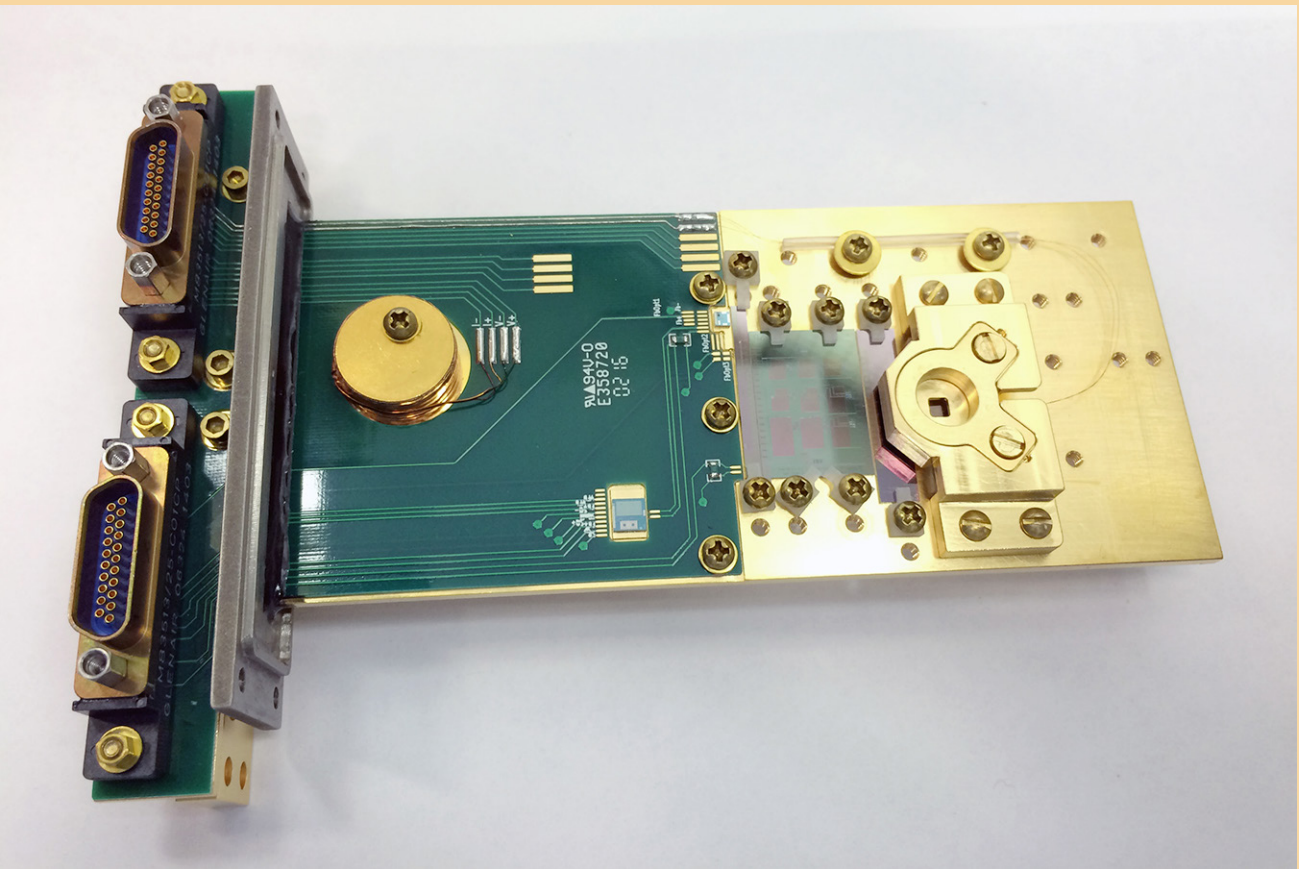


**Fig. 1.** Assembled cryogenic mount for AC-bias test showing routing PC board, SQUIDs, LC filter chip, and transformer chip. The chip with the TES detectors is barely visible through the square photon access hole.

All existing multiplexing architectures for TESs exploit the favorable properties of SQUID amplifiers. The non-linear response of SQUID amplifiers is typically mitigated by magnetic flux or current feedback. Feedback is particularly important in FDM because of the large amplitude of the fast carrier signals and the requirement that one SQUID simultaneously measure signals from many sensors. As a result, FDM system performance can depend strongly on the particular feedback implementation, and feedback systems with additional capability will likely be needed [3].

The motivation for the NIST AC-bias measurement platform is to measure AC-biased TESs without the use of feedback, by using microwave SQUIDs. In this setup, the microwave SQUID can be operated open-loop, allowing the TESs to be characterized independent of the complications of a fixed-bandwidth feedback loop. The microwave SQUID has the option of linearizing the SQUID response using flux ramp modulation [6]. The effect of this modulation on the measured response of the TES is directly calculable and can be separated from the response of the TES to AC bias. In this setup, the SQUID is embedded in a passive microwave resonator and probed using microwave tones. This approach, shown schematically in Fig. 2 left panel, has the potential to provide very large readout bandwidths and high dynamic range without the use of feedback.

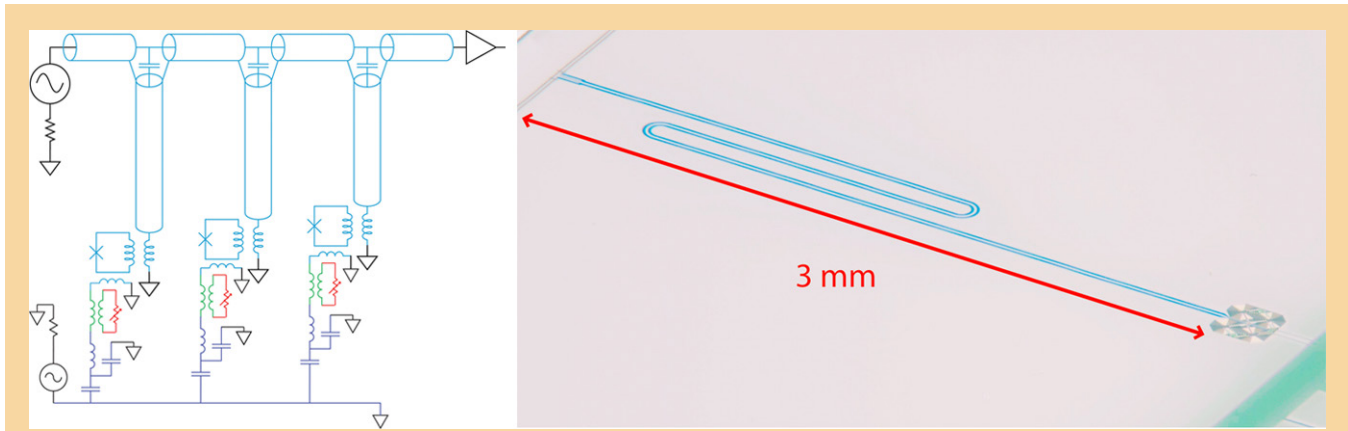


**Fig. 2.** Circuit schematic (left) depicting a microwave SQUID multiplexer to read out AC-biased TESs, and micrograph (right) of a microwave SQUID multiplexing element showing the superconducting resonator coupled to the shared feedline in the top left corner and the SQUID coupling coils in bottom right corner.

To meet the bandwidth requirements of the 1-5 MHz range for the Athena AC bias, new microwave SQUIDs with 15 MHz of open-loop bandwidth were designed and fabricated (Fig. 2, right panel). These designs were tested with direct current inputs. The shift of the resonance frequency of one of the microwave SQUIDs as a function of input flux is shown in Fig. 3. After testing the microwave SQUIDs separately, they were integrated into the sample box with the AC-bias circuit using the SRON LC-filter and transformer chips. Four microwave SQUIDs are fabricated on the same chip, sharing a common microwave feed-line. These four SQUIDs can be probed independently, and act as four independent readout channels. Each of the four channels can measure either an AC- or DC-biased TES. Initial tests demonstrated the functionality of the microwave SQUID readout. The open-loop bandwidth was confirmed to be 15 MHz, and a flux ramp modulated sampling rate of 8 MHz was achieved. Integration into circuits with AC-biased TESs is commencing (Fig. 4).

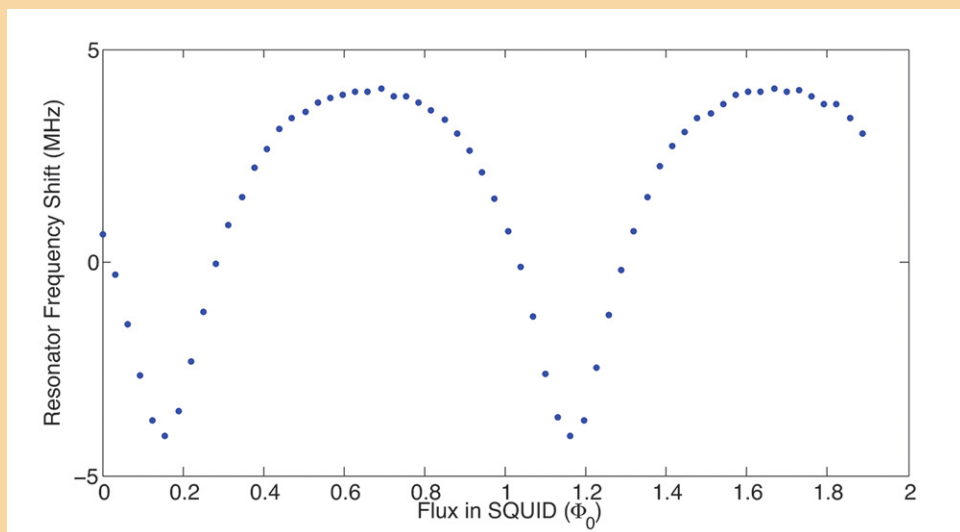


**Fig. 3.** Modulation of the resonant frequency as a function of input flux for a microwave SQUID readout optimized to measure AC-biased TESs at the frequencies targeted for the Athena X-IFU instrument.



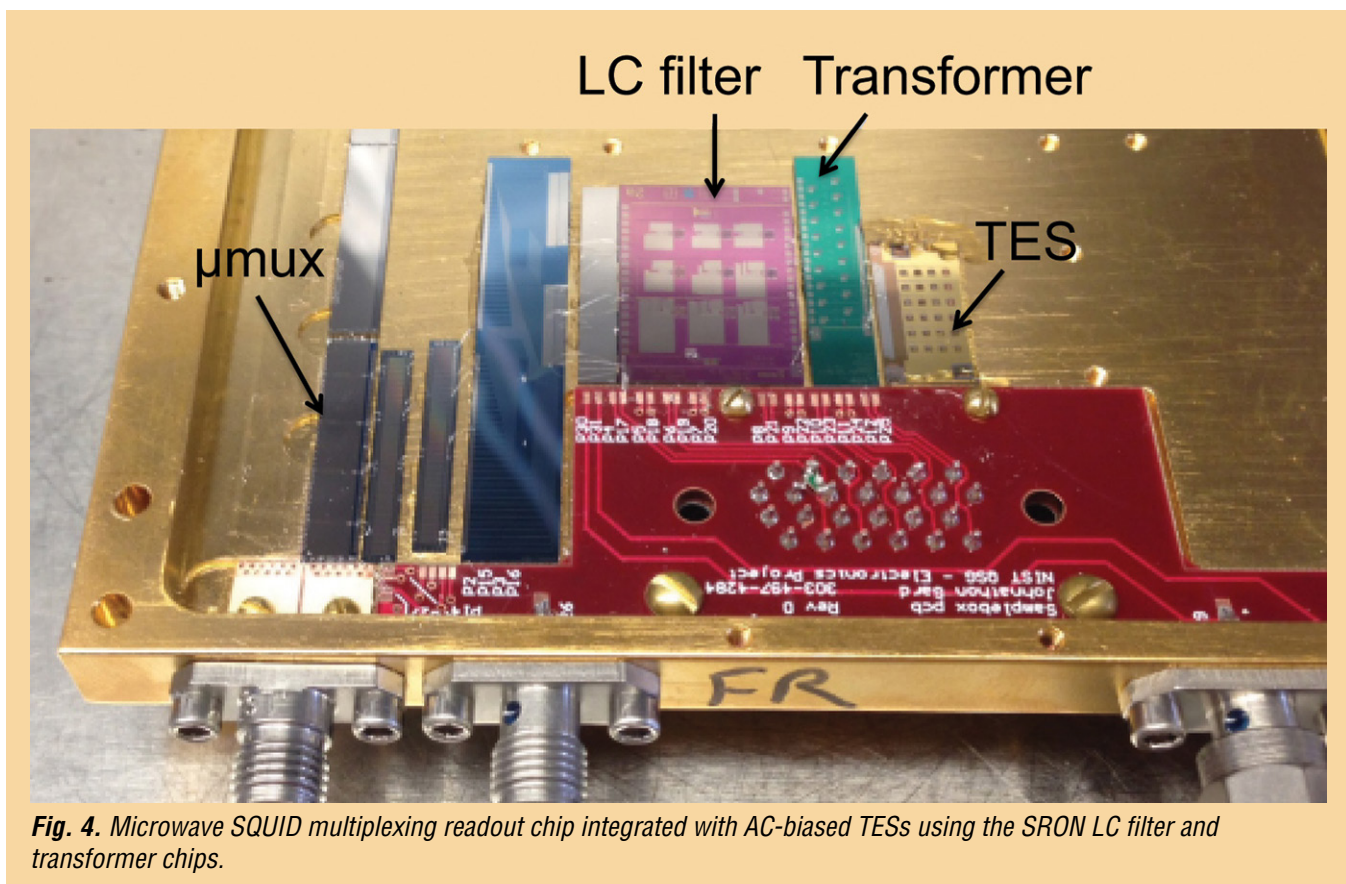


**Fig. 4.** Microwave SQUID multiplexing readout chip integrated with AC-biased TESs using the SRON LC filter and transformer chips.

In addition to expanding capability to measure AC-biased TES microcalorimeters in the US, GSFC and SRON scientists began testing new GSFC X-ray microcalorimeters using an existing test set-up at SRON. A new array was measured at SRON consisting of different TES sizes (50, 100, 120, and 140  $\mu\text{m}$ ), targeted at understanding the influence of TES geometry on the performance under AC bias. These designs were first tested at GSFC under DC bias so the two bias strategies could be directly compared. The updated arrays included improved heat-sinking and better fundamental energy resolution characteristics over a broader region of the transition than the arrays previously tested at SRON.

Frequency-domain measurements provide a natural measure of both the in-phase current (which should contain the TES signal component) and any out-of-phase current. If the TES were a pure resistive element with no reactive elements, there should be no out-of-phase component. However, detailed measurement of TES IV curves on these devices and those of a previous uniform array show the presence of oscillatory structure and discontinuities in the measurements of the out-of-phase current that are not attributable to the bias circuit. Thus, the out-of-phase current is thought to be related to the physical properties of the TES.

Theoretical efforts to understand these effects have focused on understanding the Josephson-junction-like properties of these TESs under AC excitation. We now believe these reactive features are a direct result of the non-linear Josephson inductance of the TES. In a theoretical analysis by McDonald and Clem [7], the non-linear nature of the differential equations that describe a Josephson junction are shown to result in bifurcations effects, resulting in a  $2\pi$  phase slip of the superconducting phase difference (oscillating in time) across the junction for certain values of the AC drive signal. These phase slips manifest as discontinuities in the time-averaged reactance, quite similar to the effects observed in TES data. Efforts are ongoing to compare the TES measurements to these theoretical models and extend the models to better reflect the more complex extended geometries of a TES.

Evidence of these discontinuities is also observed in the in-phase current (real part of the impedance) of the measured transition as small steps, particularly low in the transition. When the sensor response traverses these features, they degrade energy resolution. Bias points above 30% of the normal resistance ( $R_n$ ) are selected to avoid these features. When operating in the continuous regions around them, the AC spectral resolution is as good as 2.9 eV FWHM at 6 keV [8]. Biasing the TES array at 30%  $R_n$  could potentially limit the resolution and dynamic range of the X-IFU instrument. The best performance for the equivalent DC-biased TESs is achieved for bias points around 10% of the normal resistance.

## Path Forward

The ability to test AC-biased TES X-ray microcalorimeters in the US is maturing rapidly. When complete, it will allow us to rigorously compare TES energy resolution and other performance metrics under AC and DC bias. The complementary capabilities of the GSFC AC-bias setup to perform direct comparison with the SRON FDM, and the NIST AC-bias setup to separate the effects of an AC-biased TES from the readout implementation will provide significant insight into AC-biased TESs. Sharp steps observed in the transition currently limit the bias range to be above 30% of the normal resistance. Understanding how to mitigate these steps and recover the full dynamic range of the TES will be a major focus of this project and will continue as part of NASA's role in the Athena mission.

## References

- [1] K. Nandra et al., "[ATHENA, the Advanced Telescope for High ENergy Astrophysics](#)," recently accepted mission proposal submitted to ESA's L2 large mission opportunity (2014)
- [2] D. Barret et al., "*The Hot and Energetic Universe: The X-ray Integral Field Unit (X-IFU) for Athena+*," astro-ph [arXiv:1308.6784](#) (2013)
- [3] R. den Hartog et al., "*Baseband Feedback for Frequency-Domain-Multiplexed Readout of TES X-ray Detectors*," AIP Conf. Proc. **1185**, 261-264 (2009)
- [4] H. Akamatsu et al., "*Single Pixel Characterization of X-Ray TES Microcalorimeter Under AC Bias at MHz Frequencies*," IEEE Trans. Appl. Supercon. **23**, 2100503 (2013)
- [5] H. Akamatsu et al., "*Performance of TES X-ray Microcalorimeters with AC Bias Read-Out at MHz Frequencies*," J. Low Temp. Phys. **176**, 591 (2014)
- [6] J. Mates et al., "*Demonstration of a multiplexer of dissipationless superconducting quantum interference devices*," Appl. Phys. Lett. **92**, 023514 (2008)
- [7] J. McDonald and J.R. Clem, "*Microwave response and surface impedance of weak links*," Physical Review B **56**, 14723 (1997)
- [8] H. Akamatsu et al., "*TES-Based X-ray Microcalorimeter Performances Under AC Bias and FDM for Athena*," J. Low Temp. Phys. **184**, 1, 436-442 (2016)

For additional information, contact Joel Ullom: [joel.ullom@nist.gov](mailto:joel.ullom@nist.gov)



# Next-Generation X-ray Optics: High Angular Resolution, High Throughput, and Low Cost

Prepared by: William W. Zhang (PI; NASA/GSFC) and Stephen L. O'Dell (NASA/MSFC)

## Summary

This work continues technology development of X-ray optics for astronomy. Since Fiscal Year (FY) 2012, the Strategic Astrophysics Technology (SAT) program has funded this effort, which the Constellation-X project initiated and the International X-ray Observatory (IXO) project continued. This is an effort by GSFC with collaboration from MSFC.

The objective is to advance astronomical X-ray optics by at least an order of magnitude in one or more of three key metrics from the state of the art represented by the four major X-ray missions currently in operation: Chandra, X-ray Multi-mirror Mission-Newton (XMM-Newton), Suzaku, and Nuclear Spectroscopic Telescope Array (NuSTAR). These metrics are: (1) angular resolution, (2) mass per unit area, and (3) production cost per unit area. The modular nature of this technology renders it appropriate for missions of all sizes—from Explorers that can be implemented by the end of this decade, to Probes and flagship missions that can be implemented during the next decade.

Key areas of technology development include: (1) fabrication of substrates, (2) thin-film coating of these substrates to make X-ray mirror segments, (3) alignment and (4) bonding of mirror segments into mirror modules, and (5) systems engineering to ensure all spaceflight requirements are met. We expect to continually improve both image quality and overall technology readiness levels over the coming years.

## Background

The last five centuries of astronomy are a history of technological advancements in optical fabrication and optical-systems integration. Furthering our understanding of the cosmos requires telescopes with ever-larger collecting area and ever-finer angular resolution. In the visible and other wavelength bands, where radiation can be reflected at normal incidence, a large mirror area alone directly translates into a large photon-collecting area. However, due to its grazing-incidence nature, an X-ray telescope requires a combination of both large area and thin mirrors to increase photon-collecting area.

Three metrics capture the essence of an X-ray optics technology: (1) angular resolution, (2) mass per unit collecting area, and (3) production cost per unit collecting or mirror area. The X-ray optics of every successful observatory represents a scientifically useful compromise between the three metrics that was implementable in its specific technological, budgetary, schedule, and spaceflight opportunity context. The objective of this effort is to ready an X-ray telescope fabrication process that ever tilts the compromise toward better performance for given amounts of resources in terms of money and mass.

Our effort started in 2001, with the epoxy replication process developed for Suzaku. Instead of using thermally formed aluminum substrates, we used thermally formed (or slumped) thin glass for substrates. Taking advantage of the already smooth surface of float-glass sheets, by 2007 we were able to make glass substrates that no longer needed the epoxy replication process, saving both time and money. In early 2008, we X-ray-tested a pair of glass mirrors and produced X-ray images better than 15" half-power diameter (HPD), meeting the requirement of the Constellation-X mission. Between 2007 and 2011, we continued to improve the glass slumping technique, culminating in a process that consistently makes glass mirrors of 6" HPD. Since 2011, we have developed a mirror



alignment and bonding process that has produced technology development modules with three pairs of mirrors, making X-ray images better than 8" HPD. Compared with Chandra, this technology would lower mass and cost per unit collecting area by nearly two orders of magnitude. Compared with XMM-Newton, it would reduce mass per unit collecting area by a factor of eight and cost by a factor of three, while significantly improving angular resolution. Compared with Suzaku and NuSTAR, it would improve angular resolution by an order of magnitude, while preserving their advantages in mass and cost per unit collecting area.

In the last few years, funded by an Astrophysics Research and Analysis (APRA) grant, we developed a process for making mirror substrates out of single-crystal silicon. The development has advanced so rapidly that we have decided to use single-crystal silicon mirrors as our baseline. The major reasons for this change are:

1. Polished silicon mirrors have the potential for much better angular resolution than slumped-glass mirrors.
2. Silicon has far superior material properties compared to those of glass: lower density, higher thermal conductivity, higher elastic modulus, and lower coefficient of thermal expansion.
3. The silicon fabrication process does not require mandrels as needed for the glass-slumping process, saving time and money.

### ***Change in Approach***

In conjunction with the change of substrates from slumped glass to polished silicon mirrors, we have also changed the overall approach to making an X-ray mirror assembly. Figure 1 is an illustration contrasting the old approach with the new one. Both start with small mirror segments, but they differ in the intermediate step. In the old approach, a large number of wedge-like modules are built, tested, and then integrated to form the final mirror assembly. In the new approach, a relatively small number of meta-shells are built, tested, and then integrated.

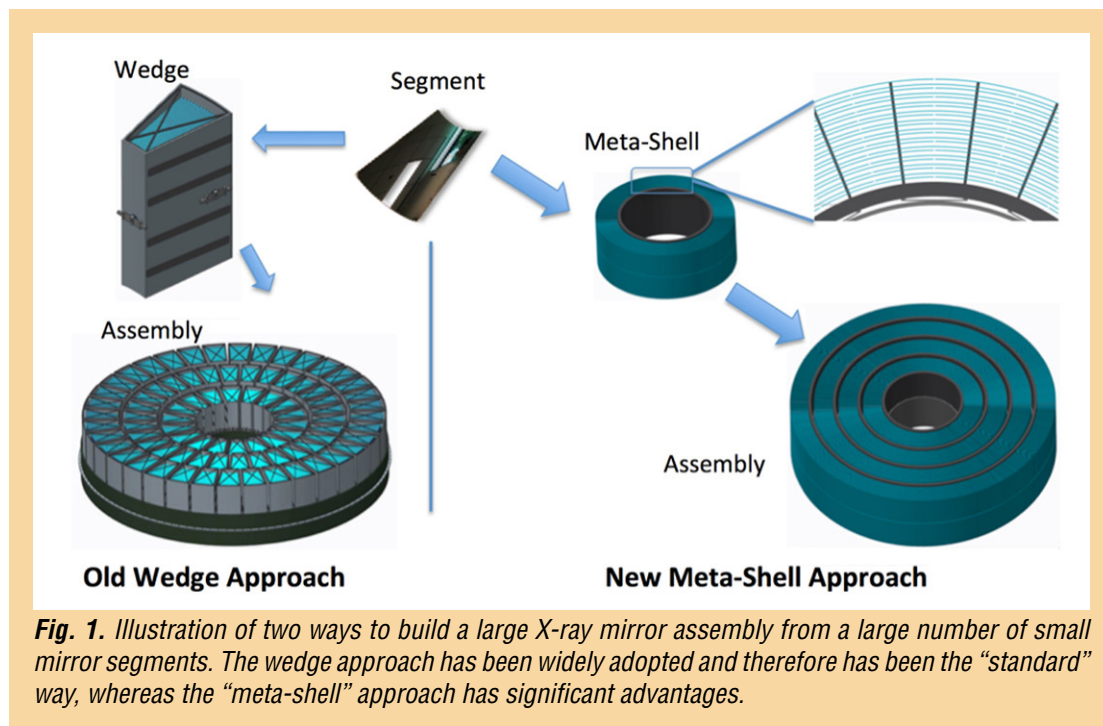


**Fig. 1.** Illustration of two ways to build a large X-ray mirror assembly from a large number of small mirror segments. The wedge approach has been widely adopted and therefore has been the “standard” way, whereas the “meta-shell” approach has significant advantages.

The new approach has several major advantages. First, its construction process naturally defines the optical axis, making it much easier to both build and integrate meta-shells into a final mirror assembly. Second, the construction process proceeds naturally from inner shells to outer shells, making it much easier to baffle against stray light and realize much smaller inter-shell spacing, essential for achieving maximum packing efficiency.

## Objectives and Milestones

The objective of this effort is to perfect a process for making mirror meta-shells that meet spaceflight environmental requirements and have progressively better performance. We expect to achieve better than 5" HPD in the near term (next two years). In the longer term (next five to 10 years), we expect to continue and improve every aspect of the process toward better angular resolution from 5" to less than 1", with the ultimate goal of achieving diffraction-limited X-ray optics in the 2020s.

The same set of milestones can be used to measure progress toward realizing both near-term and long-term objectives. They differ only in the X-ray image quality measured in arcsec. Each step or milestone has two metrics: image quality and consistency. The steps are as follows.

1. Fabricating mirror substrates.
2. Maximizing X-ray reflectivity by coating substrates with thin-film iridium or other material.
3. Aligning individual mirror segments and pairs of mirror segments.
4. Bonding mirror segments to a mechanical structure.
5. Constructing meta-shells, requiring co-alignment and bonding of multiple mirror segments.
6. Environmental-testing meta-shells, with X-ray performance tests before and after environmental tests.

Environmental tests include vibration, acoustic, and thermal-vacuum. X-ray performance tests include measurement of point spread function and effective area at representative X-ray energies – e.g., 1.5 keV (aluminum  $K\alpha$ ), 4.5 keV (titanium  $K\alpha$ ), and 8.0 keV (copper  $K\alpha$ ).

## Progress and Accomplishments

In the past year, we made progress in every area of the technology: substrate fabrication; coating; mirror alignment; mirror bonding; and module design, analysis, construction, and testing.

### Substrate Fabrication

In conjunction with our APRA-funded effort, we have developed a complete mirror fabrication process: starting with a block of commercially procured single-crystal silicon and ending with a Wolter-I X-ray mirror (parabolic or hyperbolic), with an image quality of about 3" HPD, shown in Fig. 2. This is about twice as good as the best slumped-glass mirrors, and is the best lightweight X-ray mirror in the world. We expect to continually improve this process, producing progressively better HPD and surpassing the 0.5" HPD of Chandra, eventually reaching diffraction limits.

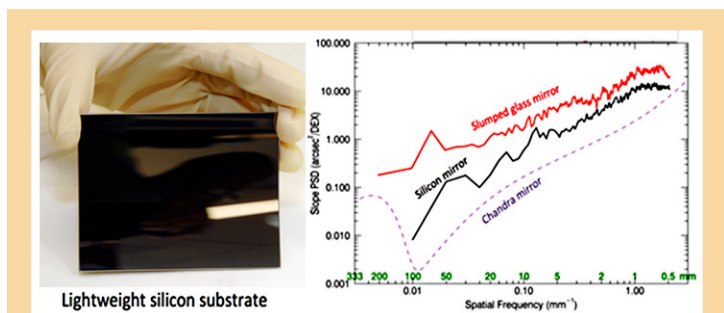


**Fig. 2.** Status of lightweight single-crystal silicon mirror fabrication. Left: Photo of a 0.7-mm-thick mirror. Right: The axial-slope power-spectral density (PSD) in comparison with typical slumped-glass mirrors and that of the Chandra mirrors. As of February 2016, the silicon mirror is about two times better than the best slumped-glass mirrors and four times worse than the Chandra mirrors. Our objective is to bridge this latter factor of four in the next four years.

The substrate fabrication process consists of the following steps:

1. Figure generation.
2. Slicing or light-weighting.
3. Edge- and backside lapping.
4. Acid etching.
5. Stress-lapping.
6. Stress-polishing.
7. Trimming.
8. Edge-polishing.

Our work in the coming years is to perfect each step, improving quality while reducing time and cost.

### **Coating**

Mirror substrates require an optical coating (e.g., 15-nm iridium) to enhance X-ray reflectivity. The stress of an iridium film, typically several Giga-Pascal, severely distorts the figure of a thin substrate, greatly degrading its imaging quality. Over the last few years we have experimented with different ways of reducing the figure distortion, including balancing the front- and back-side coating stress and thermal annealing. In the past year, we set up two magnetrons in a vacuum chamber to coat the front side (concave) and the back side (convex) of the mirror simultaneously. This work will continue into the next year with results expected by the middle of 2017.

### **Mirror-Segment Alignment and Bonding**

Traditionally, the alignment of a mirror is achieved by using a 6-dof (degrees of freedom) stage that can translate and orient a rigid body in all possible ways. We adopted and used the traditional method until six months ago, when we switched to using the fact that a Wolter-I mirror segment, or more generally, a cylindrical mirror segment, can be supported at four locations with its orientation uniquely determined. The orientation of the mirror can be fine-tuned by precise adjustment of one or more of these locations. Figure 3 shows our implementation of this concept, where each mirror segment is supported by four spacers whose radial heights are precisely machined. In practice, this is an iteration process guided by Hartmann measurements.

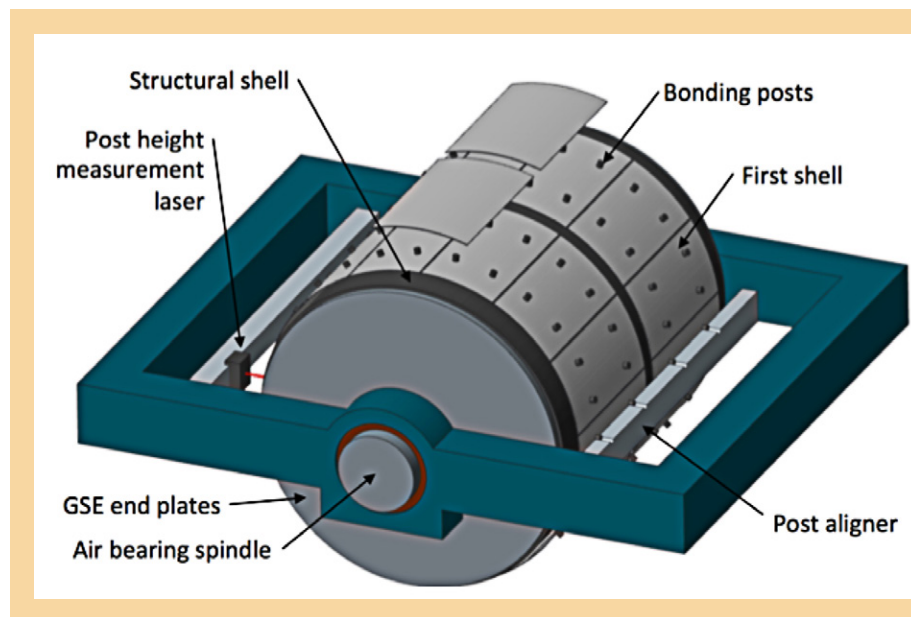


**Fig. 3.** Illustration of the mirror alignment and bonding process. Each mirror segment is supported and aligned by four spacers. The radial heights of these spacers are precisely machined in-situ, guided by Hartmann measurements (GSE, ground-support equipment).



As shown in Fig. 3, once the four spacers have been machined to achieve alignment for the mirror segment, a minute amount of epoxy is applied to each spacer. The mirror segment is then placed on the spacers and a small vibration jiggles the mirror into its optimal alignment. Once the epoxy cures, the mirror is permanently bonded.

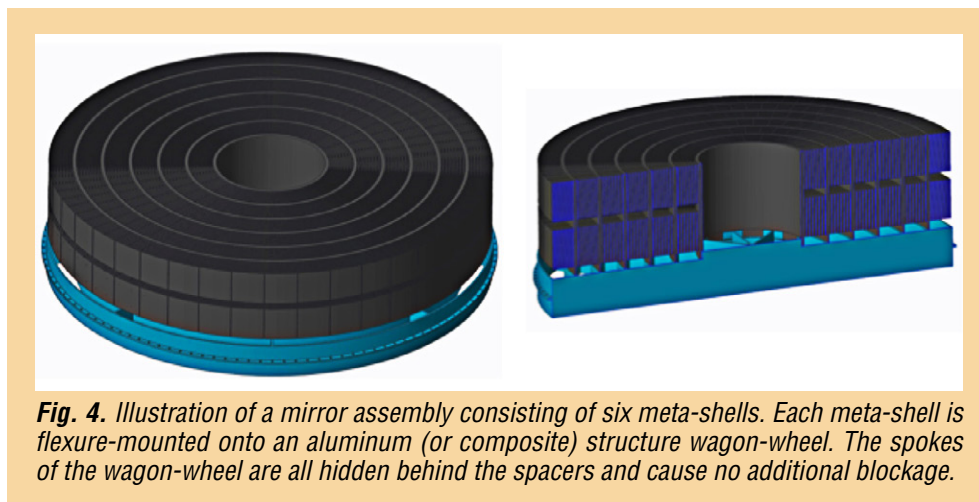
In the past year, we demonstrated with stand-alone experiments several key elements of this alignment and bonding process. First, the alignment is uniquely determined by the four spacers. A mirror was repeatedly placed and removed to show that the images of the different placement trials precisely reproduce the same quality and location. Second, a grinding and buffing process can deterministically change the height of a spacer with sub- $\mu\text{m}$  precision. Third, the application of epoxy on the spacer does not change the alignment of the mirror, implying that the epoxy thickness variation from spacer to spacer is acceptably small. We will revisit all of these conclusions in the coming year when progressively more precise alignment and bonding criteria are applied.

### ***Meta-Shell Design and Analysis***

Since the conception of the meta-shell approach a few months ago, we conducted a design and analysis exercise. Figure 4 shows the preliminary design of a mirror assembly with an outer diameter of 1.3 m. It consists of six meta-shells, each having about 20 layers of mirrors, not all of which are drawn. A set of preliminary structural and thermal analyses has led to the following conclusions:

1. Each meta-shell, with its relatively thick structural shell and interlocked mirror segments, is stiff and has good mechanical integrity. Assuming the use of a standard aerospace epoxy, such as Hysol 9309, and a reasonable bond area for each spacer, about 2 mm in diameter, the meta-shell can sustain launch loads.
2. The meta-shell construction process, as shown in Fig. 3, where the optical axis is horizontal, does not freeze in any significant amount of distortion, meaning that when the meta-shell is turned vertical, the frozen figure distortion is sub-arcsec.
3. A meta-shell can be X-ray-tested in a horizontal beam line. The images of some of the mirrors show minimal distortion. By rotating the meta-shell, we expect to be able to fully characterize the imaging performance of the entire meta-shell.
4. Because the meta-shell is made of silicon, with only trace amounts of different materials such as epoxy and iridium, a bulk temperature change of  $1^\circ\text{C}$  changes the imaging performance by only 0.1" HPD.

Overall, the analysis has shown that the meta-shell approach is sound in every aspect: performance, thermal, and structural. We note that this approach incorporates the merits of all four currently operating missions' X-ray mirror assemblies.



## Path Forward

Based on our previous work, as well as heritage of previous missions, such as Chandra, XMM-Newton, Suzaku, and NuSTAR, we have conceived and adopted the meta-shell approach for our technology development. Numerous stand-alone experiments and finite element analyses, both structural and thermal, have validated the approach. In the next year, we will start building and testing mirror modules, or meta-shells, based on this approach. Initially we will build and test single pairs. Then we will proceed to build a meta-shell with three layers of mirrors, with a total of 72 mirror segments. We will X-ray-test and then environmentally test this meta-shell.

For additional information, contact William Zhang: [william.w.zhang@nasa.gov](mailto:william.w.zhang@nasa.gov)



# Planar Antenna-Coupled Superconducting Detectors for CMB Polarimetry

Prepared by: James J. Bock (JPL, California Institute of Technology)

## Summary

We are developing advanced antenna-coupled superconducting detector-array technology for the NASA Inflation Probe (IP), a future satellite dedicated to comprehensive measurements of Cosmic Microwave Background (CMB) polarization in NASA's Physics of the Cosmos (PCOS) Program. This Strategic Astrophysics Technology (SAT) project will extend the demonstrated frequency range of antennas down to 40 GHz and up to 350 GHz, and develop dual-band antennas that offer larger wafer formats with a higher density of detectors, a valuable resource in a 100 mK space-borne focal plane.

Antenna-coupled detectors have the requisite attributes – sensitivity, frequency coverage, and control of systematic errors – called for in community studies of space-borne CMB-polarization experiments. The arrays provide integral beam-formation, spectral-band definition, and polarization analysis; and scale to operate over the wide frequency range of 30 to over 300 GHz required to remove galactic foregrounds at near-background-limited sensitivity. The devices have rapid response speed and  $1/f$  noise stability for slow-scanning observations without requiring an additional level of signal modulation.

Our program rapidly infuses new detector technology into scientific observations, the fastest way to learn about real-world performance in demanding applications. Simultaneously, the program develops aspects of the technology uniquely required for space-borne operations. We are expanding the frequency coverage of the antennas, and applying these devices to improved foreground separation between the galaxy and the CMB. We are developing broadband antennas to better exploit full access to the electromagnetic spectrum in space. We are expanding the development of focal-plane modules that integrate detectors and readouts into a package for large focal planes, and fielding these devices in the Background Imaging of Cosmic Extragalactic Polarization 3 (BICEP3) experiment. We are furthering our measurements of cosmic-ray susceptibility, based on our experience with the detectors on the European Space Agency's (ESA) Planck satellite. Finally, we are starting to develop arrays on larger 150-mm wafers, expanding to the larger formats demanded by CMB scientists.

This two-year grant began in October 2015, and includes Jeff Filippini at the University of Illinois Urbana-Champaign (UIUC); and Krikor Megerian, Hien Nguyen, Roger O'Brient, Anthony Turner, and Alexis Weber at JPL. The program actively engages postdocs and students at Caltech, including Bryan Steinbach, Jon Hunacek, Howard Hui, and Sinan Kefeli. The students characterize the devices at cryogenic temperature, and then use the arrays in astrophysical measurements of CMB polarization.

Scientifically, the devices have led the way in state-of-the-art (SOTA) CMB measurements from ground-based and balloon-borne observations. This year, the BICEP2/Keck Array collaboration published the first results incorporating measurements in two spectral bands, 95 and 150 GHz. These measurements have now constrained the amplitude of the Inflationary gravitational-wave background more strongly from CMB polarization data than with CMB temperature information, a transition predicted in the 1990s, but only achieved this year. In January 2015, the Suborbital Polarimeter for Inflation Dust and the Epoch of Reionization (Spider) balloon experiment flew with six full focal planes operating at 95 and 150 GHz. The detectors performed well in the scientific environment closest to space, with low photon backgrounds, slow-scanned observations, and a difficult cosmic-ray environment. Finally, the first season of observations completed at 220 GHz, a key band needed to constrain the level of polarized galactic foreground. Current constraints are limited by the available sensitivity of Planck satellite data on galactic emission. This year, the demonstrated 220-GHz capability will overtake Planck in constraining polarized dust emission in these deep surveys.



## Background

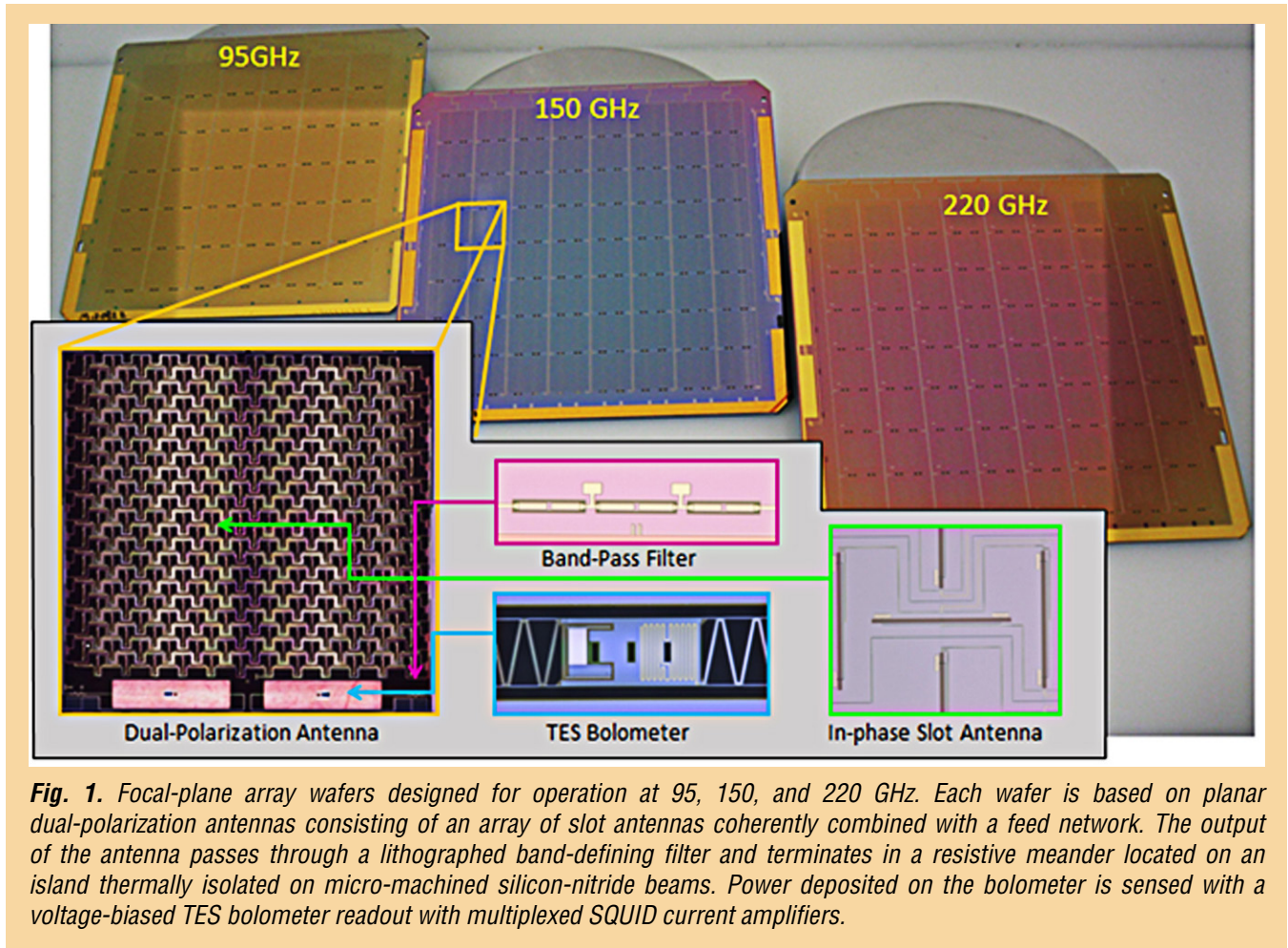
The importance of CMB-polarization research has been recognized in national reports including the 1999 National Academy Report; the 2001 Decadal Survey; and the 2003 National Research Council (NRC) report, “Connecting Quarks with the Cosmos.” In 2005, the Task Force on CMB Research stated that its first technology recommendation was “*technology development leading to receivers that contain a thousand or more polarization-sensitive detectors*”, and that “*highest priority needs to be given to the development of bolometer-based polarization sensitive receivers.*” The Astro2010 decadal report endorsed a CMB technology program of \$60M-\$200M, its second-ranked medium initiative for space. In addition, the decadal report states the amount could be increased to \$200M following a mid-decade review of the state of CMB-polarization measurements. The CMB Technology Roadmap ranked detector arrays as its highest CMB-technology priority, recommending a program that takes maximum advantage of operating the arrays in sub-orbital and ground-based CMB-polarization experiments.

The IP will measure CMB polarization over the entire sky to cosmological and astrophysical limits. The CMB is thought to carry a B-mode polarization signal imparted by a gravitational-wave background produced by the Inflationary expansion  $\sim 10^{-32}$  seconds after the Big Bang. The Inflationary polarization signal is sensitive to the energy scale and shape of the Inflationary potential, and can be clearly distinguished from polarization produced by matter-density variations due to its distinctive B-mode spatial signature. A detection of the Inflationary polarization signal would do more than just confirm Inflation — the amplitude of gravitational waves depends on the model and energy scale of Inflation, so detection would distinguish between models and constrain the physical process underlying Inflation. Such a measurement has profound implications for cosmology and bears on the current frontiers of fundamental physics: the union of general relativity and quantum mechanics, string theory, and the highest accessible energies.

The IP will also map the CMB-polarization pattern produced by gravitational lensing. Intervening matter between us and the surface-of-last-scattering slightly distorts the background CMB-polarization, imparting a B-mode signal that peaks at arcmin angular scales and probes the evolution of large-scale structure, which is sensitive to neutrino mass and dark energy. The CMB lensing signal is related to the projected gravitational potential of this matter, and provides a powerful combination with dark-energy surveys such as baryon acoustic oscillations and weak lensing.

The most recent definition study of the IP in 2008-2009 developed the basis for space-borne CMB-polarization measurements, incorporating high-sensitivity detector arrays as the key technology, operating over a wide range of frequencies to accurately measure and remove polarized galactic foregrounds. The detector system must demonstrate extreme  $1/f$  noise stability, forward-beam definition with stray-light immunity, radio-frequency (RF) and magnetic shielding, excellent spectral-band and time-constant matching, and cosmic-ray insusceptibility. Alternate implementations have been proposed, including an ESA medium-class mission and the Japanese Aerospace eXploration Agency (JAXA) Lite (Light) satellite for the studies of B-mode polarization and Inflation from cosmic background Radiation Detection (LiteBIRD) concept.

Antenna-coupled Transition-Edge-Sensor (TES) bolometer arrays (Fig. 1) are a scalable, planar focal-plane architecture that coherently sums an array of individual slot antennas with a microstrip feed network, controlling the phase and electric-field amplitude distributed to each slot. The planar antenna enables customized shaping of the detector beam-pattern for controlling detector illumination on critical optical surfaces. The antenna operates in two polarizations: an array of horizontal slots couples to one detector, and an interleaved array of vertical slots couples to another. The spectral band is defined by a three-pole RF microstrip filter. Power from the antenna is deposited in a meandered Au resistor on a thermally isolated bolometer, detected by a Ti/Al TES detector and read out by a multiplexed Superconducting-QUantum-Interference-Device (SQUID) current amplifier. As shown in Fig. 1, this technology has now been demonstrated in scientific observations in spectral bands centered at 95, 150, and 220 GHz.



Planar antennas are entirely lithographed and avoid coupling optics such as feedhorns or hyper-hemispherical lenses, ideal for a low-mass 100 mK focal plane. The devices can cover the wide range of frequencies by scaling the antenna with wavelength and keeping the detector element essentially unchanged. The antennas demonstrate excellent polarization properties and the lithographed filters provide reproducible control of the spectral band. The Ti TES detectors give predictable noise properties and low-frequency noise stability appropriate for slow-scanned observations from space.

### **Current State of CMB Polarization Measurements**

In recent years, CMB-polarization measurements have broken new ground in placing constraints on a background of gravitational waves produced in some models of Inflation. In 2016, polarization measurements surpassed constraints based on CMB-temperature measurements, and are now limited by the errors in removing galactic polarized foregrounds, requiring sensitive measurements in multiple frequency bands. Antenna-coupled TES bolometer-array technology addresses this challenge. Because the architecture scales in frequency, we have developed science-grade arrays in three frequency bands (Fig. 1). In Fig. 2 we show recent scientific measurements from the BICEP2/Keck experiment obtained at these three frequencies. The maps demonstrate SOTA sensitivity, while serving as valuable tests for controlling systematic errors. Indeed, the sensitivity at 150 GHz, about 50 nK in a square degree, is comparable to the sensitivity expected for the IP satellite. Instead of studying a small region, however, the IP will map the entire sky in multiple bands at this sensitivity.



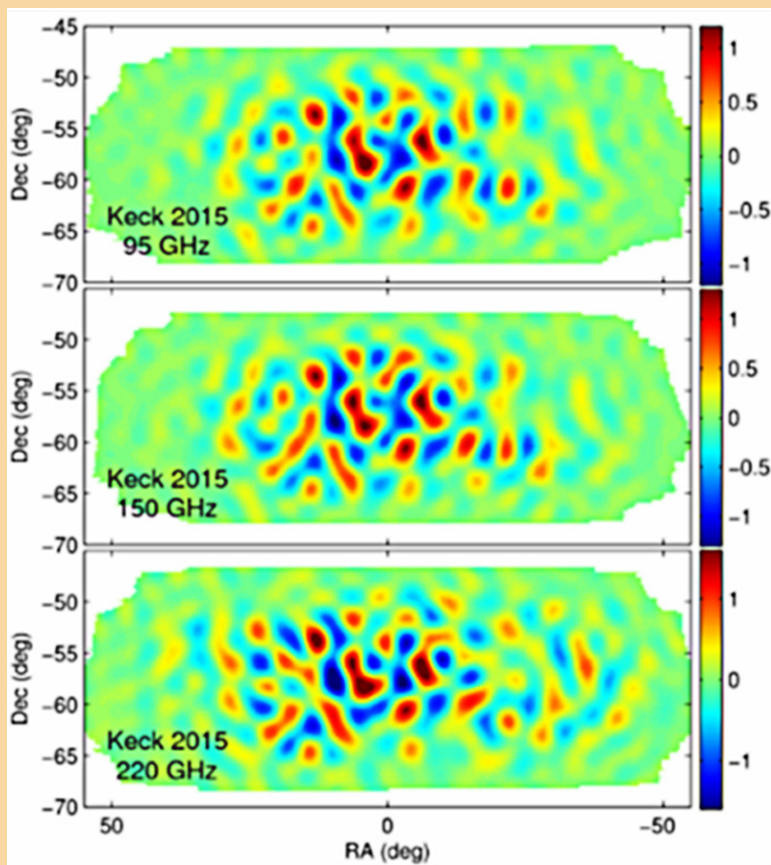


**Fig. 2.** SOTA CMB polarization measurements obtained in three frequencies from the South Pole. These images depict the amplitude of E-mode polarization in units of thermodynamic temperature in  $\mu\text{K}$ . The E-mode signal (brighter than the B-mode signal expected from Inflation) is clearly detected in all three frequencies with high signal-to-noise, evident by the structures reproduced in each band. The 220-GHz measurements are the first demonstration of sensitive polarization measurements from the ground at this frequency. After one year of integration, the 220-GHz map has comparable sensitivity to galactic dust as the Planck 353-GHz map in the same region. With two more receivers fielded in 2016, the dust sensitivity at 220 GHz will surpass Planck this year.

## Objectives and Milestones

This SAT program advances the detector attributes needed for space-borne observations, specifically developments related to frequency coverage, focal-plane packaging, RF susceptibility, beam control, cosmic-ray susceptibility, and wafer formats. The tasks for our 2016 SAT program build on current antenna-coupled detector technology to address specific challenges for a space mission as follows:

- Extend the frequency range to bands at 40 GHz and 350 GHz;
- Develop dual-band devices operating broadband antennas;
- Develop larger focal-plane modules for 150-mm wafers with larger formats;
- Characterize and reduce focal-plane RF susceptibility;
- Develop more highly tapered antennas for coupling to ambient temperature optics;
- Measure cosmic-ray particle susceptibility in arrays; and
- Scale the fabrication process up to 150-mm-diameter wafers.

## Progress and Accomplishments

Focal-plane technology developed under this SAT program has made strong scientific progress in the past year, with focal-plane modules operating successfully in the BICEP3 experiment. As shown in Figs. 3 and 4, BICEP3 operates 20 modules in a large focal plane to achieve high sensitivity at 95 GHz. The modular design enabled component-wise development and testing. Arrays operating at 220 GHz in the Keck Array produced state-of-the-art polarization measurements at the South Pole last season (Fig. 2). These maps, the deepest produced at this frequency to date, will provide leading constraints on Inflationary polarization by providing new information on the brightness and polarization of the galactic dust foreground.



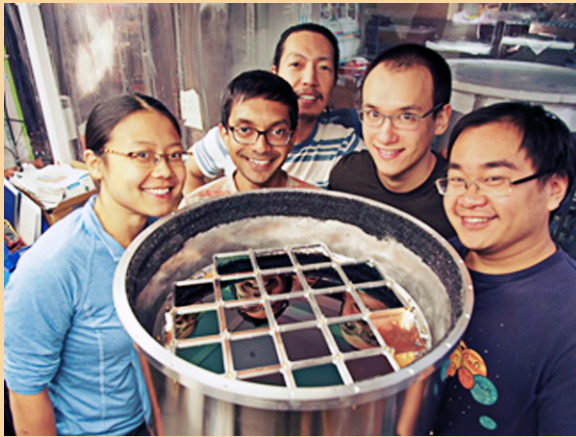


**Fig. 3.** BICEP3 deployed 20 modular focal-plane assemblies with 95-GHz antenna-coupled bolometers to the South Pole in early 2016. The experiment operates 2560 detectors to carry out leading measurements of CMB polarization at this frequency in conjunction with the multi-frequency Keck Array receivers.

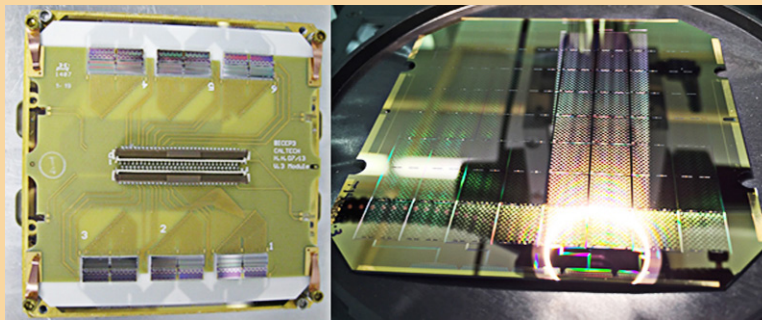


**Fig. 4.** Left: BICEP3 focal-plane module view from the back showing the SQUIDS integrated with the detector wafer. Right: Device wafer at 95 GHz. Our program will upgrade these modules to 150-mm-diameter wafers with higher detector counts.

This year, we completed testing of 40-GHz antennas, devices that were designed and fabricated under the previous SAT grant. The devices were tested for optical performance, giving controlled far-field beam characteristics (Fig. 5, left). The spectral response met the expected ~20% design bandwidth (Fig. 5, right); the dips in the spectrum are caused by the test-bed thermal filters. Preliminary measurements give an end-to-end optical efficiency, including test-bed windows and filters, of 35 – 55%. Performance is satisfactory and we intend to improve the devices by optimizing the spectral band for observations in the available terrestrial spectral band.

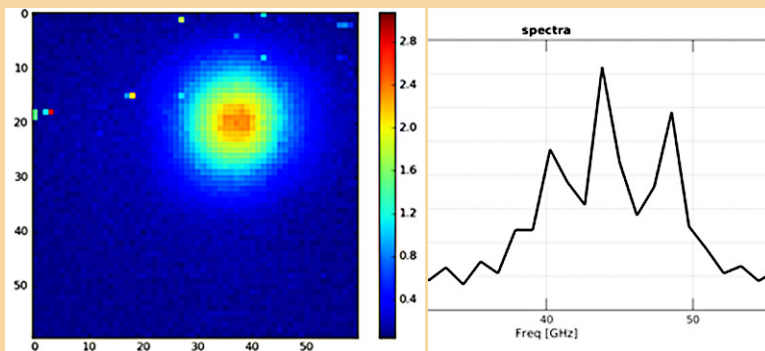


**Fig. 5.** Left: Beam map of a new 40-GHz antenna-coupled bolometer, measured in the far field of the antenna with a chopped thermal source. Right: Measured spectral response of the device. The deep notches are caused by the thermal filters, which were AR-coated for a different frequency. Now that this first test is successful, we will refine the antenna design and test with windows and filters optimized for 40 GHz.

We have also developed and fabricated a family of 200-300-GHz antennas. Under the previous SAT grant, the first round of these demonstrated a broadband 220/270-GHz dichroic filter; however, the antennas themselves were not satisfactory due to a mismatch between the antenna and resonant feed network, and an unfortunate mask layout error. We implemented three new designs based on previous test results: a 270-GHz antenna, a broadband 250-GHz antenna using a re-tuned resonant coupler, and a new 250-GHz “bow-tie” broadband antenna (Fig. 6). All of these wafers were fabricated successfully, and are currently in optical characterization, with test results expected shortly. We plan to select from these devices optimal designs for ground-based and balloon-borne observations. Based on the success of ground-based observations at 220 GHz (Fig. 2) we expect 270-GHz devices to have similar instantaneous sensitivity to galactic dust, providing a new frequency for constraining dust properties. The second flight of Spider plans to operate detectors at 270 GHz, with much lower photon backgrounds where a broadband design provides additional benefits.

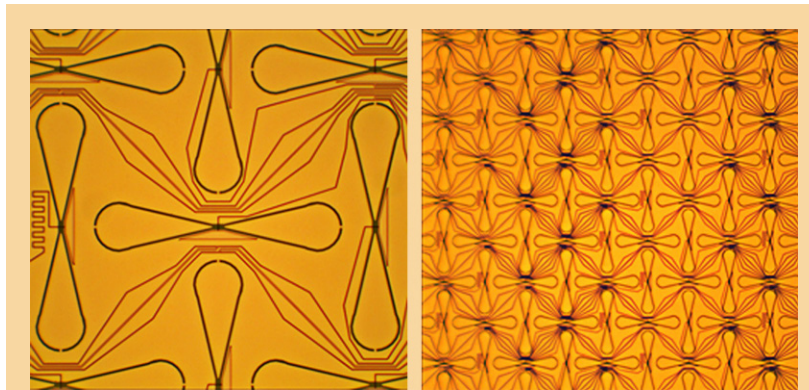


**Fig. 6.** Left: Broadband 200-300-GHz antenna designed from a unit “bowtie” sub-antenna. The bowtie is a slot design in a base Nb ground plane, back-illuminated through the Si wafer. The sub-antennas connect to a feed network of microstrip lines. Right: A larger-scale view of the broadband antenna, showing the combination of sub-antennas. The design detects vertical polarization in horizontal bowties, which are interleaved with the two feed networks.

We are gearing up to test RF susceptibility in antenna-coupled focal planes. Recent results from Spider and BICEP3 showed a degree of RF susceptibility at system level. The current design uses the ground plane of the antennas as an RF shield, connected to the housing through a series of wire bonds. We developed a new design where a bandpass filter placed over the detector array provides additional RF attenuation. This filter, developed at Cardiff University, has a high-pass inductive grid that reflects long-wavelength RF power. The filter grid is electrically connected to the housing frame. Because RF susceptibility is really a system issue, due to the many potential paths to the detector, characterizing this device requires a dedicated measurement. We are developing a new optical test bed for this purpose (Fig. 7). The test bed will also be used to measure the optical properties of future high-frequency antennas developed for bands between 200 and 350 GHz. A separate test bed is being developed at the University of Illinois to test cosmic-ray susceptibility in the array frames.



**Fig. 7.** Test bed for checking RF performance and carrying out future 200-350-GHz antenna development. The system is a small telescope cooled to 4 K using a pulse tube combined with a 300-mK cooler for operating the detectors.

Finally, our program has started on the development of 150-mm-diameter wafers. These larger wafers will increase the fabrication throughput by roughly  $\times 1.5^2 = \times 2.25$  compared to current 100-mm wafers. The lithographic deposition and etching capability at JPL's Micro Devices Lab is fully compatible with 150-mm wafers. The main performance issue is to control the uniformity of the TES, dielectric, and Nb layers over 150-mm diameters. We have carried out preliminary measurements of dielectric thickness, which becomes less uniform towards the wafer edge, as expected. We are now testing shadowing methods to improve uniformity. If these are unsuccessful, we will need to upgrade the deposition equipment to larger targets. The matching requirements for the TES normal resistance and transition temperature depend in detail on the noise properties of the devices vs. electrical bias. We also tested the Ti TES uniformity in the transition temperature (Fig. 8) which again degrades with radius, but appears to be acceptable.

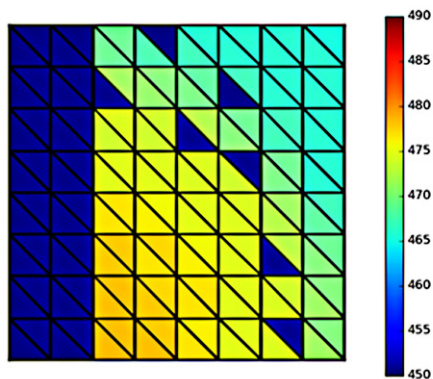


**Fig. 8.** Measured uniformity of the Ti transition temperature is  $\sim 10$  mK ( $\sim 2\%$ ) from edge to center for a 150-mm wafer. This measurement used a 100-mm wafer displaced from center to explore the radial dependence of the deposition chamber. The dark-blue missing channels on the left of the wafer are caused by a bad SQUID multiplexing channel.



Table 1 shows project milestones by topic, with each milestone's schedule and status.

Topic	Milestone	Schedule and Status
Antennas for Extended Frequencies	<b>40-GHz Arrays</b> Demonstrate antennas for the 40-GHz frequency band	<b>October 2014 – August 2015</b> Completed
	<b>270-GHz Arrays</b> Develop arrays for 270 GHz	<b>August 2014 – June 2016</b> 2 <sup>nd</sup> generation devices completed, in test
	<b>350-GHz Arrays</b> Develop arrays for 350 GHz	<b>March 2016 – December 2017</b> Design awaiting 270-GHz test results
Multi-Color Antennas	<b>Wide-Band Antenna</b> Develop wide-band antenna for 220/270 GHz	<b>August 2014 – June 2016</b> 2 <sup>nd</sup> generation devices completed, in test
	<b>Diplexer and Filters</b> Develop and test diplexer + filter components	<b>August 2014 – December 2015</b> Dichroic tested to perform nominally; full device requires improved wide-band antenna above
Large-Focal-Plane Modules	<b>Large-Format Modules</b> Develop and test designs for operating 150-mm wafers with larger formats	<b>January 2016 – November 2016</b> Mechanical design started
RF Susceptibility	<b>Focal-Plane RF-Susceptibility Mitigation</b> Test and improve RF susceptibility	<b>January 2016 – April 2016</b> RF test bed in assembly RF-shielded high-pass filter designed
Beam Spillover	<b>Highly-Tapered Antennas</b> Develop and test highly tapered 95-GHz antennas at device level	<b>January 2016 – November 2017</b> Design has not started
Particle Susceptibility	<b>Frame Response of Single-Element Device</b> Test Planck devices with modified frame to minimize events	<b>January 2014 – August 2015</b> Testing completed
	<b>Array Frame Hits</b> Measure frame susceptibility in arrays	<b>January 2016 – December 2017</b> Developing cryogenic test bed at UICU
150-mm-Diameter Wafers	<b>150-mm Wafer Fabrication Process</b> Determine engineering parameters for fabricating 150-mm-diameter wafers	<b>January 2016 – October 2017</b> Completed tests of dielectric and TES uniformity

**Table 1.** Project milestones, schedule, and status by topic.

## Path Forward

Developing antennas for extended frequencies will continue, with test results expected soon on the second-generation 270-GHz and broadband antennas. Once these tests complete, we plan to push forward one or possibly two 270-GHz designs to demonstrate science-grade devices that meet the requirements of the Keck Array and Spider experiment. We plan to start developing designs for new large modules for 150-mm wafers during the summer. The 150-mm-wafer fabrication plans will go forward with this development, starting with 35-GHz devices, which represents a convenient choice for advancing both the modules and the 150-mm-wafer capability. The RF-susceptibility test bed will be integrated and commissioned, carrying out RF-susceptibility tests with the new RF filter, starting with a well-characterized Spider focal-plane array. Future developments of 350-GHz and highly-tapered antennas will begin once the 270-GHz focal-plane development has completed.

## Publications

1. P. Ade et al., “Antenna-Coupled TES Bolometers Used in BICEP2, Keck Array, and SPIDER,” *ApJ*, **812**, 176B (2015)
2. BICEP2/Keck Collaborations, “Improved Constraints on Cosmology and Foregrounds from BICEP2 and Keck Array CMB Data with Inclusion of 95 GHz Band,” *PRL*, **116**, 1302B

3. BICEP2/Keck and Planck Collaborations, “*Joint Analysis of BICEP2/Keck Array and Planck Data*,” PRL, **114**, 1301 (2015)
4. BICEP2/Keck Array Collaboration, “*BICEP2/Keck Array V: Measurements of B-Mode Polarization at Degree Angular Scales and 150 GHz by the Keck Array*,” ApJ, **811**, 126B (2015)
5. BICEP2 Collaboration, “*BICEP2 III: Instrumental Systematics*,” ApJ, **814**, 110B (2015)
6. BICEP2/Keck Collaboration, “*BICE2/Keck Array VIII: Measurement of Gravitational Lensing from Large-Scale B-Mode Polarization*,” arXiv 1606.01968K (2016)
7. BICEP2/Keck Array Collaboration, “*BICEP2/Keck Array IV: Optical Characterization and Performance of the BICEP2 and Keck Array Experiments*,” ApJ, **806**, 206B (2015)
8. K.S. Karkare et al., “*Keck Array and BICEP3: Spectral Characterization of 5000+ Detectors*,” SPIE **9153E**, 3BK (2014)
9. I. Buder et al., “*BICEP2 and Keck Array: Upgrades and Improved Beam Characterization*,” SPIE **9153E**, 12B (2014)
10. H. Hui et al., “*BICEP3 Focal Plane Design and Detector Performance*,” SPIE, in press (2016)
11. K.S. Karkare et al., “*Optical Characterization of the BICEP3 CMB Polarimeter at the South Pole*,” SPIE, in press (2016)
12. J.A. Grayson et al., “*BICEP3 Performance Overview and Plans for a Multi-Receiver Array*,” SPIE, in press (2016)

For additional information, contact James Bock: [james.j.bock@jpl.nasa.gov](mailto:james.j.bock@jpl.nasa.gov)



# High-Efficiency Feedhorn-Coupled TES-based Detectors for Cosmic Microwave Background Polarization Measurements

Prepared by: Edward J. Wollack (PI; GSFC), David T. Chuss (Villanova University), Kevin L. Denis and S. Harvey Moseley (GSFC), Karwan Rostem (GSFC, JHU), and Tobias A. Marriage and Charles L. Bennett (JHU)

## Summary

The relic radiation from the Big Bang, the Cosmic Microwave Background (CMB), has provided a Rosetta stone for deciphering the content, structure, and evolution of the early universe. Our current theoretical understanding suggests that the universe underwent a rapid exponential expansion, called “Inflation,” in the first fraction of a second. Such an inflationary epoch would result in an observable stochastic background of gravitational waves that impress a faint polarized signature on the CMB. The cosmological importance of undertaking this measurement was highlighted in the 2010 National Research Council Decadal Survey, *“New Worlds, New Horizons in Astronomy and Astrophysics”* (NWNH) [1]. NASA consequently recognized characterization of the CMB as a high-priority science objective and a dedicated Inflation Probe (IP) mission was called out in the NASA Astrophysics Roadmap, *“Enduring Quests, Daring Visions”* [2]. These efforts are international in their scope, with collaborative mission concepts under consideration by both the Japanese and European Space Agencies. The development of enabling technologies, including large-format focal planes, for space-borne polarization missions is a priority of the NASA Physics of the Cosmos (PCOS) technology roadmap.

This two-year technology maturation effort, initiated by the Strategic Astrophysics Technology (SAT) program in December 2015, focuses on the implementation of polarization-sensitive focal-plane arrays that are compatible with the space environment. We have developed and demonstrated superconducting Transition-Edge Sensor (TES) detectors that utilize a unique combination of highly symmetric electromagnetic design elements and a single-crystal-silicon material system that results in high transmission efficiency, the required sensitivity, and low cross-polarization response. Our objective is to advance these devices to a Technology Readiness Level (TRL) of 6.

## Background

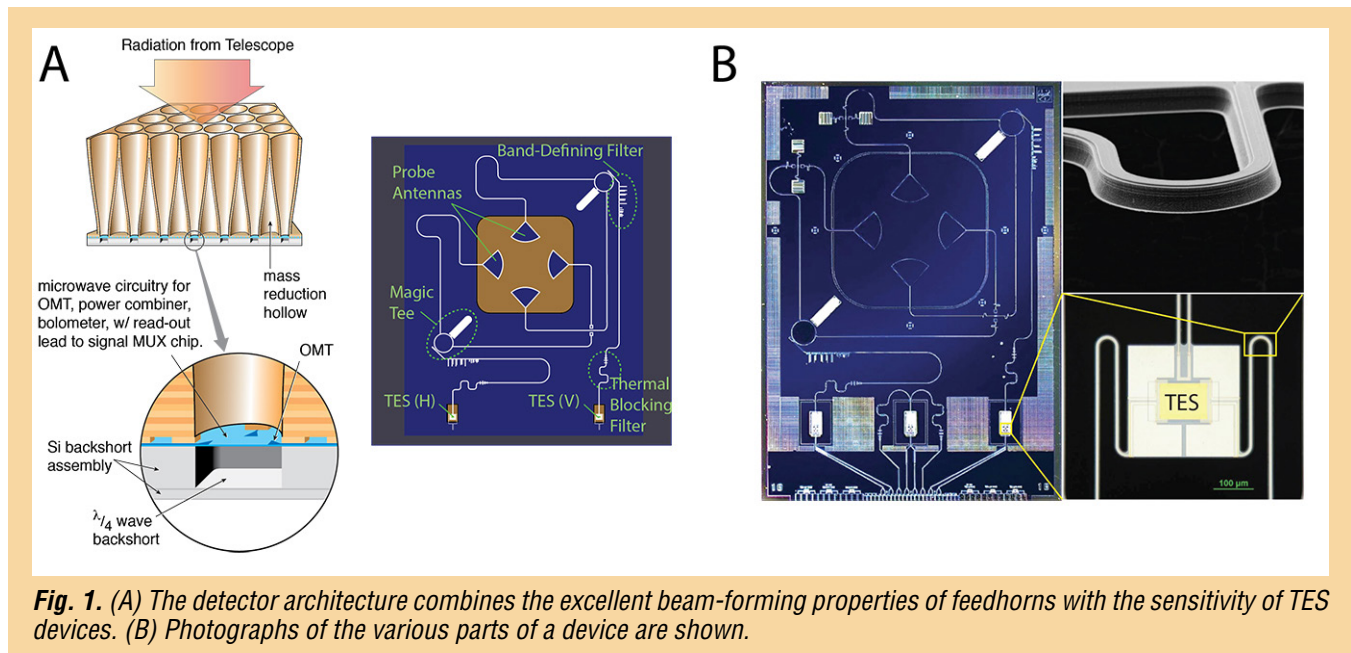
The polarized signature of inflation in the CMB offers an important tool to investigate the physics of the inflationary epoch of the early universe. Discovery of this signature would provide the first direct evidence for Inflation, and would rule out most competing explanations for the initial conditions of the early universe. Characterization of this signal provides a path to probe and quantify the physics of the first  $\sim 10^{-32}$  seconds of the universe, when energy scales vastly exceeded those accessible to current Earth-bound particle accelerators.

The measurement is arguably challenging, as the polarized signal from Inflation is anticipated to be faint, likely a mere  $\sim 10^{-8}$  of the 2.725 K isotropic component of the CMB. High sensitivity is a prerequisite; however, any mission that targets this measurement will also have to distinguish this minute polarized signal from both instrumental effects and other astrophysical sources. This requires high sensitivity and stability, multiple spectral bands for astrophysical foreground removal, control over potential systematic measurement and calibration errors, and compatibility with unique space-borne environmental conditions. Large detector arrays as well as development of calibration and observational techniques to achieve these instrumental attributes are key enabling technology considerations. We have developed a sensor architecture that addresses these needs of an IP mission.



The basic design and the fabrication processes that have been developed have been reported in the literature [3-5]. Figure 1 provides an illustration of the architecture. Radiation from the optics is coupled by the feedhorn of each sensor into microstrip circuitry. Each linear polarization is coupled to an independent microstrip line, filtered to set the desired spectral passband, and detected in a TES. This configuration directly addresses the requirements of the IP mission as follows:

- **Polarization Sensitivity:** The symmetric planar ortho-mode transducer (OMT) coupled to the symmetric feedhorn ensures that each polarization has symmetric beams and high isolation over the full spectral band.
- **Sensitivity:** The TES bolometers operate at  $\sim 150$  mK to ensure that the noise limit is set by the fluctuations in the CMB when operated in an appropriately stabilized space-borne system. In addition, the signal-mode sensor's large fractional bandwidth (60%) and high transmission efficiency ( $\sim 90\%$ ) enable improved throughput relative to alternative implementations. The architecture is demonstrably scalable to the large focal planes required for an IP mission.
- **Systematic Error Control:** On-chip thermal blocking and bandpass filters ensure that the spectral band is well-defined for radiation coupling through the optics. Boxed microstrip and electrical closeouts for the TES detectors ensure that stray (out-of-band) radiation does not couple directly to the detector. The design has been scaled to three broadband designs that span the CMB spectrum. Multiple spectral channels will be necessary to separate the CMB signal from astrophysical foregrounds such as galactic dust and synchrotron radiation. A highly uniform dielectric layer provides the control required to realize broadband circuit elements across the array reliably.
- **Prevention of Surface and Deep Dielectric Charging:** Damage can occur from interaction between exposed dielectrics surfaces and ambient space plasma. The metallic elements in the design, including the feedhorns and integrated doped-silicon package, greatly limit exposure of dielectric structures to energetic electrons in the environment. In addition, the comprehensive filtering strategy, stray light control, and metallic beam-forming elements minimize the number of quasi-optical dielectric elements required by the instrument design.
- **Mitigation of Cosmic-Ray Events:** High-energy ionizing particles that electromagnetically interact with the detector have the potential to induce signal contamination. It is not practical to mitigate cosmic-ray events via shielding. The approach adopted here is the implementation of structures having simple (easily understood) and fast thermal response, to reduce the affected portion of the data.



The basic operation of these detectors has been demonstrated at 40 GHz. Such detectors are currently being used in the Cosmology Large-Angular-Scale Surveyor (CLASS) ground-based telescope. This work focuses on extending their capabilities through a series of architectural improvements and corresponding validation.

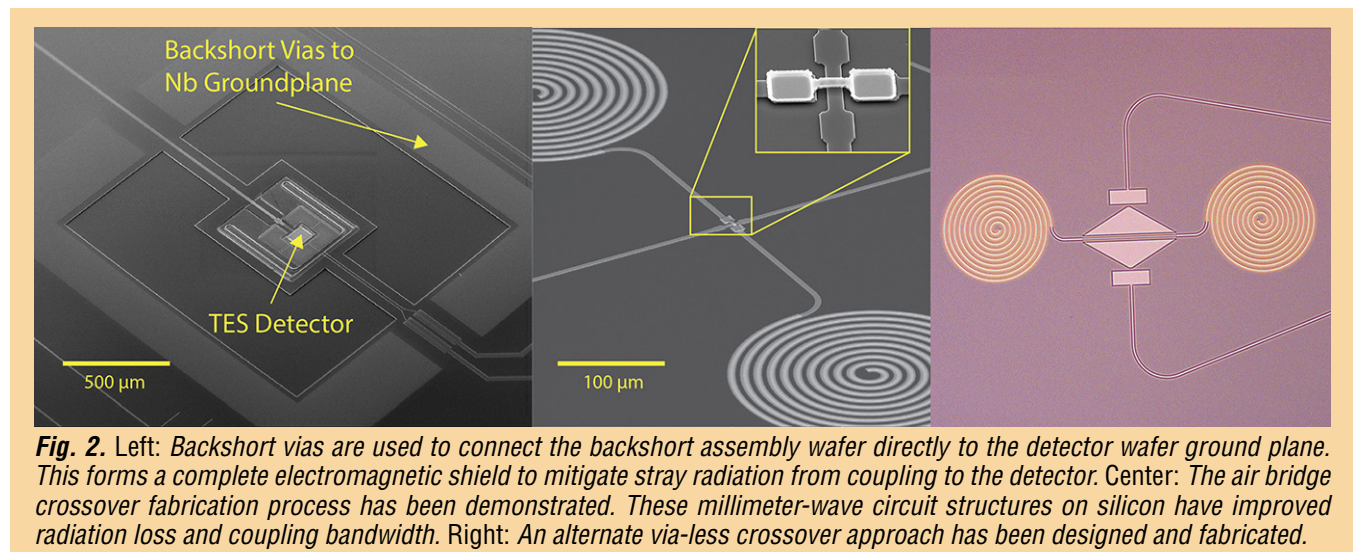
## Objectives and Milestones

This development effort centers around three targeted improvements in the focal-plane architecture. The first is to extend stray-light rejection through the 700-GHz gap frequency of the superconducting niobium circuitry. Measurements indicate that the achieved limit is ~500 GHz, limited by the closeout approach adopted in the current generation of device structures. This response will be refined by implementing vias in the silicon substrate that enable the backshort assembly to be bonded directly to the ground plane. These vias will complete the electromagnetic closeout of the detector and eliminate unintended coupling paths for out-of-band radiation. Second, we will implement direct access to the microwave ground plane to enable greater signal fidelity. This architectural improvement has been demonstrated to improve the noise performance of the devices in a prototype structure. The final architectural improvement involves the use of “crossovers,” which allow the microstrip from waveguide coupling probes to be routed on the chip.

In our 40- and 90-GHz detectors, this detail has been handled using a novel “via-less” crossover [6]. To extend these designs to higher frequencies, we will develop, test, and validate “air-bridge” crossovers, in which one line crosses over the other with an air gap between them. This concept minimizes loss and maximizes isolation. In addition to these advances, we have also targeted improvements in other aspects of our devices. Efforts are underway to enhance the TES topology and device thermalization. In addition, we are targeting improvements in our fabrication process to improve yield, reliability, and uniformity. These upgrades will be incorporated into focal planes as they are demonstrated.

## Progress and Accomplishments

In the first five months of the project, we developed fabrication processes for the ground-plane contacts and backshort assembly vias (Fig. 2). The ground-plane contacts have been integrated into device wafers and are currently being evaluated. Backshort assembly vias through the dielectric substrate have been integrated into devices (Fig. 3) and have passed basic continuity tests. Air-bridge crossovers have been fabricated along with devices using a new via-less crossover concept. Sensor arrays containing examples of these devices are currently being packaged for evaluation at millimeter wavelengths. In doing so, the performance of the two approaches will be compared. In support of these efforts, a prototype cryogenic multi-detector calibrator for arrays has been developed and will be used to characterize the efficiency and radiometric response of the sensors. This calibration source will be refined and integrated into our test facilities.





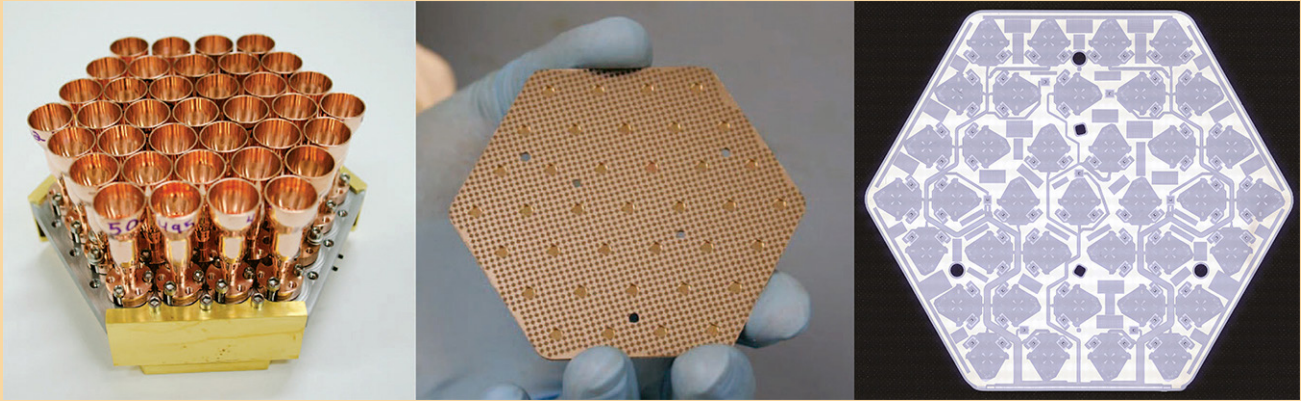


**Fig. 3.** Left: A complete 90-GHz sub-array prototype module is shown. Center: The 37-element integrated wafer. Right: This wafer includes the vias and ground-plane contacts described in the text.

## Path Forward

Over the next 12 months, the work will be advanced following the milestones summarized above. Testing of the sensor arrays that have incorporated the ground-plane contacts and backshort-assembly vias has been initiated. A new package to accommodate the array is under development, and an upgraded readout system to improve test throughput is being acquired. Wafers incorporating the air-bridges are in development, and the detailed performance of dichroic arrays (150/220 GHz) employing this approach will be evaluated relative to the via-less design. A detailed study of the sensor-array heat sinking and thermalization time scale will be performed to inform and potentially refine package design for use in ionizing-radiation environments. Representative focal-plane arrays will be integrated into the CLASS telescope [7] to achieve the desired TRL objectives.

## References

- [1] Blandford et al., “*New Worlds, New Horizons in Astronomy and Astrophysics*,” National Academy of Sciences (2010)
- [2] National Aeronautics and Space Administration, “*Enduring Quests, Daring Visions*,” Astrophysics Roadmap (2013)
- [3] D.T. Chuss et al., “*Cosmology Large Angular Scale Surveyor (CLASS) Focal Plane Development*,” Journal of Low Temperature Physics, 101007/s10909-015-1368-9 (2015)
- [4] K.L. Denis et al., “*Fabrication of Feedhorn-Coupled Transition Edge Sensor Arrays for Measurement of the Cosmic Microwave Background Polarization*,” Journal of Low Temperature Physics, 10.1007/s10909-015-1366-y (2015)
- [5] K. Rostem et al., “*Scalable Background-Limited Polarization-Sensitive Detectors for mm-wave Applications*,” Proc. SPIE **9153**, 91530B (2014)
- [6] K. U-yen, E.J. Wollack, S.H. Moseley, T.R. Stevenson, W.-T. Hsieh, and N.T. Cao, “*Via-less microwave crossover using microstrip-cpw transitions in slotline propagation mode*,” in Microwave Symposium Digest, MTT '09, IEEE MTT-S International, 1029-1032 (2009)
- [7] T. Essinger-Hileman et al., “*The Cosmology Large Angular Scale Surveyor (CLASS)*,” Proc. SPIE **9153**, 91531I (2014)

For additional information, contact Edward Wollack: [Edward.J.Wollack@nasa.gov](mailto:Edward.J.Wollack@nasa.gov)





# Appendix D

## Acronyms

### A

AAS . . . . .	American Astronomical Society
AC . . . . .	Alternating Current
ACF . . . . .	Anisotropic Conductive Film
ACIS . . . . .	Advanced CCD Imaging Spectrometer
ADC . . . . .	Analog-to-Digital Converter
ADR . . . . .	Adiabatic Demagnetization Refrigeration
AEGIS . . . . .	Astrophysics Experiment for Grating and Imaging Spectroscopy
AEI . . . . .	Albert Einstein Institute (Hannover)
AGN . . . . .	Active Galactic Nuclei
AIM . . . . .	Advanced Interferometry and Metrology
AIP . . . . .	American Institute of Physics
AIP . . . . .	Astrophysics Implementation Plan
ALD . . . . .	Atomic Layer Deposition
ANU . . . . .	Australian National University
AO . . . . .	Announcement of Opportunity
AOM . . . . .	Acousto-Optic Modulator
APD . . . . .	Astrophysics Division
APRA . . . . .	Astrophysics Research and Analysis
APS . . . . .	Active Pixel Sensor
AR . . . . .	Anti-Reflection
ASCA . . . . .	Advanced Satellite for Cosmology and Astrophysics
ASE . . . . .	Amplitude-Stimulated Emission
Athena . . . . .	Advanced Telescope for High-ENergy Astrophysics
AXAF . . . . .	Advanced X-ray Astrophysics Facility
AXSIO . . . . .	Advanced X-ray Spectroscopic Imaging Observatory

### B

BI . . . . .	Back-Illuminated
BICEP . . . . .	Background Imaging of Cosmic Extragalactic Polarization
BOX . . . . .	Buried Oxide
BRDF . . . . .	Bidirectional Reflectance Distribution Function

### C

CAD . . . . .	Computer-Aided Design
CAT . . . . .	Critical-Angle Transmission
CATXGS . . . . .	Critical-Angle Transmission X-ray Grating Spectrometer
CCD . . . . .	Charge-Coupled Device
CDM . . . . .	Code-Division Multiplexing
CDR . . . . .	Critical Design Review
CLASS . . . . .	Cosmology Large-Angular-Scale Surveyor
CMB . . . . .	Cosmic Microwave Background
CMOS . . . . .	Complementary Metal Oxide Semiconductor
CNR . . . . .	Carrier-to-Noise (density) Ratio
COPAG . . . . .	Cosmic Origins Program Analysis Group
COR . . . . .	Cosmic Origins
COTS . . . . .	Commercial off the Shelf

CRESST . . . . . Center for Research and Exploration in Space Science & Technology  
 CST . . . . . Community Science Team  
 CTA . . . . . Cherenkov Telescope Array  
 CTE . . . . . Coefficient of Thermal Expansion  
 CY . . . . . Calendar Year

## D

DAM . . . . . Detector Assembly Mount  
 DC . . . . . Direct Current  
 DLR . . . . . Dienstleistungszentrum Ländlicher Raum (German Aerospace Center)  
 DM . . . . . Demonstration Model  
 dof. . . . . degree of freedom  
 DRIE . . . . . Deep Reactive Ion Etching  
 DWS . . . . . Differential Wavefront Sensing

## E

E . . . . . Energy  
 E-beam . . . . . Electron-beam  
 EBEX . . . . . The E and B Experiment  
 EC . . . . . Executive Committee  
 ECL . . . . . External Cavity Laser  
 eLISA . . . . . evolved Laser Interferometer Space Antenna  
 EM . . . . . Electromagnetic  
 EM . . . . . Engineering Model  
 ERP . . . . . Event Recognition Processor  
 ESA . . . . . European Space Agency  
 EUSO . . . . . Extreme Universe Space Observatory  
 ExEP . . . . . Exoplanet Exploration Program  
 ExoPAG . . . . . Exoplanet Exploration Program Analysis Group

## F

FDM . . . . . Frequency-Division Multiplexed  
 FDM . . . . . Frequency-Domain Multiplexing  
 FI . . . . . Front-Illuminated  
 FOV . . . . . Field of View  
 FPA . . . . . Focal-Plane Array/Assembly  
 FPGA . . . . . Field Programmable Gate Array  
 FWHM . . . . . Full-Width at Half-Maximum  
 FY . . . . . Fiscal Year

## G

GAS . . . . . Grating-Array Structure  
 GEMS . . . . . Gravity and Extreme Magnetism Small Explorer  
 GEVS . . . . . General Environmental Verification Standard  
 GFE . . . . . Government-Furnished Equipment  
 GLAST . . . . . Gamma-ray Large-Area Space Telescope  
 GOAT . . . . . Gravitational Observatory Advisory Team  
 GOF . . . . . Guest-Observer Facility  
 GPS . . . . . Global Positioning System  
 GR . . . . . General Relativity  
 GRACE . . . . . Gravity Recovery and Climate Experiment  
 GRB . . . . . Gamma-Ray Burst  
 GRS . . . . . Gravitational Reference System

GSE . . . . . Ground Support Equipment  
 GSFC . . . . . Goddard Space Flight Center  
 GW . . . . . Gravitational Wave

## H

HabEx . . . . . Habitable Exoplanet  
 HETGS . . . . . High-Energy Transmission-Grating Spectrometer  
 HFDFC . . . . . High-Fidelity Deterministic Figure Control  
 HPD . . . . . Half-Power Diameter  
 HQ . . . . . Headquarters  
 HRMA . . . . . High-Resolution Mirror Assembly

## I

IAU . . . . . International Astronomical Union  
 IBS . . . . . Ion-Beam Sputtering  
 IF . . . . . Intermediate Frequency  
 INFN . . . . . Istituto Nazionale di Fizica Nucleare (Italian National Institute for Nuclear Physics)  
 I/O . . . . . Input/Output  
 IP . . . . . Inflation Probe  
 IR . . . . . Infrared  
 IRAD . . . . . Internal Research and Development  
 ISS . . . . . International Space Station  
 I-V . . . . . Current-Voltage  
 IXO . . . . . International X-ray Observatory  
 IXPE . . . . . Imaging X-ray Polarimeter Explorer

## J

JANUS . . . . . Joint Astrophysics Nascent Universe Satellite  
 JAXA . . . . . Japanese Aerospace eXploration Agency  
 JEM . . . . . Japanese Experiment Module  
 JPL . . . . . Jet Propulsion Laboratory  
 JUICE . . . . . JUpiter ICy moons Explorer  
 JWST . . . . . James Webb Space Telescope

## K

KAGRA . . . . . KAmioka GRAVitational-wave telescope

## L

LADEE . . . . . Lunar Atmosphere and Dust Environment Explorer  
 LBNL . . . . . Lawrence Berkeley National Laboratory  
 LCD . . . . . Liquid Crystal Display  
 LCRD . . . . . Laser Communication Relay Demonstration  
 LD . . . . . Laser Diode  
 LED . . . . . Light-Emitting Diode  
 LEO . . . . . Low Earth Orbit  
 LIGO . . . . . Laser Interferometer Gravitational-wave Observatory  
 LISA . . . . . Laser Interferometer Space Antenna  
 LiteBIRD . . . . . Lite (Light) satellite for the studies of B-mode polarization and Inflation from cosmic background Radiation Detection  
 LLC . . . . . Limited Liability Company  
 LP . . . . . Line Processor  
 LPA . . . . . Large-Pixel Array  
 LPF . . . . . LISA Pathfinder  
 LRI . . . . . Laser-Ranging Interferometer



LRP . . . . .	Laser-Ranging Processor
LSF . . . . .	Line Spread Function
LTP . . . . .	LISA Technology Package
LUPI . . . . .	Laser Unequal Path-length Interferometer
LUVOIR . . . . .	Large UV/Optical/IR
LVS . . . . .	Leon Van Speybroeck
L1 . . . . .	Level 1
L2 . . . . .	Level 2
L2 . . . . .	Second large space mission of ESA's Cosmic Vision program
L3 . . . . .	Third large space mission of ESA's Cosmic Vision program
L3ST . . . . .	L3 Study Team

## M

MAXI . . . . .	Monitor of All-sky X-ray Image
MBE . . . . .	Molecular-Beam Epitaxy
MCC . . . . .	Magnetically Coupled (micro-)Calorimeter
MEMS . . . . .	Micro-Electro-Mechanical System
MIDEX . . . . .	Medium-class Explorer
MIT . . . . .	Massachusetts Institute of Technology
MKI . . . . .	MIT Kavli Institute
MO . . . . .	Mission of Opportunity
MOPA . . . . .	Master Oscillator Power Amplifier
MPPC . . . . .	Multi-Pixel Photon Counter
MSFC . . . . .	Marshall Space Flight Center
MSM . . . . .	Magnetic Smart Material
mux . . . . .	multiplexer

## N

NANOGrav . . . . .	North American Nanohertz Observatory for Gravitational waves
NASA . . . . .	National Aeronautics and Space Administration
Near-IR . . . . .	Near-Infrared
NGO . . . . .	New Gravitational-wave Observatory
NISP . . . . .	Near-Infrared Spectrometer and Photometer
NIST . . . . .	National Institute of Standards and Technology
NITPC . . . . .	Negative-Ion Time Projection Chamber
NPR . . . . .	NASA Procedural Requirements
NPRO . . . . .	Non-planar Ring Oscillator
NRC . . . . .	National Research Council
NSF . . . . .	National Science Foundation
NuSTAR . . . . .	Nuclear Spectroscopic Telescope ARray
NWNH . . . . .	New Worlds, New Horizons in Astronomy and Astrophysics (2010 Decadal Survey)
N-XGS . . . . .	Notional X-ray Grating Spectrometer

## O

OBA . . . . .	Optical Bench Assembly
OBF . . . . .	Optical Blocking Filter
OCT . . . . .	Office of the Chief Technologist
OGRE . . . . .	Off-plane Grating Rocket Experiment
OLED . . . . .	Organic Light-Emitting Diode
OMT . . . . .	Ortho-Mode Transducer
OP-XGS . . . . .	Off-Plane X-ray Grating Spectrometer
OSIRIS-REx . . . . .	Origins, Spectral Interpretation, Resource Identification, and

	Security-Regolith Explorer
OWL . . . . .	Orbiting Wide-angle Light collectors
<b>P</b>	
PAG . . . . .	Program Analysis Group
PATR . . . . .	Program Annual Technology Report
PBS . . . . .	Polarizing Beam-Splitter
PCI . . . . .	Peripheral Component Interconnect
PCOS . . . . .	Physics of the Cosmos
PDR . . . . .	Preliminary Design Review
PER . . . . .	Polarization Extinction Ratio
PHARAO . . . . .	Projet d'Horloge Atomique par Refroidissement d'Atomes en Orbit (On-Orbit Cooled-Atom Atomic Clock Project)
PhysPAG . . . . .	Physics of the Cosmos Program Analysis Group
PI . . . . .	Principal Investigator
PIPER . . . . .	Primordial Inflation Polarization Explorer
PLC . . . . .	Planar Linear Cavity
PMS . . . . .	Phase-Measurement System
PMT . . . . .	Photomultiplier Tube
POET . . . . .	Polarimetry of Energetic Transients
PRAXyS . . . . .	Polarimeter for Relativistic Astrophysical X-ray Sources
PRN . . . . .	Pseudo-Random Noise
PRT . . . . .	Platinum Resistance Thermometer
PSD . . . . .	Power Slope Density
PSF . . . . .	Point Spread Function
PSM . . . . .	Point-Source Microscope
PSU . . . . .	Penn State University
PTB . . . . .	Physikalisch-Technische Bundesanstalt (German National Metrology Institute)

**Q**

QE . . . . .	Quantum Efficiency
--------------	--------------------

**R**

RAM . . . . .	Random Access Memory
R&D . . . . .	Research and Development
REXIS . . . . .	REgolith X-ray Imaging Spectrometer
RF . . . . .	Radio Frequency
RFI . . . . .	Request for Information
RGS . . . . .	Reflection-Grating Spectrometer
RIN . . . . .	Relative Intensity Noise
RIO . . . . .	Redfern Integrated Optics
rms . . . . .	root mean square
ROC . . . . .	Radius of Curvature
RTD . . . . .	Resistance Temperature Detector
RTF . . . . .	Roman Technology Fellowship
RXTE . . . . .	Rossi X-ray Timing Explorer

**S**

SAC-B . . . . .	Satelite de Aplicaciones Cientificas-B
SAO . . . . .	Smithsonian Astrophysical Observatory
SAT . . . . .	Strategic Astrophysics Technology
SBIR . . . . .	Small Business Innovation Research
SBS . . . . .	Stimulated Brillouin Scattering
SEM . . . . .	Scanning Electron Micrograph

SGO . . . . .	Space-based Gravitational-wave Observatory
SGR . . . . .	Soft-Gamma Repeater
SiPM . . . . .	Silicon Photomultiplier
SLF . . . . .	Stray-Light Facility
SMART-X . . . . .	Square Meter, Arcsecond Resolution Telescope for X-rays
SMBH . . . . .	Supermassive Black Hole
SMD . . . . .	Science Mission Directorate
SMEX . . . . .	Small Explorer
SOI . . . . .	Silicon-on-Insulator
SOTA . . . . .	State of the Art
SPA . . . . .	Small-Pixel Array
SPC . . . . .	Scientific Programme Committee
Spider . . . . .	Suborbital Polarimeter for Inflation Dust and the Epoch of Reionization
SPIE . . . . .	Society of Photo-Optical Instrumentation Engineers
SQUID . . . . .	Superconducting QUantum Interference Device
SRON . . . . .	Space Research Organization Netherlands
SR&T . . . . .	Supporting Research and Technology
STD . . . . .	Solar Time Delay
STDT . . . . .	Science and Technology Definition Team
STI . . . . .	SpaceTech International (Germany)
STMD . . . . .	Space Technology Mission Directorate
STOP . . . . .	Structural Thermal and Optical Performance
ST-7 . . . . .	Space Technology 7

## T

TC . . . . .	Thermocouple
TDM . . . . .	Time-Division Multiplexing
TDR . . . . .	Technology Development Roadmap
TES . . . . .	Transition-Edge Sensor
TES . . . . .	Transition-Edge Superconducting
TFB . . . . .	Tapered Fiber Bundle
TFT . . . . .	Thin-Film Transistors
TIS . . . . .	Total Integrated Scatter
TM . . . . .	Test Mass
TMB . . . . .	Technology Management Board
TPC . . . . .	Time Projection Chamber
TPCOS . . . . .	Technology development for Physics of the Cosmos
TRL . . . . .	Technology Readiness Level
TVAC . . . . .	Thermal Vacuum

## U

UHECR . . . . .	Ultra-High-Energy Cosmic Ray
UIUC . . . . .	University of Illinois Urbana-Champaign
UK . . . . .	United Kingdom
UROP . . . . .	Undergraduate Research Opportunities
US . . . . .	United States
USO . . . . .	Ultra-Stable Oscillator
USRA . . . . .	Universities Space Research Association
UV . . . . .	Ultraviolet

## V

V5 . . . . .	Virtex-5 (FPGA)
--------------	-----------------



## W

WDM . . . . .	Wavelength-Division Multiplexer
WFI . . . . .	Wide-Field Imager
WFIRST . . . . .	Wide-Field Infrared Survey Telescope
WFS . . . . .	Wavefront Sensor
WHIM . . . . .	Warm-Hot Intergalactic Medium
WHIM . . . . .	Warm-Hot Interstellar Medium

## X

XCSR . . . . .	X-ray mission Concepts Study Report
XGS . . . . .	X-ray Grating Spectrometer
X-IFU . . . . .	X-ray Integral Field Unit
XMM-Newton . . . . .	X-ray Multi-mirror Mission-Newton
XMS . . . . .	X-ray Microcalorimeter Spectrometer
XRS . . . . .	X-Ray Surveyor
XRT . . . . .	X-Ray Telescope
XTiDE . . . . .	X-ray Time Domain Explorer

## Other

3NT . . . . .	Three-Noise Tester
---------------	--------------------



